DESIGN OF EXPERIMENTAL PROCEDURES FOR THERMAL PROPERTIES ANALYSIS OF PRISMATIC $LiFePO_4$ BATTERY

CHAYANGKUN SANGUANWATANA

A THESIS SUBMITTED IN PARTIAL FULFILLMENT
OF THE REQUIREMENT FOR THE DEGREE OF
MASTER OF ENGINEERING IN AUTOMOTIVE ENGINEERING
(INTERNATIONAL PROGRAM)
INTERNATIONAL COLLEGE
KING MONGKUT'S INSTITUTE OF TECHNOLOGY LADKRABANG
2014

KMITL-2014-IC-M-004-0010

DESIGN OF EXPERIMENTAL PROCEDURES FOR THERMAL PROPERTIES ANALYSIS OF PRISMATIC $LiFePO_4$ BATTERY

CHAYANGKUN SANGUANWATANA

A THESIS SUBMITTED IN PARTIAL FULFILLMENT

OF THE REQUIREMENT FOR THE DEGREE OF

MASTER OF ENGINEERING IN AUTOMOTIVE ENGINEERING

(INTERNATIONAL PROGRAM)

INTERNATIONAL COLLEGE

KING MONGKUT'S INSTITUTE OF TECHNOLOGY LADKRABANG

2014

KMITL-2014-IC-M-004-0010

Thesis	Design of Experimental Procedures for thermal properties analysis in $LiFePO_4$ Battery
Student	Mr. Chayangkun Sanguanwatana
Student ID.	
Degree	Master of Engineering
Program	Automotive Engineering (International Program)
Year	2014
Thesis Advisors	Asst. Prof. Dr. Monsak Pimsarn Dr.-Ing Chadchai Srisurangkul Prof. Tsushima Shohji

ABSTRACT

As a main objective of this thesis, a set of experimental procedures has been developed in order to study thermal behavior of selected lithium ion battery. The thermal model of the battery is used for the concept of the design along with the information of the battery performance characteristics. The results from the performed experiments such as internal, surface temperature and cell voltage from different load conditions can be used in order to analyze for the heat generated as well as heat capacity from the battery which is essential for the design of thermal management system (BTMS).

At the first stage, characteristics of the selected battery is studied by performing charge and discharge tests to observe the capacity and voltage profiles of the battery. Then, the derived 1D thermal model of the battery was shown that heat generated is indicated from two sources, over-potential heat which is irreversible and entropic heat which is reversible. The difference between heat generated and heat transferred to the surroundings result in the product of heat capacity and temperature-time gradient of the battery. Designed experiments include constant current discharge, pulse current discharge, temperature coefficient experiment and heat capacity experiment. For constant current experiment, various discharge rates were applied to the battery and at the same time, temperature inside and on the surface of the battery are recorded for the analysis of heat generation stated above. Separated experiment of adjusting battery temperature to

observe the change in open circuit potential is designed for the evaluation of entropy coefficient value at different state of charges. Pulse current test can be used for analyzing the internal resistance of the battery which can be used to express the relationship to the state of charge and temperature of the battery. The heat generation results from discharging the battery shows the heat generated mostly followed the trend of over-potential heat but entropic heat tend to reduce the total heat generated at the start. Then, it was found that higher discharge current applied can produce less internal resistance and vice versa for lower discharge rate. For surrounding heat transfer, heat transfer coefficient was referred to the specification from heat flux sensor which was used directly for the calculation. The internal heat transfer coefficient was also calculated by using the internal and surface temperature data. In the heat capacity experiment, the procedure is similar to pulse current test except that both charge and discharge processes were applied to maintain average state of charge at constant. Then, heat capacity was calculated to average value of 2112.84 J/K. Finally, open circuit voltage of the battery was observed through the long pulse test and the voltage recovery curve was fitted to sixth degree polynomial curve which can be used to predict the final value of open circuit voltage.

ACKNOWLEDGEMENT

The study was a scholarship in automotive program under Thailand Advanced Institute of Science and Technology and Tokyo Institute of Technology (TAIST Tokyo Tech) which is a collaboration of National Science and Technology Development Agency, Thailand (NSTDA), Tokyo Institute of Technology, Japan, and King Mongkut's Institute of Technology Ladkrabang, Thailand. This study has been carried during the year 2009 - 2013 as a part of a research project in the Automotive Laboratory, National Metal and Materials Technology Center, Thailand.

I would like to express my gratitude to my advisors, especially, Dr.-Ing Chadchai Srisurangkul, Automotive Laboratory MTEC, Associate Professor Dr. Monsak Pimsarn, department of Mechanical Engineering, KMITL and Professor Tsushima Shohji, Osaka University, and Dr. Preechar Karin, International College for their guidance and encouragement during the work. For providing equipment and location for performing experiments, I would like to thank the members of Automotive Laboratory and Electrochemical Materials and System Laboratory. Also, I would like to thank all of my friends from TAIST Tokyo Tech class, especially, Mr. Prabij Joshi, Mr. Saharat Chanthanumataporn and Mr. Wisit Wiputgasemsuk for their help in my research work.

Furthermore, I would like to thank Miss Daoprakai Loupilai for being such a great companion beside me in difficult times. Finally, I would like to express my gratitude to my mother for such a great support financially and spiritually.

April 13, 2015

Chayangkun Sanguanwatana

TABLE OF CONTENTS

LIST OF TABLES

TABLE Page

LIST OF FIGURES

FIGURE Page

LIST OF FIGURES (CONT)

LIST OF FIGURES (CONT)

FIGURE PAGE

LIST OF FIGURES (CONT)

FIGURE PAGE

LIST OF FIGURES (CONT)

FIGURE PAGE

LIST OF FIGURES (CONT)

FIGURE PAGE

CHAPTER 1

INTRODUCTION

1.1 Background

Nowadays, two of the major problems which facing the humanity are the rapid decrease in fossil fuels which are the main energy resources and the global warming effect which cause the temperature of the earth's surface to rise gradually. The cause of this started from the discovery of fossil fuels results in the invention of gasoline and diesel engine technologies for almost all of automobiles used today. Then, it is realized that the emission from these kinds of engines are the main cause of global warming judging from the great numbers of automobile usage around the world. To counter this, zero emission technologies are developed. Being one of the alternatives, electric vehicle has slowly become popular through the late 20^{th} century after being dominated by the fossil fuels powered engine earlier.

The advantage of electric vehicle apart from being the zero emission vehicles is that the power conversion efficiency is much higher compared to the fossil fuel engines. This is because the wheels receive the power directly from the main power source of the vehicle, batteries. Battery is the main key which can determine the overall performance of the electric vehicle such as range and power delivered. Many types of batteries are used for the application of electric vehicles (EV), including lead acid, nickel metal hydride and lithium ion batteries.

Lithium ion batteries quickly become the most attractive type in the EV application because of their advantages such as higher operating voltage, higher power density, less self-discharge rate, has no memory effect and etc. The only issue which is the most concern to the users of lithium ion batteries is regarding to the temperature. As the rise of demand in EV, batteries are to be charged quickly with high current and therefore can concern heat issue.

Temperature has significant effects to the lithium ion battery. Extremely high temperature condition can give high resistive heat generation which can damage battery from the inside and leads to thermal runaway which destroys the battery. For extremely low temperature condition, chemical reaction rate is slowed down and thus reduce the power output and permanently reduce battery capacity. To prevent this from happening, battery thermal management system (BTMS) is necessary. The function of BTMS is to protect, monitor and control the battery condition and the

environment. It is used for balancing the cell in order to maintain the battery in a state which can fulfill the requirement of the specified application. The system requires integrated circuits which has the data of battery operating temperature limit and thermal properties. Therefore, to design the BTMS, the selected battery must be studied in terms of structure and thermal performance characteristics.

The essence of this work is to understand thermal model which express relationship of battery voltage and temperature that can lead to the calculation of heat generation and evaluation of thermal properties. To see the results practically, experiments are performed on the selected battery with different conditions of current load and environmental temperatures. When temperature output response in recorded, the data is used for further investigation of battery thermal behavior. The experimental procedures are purposely designed and simplified in order to determine the battery properties having to take least amount of time with obtaining as many results as possible with the acceptable accuracy. Then, the results can be applied as controlling parameter for the BTMS configurations of battery operating limits.

1.2 Objectives

- To design experimental procedures for evaluating thermal performance of the selected lithium ion battery.
- To study thermal properties of the selected lithium ion battery.
- To evaluate thermal performance at different operating current loads.

1.3 Scopes

- Study the battery specifications and performance characteristics such as dimensions, capacity, internal resistance, operating voltage and etc.
- Study thermal model for the lithium ion battery including heat generation terms and thermal properties.
- Design experimental procedures based on thermal model for the battery.
- Determine thermal properties such as heat capacity, heat generation and heat transfer coefficient of the battery.

1.4 Thesis Outlines

The thesis is organized in 6 Chapters, the contents of which are summarized as followed:

Chapter 1 : Introduction

This chapter introduces the general background of batteries, the important of thermal management system, the objectives of this study, and the scopes of work in this study.

Chapter 2 : Literature Reviews

This chapter citations reviews the published literature on the battery thermal effects, the previous studies of methods for thermal analysis, and thermal model for the lithium ion batteries.

Chapter 3 : Research Methodology

This chapter explains the process of experimental design. The procedures of research include the charge and discharge with measurement of temperature. Additionally, procedures for determining temperature coefficient and heat capacity are also included.

Chapter 4 : Results

This chapter demonstrates the experimental results such as discharge voltage curves and temperature responses. Then, the calculation results of thermal properties of the battery are presented.

Chapter 5 : Analysis and Discussions

The obtained results from the previous chapters would be discussed in this chapter. The discussions are included with experimental temperature results, thermal model and calculation results of thermal properties are different experiment conditions are compared.

Chapter 6 : Conclusions and Suggestions

A brief summary of the work is presented in this chapter.

CHAPTER 2

LITERATURE REVIEWS

From the day it was invented, battery becomes more and more important for us due to its ability to store energy. The first cell was made by Alessandro Volta in 1800. He discovered that a continuous flow of electrical force was generated when using certain fluids as conductors to promote a chemical reaction between the metals and voltage would increase when voltaic cells were stacked on top of each other [1]. Undeniably, this is considered to be one the greatest inventions in human history because batteries can be found in almost every electrical application today. From 19^{th} to 20^{th} century, batteries were constantly developed in terms of chemical and physical characteristics in order to enhance their performance. Table 2.1 Timeline History of battery [1] shows a brief timeline of battery development.

Table 2.1 Timeline History of battery [1]

Year	Inventor	Discovery
1800	Volta (Italy)	Invention of the voltaic cell
1820	Ampère (France)	Electricity through magnetism
1836	Daniell (England)	Invention of Daniell cell
1859	Planté (France)	Invention of lead acid battery
1868	Leclanché (France)	Invention of the Leclanché cell
1888	Gassner (USA)	Completion of dry cell
1899	Jungner (Sweden)	Invention of the nickel-cadmium battery
1901	Edison (USA)	Invention of the nickel-iron battery
1947	Neumann (France)	Successfully sealing the nickel-cadmium battery
Mid 1960	Union Carbide (USA)	Development of primary alkaline battery
1970s	M.S. Whittingham (USA)	Lithium-ion battery proposed
1996	J. Goodenough (USA)	Lithium iron phosphate ($LiFePO_4$) first used as cathod material
1999	-	Commercialization lithium-ion polymer
2002	Y.M. Chiang (USA)	Conductivity improved by doping with Aluminum or Zirconium
2011	-	66% of rechargeable batteries in Japan are Li-ion type
2013	-	LVP* Battery developed to increase energy efficiency

* LVP = Lithium Vanadium Phosphate

2.1 Review of Lithium ion battery

2.1.1 Working principle of a lithium ion battery

A single cell of lithium ion battery consists of several parts. This includes a positive electrode (cathode), a negative electrode (anode), electrolyte and a separator. Energy cells are the smallest individual electrochemical unit which delivers a voltage depends on the chemistry. A battery is formed when these cells are assembled together. The construction may come in many forms for examples; cylindrical, prismatic, pouched, or coin cells. Readers are welcome to do further readings to learn more about battery construction in [2].

Figure 2.1 Lithium ion batteries in different sizes and construction

In discharging process, the cell is connected to an external load, electrons flow from the oxidized anode, passed the external load, electrons to the cathode, where the electrons are accepted and the cathode material is reduced. When the battery is fully discharged, the voltage will have a sudden drop to its specified value. For the charging process, the process is reversed only for the case of secondary lithium ion battery. The chemical reaction is shown here below for the case of lithium cobalt oxide [3]. See figure 2.2 for chemical reaction of such process.

$$LiCoO_2 + \square C_6 \underset{\text{discharge}}{\overset{\text{charge}}{\rightleftarrows}} \square CoO_2 + LiC_6$$

Figure 2.2 Chemical Reaction of charging and discharging battery

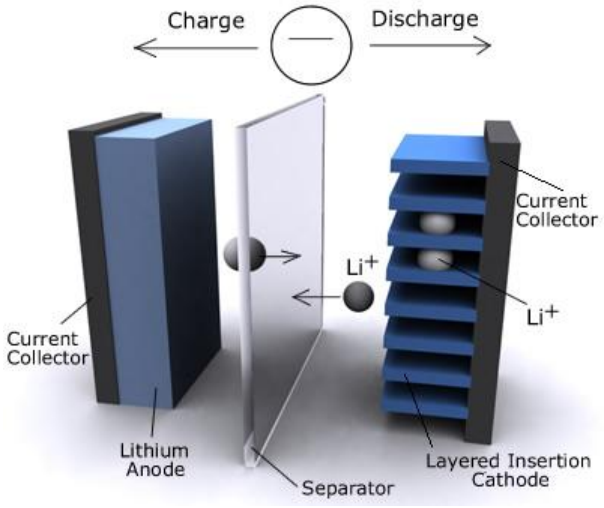

Figure 2.3 Operation of Secondary lithium ion battery [4]

2.1.2 Comparison of battery types

Many types of battery were developed since the first kind was invented. The purpose of this is to improve the performance and fill in the gaps of disadvantages of the previous types. Lithium-ion battery is considered to be the newest technology which has many advantages over other types. Factors which indicate the performance of the battery include cell operating voltage, energy density, specific energy, self-discharge rate, cycle life, environmental effect and etc. Figure 2.4 compares common lithium ion batteries in several aspects.

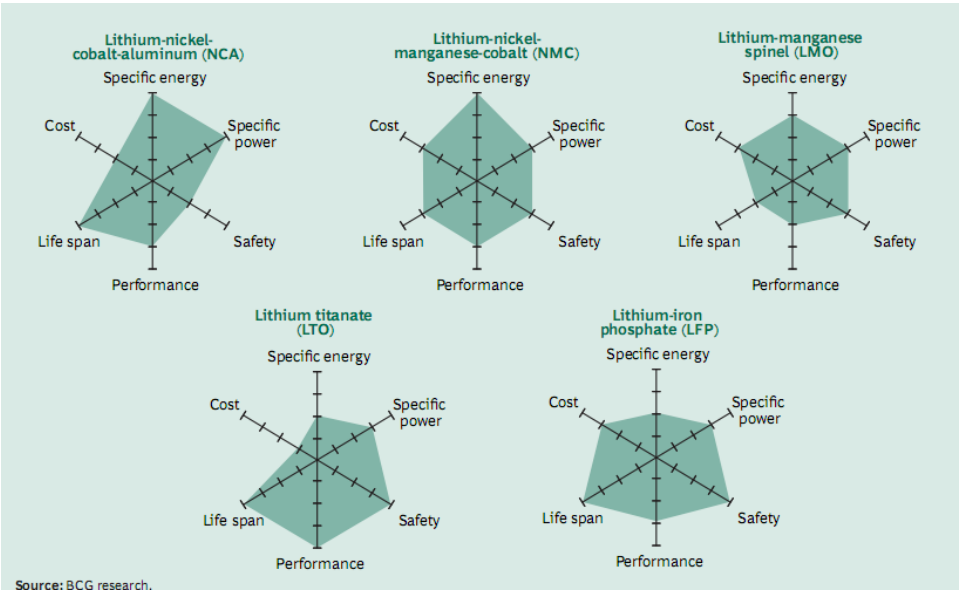

Figure 2.4 Energy density and Specific Energy comparison [5]

Other than the superior in specific energy, lithium-ion batteries also have the advantages in terms of operating voltage, which is 3 times higher (typically 3.6 V) than lead acid battery. This is because lithium is the element which can produce the lowest standard reduction potential. There is no memory effect which occurs in the nickel cadmium type. While being expensive, new materials for manufacturing lithium-ion batteries are constantly explored to reduce the cost. Lithium-ion batteries are also developed into many types based on different materials used for cathode. Comparison in general characteristics of lithium ions with other types are in the table 2.2 [6]

From table 2.2, comparing between the lithium ion battery types, both manganese and phosphate are capable of fast charging at 1 hour or less. Also, they have the same peak load current less than 10C for best result. In comparison for cycle life, phosphate type has the highest value among the others with maximum of 2000 cycles. Cell voltage for phosphate type is lower than other types (3.6V) which makes this type deliver less energy. When considering safety factor, phosphate type is proved to have a very good thermal stability [7]. Despite this, protection circuit is a mandatory.

Table 2.2 Performance comparison of several types of batteries [6]

Specifications	Lead-Acid	NiCd	NiMH	Li-Cobalt	Li-Manganese	Li-Phosphate
Specific energy density (Wh/kg)	30 - 50	45 - 80	60 - 120	150 - 190	100 - 135	90 - 120
Internal resistance (mΩ/V)	<8.3	17 - 33	33 - 50	21- 42	6.6 - 20	7.6 - 15.0
Cycle life (80% discharge)	200 - 300	1000	300 - 500	500 - 1000	500 - 1000	1000 - 2000
Fast-charge time (hrs.)	8 - 16	1 typical	2- 4	2- 4	1 or less	1 or less
Overcharge tolerance	High	Moderate	Low	Low	Low	Low
Self-discharge/month (room temp.)	5 - 15%	20%	30%	<5%	<5%	<5%
Cell voltage	2.0	1.2	1.2	3.6	3.8	3.3
Charge cutoff voltage (V/cell)	2.4	Full charge indicated by voltage signature	Full charge indicated by voltage signature	4.2	4.2	3.6
Discharge cutoff voltage (V/cell)	1.75	1	1	2.5 - 3.0	2.5 - 3.0	2.8
Peak load current**	5C	20C	5C	> 3C	> 30C	> 30C
Peak load current* (best result)	0.2C	1C	0.5C	< 1C	< 10C	< 10C
Charge temperature	-20 - 50°C	0 - 45°C	0 - 45°C	0 - 45°C	0 - 45°C	0 - 45°C
Discharge temperature	-20 - 50°C	-20 - 65°C	-20 - 65°C	-20 - 60°C	-20 - 60°C	-20 - 60°C
Maintenance requirement	3 - 6 months (equalization)	30 - 60 days (discharge)	60 - 90 days (discharge)	None	None	None
Safety requirement	Thermally stable	Thermally stable, fuses common		Protection circuit mandatory		
In use since	1881	1950	1990	1991	1996	1999
Toxicity	High	High	Low	Low	Low	Low

*C refers to battery capacity and this unit is used when specifying charge or discharge rates. For example: 0.5C for a 100 Ah battery = 50A. **Peak load current is maximum possible current which could permanently damage a battery.

2.1.3 Electrical fundamentals of batteries

In this thesis, phenomenological model is used for the study of electrical characterization of the battery. The term "phenomenological" means the investigation of input and output without considering the fundamental physics which is more complex [8]. To understand the mechanism of a battery, a simple equivalent circuit is considered. The circuit in figure 2.5 demonstrates the relationship between the open circuit voltage, E_0, internal resistance R_i (which is the combination of R and R_0 and capacitance C_0). Electrical model equation 2.1 and 2.2 then can be derived from Kirchhoff's Law.

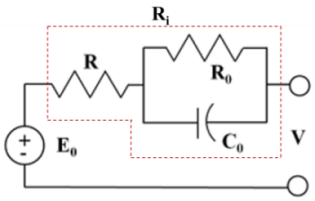

Figure 2.5 Simplified battery circuits

$$V = E_0 - IR_i - V_C \tag{2.1}$$

$$V_C = \eta_{ct} + \eta_c \tag{2.2}$$

Where the cell voltage, V is the output which depends on the input parameters including open circuit voltage (E_0) with the product of current (I) and resistance (R) and the capacitance voltage (V_c). Here, V_c can also be related to the concentration polarization (η_c) and charge transfer (η_{ct}) effects. Figure 2.6 shows cells voltage as a function of current.

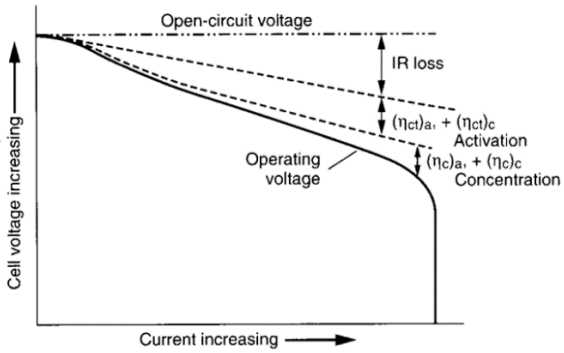

Figure 2.6 Cell polarizations as a function of current [9]

State of charge (SOC) is the parameter which determines the amount of charge which the battery can supply with reference to its capacity.

$$\frac{dSoC}{dt} = -\frac{I(t)}{C_n} \tag{2.3}$$

Here, state of charge depends on the current (I) and the nominal capacity of the battery (C_n) in Amp-Hour. This is one of the methods for determining the state of charge of the battery which is called "Amp-Hour counting". Ampere-Hour (Ah) is the unit for indicating the capacity of the battery. If the battery has 60 Ah rating, it takes 60 Amperes to fully discharge the battery in one hour.

Internal resistance is the other important factor for determining performance of the battery. From equation 2.1 while neglecting the charge transfer and activation polarization effects which is small compared to IR loss, resistance depends on the open circuit, cell voltage and the current load. From Hans Georg et al [10], several methods can be used to find the resistance of a battery. VDA current step method is one of methods reported in this literature. In this method, charge and discharge pulses were applied to the battery for a period of time. The changes in voltage resulted from the charge and discharge pulses were used for the calculation of internal resistance. Equation 2.4 shows that the internal resistance (discharge condition only) is the result of voltage change divided by the loaded current which also depends on discharge time.

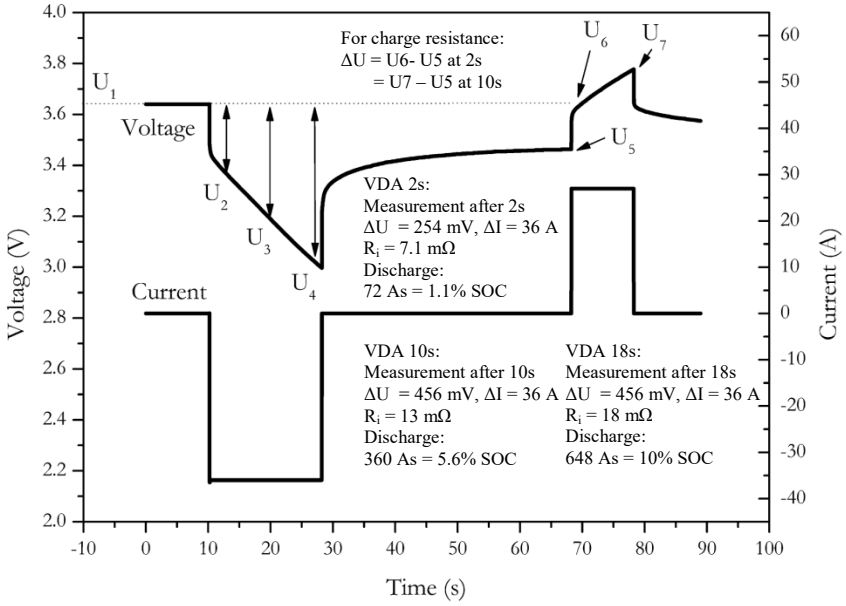

Figure 2.7 VDA Current Step method procedures [10]

$$R_{i,t} = \left|\frac{\Delta U}{I}\right| = \left|\frac{U_1 - U_2}{I}\right|_{t=2s} = \left|\frac{U_1 - U_3}{I}\right|_{t=10s} = \left|\frac{U_1 - U_4}{I}\right|_{t=18s} \tag{2.4}$$

2.1.4 Temperature Effects on batteries

The most important factor which affects the performance and life of a lithium ion battery is the temperature. According to Arrhenius Law [18], as the battery gets hotter, the rate of chemical reaction will be increased and reduce the life of the battery. Figure 2.8 shows that performance of a battery depends on both voltage and temperature. This shows that the safe operating value must be in the area of the green zone which is between 2.2 – 4.2 V and -5 to 95ºC of voltage and temperature range respectively. Severe consequence can start from lithium plating which resulted from overvoltage or low temperature operation. Lithium plating occurs when excessive currents the Lithium ions cannot be accommodated quickly enough between the intercalation layers of the anode and Lithium ions accumulate on the surface of the anode where they are deposited as metallic Lithium. Consequently, the capacity will be reduced permanently. With higher operating current, the result of heat from I^2R heating (resistive heating) is also higher. When the temperature reaches 80ºC, SEI (Solid Electrolyte Interface/Interphase) layer will start to breakdown and at 150ºC, the separator will starts to melt, allowing the cathode and anode plates to be in contact, which short circuit the battery. At the point above 250ºC, temperature will increase dramatically, with the release of oxygen. Above 300ºC, thermal runaway will occur and the battery will be completely destroyed.

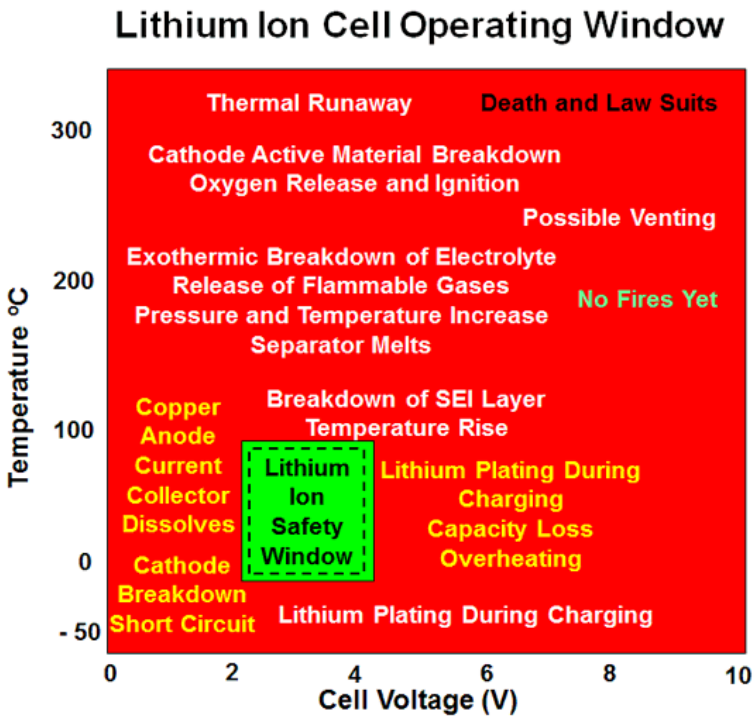

Figure 2.8 Lithium ion cell operating window [11]

2.1.5 Batteries in electric vehicle application

Historically, development of electric vehicle grows in parallel with the batteries applied inside. From the invention of Gaston Plante, lead acid battery was used in the earliest practical design of electric car built by Thomas Parker [12]. This kind of battery was also applied in General Motors EV-1, the first mass-produced and electric car in 1996 [13]. Then the nickel metal hydride battery was developed with higher energy density than lead acid and longer lifetime but less efficient in charging and discharging. When the lithium ion batteries were developed, it was found that this type has higher energy density and gives higher efficiency in charge and discharging. In the early development, lithium ion batteries has shorter cycle life (500 – 1000 cycles for lithium cobalt and lithium manganese) [14] and also sensitive to temperature. This leads to the new development of cathode materials to improve the performance. Lithium iron phosphate battery, one of the youngest technologies of Li-ion battery is proved to have longer cycle life (1000 – 2000 cycles) and have better thermal stability comparing to other types. Table below shows the types of battery used in the electric vehicle throughout the history.

In first commercialized battery electric cars, lead acid and NiMH batteries was used as a power source. However, due to low energy density, this cause power rating and range to be low. When lithium ion battery was applied to electric car application, driving range becomes amplified. The because of higher energy density in lithium ion batteries which allows the electric car to store more batteries which can deliver more power with less weight.

Table 2.3 Batteries for commercialized battery electric cars [15]

Production Year	Model	Battery Chemistry	Power Rating	Range
1996	General Motors EV1	Lead Acid and NiMH	16.5 kWh	70 – 100 miles
2001	REVAi	Lead Acid	9.6 kWh	50 miles
2006	ZAP Xebra	Lead Acid	7.2 kWh	40 miles
2008	Tesla Roadster	Lithium ion	53 kWh	221 miles
2009	BMW Mini E	Lithium ion	35 kWh	100 miles
2010	Nissan LEAF	Lithium ion	24 kWh	109 miles
2011	Mitsubishi iMiev	Lithium ion	16 kWh	62 miles
2012	Tesla Model S	Lithium ion	85 kWh	300 miles
2014	BMW i3	Lithium ion	18.8 kWh	81 miles

2.2 Battery Thermal Management System (BTMS)

2.2.1 Definition and purpose

From figure 2.8, it is seen that to maintain the battery in the safe area, the temperature and voltage conditions must be controlled in certain boundaries according to the specifications. These factors also impacts on battery life and its performance, battery thermal management system is essentially required. Also, in the electric car battery application, the battery has to deal with occasional extreme condition from fast charging which most of the electric car user needs. Battery thermal management system or BTMS in short is the system which regulates and monitors the temperature of the battery within the requirements. The main objectives of BTMS design are;

- Protection from Overheating: Protection circuit is installed in order to cut off the battery before the excessive condition of temperature is reached.
- Dissipation of surplus heat generated: Examples are keeping the ambient temperature low to maximize the natural heat flow or using metallic cooling plates mounting as a good heat conducting part on the conductive surface of the battery.
- Uniform heat distribution: This is to monitor the “hot spot” which is localized inside the battery located in the surroundings of other hot batteries. The use of PCM (Phase-change material) is one of the solutions which can dissipates heat by convection and brings the temperature down to the safe zone. Thermal imaging can also be used for the analysis of this part.
- Minimum additional of weight: A complex design of BTMS can cause the battery pack to be heavier. For the tractions batteries in Electric Vehicle application, this will require higher power consumption as the battery pack gets heavier. In this case, batteries with high energy density can be used as one solution.

2.2.2 BTMS Development and Design

The term “battery management system” or BMS in short, is defined as any electronic system that manages a rechargeable battery such as by protecting the battery from safe operating area, monitoring its state, calculating secondary data, reporting that data, controlling its

environment, authenticating it and / or balancing it [16]. BTMS is a branch of BMS which focuses mainly on the battery temperature.

One of the very first battery management systems was designed to monitor the state of charge (SOC) of the battery. Figure 2.9 shows such technology developed by Heyer [17]. From the figure, the measurement is indicated from the ratio between battery voltage and the voltage drop on the sense resistor. This is for user to recognize replacement time for the battery.

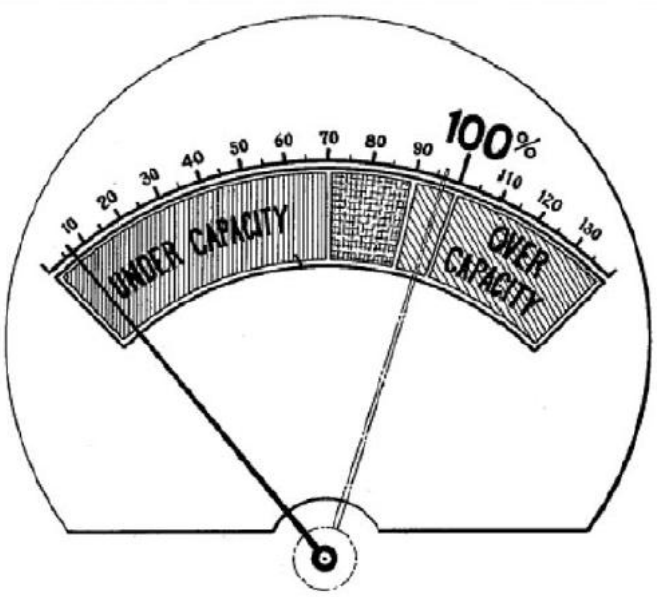

Figure 2.9 Battery capacity indicator developed by Heyer

From figure 2.8, temperature is the most critical factor which impacts on battery performance and lifetime. To explain this, Arrhenius Law states that the chemical reaction rate depends on the temperature [18]. This makes the battery which operates in high temperature give higher performance due to improved electron mobility. However, if the operating temperature is too high, irreversible chemical reactions can occur and can cause permanent damage to the battery. On the other hand, if the operating temperature is too low, the rate of reaction will be reduced along with the performance. Considering automotive applications, batteries usually are subjected to many thermal abuses such as accelerating the vehicle which creates sudden high load or fast charging. Therefore, battery thermal management system is critically required.

Battery Thermal Management System can be categorized into 2 types, active and passive. The active BTMS requires fluid such as air and water for regulating the temperature. From figure 2.10, the study in BTMS system in Toyota Prius by Zolot et al [19] shows the system can operates well under HWFET, FTP and US06 driving cycles and operating temperature of 0°C,

25°C and 40°C. Conditioned air from the cabin is supplied as thermal management forced air system. Please refer to the literature for the experimental results of this work.

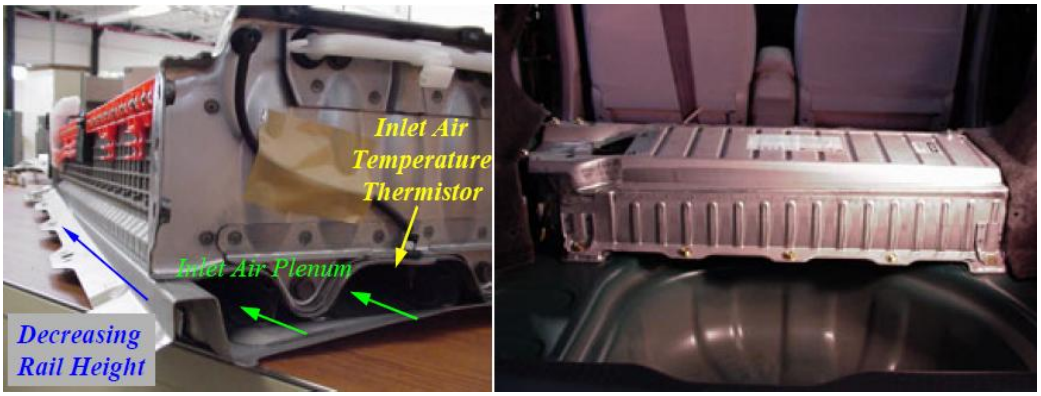

Figure 2.10 Toyota Prius Battery pack with thermal management system [19]

The BTMS system inside Chevrolet Volt is also treated as one of the examples of active type which use liquid coolant as the cooling fluid. The overall system explanation can be observed from figure 2.11 below. A 12 V coolant pump create and control the coolant flow which passes the plug-in battery charger assembly, the radiator, the power inverter module and then back to the pump. The coolant also flows through the system to comfort the passenger cabin.

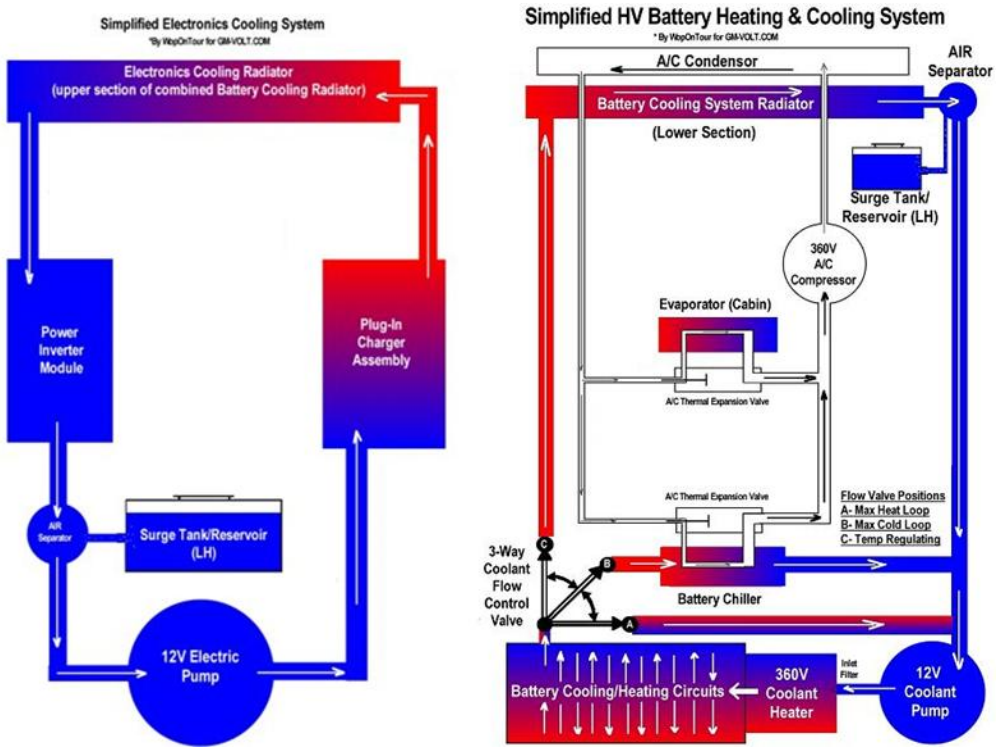

Figure 2.11 Chevrolet Volt battery thermal management system [20]

For the passive type of BTMS, there are no complex systems installed to regulate the temperature with simpler and smaller in size due to the elimination of mechanical components. PCM or Phase-Change Material is best example for the passive BTMS. By changing the phase, it can absorb and release heat while the temperature is maintained constant. From the study of Khateeb et al [21], the comparison between different thermal management (heat dissipation) methods under different C-Rates was performed. The result of experiments found that the use of PCM alone can cause the temperature to drop significantly but in the abusive operation, the slow heat dissipation can cause the PCM to melt. For the case of combining PCM with the aluminum foam, it was found that the foam could help prevent the PCM temperature reaching the melting range with the comparable cooling efficiency.

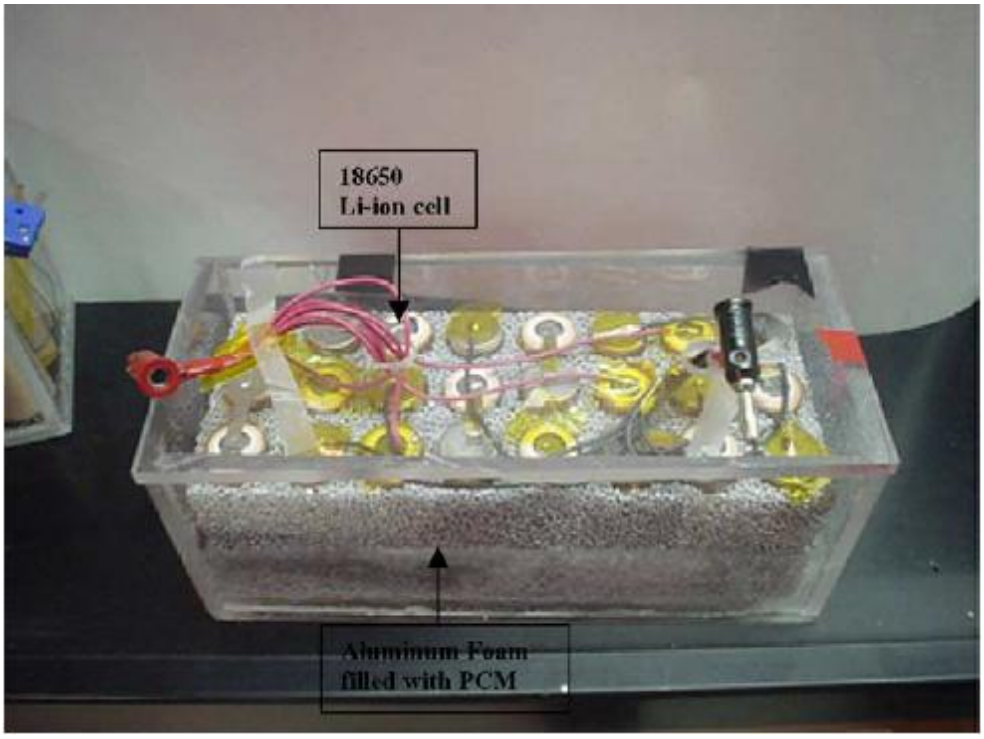

Figure 2.12 Experiments of heat dissipation by using PCM

The timeline of thermal management system development can be shown in table 2.4. This shows the development from the patents of battery temperature monitoring to the development of BTMS in commercialized electric car. From the table, the progression started from development of battery testing apparatus by Heyer which focused on voltage measurement that can be translated into battery condition. In 1977, Benham put more focus on temperature by designing a system which detects thermal runaway from the slope of the charge current.

Table 2.4 Timeline of BTMS development

Year	Developer	Developments
1937	Heyer et al.	Battery testing apparatus [22]
1977	Benham et al.	Battery thermal runaway monitor and alert [23]
1985	Esrom	Battery storage with double wall housing design [24]
1993	Harm et al.	Battery charger with thermal runaway protection [25]
1996	McShane et al.	Method for detection and control of thermal runaway under charge [26]
1997	Waters et al.	Battery design for uniform cooling and heating [27]
2000	Lake et al.	System for cooling electric vehicle battery [28]
2002	Oweis et al.	Battery module thermal management blanketing and jacketing [29]
2003	Oda et al.	Power supply apparatus including fan cooling [30]
2007	Yahnger et al.	Thermal management system for battery pack [31]
2010	Zhou	EV thermal management system (3-loop heat exchanger) [32]
2012	Schaller et al.	Battery thermal management with phase transition [33]
2013	Bandhauer et al.	Li-ion battery thermal runaway suppression system using microchannel coolers and refrigerant injections [34]

Esrom, Waters and Oweis designed battery housing for applying temperature regulation by air or liquid flow. Thermal runaway control was developed by McShane so that the current can be adjusted when the temperature reaches the limit. In 2000, the battery cooling system with one loop heat exchanger was developed by Lake and then improved to three-loop heat exchanger by Zhou. In 2003, Oda designed the forced air cooling by fan and later PCM was applied to the design by Schaller. In 2013, a system was designed by attaching sensors to batteries and release cooling fluids when a thermal runaway condition is at risk.

2.3 Reviews on battery thermal analysis methods

As the temperature of the battery affects its performance largely, thermal management must be carefully designed to achieve the target performance and to prolong battery life. According to National Renewable Energy Laboratory (NREL), the design of BTMS requires several analysis procedures in order to maximize the efficiency of the system. These include computer aided thermal analysis, thermal imaging, fluid and heat transfer experiment, vehicle simulation, field testing and thermal characterization. [35]

In this work, thermal characterization is the main focus. This has three parts of analysis which include cell characteristics, module cooling strategy, operating conditions. The input of these data into design analysis can produce the output of battery thermal responses. Figure 2.13 demonstrates in this part.

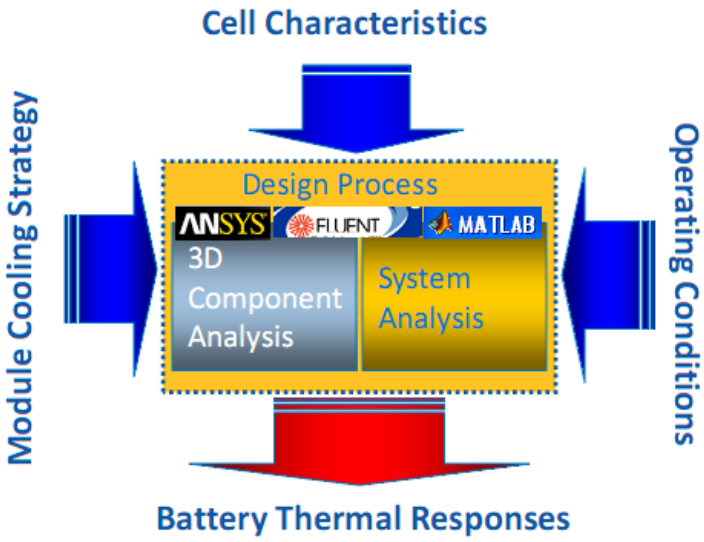

Figure 2.13 Process of battery thermal characterization modeling [35]

Thermal performance analysis is one of the initial steps of designing BTMS. The first sequential step starts from defining the BTMS design objective and constraints. This is to define the desired thermal performance according to the safety requirement which stated by the manufacturer. Then the battery characteristics such as dimensions, geometry, number of modules and orientation are studied for the BTMS layout establishment. Next, heat generation and heat capacity of the battery are analyzed along with the first order BTMS evaluation. This requires the use of principles of heat transfer and energy balance to determine transient and steady-state temperature of the battery pack while operated at the simulated conditions.

The size and design of BTMS has the direct effect from the magnitude of heat generation from the selected battery. Heat generation depends on many parameters such as load profile, battery temperature, internal resistance and chemical structure of the battery. Heat capacity, the property which defines the amount of heat that can be stored inside the battery, also affects the design of BTMS. Many approaches were applied to perform analysis to obtain such thermal properties.

In NREL research facility, many tools are provided for battery analysis. They are battery cycling devices for simulating load profile, finite element analysis (FEA) software for simulating thermal response, thermal environment chambers for temperature controlled test, glove box for battery physical examination and isothermal calorimeter for heat generation analysis [36]. Furthermore, NREL has designed a custom cell calorimeter in order to test cells with improved specification with more capability than most of calorimeters in the market. Figure 2.14 shows the diagram of the designed calorimeter. It is designed to obtain accurate heat generation data for batteries from 0.5 Ah to 100 Ah. Its sustained maximum current is 500 Amps. Maximum battery weight for testing is 200 kg. The dimension is 60x40x40 cm with test cavity volume of 96 liters. Operating temperature range is from -40 to 100°C. This system is also capable of testing liquid-cooled batteries. The main objective of this calorimeter design is to obtain accurate heat generation data for battery modules under different operating conditions such as power profiles and operating temperatures. The power profiles can be simulated from actual electric vehicle driving cycle. Furthermore, this device can also be used to analyze for heat capacity of the selected battery. The method involves the measurement of exchanged heat by using the heat flux gauges which installed next to the battery. Then data from heat flux gauges and the difference between battery and chamber temperature are used to calculate the heat capacity [37].

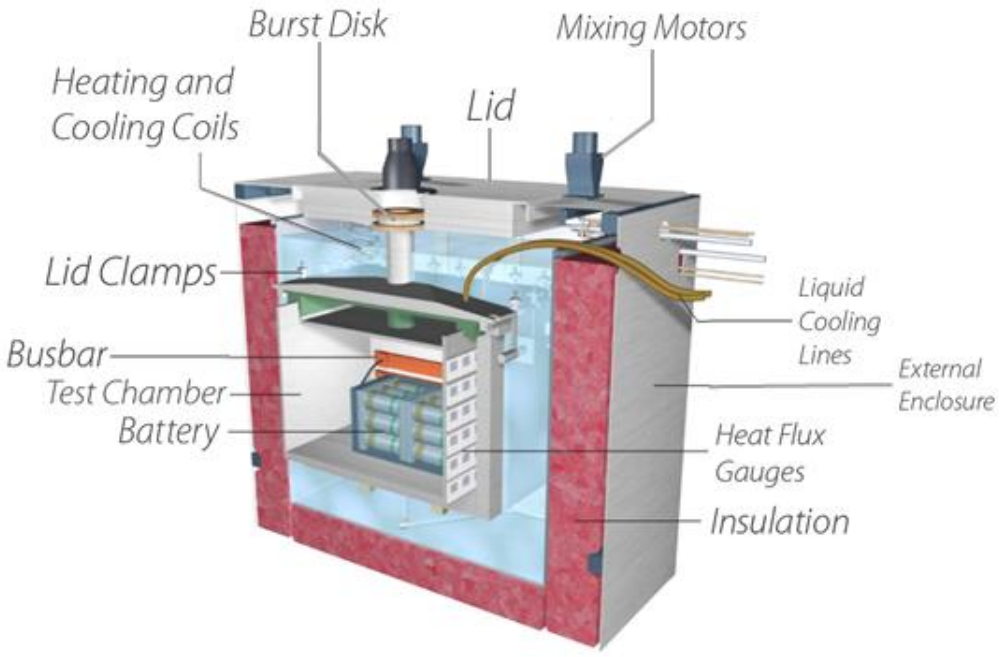

Figure 2.14 Custom made Calorimeter by NREL [37]

Calorimeter is widely used for analyzing thermal behavior of batteries. In the work of Hong et al [38], heat dissipation and heat accumulated of a commercial Sony 18650 1.35 Ah nominal capacity lithium ion cell were measured by using ARC 2000 accelerated calorimeter. The heat effects were observed from the charging and discharging process. The battery is brought to the desired initial temperature by using Arbin BT-2042 battery cycler. This device feeds current to the coil heater which was wrapped around the cell for heating the cell by means of different constant current values. The heater around the calorimeter cavity is used for regulating the temperature at 30°C. The temperature difference between the cell and the calorimeter was measured by using a precision multi-meter. The discharge capacity of the battery is first tested with the conditions of initial temperature of 35ºC, 45ºC and 55ºC. The overall cell impedance value is expressed as an area-specific impedance or ASI. This depends on the difference between open circuit voltage and the operating voltage. The value of ASI in each temperature condition is obtained from 15 seconds DC current interruption experiment (see figure 2.17 for the results and calculation method). The surface temperature rises in each condition are also observed. Heat dissipation rate is calculated as a function of discharge rate and surface temperature. Heat dissipation tends to increase with the increasing discharge rate and rise sharply towards the end of discharging process (see figure 2.16). This can be related to the increase of impedance at the end of discharge. The experimental setup in the work of Hong et al is shown in figure 2.15 below.

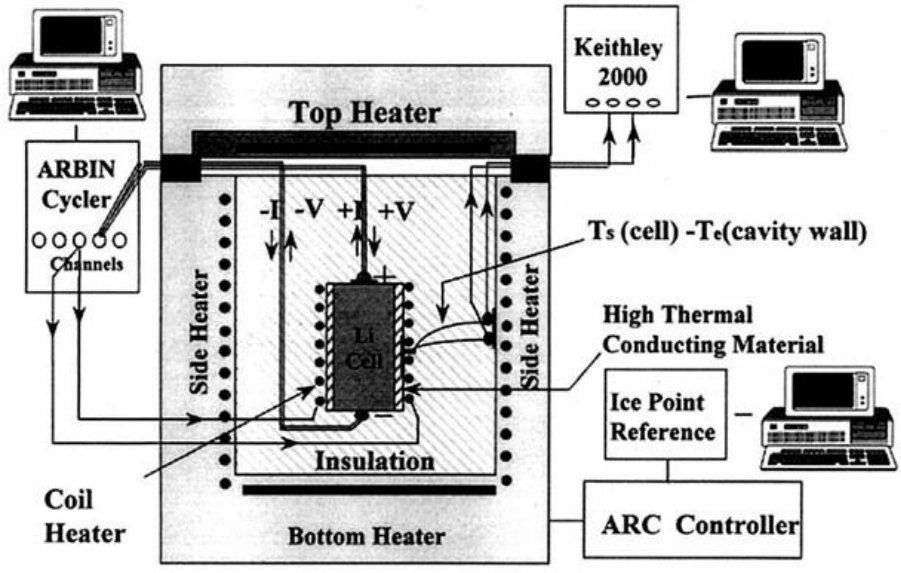

Figure 2.15 Experimental Schematics of Hong et al [38]

Heat capacity was found to be ranged from 0.82 to 1.07 J g^{-1} K^{-1} and is independent from temperature. Heat dissipation rate is maximized peak is at approximately 0.6 W for C/1 rate. To obtain this, controlled heater power is applied and knowing the measure heat dissipated value, heat capacity can be calculated using energy balance equation (will be explained later in section 2.4).

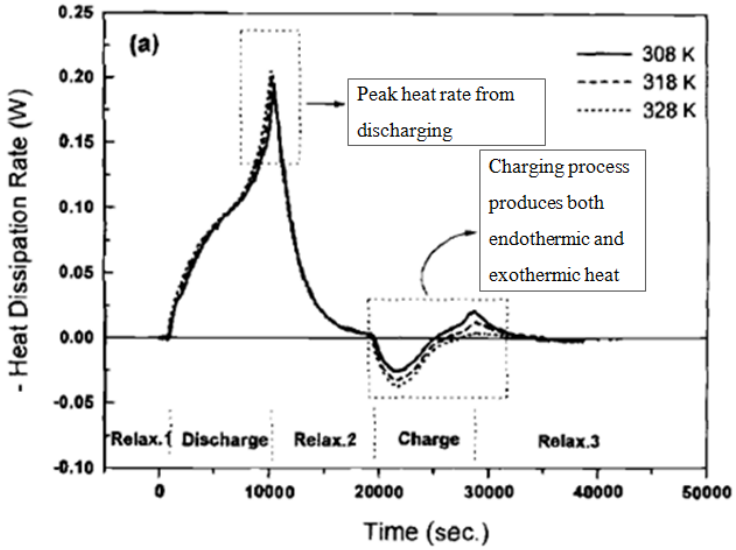

Figure 2.16 Results of heat generation from Hong et al [38]

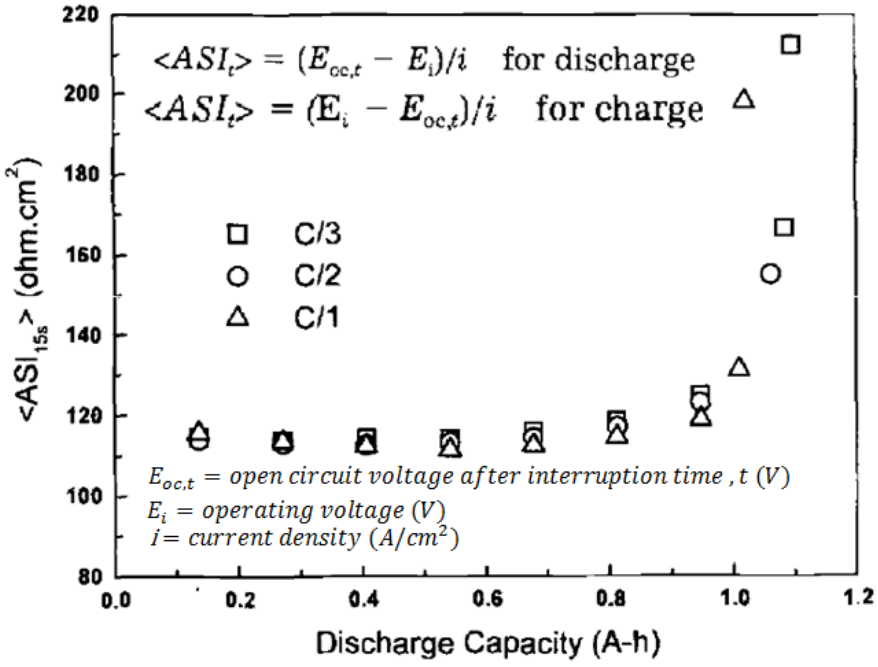

Figure 2.17 Results of ASI measurements from Hong et al [38]

The other related work in thermal properties analysis of lithium ion battery which applied the calorimetry method was done by Maleki et al [39]. The same type of battery as in Hong et al was used (Sony 18650 lithium-ion, 1.35 Ah). This illustrated the techniques for determining thermal properties of the battery and the relationships between thermal properties were investigated. The first measurement method for heat capacity was the cooling transient method having shown the setup in figure 2.18. The battery is put in heat flux calorimeter and is heated to 60°C and then heater power was cut off to cool down the battery to ambient temperature until the difference between ambient and battery temperature became less than 1 K. Insulator was designed to prevent convection cooling. Then energy balance equation was used to determine heat capacity. In the second method, adiabatic calorimeter was used with the schematics shown in figure 2.19. The setup contains upper and lower parts. The lower part of the setup is contained with oil which was heated by the heating coil. When the steady-state temperature of oil is reached, the cell is slowly immersed. The temperature change of battery cell and the oil bath are compared and when the heat capacity of the oil is known, heat capacity of battery can be calculated from the equation shown in figure 2.19. When the battery is immersed in oil, the temperatures of the battery slowly increase and the temperature of the oil bath is reduced. Finally, at approximately 200 minutes of time elapsed, both temperatures of battery and oil converged to the same value. Figure 2.20 shows the temperature profile from this test.

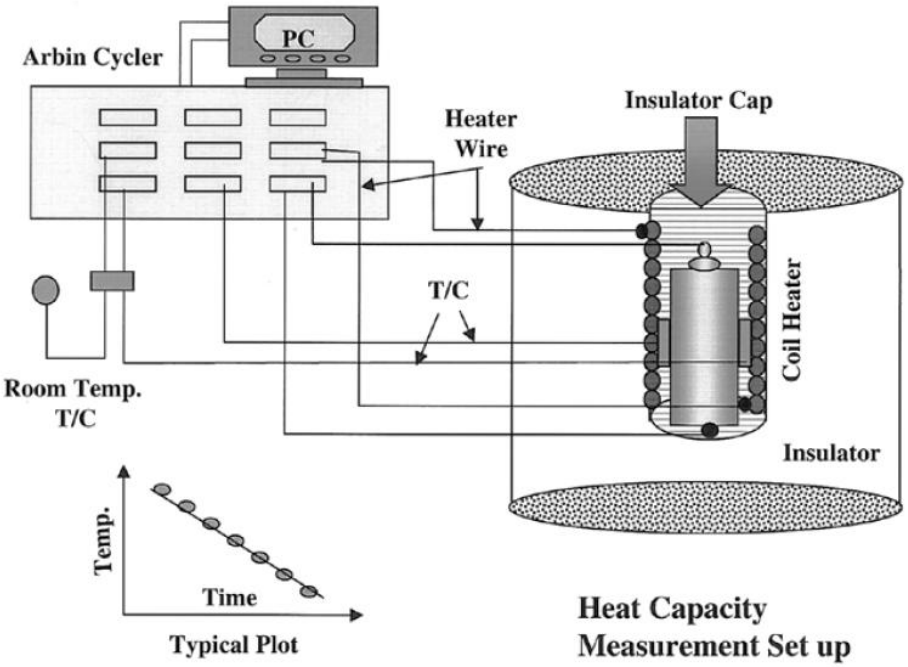

Figure 2.18 Specific heat capacity test by cooling transient method setup, Maleki et al [39]

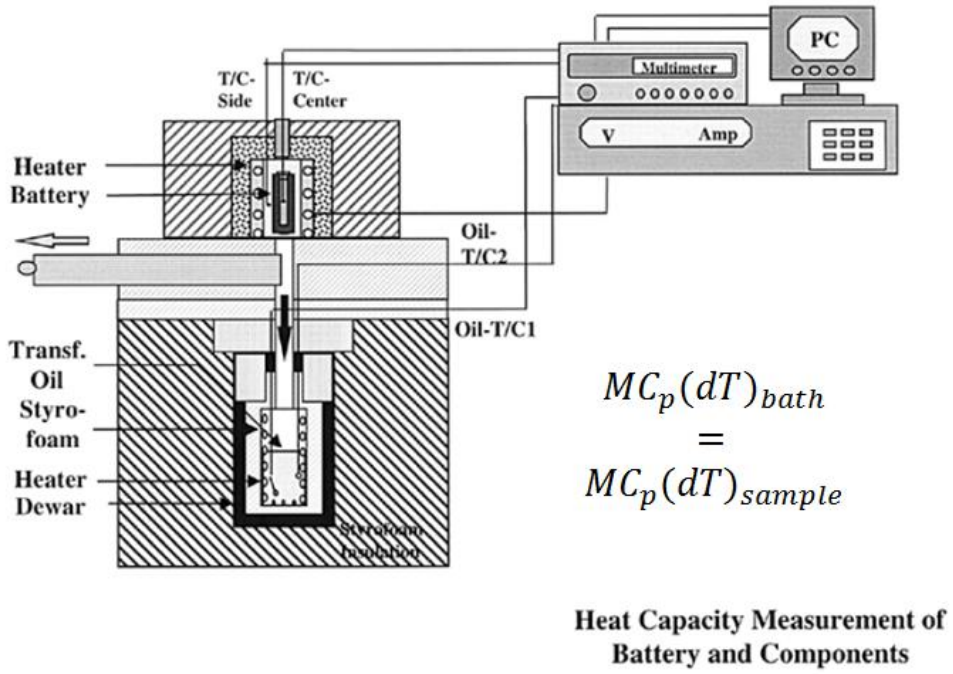

Figure 2.19 Specific heat capacity test by adiabatic calorimetry setup, Maleki et al [39]

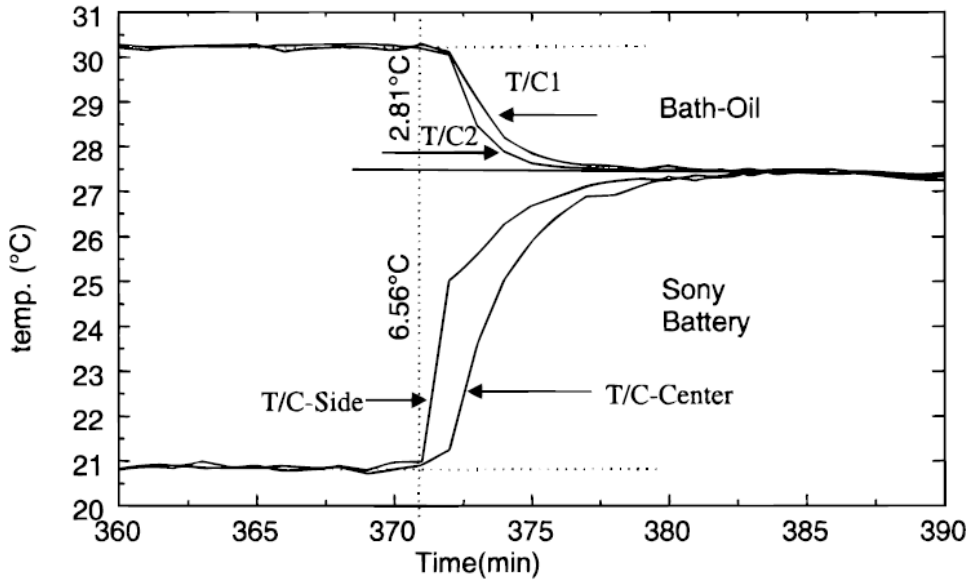

Figure 2.20 Temperature of the battery in adiabatic calorimetry test, Maleki et al [39]

From the first method, heat capacity was calculated to 0.800 J g^{-1} K^{-1}. From the second method, the results of heat capacity are 0.96 ± 0.02 J g^{-1} K^{-1} and 1.04 ± 0.02 J g^{-1} K^{-1} for open circuit voltage of 2.75 and 3.75 V respectively.

Another case of calorimeter application for thermal properties analysis of lithium ion battery is from the work of Vaidyanathan et al [40]. In this case, radiative calorimeter is used for analyzing lithium cobalt oxide and lithium nickel oxide cells with spirally wound electrodes for both cases. The copper chamber is maintained at very low temperature at 105 K by the circulation of liquid nitrogen. The chamber inside is painted black and the cell is suspended using a lacing cord. The calorimetric chamber is maintained at 10^{-5} Torr. The battery placed inside the copper chamber is wrapped with thermofoil heater tape. Dissipated heat terms include radiated heat, heater power, conductive heat and energy stored. For determining heat capacity, similar method as in Maleki et al was used. This was to observe temperature transients during the warming up stage of heater and during the cool-down stage while there was no heater power. Then, by using battery energy balance equation (which will be explained in the next section) was used to calculate the specific heat capacity. The result of normalized value is 0.946 J/ºC g. Voltage profiles of the cells were observed for both charging and discharging processes along with temperature responses. Heat dissipation rate of discharge rates were also observed. It was found that at low discharge rate (C/5), small changes were observed in heat rate. In contrast, for C/1 discharge rate, heat rate quickly rose up sharply above 0.5 W.

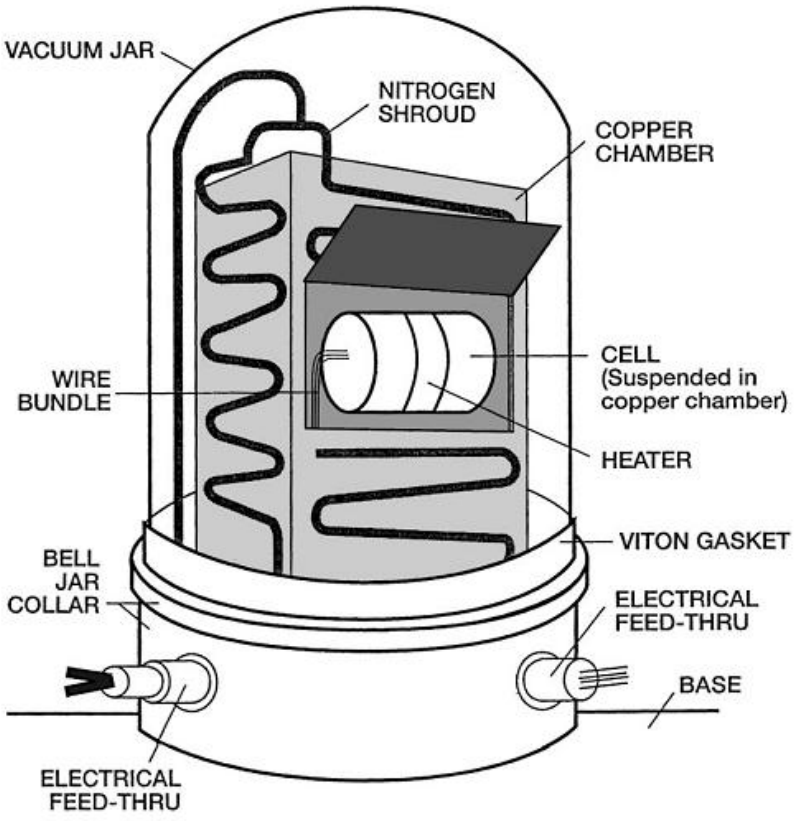

Figure 2.21 Schematics of thermal analysis in Vaidyanathan et al [40]

In 2003, Onda et al [41] studied the heat generation behavior of the lithium ion battery by considering mainly on the heat effects from over-potential resistance and the change in entropy. Two lithium ion batteries tested here were SONY-US 18650 and a SONY-US 18650 G3 with capacity of 1.35 Ah and 1.80 Ah respectively. As shown in figure 2.22, the selected batteries were charged and discharged by the Bipolar Power Source. The cell temperature and voltage are recorded by the Hybrid Recorder. Then data is input to the computer. General purpose interface bus (GPIB) was used to control the charge and discharge conditions. The battery is wrapped in thin film for electrical insulation and was put in water thermostat in order to have the constant temperature condition. Over-potential resistance of the battery was measured by four methods. These included the V-I characteristics, difference between E_{eq} (Open Circuit Voltage) and cell voltage, intermittent discharge and AC impedance meter. The measurement of entropy change included the observation of temperature gradient with E_{eq} and heat production differences methods. The constant current characteristics at different discharge rates were obtained for calculating resistance. The tendencies of the resistance measured by first three methods are the same as they increases when discharged and then peaked quickly at the end. At lower ambient temperature, cell resistance becomes higher than higher temperature condition. The results between V-I characteristics and E_{eq} vs. cell voltage methods provided small differences. The intermittent discharge and AC methods resulted in lower value of cell resistance. The observation of change in E_{eq} by temperature shown that as the temperature is increased, the E_{eq} decreased. The measurement of heat capacity is similar to that of Maleki et al [39], where the battery is heated to 60ºC and then cooled down to steady-state temperature. Then, heat balance is used for calculating the heat capacity.

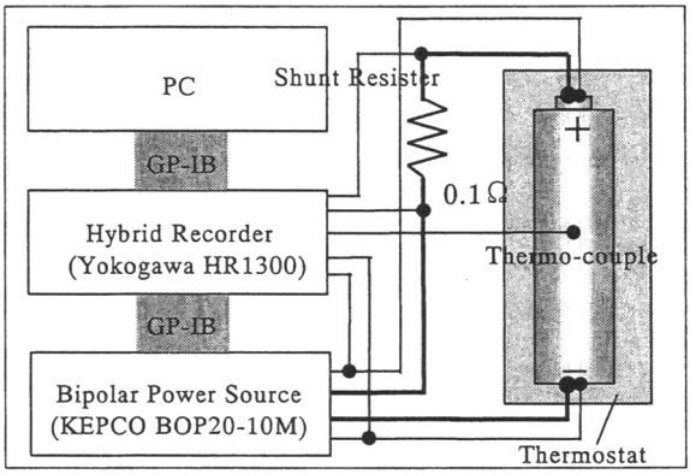

Figure 2.22 Schematics for experiments in Onda et al [41]

As calorimeter can be very helpful in heat generation analysis for lithium ion batteries, it can be quite cumbersome to build one and also can be expensive to purchase one. Forgez et al [42], perform thermal analysis on $LiFePO_4$/graphite lithium ion battery (26650 cylindrical cell, 2.6 Ah) without using the calorimeter. Here, the focus is put on thermal properties such as heat capacity and heat transfer coefficient. Two T-type thermocouples were used for temperature measurement. One is mounted on the surface and another is inserted inside the battery. Then the battery is connected to the power amplifier in order to raise the battery temperature with 2 Hz current pulses (±10, ±15 and ±20A). The current pulses was applied for 1 hour and then relaxed. Thermal chamber is used to perform the temperature coefficient test while the ambient temperature is altered in order to see the change in E_{eq}. In analysis part, steady-state condition in temperature response from current pulse is considered for calculating heat transfer coefficient and transient condition is considered for heat capacity calculation. Thermal model of lithium of lithium ion battery was used for the calculation of thermal properties. The analysis of thermal resistance or the reciprocal of heat transfer coefficient is done by using the lumped model of the battery. The heat capacity values calculated from different current pulses are ranged from 73.2 J/K to 77.9 J/K.

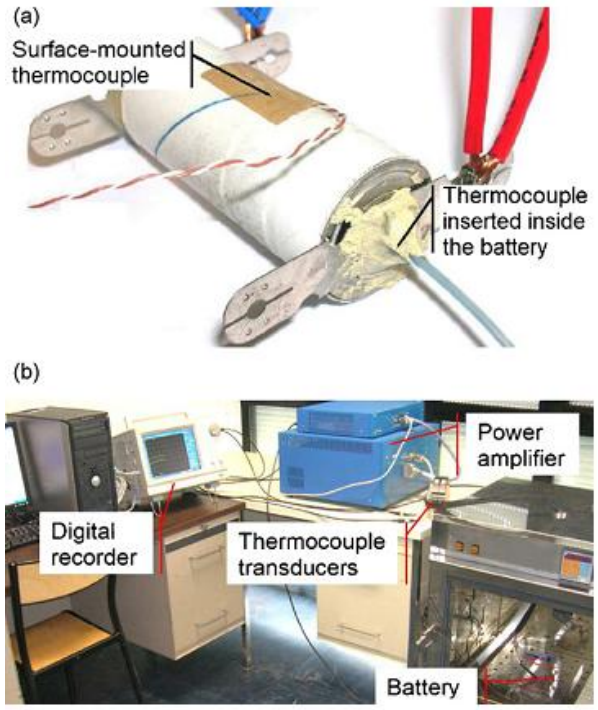

Figure 2.23 Schematics experiments in Forgez et al [42]

2.4 Battery Thermal Model Review

To investigate battery thermal behavior, several inputs are needed for thermal model which can be expressed in figure 2.24. These include cell specification, charge/discharge profile, thermal properties and cooling method.

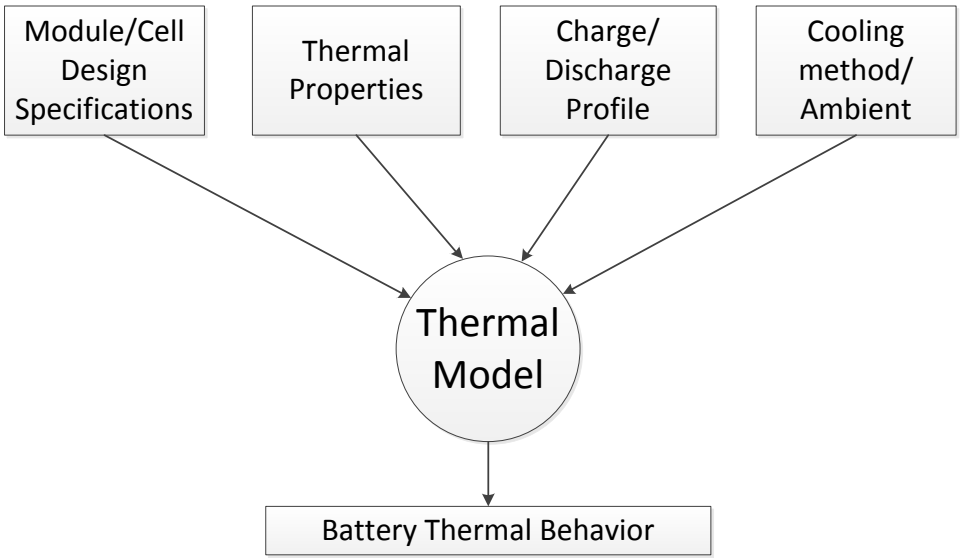

Figure 2.24 Battery thermal model inputs

Developed by Bernardi et al [43], general energy balance for battery systems is derived from considering the cell temperature effect from electrochemical reactions, phase changes, mixing effects and joule heating. In this case uniform temperature distribution assumption was applied. Most applicable term for common battery application excludes the mixing effects and phase changes term. The heat of mixing term can be neglected when the chosen electrochemical system has good transport properties and provides the smaller effect compared to those from joule heating and chemical reaction effects [44]. The phase change term can also be neglected when the battery is assumed to be contained at the same phase in the operation. This left with two most important terms which are chemical reaction and joule heating (see section 2.4.1). The study of thermal model starts from considering Gibbs free energy relationship with the product of temperature and entropy with the enthalpy [21]. Then the thermodynamic expression of each terms are related to voltage current and temperature as shown in equation 2.4 – 2.9.

Explanations of this battery thermal model can be started from Gibbs free energy (ΔG) which related to the change in enthalpy (ΔH) and the residual energy (TΔS). The expression of (ΔG) can also be in the product of Faraday constant (F), number of electrons (n) and equilibrium potential or open circuit voltage (E_{eq}) which is the same as the product of current and open circuit voltage. The expression of W_{el} indicates the electrical power generated which is from the product of current (I) and cell voltage (E). The expression of entropy change (ΔS) is related to the product of current and the change of open circuit voltage over the change in temperature ($\frac{dE_{eq}}{dT}$). Finally, heat generation can be expressed as in equation 2.9

$$\Delta G = \Delta H - T\Delta S \tag{2.4}$$

$$\Delta G = -nFE_{eq} = -IE_{eq} \tag{2.5}$$

$$\Delta S = nF\frac{dE_{eq}}{dT} = I\frac{dE_{eq}}{dT} \tag{2.6}$$

$$W_{el} = IE \tag{2.7}$$

$$\dot{Q} = \Delta G + T\Delta S + W_{el} \tag{2.8}$$

$$\dot{Q} = I(E - E_{eq}) + IT\frac{dE_{eq}}{dT} \tag{2.9}$$

Table 2.5 Researches involves the usage of battery thermal model

Year	Researchers	Experiments performed using Li- ion battery thermal model
1995	Pals and Newman [45]	Thermal modeling simulation to observe heat effects in single cell
1998	Hong et al. [38]	Electrochemical-Calorimetric Studies by accelerated rate calorimeter
1999	Maleki et al. [39]	Thermal properties study by using heat flux and adiabatic calorimeter
1999	Hallaj et al. [46]	Temperature profile for thermal runaway temperature study
2000	Vaidyanathan et al. [40]	Heat dissipation study by using radiative calorimeter
2003	Onda et al. [41]	Heat generation study from normal charging and discharging cycle
2005	Onda et al. [3]	Thermal behavior study during rapid charge and discharge cycle
2009	Forgez et al. [42]	Thermal properties study by using current pulse experiment

2.4.1 Heat Generation Terms

As shown in equation 2.9, there are two main terms indicating heat generation from the battery. The first term is called "over-potential" heat term which is irreversible ($\dot{Q}_p$). It is the heat effect from the battery resistance when loaded. As noted in equation 2.8, this term relates to the difference in open circuit (E_{eq}) and cell voltage or according to Ohm's law, this is directly related to the resistance which is called "over-potential resistance". Also, over-potential resistance can be considered to understand the behavior of this term. Onda et al [3], [41] approached this term by using the method of V-I characteristics with SOC. This will always produce exothermic heat generation for both charging and discharging processes. Equation 2.10 shows this relationship.

$$\dot{Q}_p = I\left(E_{eq} - E\right) = I^2 R_\eta \tag{2.10}$$

The second term of heat generation is the reversible term related to the chemical reaction. As the electrons move back and forward from cathode to anode, endothermic and exothermic heat effects can be created from the charge and discharge processes respectively. This second term here is called reversible entropic heat ($\dot{Q}_s$). In equation 2.11, the key parameter here is the temperature coefficient or sometimes denoted as temperature coefficient which is related to the entropy change ($\frac{dE_{eq}}{dT}$). In the work of Onda et al [41], Hong et al [38] and Forgez et al [42] all demonstrated the methods for acquiring temperature coefficient. Generally, the battery in contained in thermal chamber and E_{eq} dynamics is observed while ambient temperature is altered.

$$\dot{Q}_s = IT\frac{dE_{eq}}{dT} \tag{2.11}$$

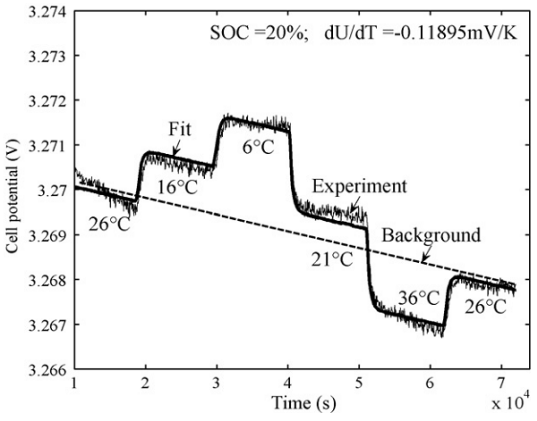

Figure 2.25 Results from temperature coefficient experiment [42]

2.4.2 Energy Balance of a single cell battery

To apply this thermal model, the assumption of uniform temperature distribution of the battery cell is needed. Here in equation 2.12, the heat generation terms are located on the left side and on heat transfer to the surroundings and heat capacity terms are on the right side. In some literatures, surrounding heat transfer ($\dot{Q}_B$) can be calculated as in equation 2.13. The heat transfer coefficient or h can be considered for both from inside the battery to the surface and from surface to the ambient. These sets of equations are very helpful for analyzing thermal properties of lithium ion batteries which are heat transfer coefficient (h) and heat capacity (C_p).

$$\dot{Q} = I\left(E_{eq} - E\right) + IT_{in}\frac{dE_{eq}}{dT} = \dot{Q}_B + C_p\frac{dT_{in}}{dt} \tag{2.12}$$

$$\dot{Q}_B = h_{in}\left(T_{in} - T_{surf}\right) = h_{out}\left(T_{surf} - T_{amb}\right) \tag{2.13}$$

Where $\dot{Q}$ = Heat generation rate (W)

I = Current load (A)

E_{eq} = Equilibrium potential and E for cell voltage (V)

T_{in} = Inside of cell temperature (K)

T_{surf} = Cell surface temperature (K)

T_{amb} = Ambient or environment temperature (K)

h_{in} = Heat transfer coefficient inside the battery (W/K)

h_{out} = Heat transfer coefficient outside the battery (W/K)

C_p = Heat capacity of the battery (J/K)

As explained in the previous section, thermal properties are one of the inputs for studying thermal behavior of lithium ion battery. Also, for the design of battery thermal management system, thermal properties are needed for the simulations in order to maximize the system. To analyze this, battery thermal model is essential. It can be used to determine the limits of temperature that the battery can operate under the actual load conditions. In the next chapter, details of experimental procedures will be demonstrated by applying this thermal model.

2.4.3 Review of thermal properties results

There are many literatures which applied the use of thermal model to determine thermal properties from batteries. Table 2.6 shows the summary of those results especially from the lithium ion batteries.

Table 2.6 Comparison of thermal properties results from several literatures

Battery Type	Researchers	Heat Generation	C_p	h
$LiCF_3SO_3$	Pals and Newman	0.6 – 5.8 W/m^2	0.747 kJ/kg·K	6 – 30 $W/m^2·K$
$LiCoO_2$	Hong et al.	- 2.94 – 3.53 W/m^2	0.82 – 1.07 kJ/kg·K	9.19 $W/m^2·K$
$LiCoO_2$	Maleki et al.	Not investigated	0.96 – 1.04 kJ/kg·K	13.43 $W/m^2·K$
$LiCoO_2$	Hallaj et al.	0.11 - 0.23 W/m^2	1.0 kJ/kg·K	10 $W/m^2·K$
$Li_xC/LiNiO_2$	Vaidyanathan et al.	-2.06 – 5.51 W/m^2	0.95 – 0.97 kJ/kg·K	Not investigated
$LiCoO_2$	Onda et al.	Shown in other terms	0.83 – 0.88 kJ/kg·K	11.5 – 13 $W/m^2·K$
$LiFePO_4$/graphite	Forgez et al.	Shown in other terms	0.85 – 0.91 kJ/kg·K	16.92 – 18.28 $W/m^2·K$

The results from table above expressed results in various literatures. For simplicity in comparison, all data were expressed in the same units. For heat generation, some literatures expressed the results in unit of Watt, so the specification of the battery was taken into account for heat generation per unit area. For example, in the work of Hallaj et al. [46], heat generations was expressed in per unit volume (W/L), which was ranged from 28 – 60 W/L in 1C discharge rate condition. With the specification of 18 mm diameter and 65 mm height, this yield volume of 1.654×10^{-5} m^3 and surface area of 4.18×10^{-3} m^2. Therefore, heat generation per unit area was calculated to be the range of 0.11 – 0.23 W/m^2. It can be seen that different results are provided for heat generation. This is due to the different conditions in experiments such as the battery types, discharge profile and etc. Some literatures expressed heat generation in different manner, for examples, in the work of Onda et al. [3], it was shown as the voltage-current (V-I) characteristics and resistance. In Forgez et al. [42], heat generation results were not present but it was rather shown as the product of current and the difference between equilibrium and cell voltage. However, the value of heat capacity (C_p) and heat transfer coefficient (h) are found to be in fairly same range in different literatures. For more details on battery specifications in each literature, see Appendix F.

CHAPTER 3

RESEARCH METHODOLOGY

3.1 Selected Lithium Ion Battery Specifications

Researchers of Automotive Laboratory, National Metals and Materials Technology Center of Thailand (MTEC) initiated the electrical conversion project. This requires replacing drive-train components in a conventional gasoline car into electric drive-train. The most important component for power supply here is the battery. In this case, selected type of battery has the chemistry of lithium iron phosphate. This type has a wide range of advantages. Considering figure 2.4, safety rating of this type is at highest among the lithium ion battery family. Specification of the selected battery is shown here in table 3.1

Table 3.1 Technical specifications of the selected battery

Type	Specifications
Nominal Capacity	60 Ah
Manufacturer	Thunder Sky Battery
Chemistry	Lithium iron phosphate
Nominal Voltage	3.3 V
Charge Voltage Cut-off	4.0 V
Discharge Voltage Cut-off	2.8 V
Max charge current	≤ 3C
Max discharge current	≤ 3C (Constant) and ≤ 20C (Pulse)
Cycle Life	≥ 3000 times (80 DOD%)
Temperature durability of case	≤ 200 ºC
Operating Temperature	(-45ºC - 85ºC)
Self-discharge rate	≤ 3% monthly
Weight	2.3 kg ± 50 g

In terms of battery configuration in electric car, prismatic batteries can provide the ease of installation. Construction of this battery has each cell comprised of positive electrode, separator and negative electrode stacked together. A combination of many stacks becomes the core. The bolts on the top of the battery denote positive and negative terminals. Then the whole core is

wrapped around with plastic case. Pressure valve is located between positive and negative terminals. This is designed in order to vent out the gas resulted from overcharging the battery as shown in Figure 2.8 Lithium ion cell operating window [11] for the battery operating window.

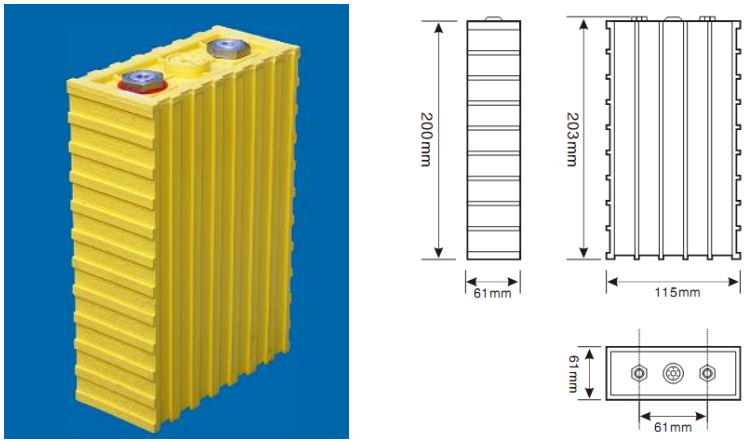

Figure 3.1 Physical appearance and dimensions of selected battery

3.2 Experimental Setup Apparatus

In this section, the summarize of available devices and tools for experimental setup will be shown. Here the devices will be considered in terms of accuracy, safety, connectivity and space requirement for the experimental procedures design.

3.2.1 Agilent Electronic Load N3306A

Figure 3.2 Agilent Electronic Load N3306A

This electronic load or “load cell” is capable of generating DC load in order to discharge the battery. The DC load can be programmed via using the front panel control or the by using software. There are three modes of operation, constant current (CC), constant voltage (CV) and constant resistance (CR). In this model, the maximum power the device can operate is at 600 W. Voltage and current operation range are 0 – 60 V and 0 – 120 A respectively. The dimension is 625 x 426 x 178 mm with net weight of 4.6 kg. Operating conditions such as voltage and current can be observed through the front panel display. Manually tightened Connectors can be used for connecting power cables between the electronic load and the battery. This needs the cable with pure copper or other material which gives good electrical conductivity for connecting with the manual tightened connectors. Figure 3.3 shows the connector which is located at the backside of the electronic load. Data can be transferred from the device by using GPIB (General Purpose Interface Bus).

As shown in figure 3.3, a bunch of wire with the size according to the specification has to be inserted in order to make a connection. This applies for both positive and negative terminals. In figure 3.4, the buttons for programming the load operation is shown. This can be used to select the mode operation (CC, CV and CR) and also to set the value of load applied.

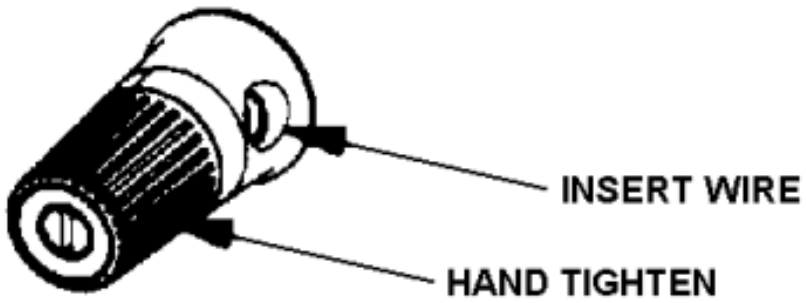

NOTES:

1. **WIRE SIZE AWG 4 MAXIMUM**
2. **STRIP BACK INSULATION (13mm FOR AWG 6 OR 8)**
3. **INSERT WIRES INTO CONNECTOR**
4. **TIGHTEN TO 8 in-lb (90 N-cm)**
5. **OBSERVE POLARITY WHEN CONNECTING LEADS TO SOURCE**

Figure 3.3 Manual Tightened Connector for Agilent N3306A

Figure 3.4 Front Panel Controller Buttons for Agilent N3306A

3.2.2 Agilent Electronic Load N3306A

Figure 3.5 Agilent Power Supply N6692A

This device is used for charging the battery at desired current rate within the specification ratings. Same as N3306A, the device can be programmed by setting the values at the

front panel or by using software. At the front panel control, the settings can also be adjusted by using the control knob located under the display. The buttons for front panel control is the same as for N3306A. This device requires 3-phase power supply. The output rating for current and voltage are 0 – 110 A and 0 – 60 V respectively. The dimension is 426 x 574 x 222 mm. For connecting to the battery, the device is designed with a pair of bus bar which is located at the back of the power supply (shown in figure 3.6) which can provide simpler approach for the battery cable design.

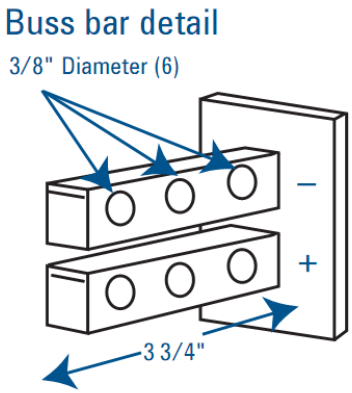

Figure 3.6 Agilent N6692A Bus bas

3.2.3 Agilent 82357B GPIB/USB Interface

Figure 3.7 Agilent 82357B GPIB/UBS Interface Connector

This device is an essential part for the data transfer and for controlling the Agilent Electronic load and Power Supply remotely by using a computer. It requires no switch, no power supply as it can get from the connected device. This uses standard USB and IEEE-488 interfaces which requires installation of IO suites software. Three LED lights are the indicator for the status of the connection. These include “Ready”, “Fail” and “Access”. The “Ready” LED sign will turn

yellow when the USB is initially inserted and then will change into green color when the connection is successful. Otherwise, the red light on the “Fail” LED will be shown. When the data is transferred from the device to the computer, the light on “Access” LED will blink continuously. The GPIB connection port is located at the backside of both Agilent electronic load (N3306A) and power supply (N6692A) as shown in figure 3.8

Figure 3.8 Location GPIB/USB Port at the back of N6692A

3.2.4 Battery Cables

For connecting the battery to the device i.e. electronic load or power supply, the battery cable must be carefully prepared. This can affect in terms of performance and safety while performing experiments on the selected battery. The cables can be categorized by the amount of copper wire inside. With more copper wire, less voltage drop will be produces and thus provide the accurate results for voltage measurement. This also depends on the connection at the terminals of the battery. While using clamp-end cables can be easier for installation than using terminal-end cables, the latter one can provide more accurate results in measurement.

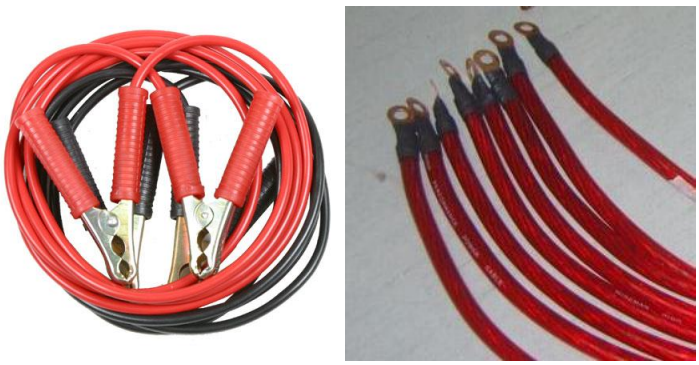

Figure 3.9 Clamp-end (left) and Terminal-end (Right) battery cables

3.2.5 Voltage Measurement Set

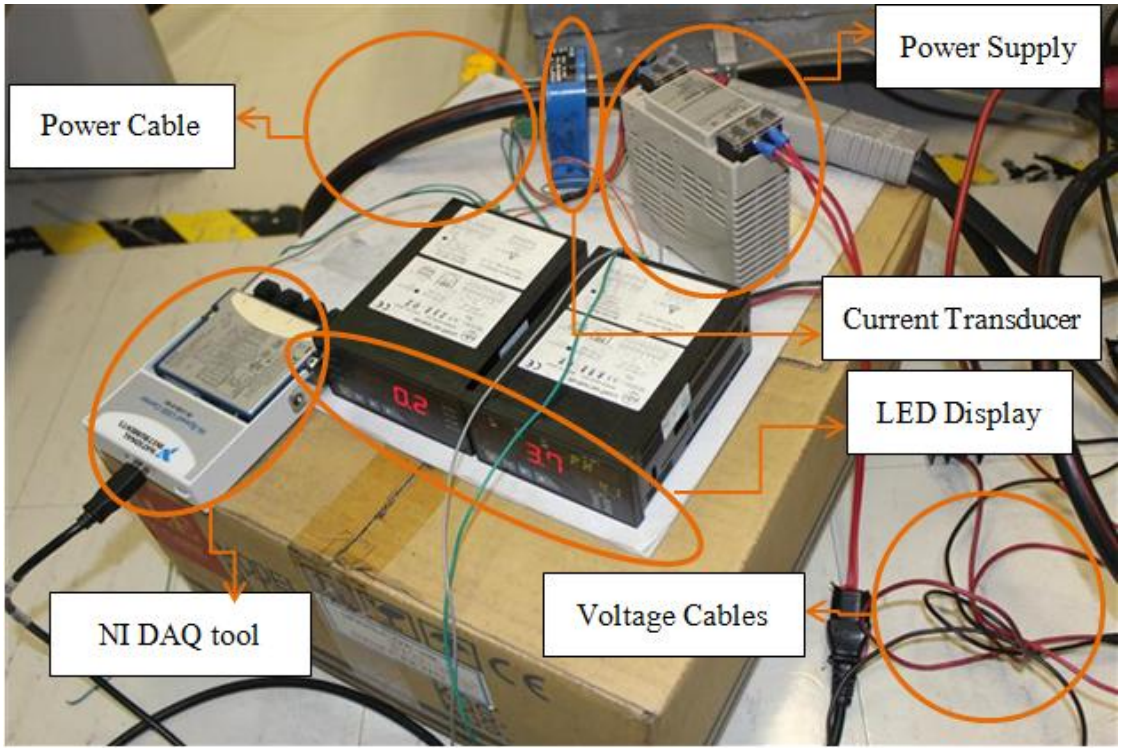

Figure 3.10 Voltage measurement set

This is a set of device combination which used for measuring voltage and current of the battery. The values are measured directly similar to a multi-meter. The measured value is shown in the LED display which requires an external power supply which is provided by OMRON S8VS-06024 in this case. There are two pairs of cables which used for measuring current and voltage separately. Power cable is setup through the LEM AC/DC Current Transducer DHR-C10 which was used for measuring current in the cables and transmits data as voltage output to the NI DAQ 9205 then converted to current data again in the LabVIEW software. The voltage output signals is transferred through wires which can be connected to the National Instruments Data Acquisition (DAQ) Module 9205 and then transfer data to the computer. As the connection of cables between the electronic load and the battery can cause the voltage to drop, direct measurement of voltage is needed. The results of measurement here can be used to compare with the measurement value from the electronic load or power supply in order to obtain more accurate measurement.

3.2.6 National Instruments Data Acquisition (DAQ) Tools

Data acquisition tools (DAQ) are very powerful for obtaining the data from the measurement devices. The selection criteria of the DAQ modules are based on the suitability of this work. In this work, output voltage and temperature are the main focus. Table 3.2 shows the utilized DAQ tools for this experimental design. The NI 9205 module is for obtaining analog voltage input with the range from ±0.2 V to ±10 V. This is in the range of the selected battery which has the nominal voltage of 3.3 V and the 16 channels input ports can be applied for acquiring data from device which provide voltage output data such as infrared thermal sensor (see section 3.2.8) . The module 9213 is used for acquiring temperature data which measured from thermocouples attached to several locations of the battery. This module has the operating range from -40 °C to 70 °C. This 9213 module also has 16 channels of input ports which is suitable for measuring many locations of surface temperatures to prove the assumption of uniform temperature distribution. The module 9211 serves the same purpose as 9213 (same operating temperature and can support type-K thermocouple) but with only four input ports. The main difference between 9211 and 9213 is that the 9211 type has the bigger port which is applicable for the thermocouple with fork end terminal (figure 3.11). The ring end terminal (figure 3.11 middle) is suitable for connecting the cables to the battery because it has holes which the screw can be fitted. The normal wire end (figure 3.11 left) is suitable for inserting into 9205 and 9213 input ports for accuracy of data transfer with less voltage drop. The NI cDAQ 9172 chassis is the device for transmitting outputs up to 8 NI modules at the same time between the computer via hi-speed USB. For more details of the specifications, see Appendix B.

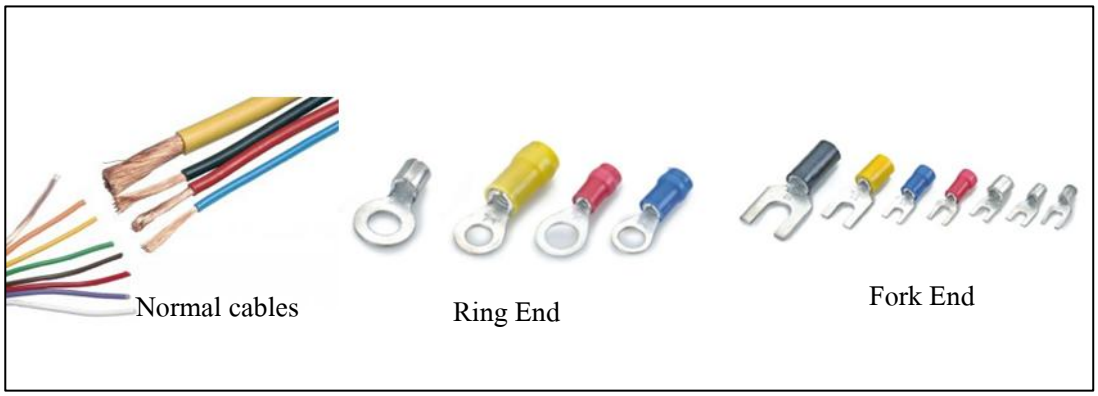

Figure 3.11 Cable ends types applied for this work

Table 3.2 NI DAQ tools for obtaining voltage and current data

Module Name	Picture	Details
NI 9205		• 16 channels of voltage analog inputs
NI 9213		• 16 channels of thermocouple analog inputs
NI 9211		• 4 channels of thermocouple inputs
NI cDAQ 9172	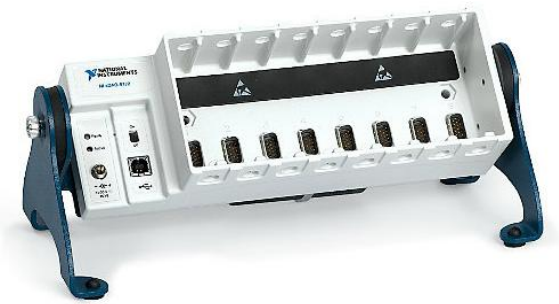	• Compact DAQ chassis which compatible for operating 8 NI modules

3.2.7 Thermocouple

For the temperature measurement, thermocouple is considered to be the simplest approach and capable of producing acceptable accurate results. A thermocouple consists of two dissimilar conductors in contact with each other. Here, when it is heated, voltage will be produced. The reading of this voltage can be converted into temperature. This was discovered by the German-Estonian Physicist Thomas Johann Seebeck and thus the theory of thermocouple working principle is called the "Seebeck Effect" [47]. There are many types of thermocouples depending on the material used as a conductor. In this case, type K thermocouple which consists of chromel (90% nickel and 10% chromium) and alumel (95% nickel, 2% manganese, 2% aluminium and 1% silicon) is used. The temperature range is from -200ºC to +1350ºC. Figure 3.12 shows the basic diagram for thermocouple.

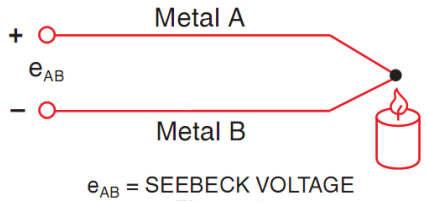

Figure 3.12 Thermocouple diagram [48]

From figure 3.11, the small change in Seebeck voltage is linearly proportional to temperature. Equation 3.1 can be used to explain its working principle. α denotes the Seebeck coefficient.

$$\Delta e_{AB}=\alpha\Delta T \tag{3.1}$$

The advantage of thermocouple is that in can be easily installed on any target temperature measurement surface due to the size and shape of thermocouple probe. It is also very responsive to rapidly changing temperatures and contains large temperature scale. Therefore, thermocouples are used for measuring surface temperatures of the battery. However, from thermal model presented in chapter 2, battery internal temperature is also required. For this case, contact type temperature measurement device such as thermocouple can cause a short circuit if attached to the battery core. Therefore, infrared temperature sensor is applied.

3.2.8 Infrared Temperature Sensor

The technology of infrared offers a convenient and accurate approach for temperature measurement. Discovered by William Hershel in 1800 when he was using mercury thermometer. The temperature rose from violet to red while moving the peak of the blackened thermometer through the colors of spectrum. The temperature increased and peaked behind the red area. Thus, this becomes the "infrared wavelength area". The lens in the sensor can sense the infrared radiation then the electrical signals will be generated and transformed into output signal which proportional to the object temperature. The infrared sensor provides many advantages such as the capability of measuring moving, overheated objects or objects which located in hazardous surroundings. The response and exposure time is very fast and provides no influence on the measuring object. It is a non-destructive measurement and has no mechanical wear. [49] In this work, Micro-Epsilon SF-15 is used for battery internal temperature measurement because it does not require the sensor to contact the surface which avoids the risk of short circuit. The disadvantage of this type is the higher cost and more complicate installation. The specification is shown in table 3.3 and figure 3.13 shows the dimension of the sensor.

Table 3.3 Technical specifications of Infrared Thermal Sensor employed in this work

Temperature Range	-40 ….. 1030˚C
Spectral Range	8…..14μm
Optical Resolution	15:1
Accuracy	±1.5˚C or ±1.5%
Emissivity/Gain	0,100….1,100 (adjustable to software)

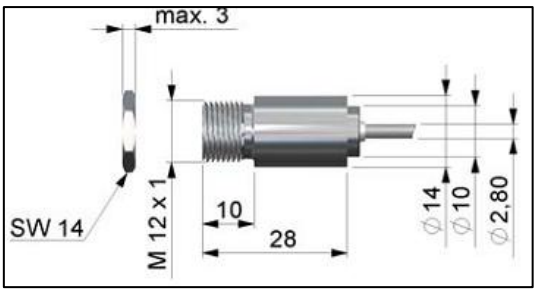

Figure 3.13 Dimensions of infrared thermal sensor

3.2.9 OMEGA Thin Film Heat Flux Sensor

For measuring the surface temperature of the battery, thermocouple would be sufficient. However, it is important to know the heat which flows from the surface of the battery to the surroundings. Therefore, heat flux sensors with thermocouples are attached to both sides of the sensor for this purpose. The temperature of the surface and the surrounding can be measured simultaneously from thermocouple type K in the sensor. Then, heat transfer can be calculated from using the thermal resistance value (0.002 $^{\circ}C \cdot m^2/W$). The dimension of selected sensor is shown in figure 3.14. The upper temperature limit is approximately 150˚C. The carrier of thermal junction is polyimide film (Kapton). Lead wires are made up of #30 (American wire gauge) AWG Solid, Teflon insulated color coded.

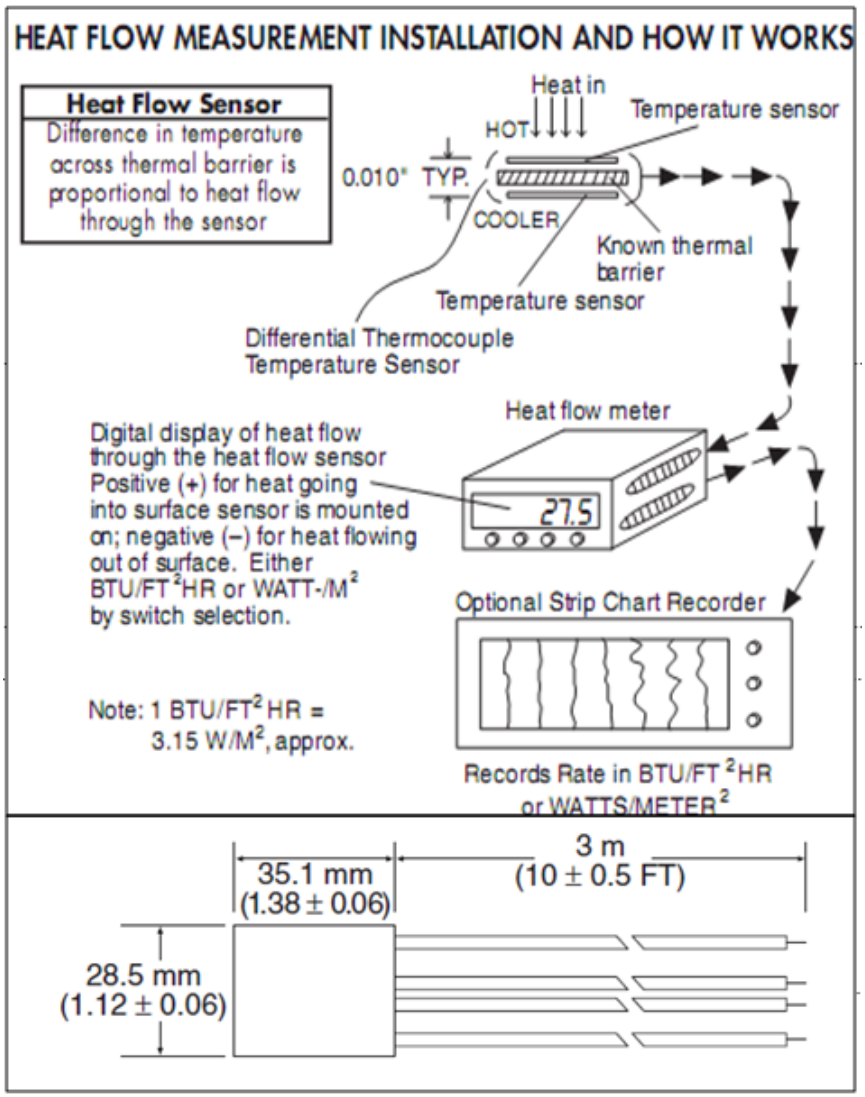

Figure 3.14 OMEGA Heat Flux Sensor working principal and specifications

3.2.10 MACCOR battery testing system

For improved accuracy in the application of battery testing, MACCOR has provided the solution for this. MACCOR battery tester has two pairs of cables, one for charging and discharging the battery and one pair for measuring voltage of the battery. MACCOR series 4000 provides 8 channels with maximum voltage of 100 V and maximum current of 60 A. Also, thermocouple channels are available for temperature measurement. Figure 3.15 shows the picture of MACCOR series 4000 used in this work. Table 3.4 shows the specification of this system.

Figure 3.15 MACCOR Series 4000

Table 3.4 MACCOR Series 4000 Specification

Number of test channels	1 to 192 per system
Voltage Ranges	Available up to 180 V Maximum
Current Ranges	Single Current Range 1mA to 2000A; Four Current Ranges: 150μA, 5mA, 150mA, 5A
Data Recording Rate	200 data points per second per system standard
Operating Modes	Constant Current, Constant Voltage, Constant Power, Constant Resistance, Cyclic Voltametry

3.2.11 Thermal Chamber

In the actual application of batteries, thermal conditions may vary depend on the climate of the environment. Therefore, it is necessary to use temperature chamber for simulating different thermal environment for battery testing. As explained before, thermal model for heat generation of the battery requires the value of temperature coefficient, dE_{eq}/dT (see equation 2.11). This can also be obtained by using thermal chamber. In this work, a refrigerator with temperature controller is used as a thermal chamber. The range of programmable temperature is from 5˚C to 40˚C with the 0.5 ˚C incremental. The size is 8.8 cubic ft. Picture of the refrigerator and temperature control unit is shown below.

Figure 3.16 Thermal Chamber

3.3 Experimental Setup

In this work, main interested parameters are temperature and voltage according to the thermal model. Summarize of experiments preparation is shown in figure 3.17.

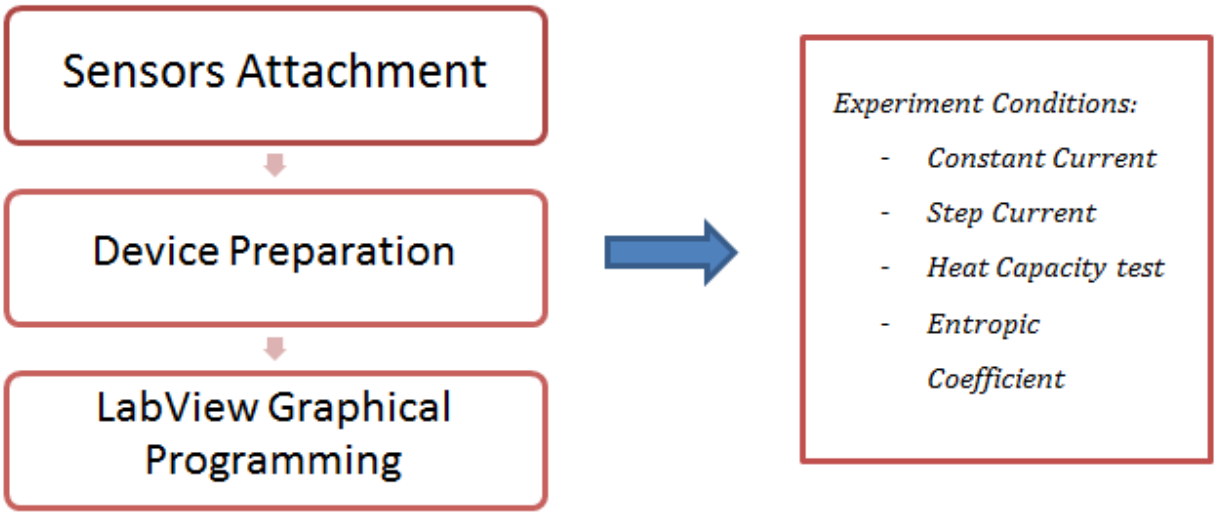

Figure 3.17 Preparation of experimental setup

From figure 3.17, there are three main parts for the preparation of experiments. In the first step, temperature sensors are prepared and attached to specified location of the battery. This includes the thermocouples and infrared sensor. Then, battery testing system such as electronic load and power supply are prepared for voltage measurement. Finally, the output of data from sensors and the devices are logged by using National Instruments LabVIEW software. This software provides the graphical programming which can also be used for controlling the devices. When all the components are connected together, experimental conditions can be applied to obtain the targeted data.

3.3.1 Temperature Sensors Setup

For proving uniform temperature distribution assumption to apply thermal model, thermocouples are attached in several points on the surface of the battery by using aluminum insulator foil. Figure 3.18 shows the positions of each thermocouple. After this assumption is proved for x, y and z axis, heat flux sensor with thermocouples are attached in three positions of x, y and z axis of the battery to localize the data for simpler calculation. Adhesive tapes were used for heat flux sensor installation. Figure 3.19 shows correspondingly of those positions.

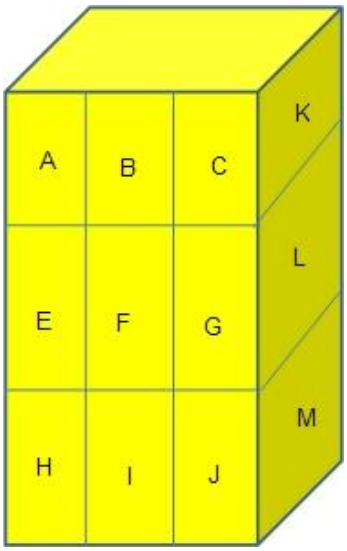

Figure 3.18 Surfaces for thermocouple attachment for proving uniform temperature

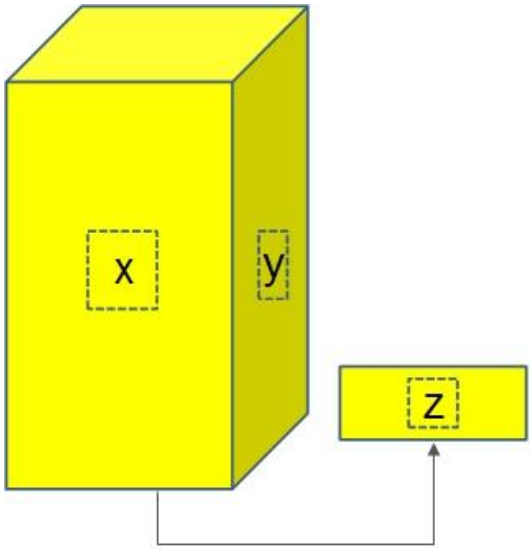

Figure 3.19 Surfaces for thermocouple attachment after proving the assumption

For measuring internal temperature of the battery, it is required that non-contact measurement must be applied to prevent short circuit. In this case, infrared (IR) thermal sensor is applied because it can measure temperature from a distance. Primary investigation on physical structure at the top portion was reviewed by using X-ray scan image shown in figure 3.20. From the scan image it was found that IR thermal sensor can be installed by having the modifying the pressure valve to fit the dimension of the sensor. Then the pressure valve is only for releasing gas when the battery is overcharged, this is not the condition of this work and thus it is safe to modify the valve. The dimension of the battery was reviewed and the distance between the measured

surface and the sensor is obtained from the specification sheet. The materials of the battery core was reviewed from the material safety data sheet in the battery instruction manual and found that there is nothing that can damage selected thermal sensor. Figure 3.21 shows the dimension from the top surface of battery core with the blue rectangle indicates the z axis cross section dimension.

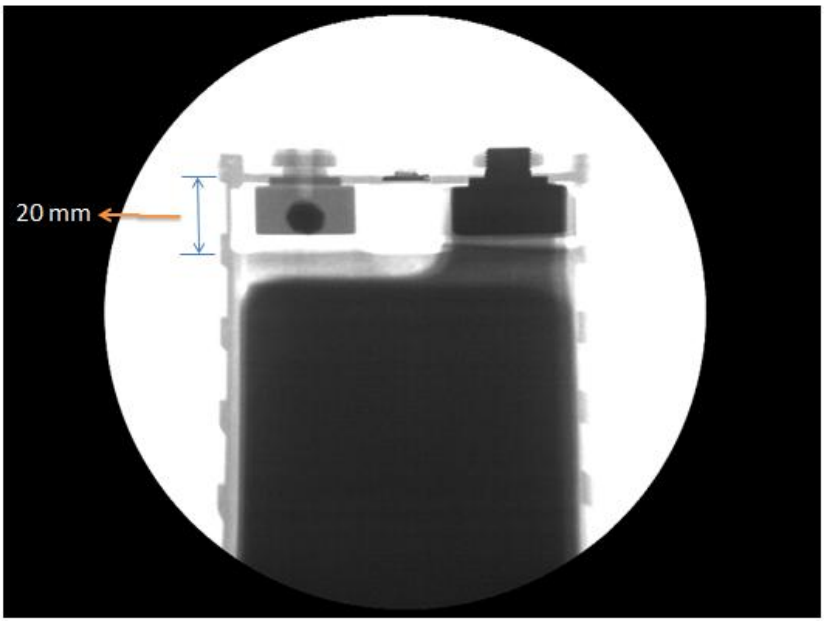

Figure 3.20 X-ray image displays depth from the lid to the battery core

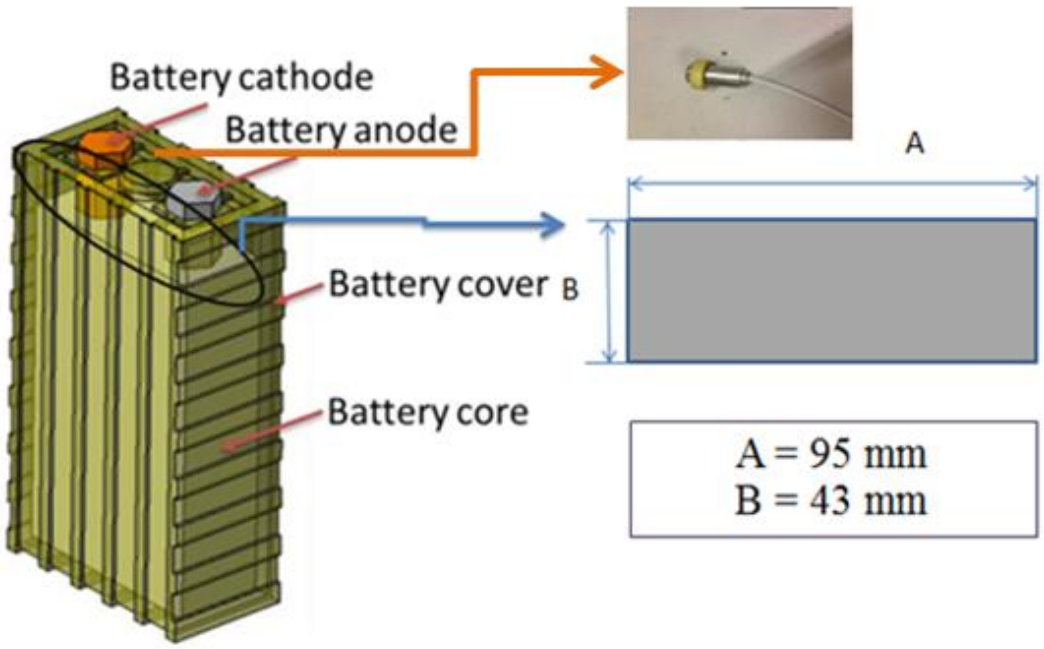

Figure 3.21 Dimension of the top surface of battery core

Aspect ratio is important for selecting IR sensor because it describes the ratio between width and height of measuring surface. In this case, the ratio of 2:1 is qualified but the sensor with 15:1 aspect ratio was selected just in case of future operations. To install IR sensor, the pressure vent lid is removed from the top and modified so that the IR sensor can be installed at the position of pressure vent. IR sensor project infrared to the battery core directly and measure battery internal temperature according to the X-ray image.

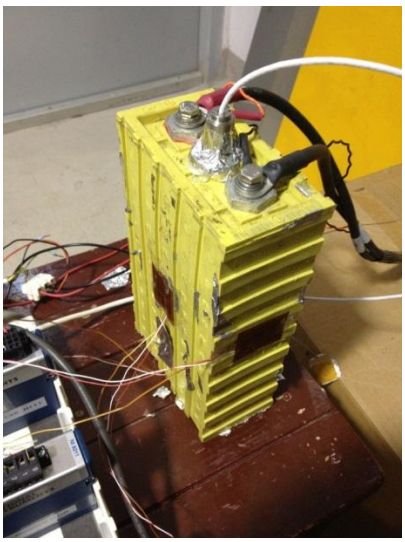

Figure 3.22 Battery installed with heat flux sensors and connected to MACCOR system

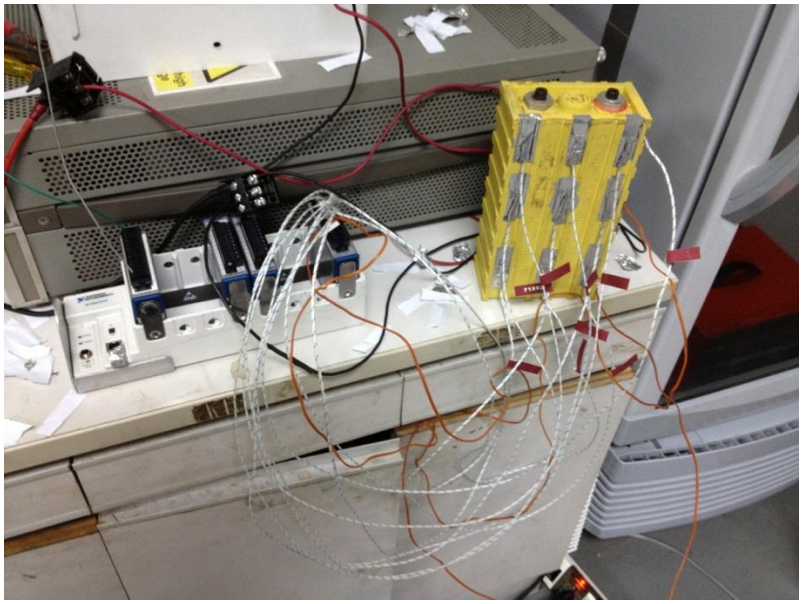

Figure 3.23 Multi-surface temperature measurement test setup

3.3.2 Electronic Load/Power Supply Setup

In the setup shown in figure 3.24, an Agilent device (either electronic load or power supply) is connected to the battery via cables to generate electrical load and at the same time, measure voltage. To get more precise value of voltage measurement, direct measurement system is also applied to compensate with the voltage drop in the battery cables connected to the Agilent device. Thermocouples are attached to the surface of the battery and IR thermal sensor is installed at the top of the battery. The output signal from thermal sensors and voltage measurement system are transmitted via National Instruments Data Acquisition tool and then processed in the LabVIEW software. Data output from Agilent devices are transmitted through the GPIB USB port and then to the LabVIEW software to further analysis.

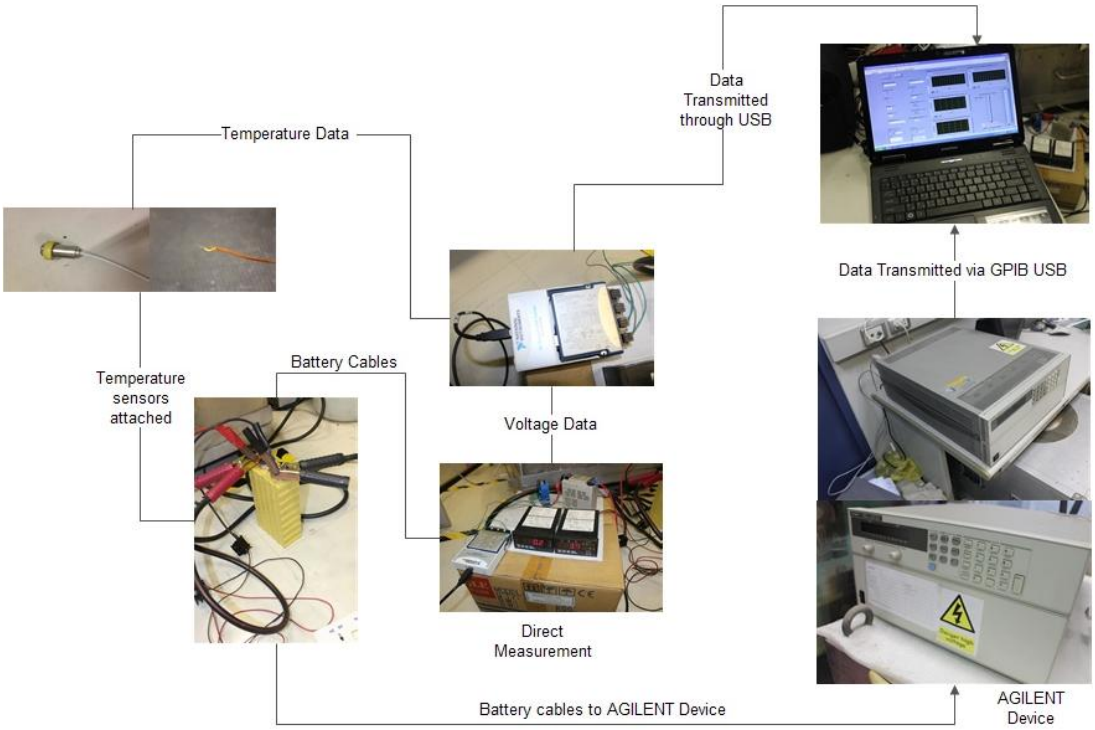

Figure 3.24 Experimental Setup for Agilent devices

In heat capacity test, the selected battery needs to be charged and discharged in the same test procedure. In this case, it is complicated to setup using both electronic load and power supply at the same time due to safety reasons such as possibility of overheat and short-circuited. Therefore, a MACCOR 4000 battery testing system is applied to achieve this purpose. Figure 3.25 shows the schematic for this experimental procedure.

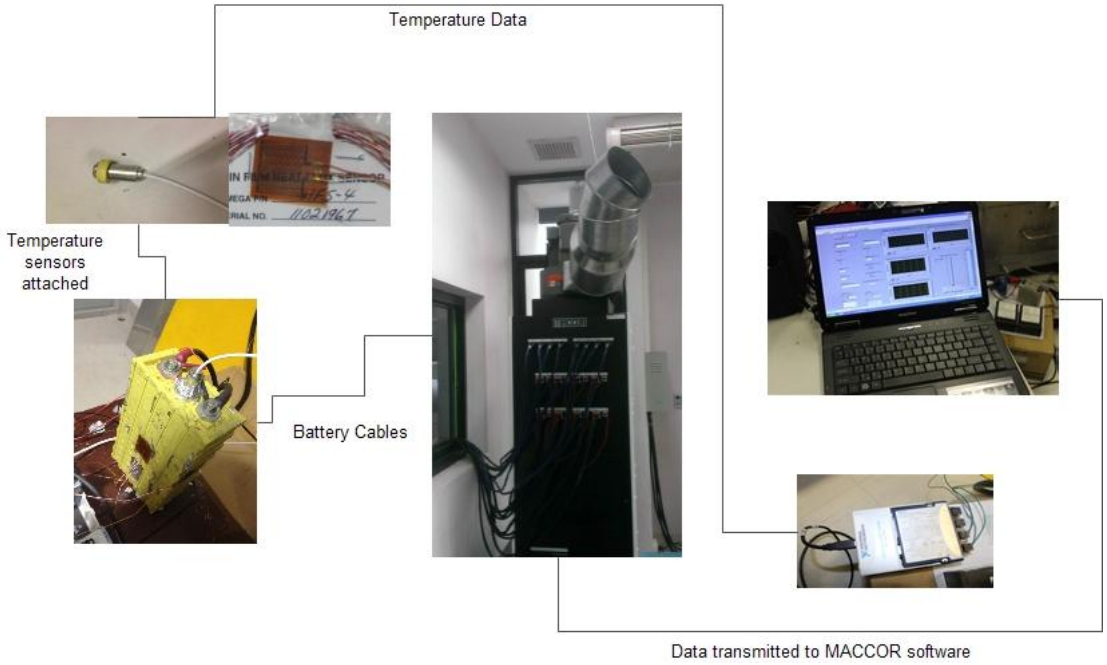

Figure 3.25 Experimental Setup for MACCOR 4000 system

In the setup of MACCOR 4000 system (figure 3.25), direct voltage measurement is not applied because the system already have the separated cables for measuring voltage and supply current. Therefore, voltage drop issue is not concerned with this setup. As this setup is aimed to obtain experimental results for heat capacity, heat transfer from the surface to the surrounding has to be calculated according to thermal model. Therefore, heat flux sensor is mounted on the three surfaces of the battery for x, y and z axis for this purpose. Same as the setup for Agilent devices, infrared temperature sensor is used for measuring internal temperature of the battery. The electrical data such as voltage, current, state of charge and etc. are transmitted to the computer with MACCOR owned software. At the same time, temperature data are transmitted via NI 9205 device, and then to NI LabVIEW software.

In figure 3.26, the experimental setup for determining temperature coefficient is shown. This property is essential for calculating the heat generation for the battery according to thermal model (see chapter 2). In this setup, battery is connected to Agilent electronic load for monitoring voltage. At the same time, battery is contained in thermal chamber (in this case, a refrigerator) and surrounding temperature is controlled as designed. Temperature of the battery is also monitored with the same setup of sensors as the first setup. Temperature inside the chamber is monitored by thermocouple and temperature data are transmitted through NI 9213 module.

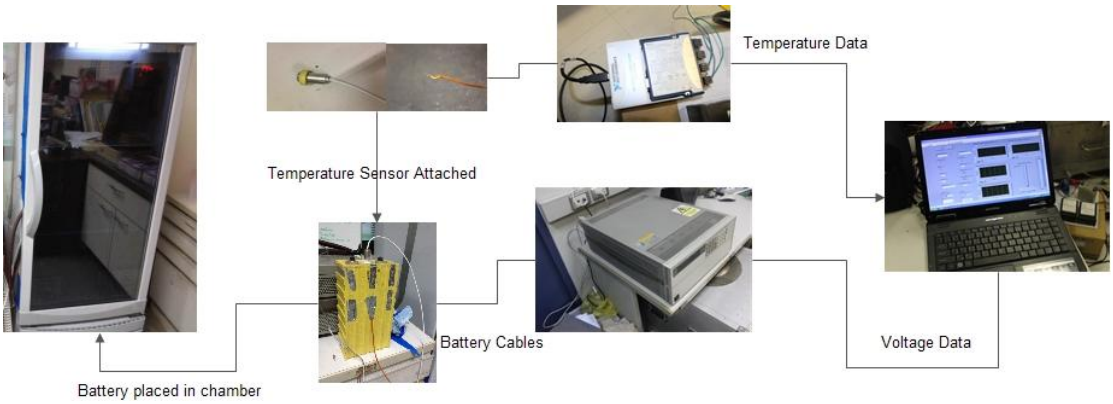

Figure 3.26 Experimental Setup for Temperature Coefficient experiment

3.3.3 LabVIEW Graphical Programming

To control electrical devices and manage data which recorded from sensors, LabVIEW (Laboratory Virtual Instrument Engineering Workbench) program is used. This program communicates with Data Acquisition (DAQ) devices which are connected between sensors and the computer. The applications of this program include data acquisition, instrument control and industrial automation with the support on main platforms such as Windows, MAC OS X or Linux. One of the main advantages of LabVIEW is the dataflow programming type which uses graphical codes. Two main parts of LabVIEW are “block diagram” and “front panel”. The block diagram page is for creating and editing the graphical programming codes. In each code, the user can easily understand the functions of each block diagram by turning on the help features. Then blocks can be connected together to create a more complex sequence to drive the program displayed in front panel. Another outstanding feature of this program is the capability in connecting with wide range of hardware and the user can also do custom user interface from the front panel to suit the purpose. Connections can be chosen from analog to digital according to user’s application. To transfer data from controlled hardware to computer, DAQ device can be used with simple connection via USB (Universal Serial Bus). Figure 3.27 shows the block diagram for discharge tests. Here, the dataflow shows that the data of voltage, current and temperature are processed and recorded to text file. The front panel reflects to the design of graphical codes in block diagram. Figure 3.27 and 3.28 show block diagram for discharge and charge experiments respectively. Here, input parameters such as current and cut-off voltage are set and real-time data of voltage and temperature can be observed. For block diagrams designed for this work, see Appendix C and D.

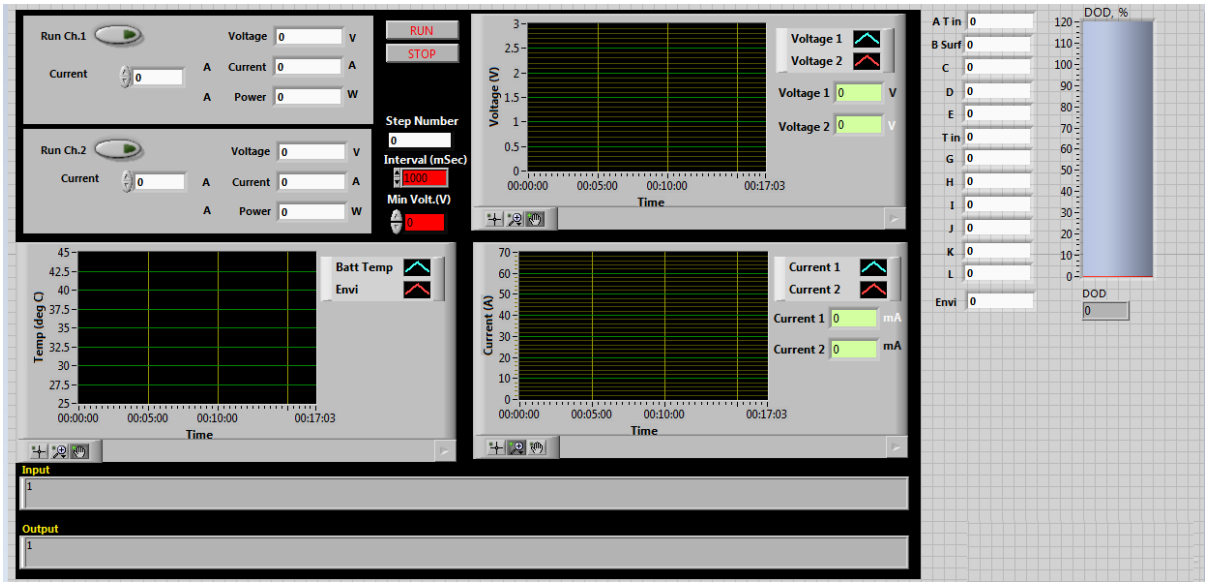

Figure 3.27 LabVIEW front panel for discharge experiment

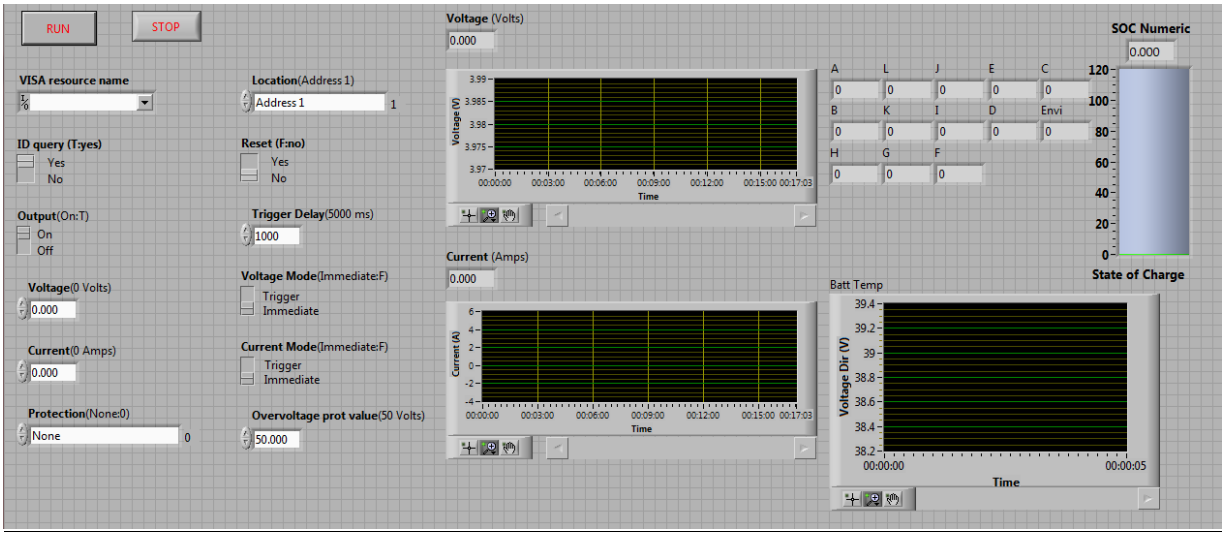

Figure 3.28 LabVIEW front panel for charge experiment

From figure 3.27 and 3.28, main parameters such as voltage, current and temperature are measured from devices explained previously. Then, the data of voltage and current are plotted into the chart relative to time for real-time observation. The numerical values are also displayed for more precise observation. For state of charge (SOC) observation, coulomb counting method was applied and data of SOC is displayed at the gauge on the right side of front panel.

3.3.4 MACCOR software

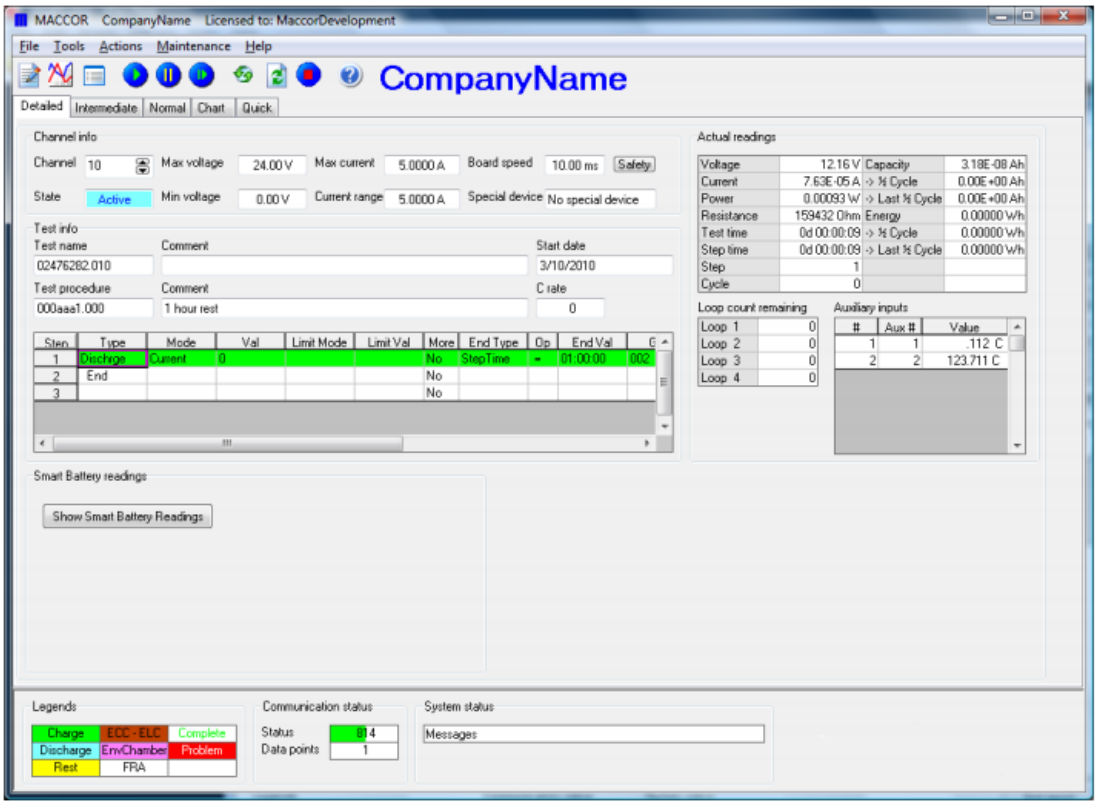

Figure 3.29 MACCOR software front panel

Figure 3.29 shows the software for MACCOR 4000 which comes with the package of the battery testing system. In this software, multiple test channels can be observed. Both charge and discharge test can be programmed with multiple channels. The data of voltage and current are recorded to the computer without using DAQ tools. One of advantage compared to LabVIEW software is that step discharge test can be programmed to have the current load altered according to the programmed values. In “detailed” tab, several real-time readings of battery conditions can be monitored such as voltage, current, power and active test procedures can be monitored. For intermediate tab, real time conditions such as voltage, current and capacity in all channels are displayed here. The normal tab shows overall status of the test system with colors indicating test progress. The chart tab shows real time graphic display with selectable inputs. Finally, “Quick” tab displays the selected condition (voltage, current, capacity and etc.) which can be seen from a distance with bigger fonts and colored in the background. To create or edit test procedures, “Build Test Program” can be used (see figure 3.30). In the type tab, procedures such as charge, discharge, rest or loop can be applied for operation. Also, several end types can be set such as step time, loop count, voltage, current, power and etc.

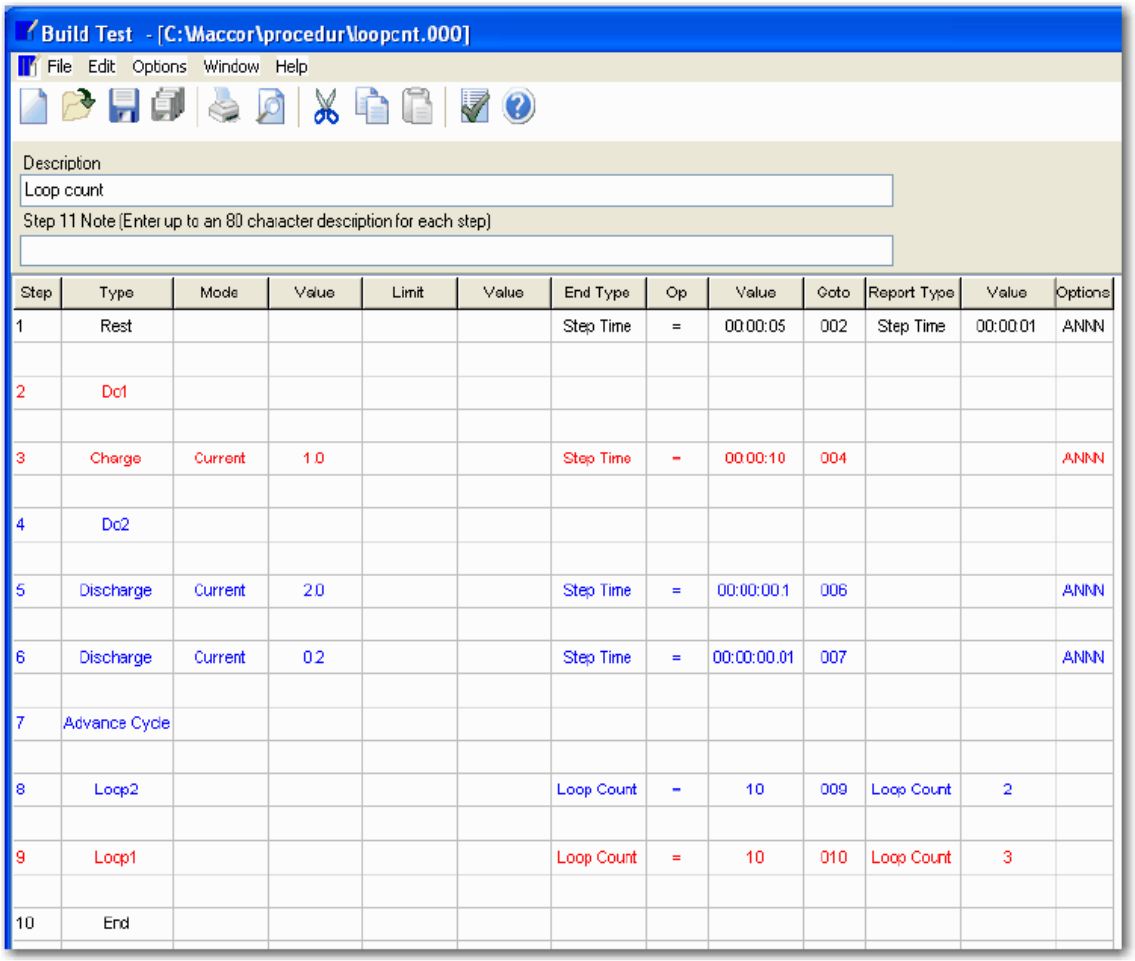

Step	Type	Mode	Value	Limit	Value	End Type	Op	Value	Goto	Report Type	Value	Options
1	Rest					Step Time	=	00:00:05	002	Step Time	00:00:01	ANNN
2	Dc1											
3	Charge	Current	1.0			Step Time	=	00:00:10	004			ANNN
4	Dc2											
5	Discharge	Current	2.0			Step Time	=	00:00:00.1	006			ANNN
6	Discharge	Current	0.2			Step Time	=	00:00:00.01	007			ANNN
7	Advance Cycle											
8	Locp2					Loop Count	=	10	009	Loop Count	2	
9	Locp1					Loop Count	=	10	010	Loop Count	3	
10	End											

Figure 3.30 Build test program window

3.4 Experimental Procedure design

For step-by-step experimental procedures, each test is based on the conditions applied to the battery. The basic concept is based on thermal model which shown the measurable parameters such as temperature, voltage and current. Then after the data of measured parameters were obtained, they were applied to thermal model to find heat generation, heat transfer coefficient and heat capacity. State of charge can also be measured in real time by using the coulomb counting method. In this case, the test conditions are discharge test, charge test, temperature coefficient test and heat capacity test. To see the demonstration of thermal data obtaining approach, see figure 3.31.

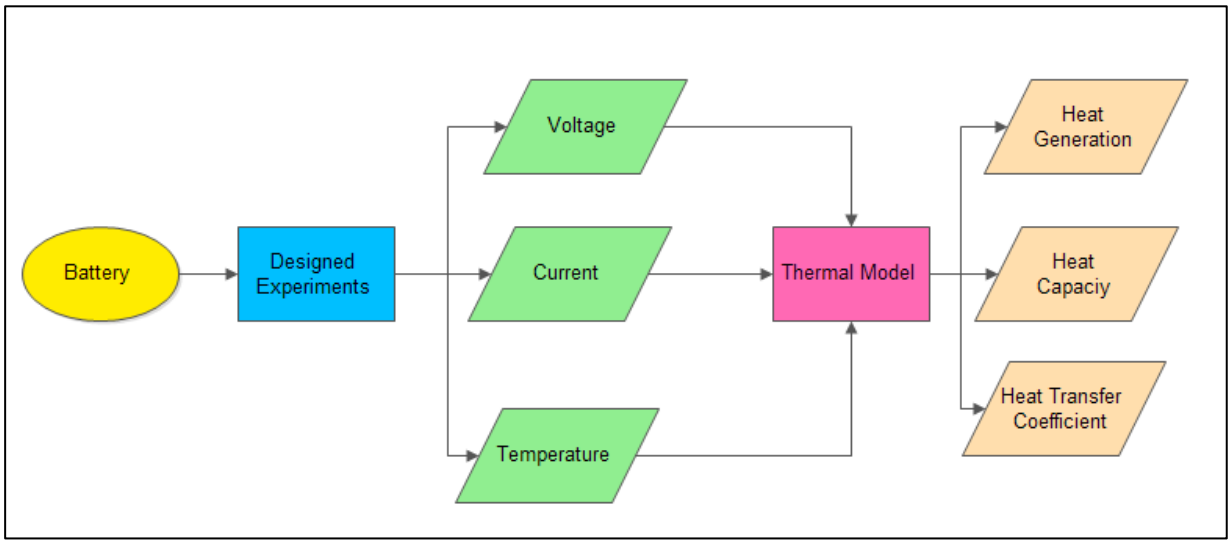

Figure 3.31 Approach to thermal properties in this work

From figure 3.31, temperature, current and voltage can be directly measured from the battery. With the data obtained, thermal model can be used to analyze for heat generation, heat capacity and heat transfer coefficient. In each thermal property, different experiments are designed with different conditions.

In all experiments performed in this work, same primary preparation process is applied. The sequential steps are shown below;

1. Inspect physical conditions of the battery for wear or tear and measure voltage and temperature by using simple devices such as multi-meter.
2. Inspect conditions of experimental devices (such as electronic load and power supply) and accessory tools such as power cables and data transfer devices (DAQ and NI modules).
3. Connect power cables between the battery and the load device
4. Connect measurement devices such as thermocouples, heat flux sensor, infrared thermal sensor and voltage measurement wire.
5. Turn on the load device and observe battery readings from the display on the connected device such as voltage, current and temperature.
6. Adjust the load device setting to according to the conditions for the selected experiment.

Therefore, different experiments will reflects on different types of load device used, settings on load conditions and measurement devices attached to the battery.

3.4.1 Charge/Discharge experimental procedure

This section explains the procedures for charge and discharge experiment. This type of experiment is the fundamental test for understanding the battery behavior. The outcome of the test can predict many attributes of the battery such as thermal behavior (temperature profile, heat generation), battery capacity, electrical properties such as open circuit voltage and internal resistance. In figure 3.32, the approach to heat generated in battery can be seen. The charge and discharge test can be performed to obtain heat generation and in the same time, state of charge can be monitored by using the coulomb counting method. Table 3.5 shows required conditions for charge/discharge experiment.

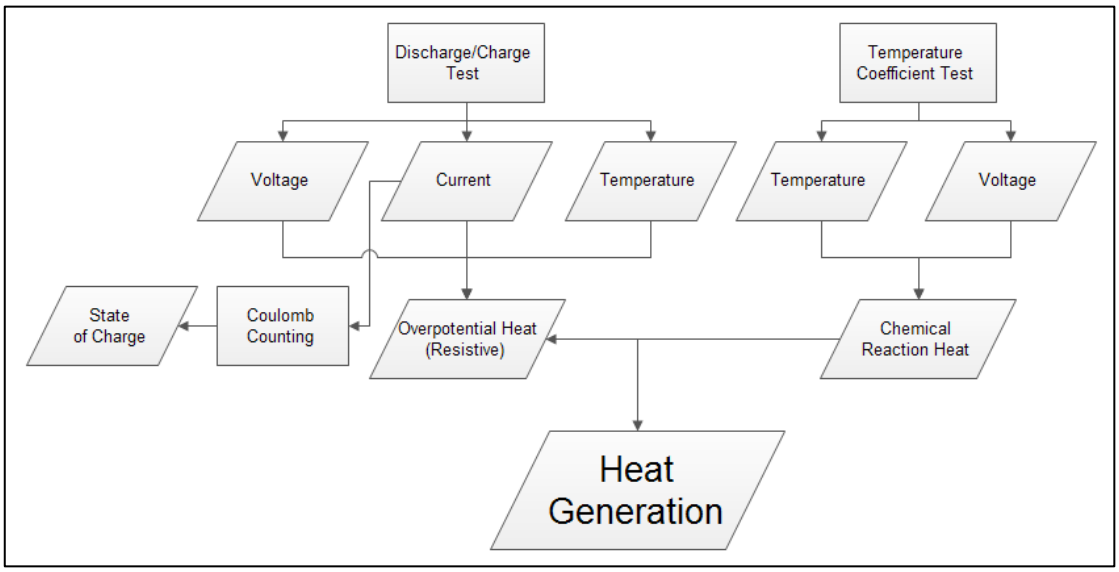

Figure 3.32 Heat Generation Approach

Table 3.5 Experimental Conditions for Charge/Discharge tests

Devices required	Agilent devices or MACCOR system
Current load applied	20A, 30A, 60A
Temperature limits	Follow battery specifications
Measurement device required	Thermocouple/heat flux sensor and IR thermal sensor
Targeted properties	Heat Generation, Battery Capacity, Resistance

For discharge test, the experiment flow is shown in figure 3.33. Load current input can be set from the LabVIEW front panel which controls Agilent electronic load (shown in red rectangle of figure 3.34). This was taken from the part of discharge test front panel in figure 3.27.

The cutoff voltage can be set in the “Min Volt” box. After finishing the condition input, the “run” button can be used to initiate the experiment. For cutoff temperature, the feature only available in MACCOR battery test system. The blue rectangle section shows the real time status in voltage, current and power of the battery.

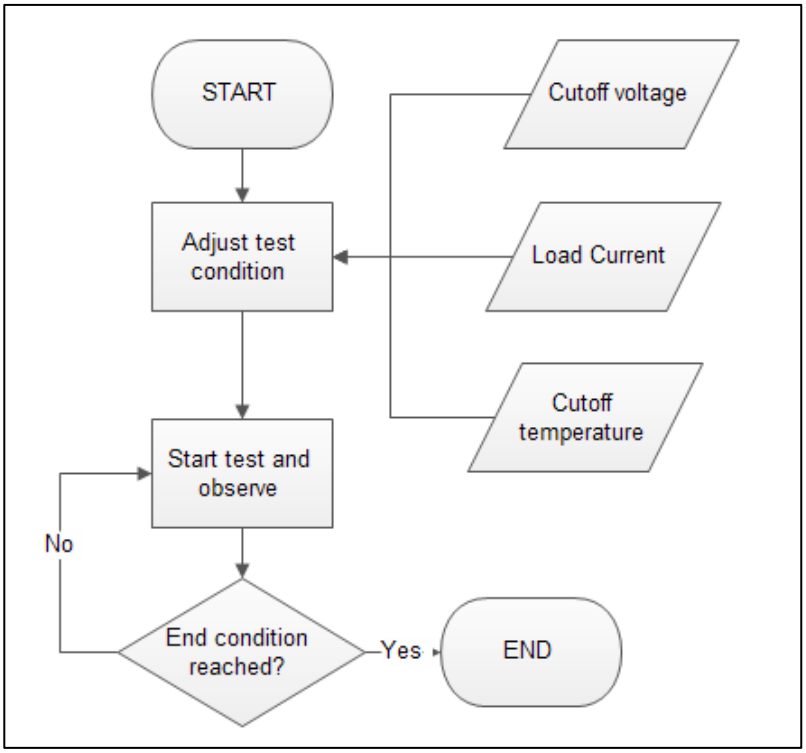

Figure 3.33 Flowchart for charge and discharge experiment

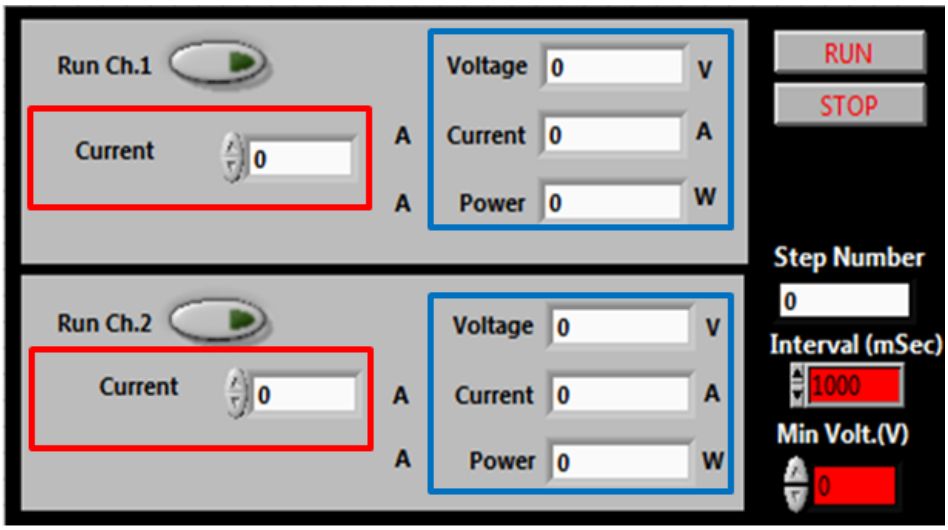

Figure 3.34 Condition input for Electronic load controller

In the other section of discharge test front panel located on the right side, battery conditions can be monitored in real time from charts and text display. The state of charge of the battery is monitored through its opposite attribute, the depth of discharge (DOD) from the DOD tank level display. When the DOD reach 100%, the cutoff voltage is reached and the experiment is ended. For MACCOR system, the input setting for load condition can be input in "Build Test Program" window shown in figure 3.30. MACCOR allows the battery to be charged and discharged by using same testing device and software. For LabVIEW which controls Agilent devices, the programs are separated and therefore the charge and discharge experiments had to be done separately.

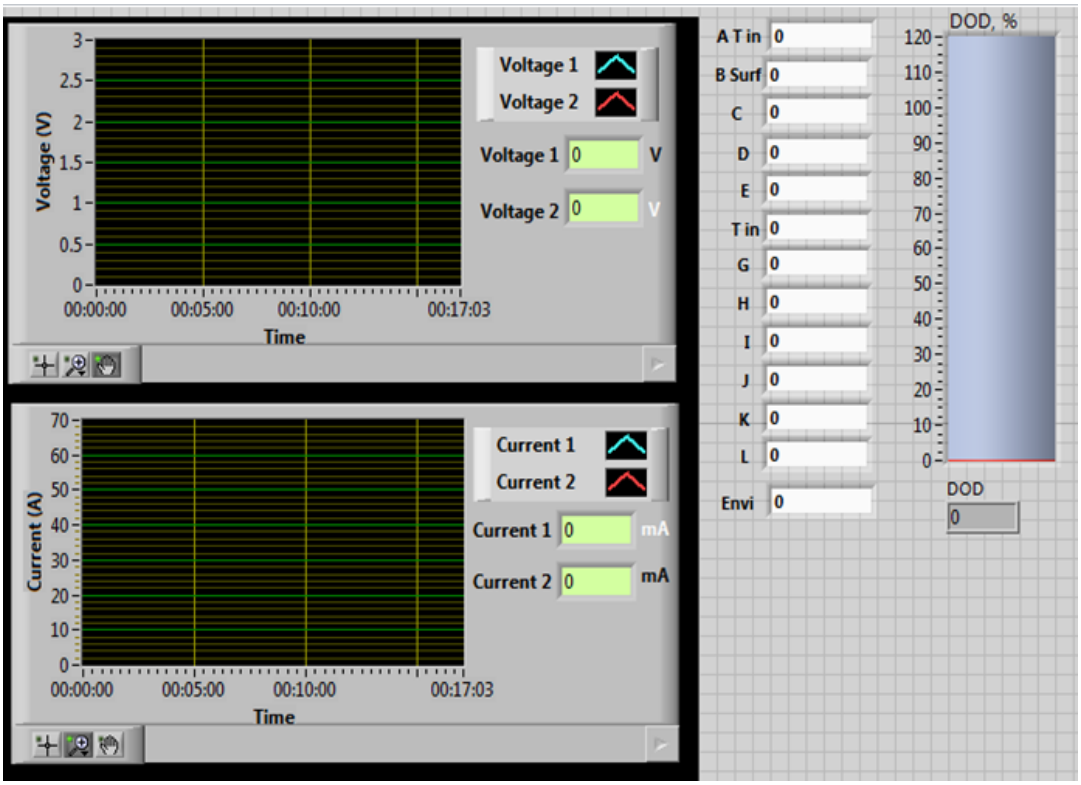

Figure 3.35 Real-time monitoring at discharge test front panel

In charge test, power supply was used to perform the experiment. For setting input conditions, the procedure is similar to that of electronic load but the selection of device is needed at the "VISA resource name" box. In figure 3.36 which was taken from the power supply, the output switch must be turned on and voltage and current can be set from boxes below output toggle switch. Similar to electronic load, the real time data displayed is demonstrated in figure 3.37.

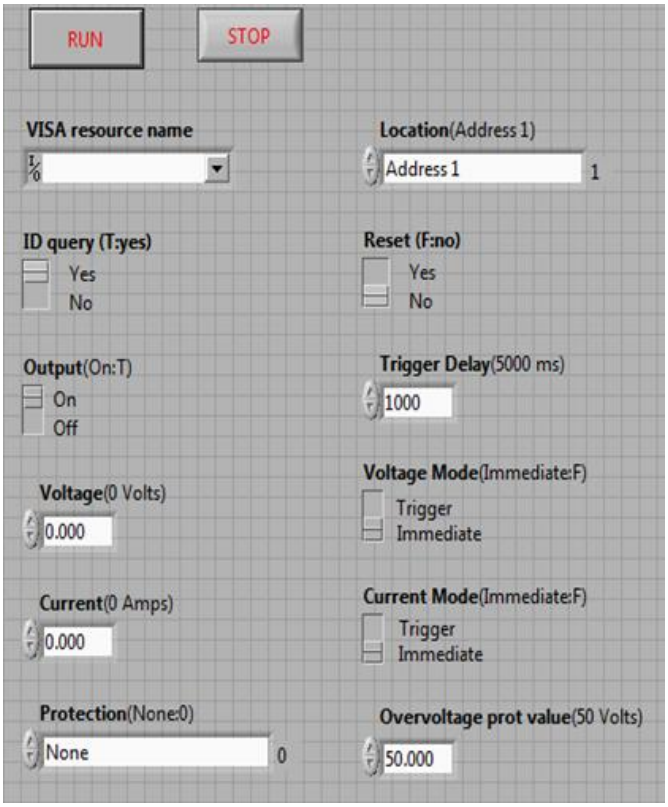

Figure 3.36 Condition input for power supply front panel

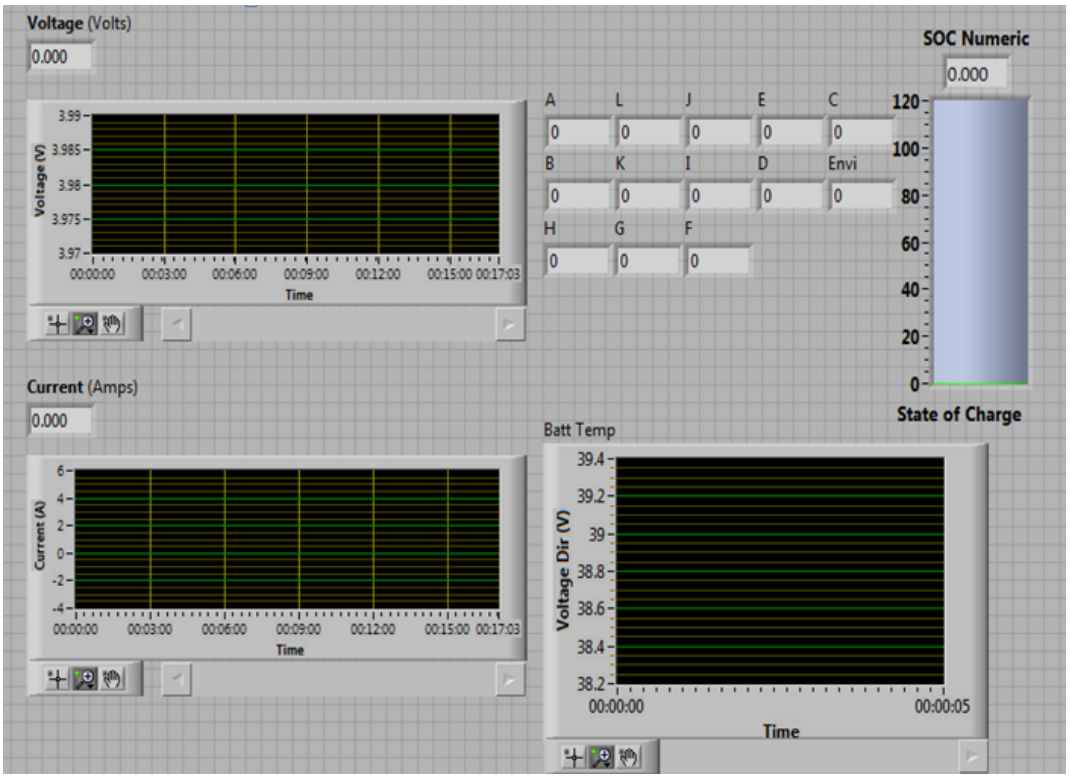

Figure 3.37 Real-time monitoring at charge test front panel

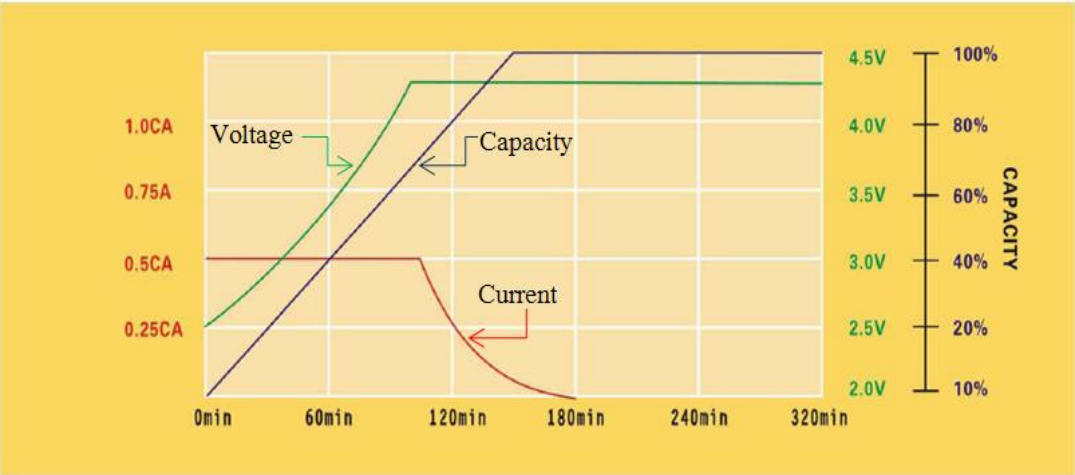

Figure 3.38 Charging sequence for selected battery

The sequence steps of charge test for lithium ion batteries are more complex than the discharge test. In this test, the initial step start with the constant current charging which the value of charge current can be set in the current box in figure 3.36. In this step, the battery voltage (galvano-static) will gradually increase until it reached the charge voltage which can be set from the voltage box at the front panel of charge test. This initiates the second step which is called the constant voltage (potentio-static) charging. In this step the battery voltage will remain constant and the charge current will gradually decreased until the cutoff current condition is reached .In theory, the cutoff current is less than 3% of the rated current applied to the battery. For this work, the selected battery has the capacity of 60A which means it takes 1 hour to fully discharge the battery with current load of 60A. Therefore, the cutoff current for this case is 3% of 60A which equals to 1.8A. Figure 3.38 demonstrates the explained sequence. This figure shows current supplied in left y-axis with the unit of CA or Capacity Ampere which based on the battery capacity (i.e. 1CA = 60A, 0.5CA = 30A). The voltage and capacity of the battery are shown on the first and second scale of the right y-axis respectively. For the case of discharge test, the constant current (galvano-static) process is only applied to the battery.

3.4.2 Temperature Coefficient experimental procedure

From the battery thermal model, it can be seen that temperature coefficient is required for calculating the heat from chemical reaction or reversible entropic heat of the battery. This term is defined as equilibrium or open circuit voltage variation to the temperature (dE_{eq}/dT).

Here, separated experiment must be performed to obtain this coefficient. Referred to the works from several researchers the methodology for approaching this parameter is similar. The tested battery with attached voltage and temperature sensor is put into thermal cycling. When the temperature of battery becomes stable, open circuit voltage of the battery is observed. Finally the data of voltage and temperature are put into the calculation of temperature coefficients. From Hong et al [38], battery was heated by the wounded coil around the cell and kept the temperature constant for 4 hours in each temperature step. The results of dE_{eq}/dT from Hong et al were -0.429 mV/K and -0.753 mV/K from open circuit voltage of 4.044 V and 3.22 V respectively. From Onda et al [41], the battery was set in thermostat and kept at 10, 20, 30 and 40°C respectively for 3 hours to see the voltage change. There was no report of dE_{eq}/dT results in Onda et al but the entropy change which was influenced by this term was negative in most SOC. From Forgez et al [42], the tested battery was out to the programmable climatic chamber and thermal cycle from 6°C - 36°C was applied to observe the voltage change. The results of dE_{eq}/dT from this work were found to deviate with the state of charge but have no definite relationship. In the range of 0 – 30 % SOC, dE_{eq}/dT was found to be negative around -0.3 to -0.05 mV/K. From 30% to 100% state of charge, the results were positive with the range from about 0.025 to 0.1 mV/K. This can be observed that depending on the state of charge, the chemical reaction heat term can be endothermic or exothermic. For the applied method in this thesis, climatic thermal chamber method was chosen. The battery was attached with thermocouples and temperature surrounded was altered after temperature of the battery reaches the chamber temperature. The experiment was performed having the battery in the same state of charge from 0 to 100% with 10% SOC incremental. Experimental conditions are summarized in table 3.6 below.

Table 3.6 Experimental Conditions for temperature coefficient test.

Devices required	Agilent Electronic load
Current load applied	None (to keep State of Charge constant)
Temperature variations (°C)	10°C - 35°C
State of charges observed (%)	0, 10, 20, 30, 40, 50, 60, 70, 80, 90, 100
Measurement device required	Thermocouple and IR thermal sensor
Targeted properties	Temperature Coefficient (dE_{eq}/dT)

Figure 3.39 shows flowchart for performing temperature coefficient test. The initial step is to have the battery fully charged. Then battery is discharged by 10% for testing for this parameter at 90% SOC. Battery temperature must be in steady state with the room temperature before it is put into thermal chamber. In thermal chamber, open circuit voltage will be observed to the variation of temperature around the battery. The temperature range can be referred from table 3.6.

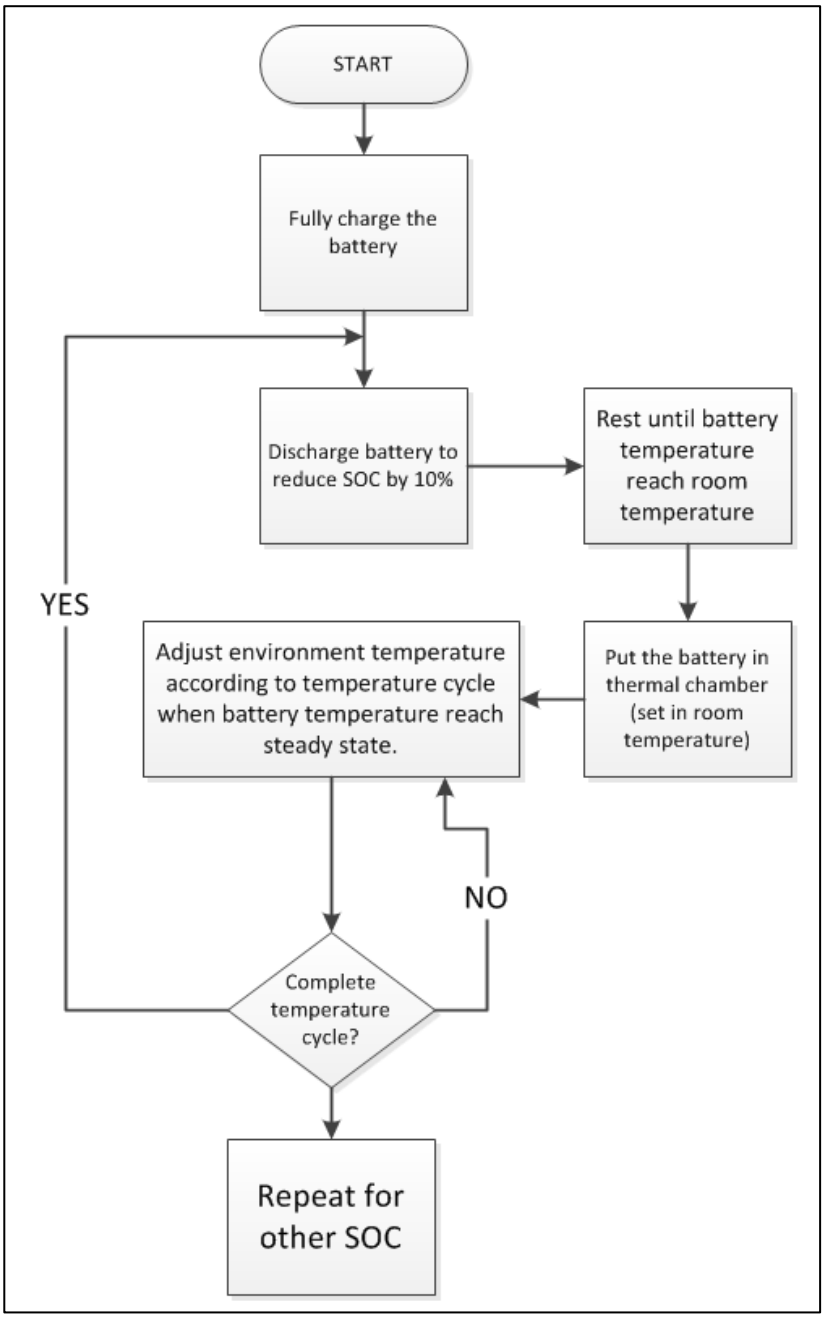

Figure 3.39 Temperature coefficient test sequence for selected battery

3.4.3 Heat Capacity (C_p) experimental procedures

Heat capacity of the battery is very useful for the design of thermal management system. In most works, this was either analyzed from material properties or from the use of calorimeter. For this work, energy balance of the battery was applied. The charging and discharging sequence was applied to battery to contain the state of charge in the range of target value, in this case ±4% SOC was used. The sequence starts from discharging the battery to reduce the state of charge by 4% then charge to bring the state of charge to 4% higher than its initial value. In this case, the current applied for charging and discharging cycle is at 1C and the target SOC for C_p analysis is at 50%. The data from targeted state of charge then was used for heat capacity calculation. Also, the internal heat transfer coefficient (h_{in}) from each axis of the battery can be calculated from the obtained data (will be shown later in chapter 4). The output temperature can be used to find temperature-time gradient. Flowchart in figure 3.40 shows the steps of performing the heat capacity procedure.

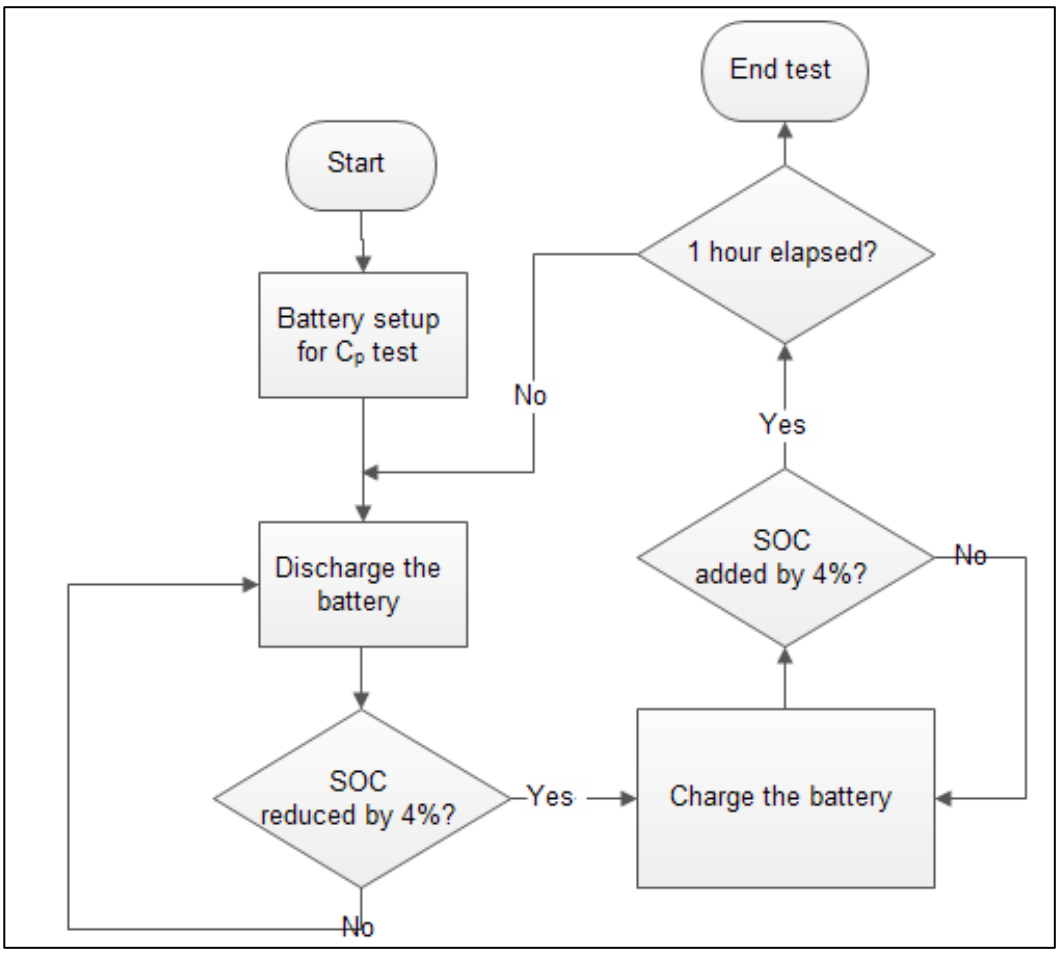

Figure 3.40 Flowchart for heat capacity test procedures

Table 3.7 Experimental Conditions for heat capacity test.

Devices required	MACCOR Batterty testing system
Current load applied	1C (60A)
Temperature limits	Follow specifications on the manual
Measurement device required	Heat flux sensor and IR thermal sensor
Targeted properties	Heat capacity

3.4.4 Pulse (Step) Current discharge test procedure

Additionally, pulse or step current discharge test was also performed to observe electrical properties of the battery such as open circuit and internal resistance. For the open circuit, the long step pulse was applied initially to observe the time taken for battery to reach equilibrium voltage. Then using the value of equilibrium and loaded voltage, the internal resistance of the battery can be calculated from the simple ohm's law. Figure 3.41 shows the flowchart of step current test procedures. The conditions of this test are similar to that of discharge test but the rest time can be different due to the purpose of test.

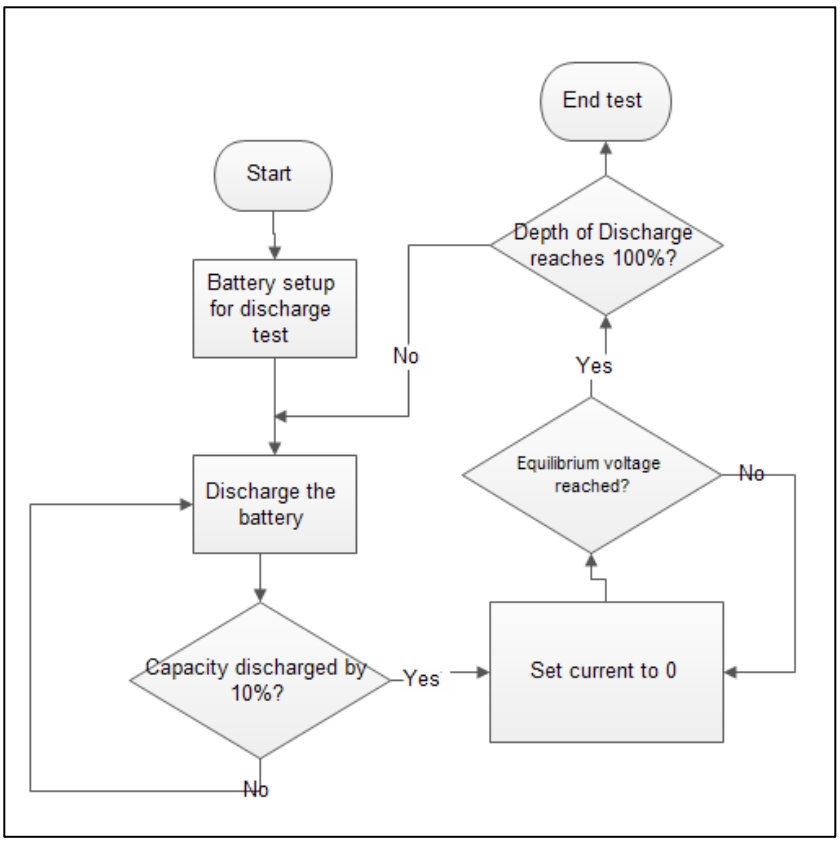

Figure 3.41 Flowchart for step current discharge test

CHAPTER 4

RESULTS

4.1 Constant Current Discharge/Charge Tests

In this section, results from constant current tests are shown. The objective here is to see the performance characteristics of the battery in terms of discharge capability and capacity. Comparisons between several methods for conducting the constant current tests are displayed here. Also, findings from battery performance in general are shown in this section.

4.1.1 Constant current discharge and charge tests (30°C)

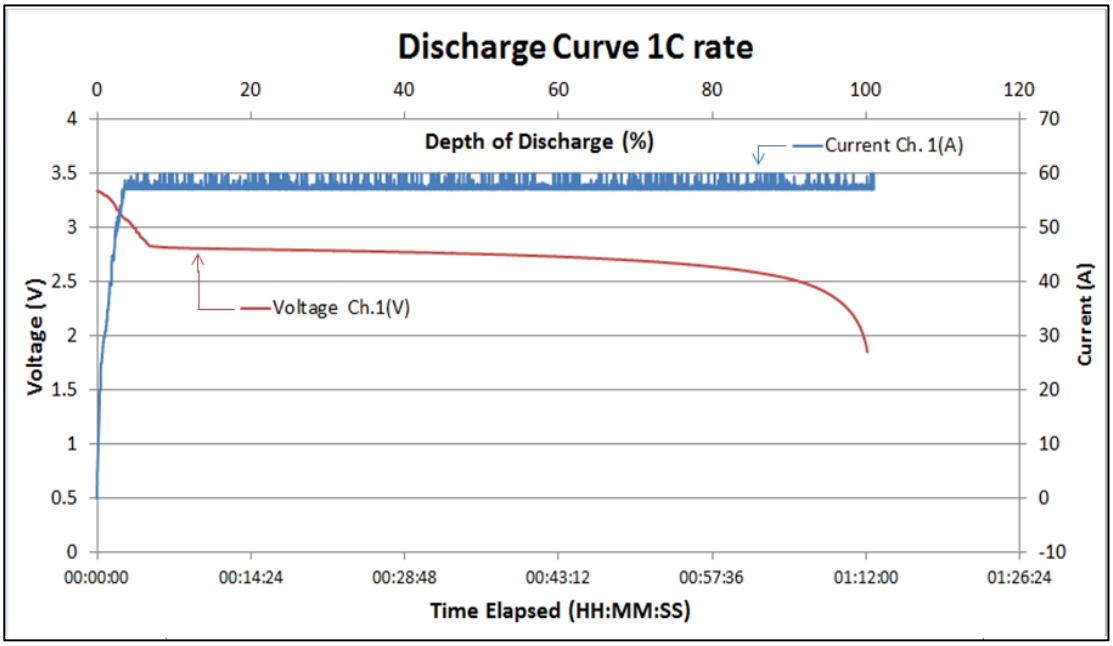

Figure 4.1 1C Constant current discharge test

In Figure 4.1, the data of voltage and current is displayed from 1 C discharge test. In this case, 1 C shows the amount of current that can fully discharge the battery in 1 hour which is 60 A according to the specification. The voltage behavior at the start decreased accordingly to the current applied. After it was discharged to 5% DOD (depth of discharge), voltage shows little change until the sudden drop when reaching 100% DOD in opposite, when the state of charge (SOC) reaches 0. This voltage behavior displays the advantage of lithium ion battery which can provide constant voltage under load. According to the coulomb counting method, the capacity of the battery was measured to follow the specification of 60 Ah.

Figure 4.2 shows the same results from discharging at 1 C rate with the comparison between the reading from Agilent Electronic load and from direct measurement of voltage. Here, the blue line shows the result which obtained from electronic load via GPIB port and the red line shows directly measured voltage. At the start of the test when the current load is gradually increased to the target value, the voltage measured from electronic load dropped to about 2.9 V. At the same time, the actual reading of voltage also has the voltage dropped but only to about 3.3 V. Both curves show similar trends except that the direct measured voltage reduced slower than measurement from electronic load due to less electrical resistance between the cable and the meter. At the end of the test, the actual (directly measured) voltage was about 2.6 V and the electronic load result shows the value below 2.4 V. This depicts that the use of direct measurement can provide more accurate results of voltage response from the battery. From coulomb counting, the results show that Ah rating for battery is higher than specified.

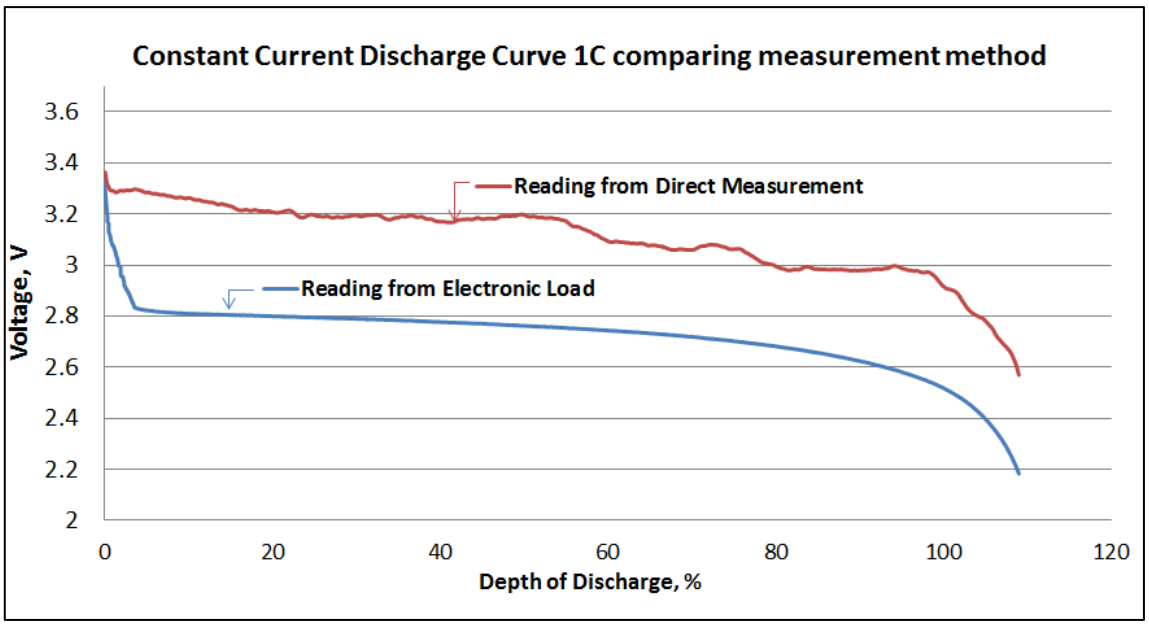

Figure 4.2 60A CC discharge voltage profile from using Agilent device

In figure 4.3, constant current discharge test from MACCOR battery tester is shown with initial environment temperature is at 30°C. Here, it can be noticed that the trend line is very similar to the results from electronic load. However, the voltage range is higher and close to the direct measurement of voltage because MACCOR device setup contains separated pair of voltage measurement cables. When the current load is applied, voltage is dropped to about 3.2 V and then was constantly reduced until it reached the cut off voltage, which is at 2.6 V.

It can be noticed that the depth of discharge (DOD) of the battery at the end of discharge test with MACCOR device (about 97%) is less than the DOD at the end of test which used Agilent device. This is because the battery was modified to be installed with infrared temperature sensor which causes the reduction of battery capacity due to the reduction in active material while the battery core is exposed to air. Despite capacity reduction, the battery performance in terms of discharge voltage profile and temperature profile are applicable for the calculation of thermal properties.

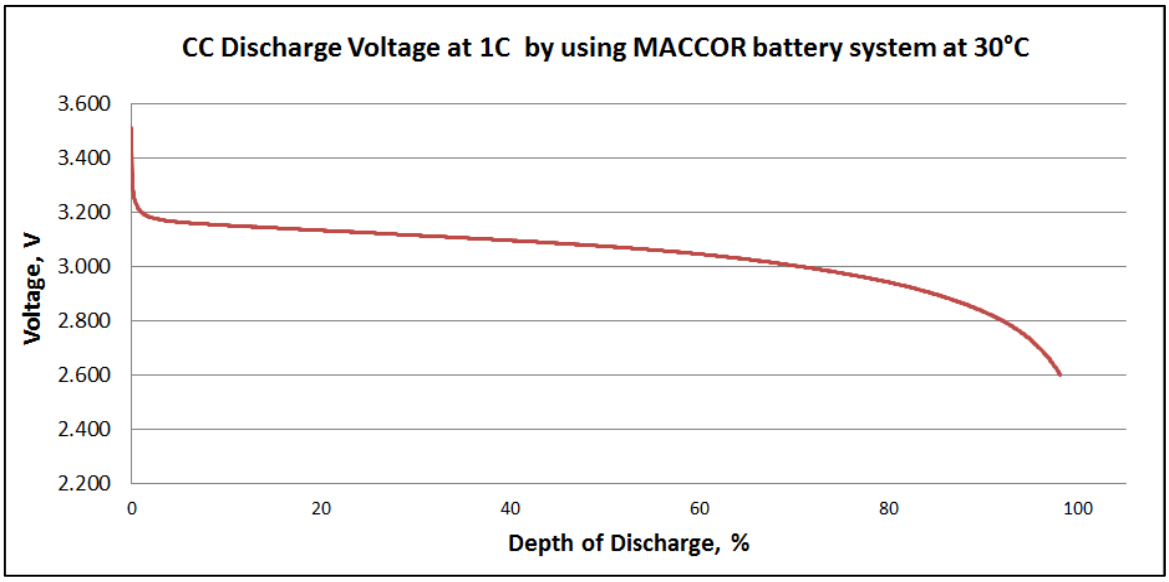

Figure 4.3 1 C CC Discharge voltage from MACCOR battery test system

Comparison of discharge voltage profile in each load is shown in figure 4.4. This is performed by using MACCOR battery tester with the current load of 20, 30 and 60A. The cut off voltage is the same as 2.6 V and initial voltage is at 3.6 V. With higher discharge rate, the quicker that voltage reaches the end condition. With lower discharge rate, it is observed that the depth of discharge at the end of the test is higher which shows the relationship between battery available capacity and discharge rate. Relatively, the discharge time can take longer with less discharge rate for example 0.5 C rate will take 2 hours to fully discharge the battery. Also, the results proved that the battery capacity is met with the condition in the specification manual with 60 Ah rating.

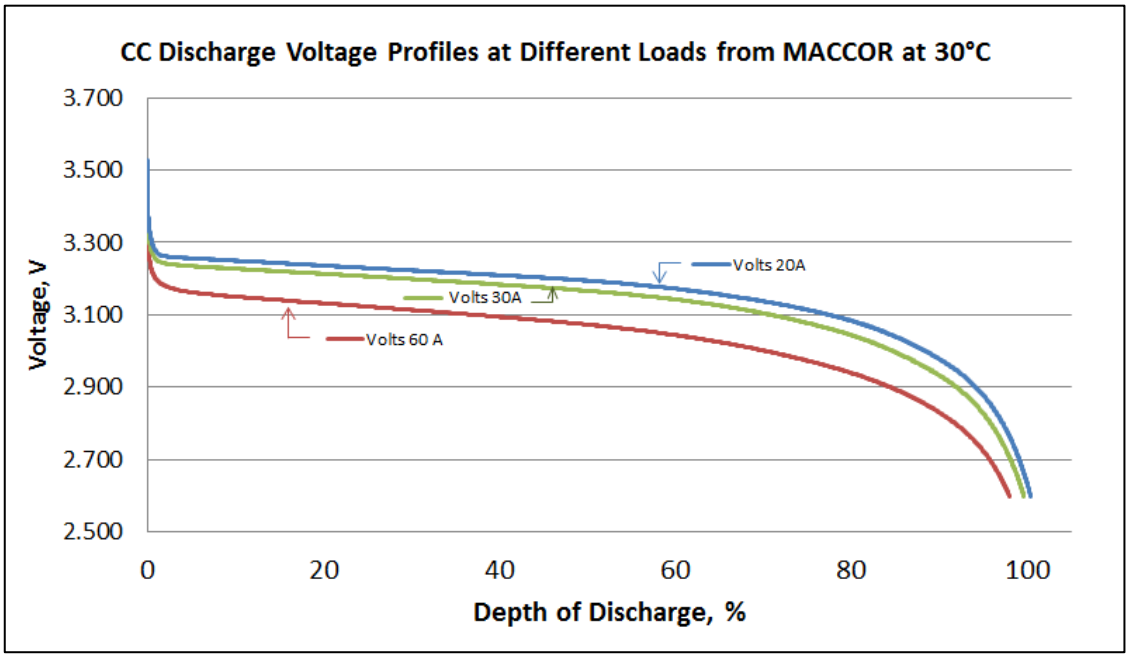

Figure 4.4 Comparison of discharge voltage at different loads

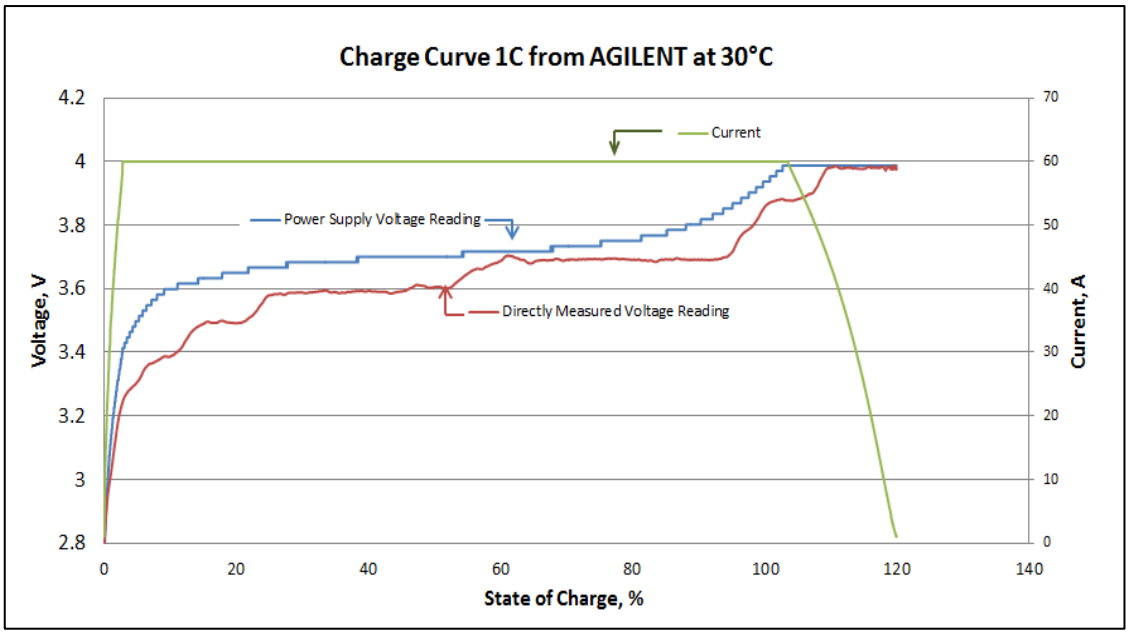

Figure 4.5 Charge curve results from Agilent Power Supply

In the constant current charge test, figure 4.5 shows results from using Agilent power supply device. At constant current phase, voltage increased until charged voltage of 4 V is reached. Then at the constant voltage phase, current dropped until reach cutoff condition of 1 A. In this process, the output voltage from power supply rise to the target voltage earlier than the directly measured voltage. The actual voltage reached target near the end of the test but the

voltage from power supply readings reaches the target earlier. Noise is one of the disadvantages of using direct measurement at Agilent setup which requires the data transmitted through NI module. To eliminate this, measured data was processed though low-pass filter in MATLAB for smoother plot. The frequency used for filtering was at 100 Hz. See Appendix E for MATLAB code used here.

Figure 4.6 shows the result of charge test from MACCOR battery tester. The voltage reading is closer to the direct measurement which is more accurate than the readings from Agilent power supply. As soon as the voltage reached 4 V (target charge voltage), the current load dropped immediately and then the test is ended when current load is reduced to 1 A (2% of rate current). Data used for plotting charge curve in figure 4.6 was used from the recorded data in MACCOR system directly without any further process such as filterng. This is because the MACCOR system can record the voltage data and eliminate interruption noises. Thus, unlike Agilent device, this system does not required another measurement settings of voltage directly.

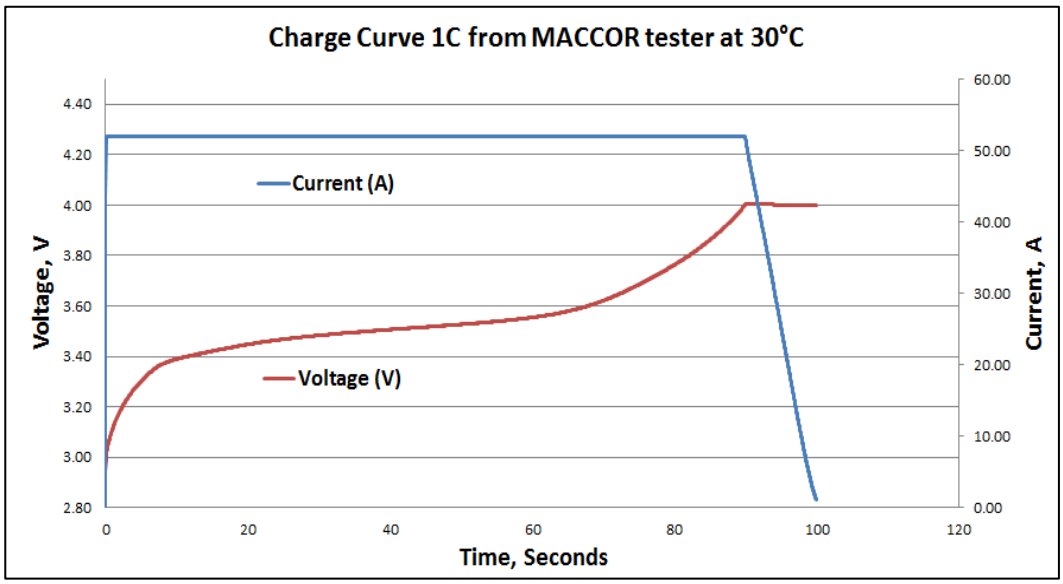

Figure 4.6 Charge Curve from MACCOR battery tester

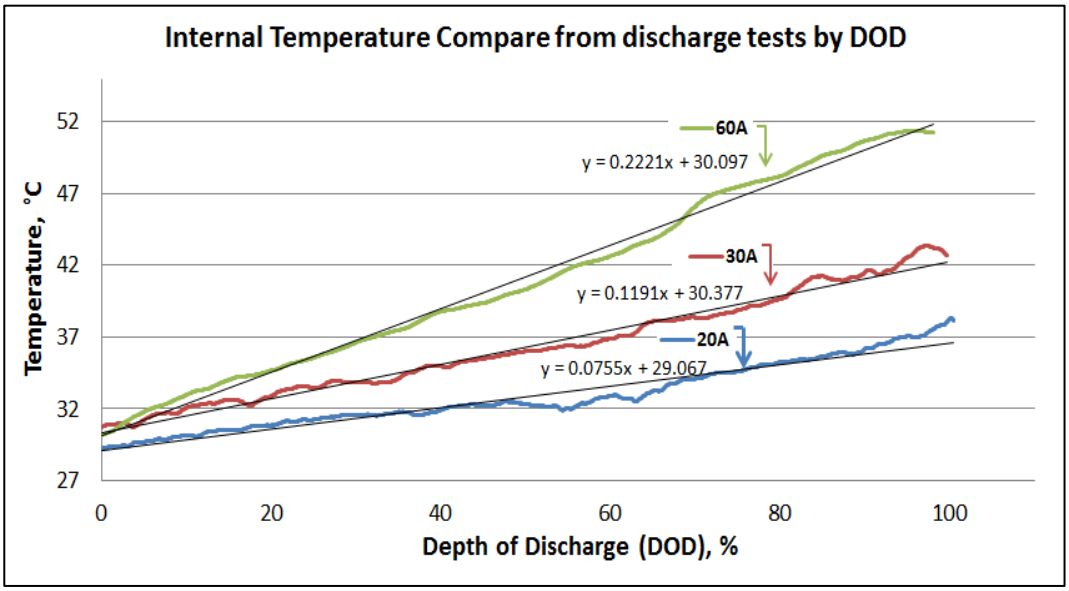

Figure 4.7 Internal Temperature Comparison between loads by depth of discharge

In figure 4.7, the corresponding result of internal temperature response from discharge test in each load (according to figure 4.4) are displayed. All of the tests started at ambient temperature at approximately 30˚C. The peaked temperature here is 51.7˚C (ΔT = 21.5 ˚C) for 1C (60A) discharge whereas in the C/2 (30A) rate of discharge, the peaked temperature at the end is about 38 ºC (ΔT = 7.3˚C). Also in perspective of time based analysis, figure 4.8 shows that the highest discharge rate (1C, 60A) produced largest temperature-time gradient. Equations in each curve are obtained by linear regression method.

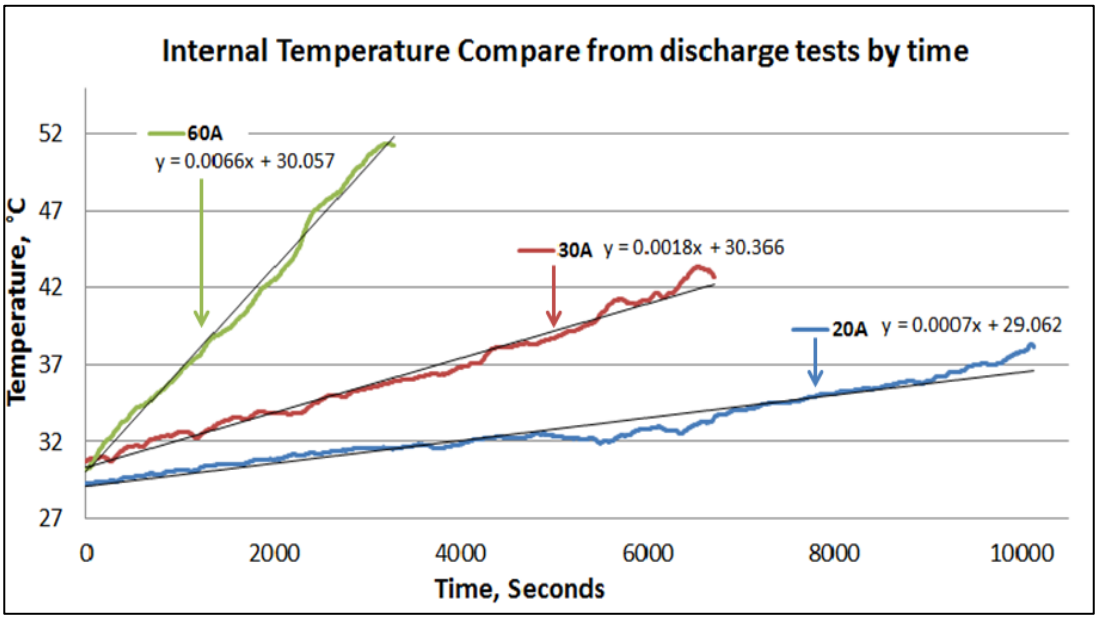

Figure 4.8 Internal Temperature Comparison between loads by time

From figure 4.9, the temperature measured inside and the surfaces of the battery are compared. From this figure, it can be noticed that all curves are in linear relationship while internal temperature produced steeper curve than the surface temperature results. It can also be noticed that the temperatures on the front, side and bottom surface of the battery have only slight difference between each other. This is due to the uniform temperature distribution across the surface of the battery. To clarify further on this, an experiment was performed as having thermocouples attached to the various positions on the battery surface according to figure 3.18 while the battery was discharged with the rate of 1 C. The actual setup is shown figure 3.23 with initial temperature was 31˚C which was the environment temperature at that time of test. The results from figure 4.10 to 4.12, most of the temperature changed in the same way in each position with the same range. The difference between the initial and final temperature is not more than 2˚C. Therefore, measurement of temperature was simplified by attaching only one thermocouple of each axis (front, side and bottom for x, y and z respectively). Furthermore, the data of temperature on the surfaces of the battery are important for the calculation of heat generation and heat capacity which will be demonstrated in the next chapter.

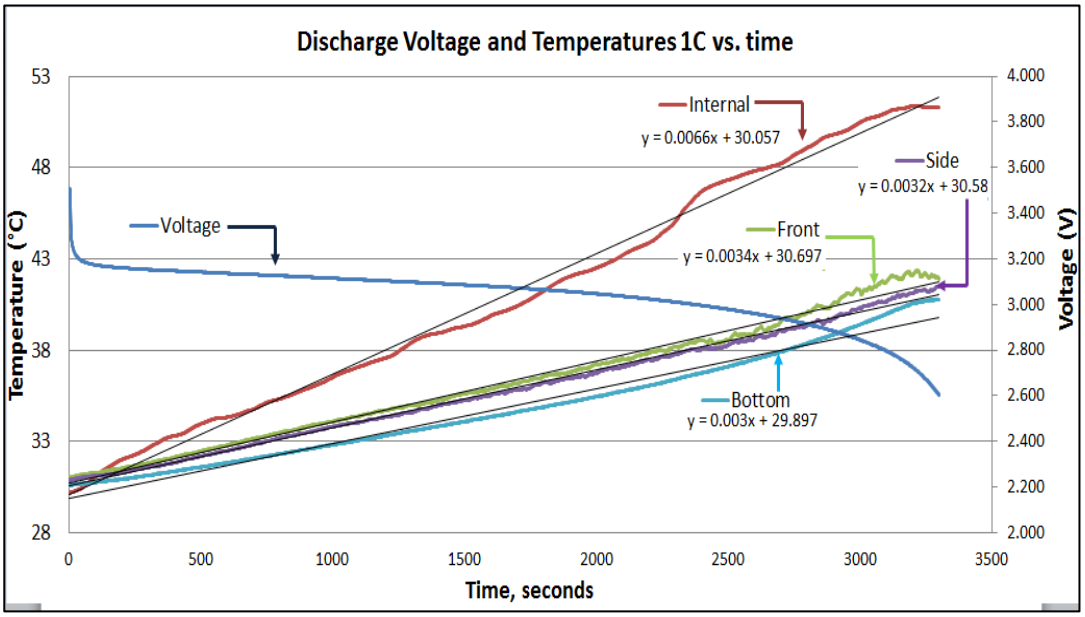

Figure 4.9 Temperature results from 1C constant current discharge test by time

Figure 4.10, 4.11 and 4.12 shows temperature responds for the uniform temperature test on the front, side and bottom surfaces of the battery respectively.

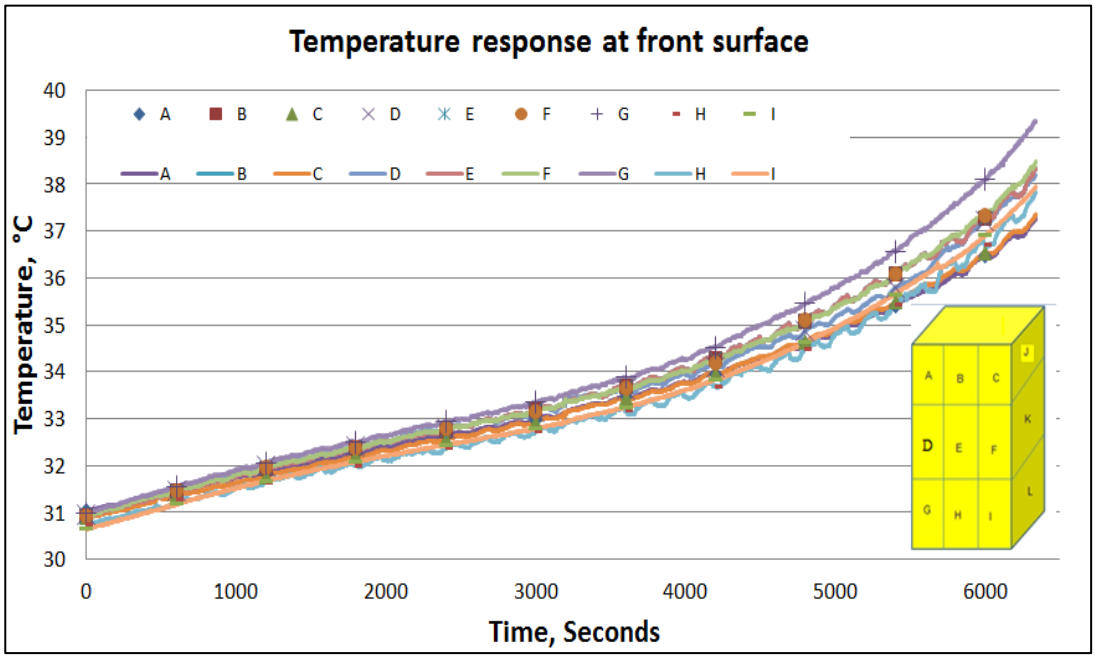

Figure 4.10 Front surface temperature responses

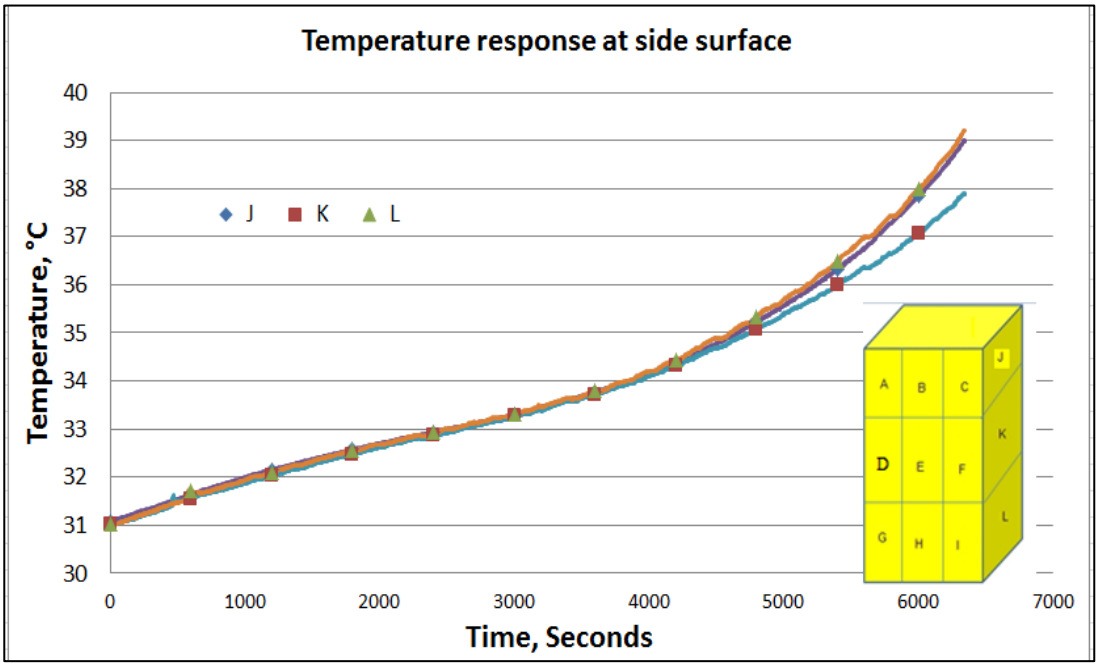

Figure 4.11 Side surface temperature responses

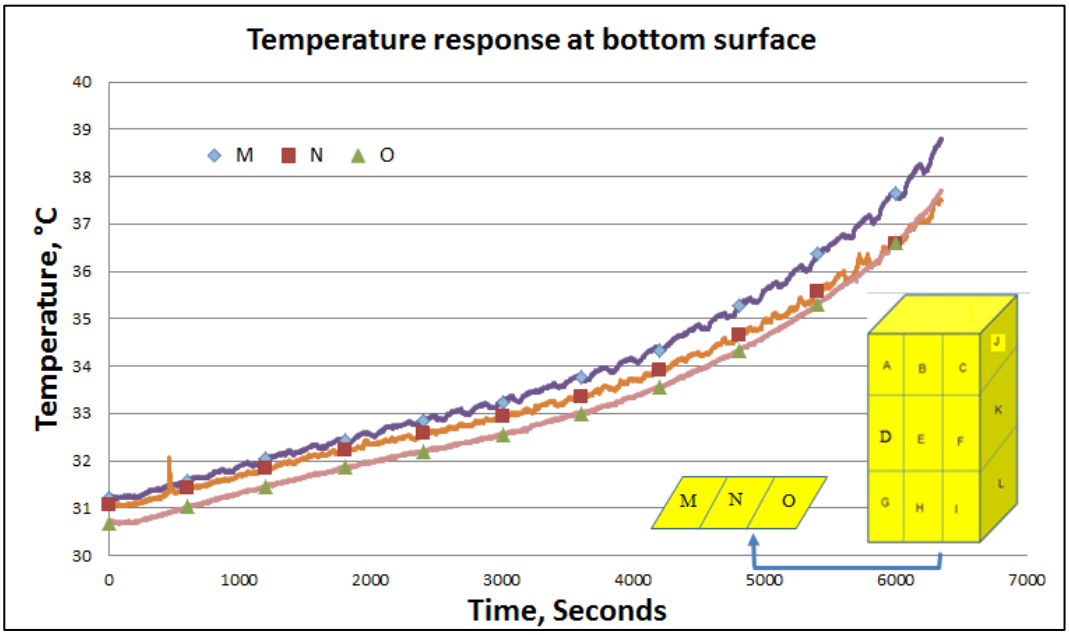

Figure 4.12 Bottom surface temperature responses

In figure 4.13, temperature responses from charge test with constant current of 1 C rate is demonstrated. Here, the results are similar to that of CC discharge test as the temperature rise with the constant slope. However, at the constant voltage (CV) period when the current supplied to the battery is reduced as the battery voltage reached the charging target, it can be seen that the temperature decreased. The peak temperature of battery internal core was slightly over 51 ºC after about 1 hour and then it was reduced at the CV phase and reached 37.6 ºC at the end.

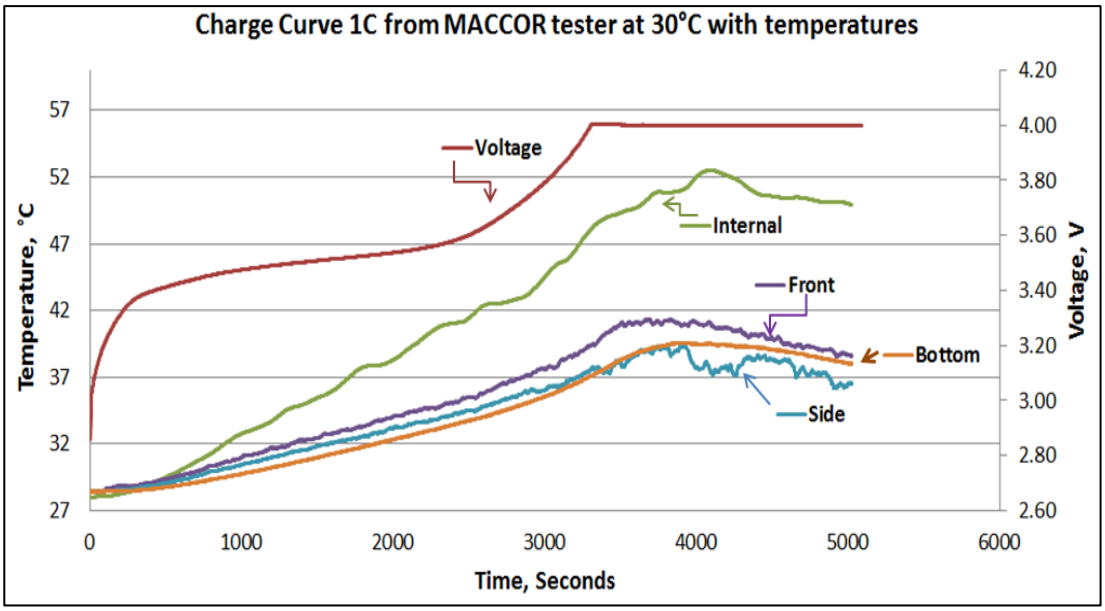

Figure 4.13 Charge Experiment with Temperature responses

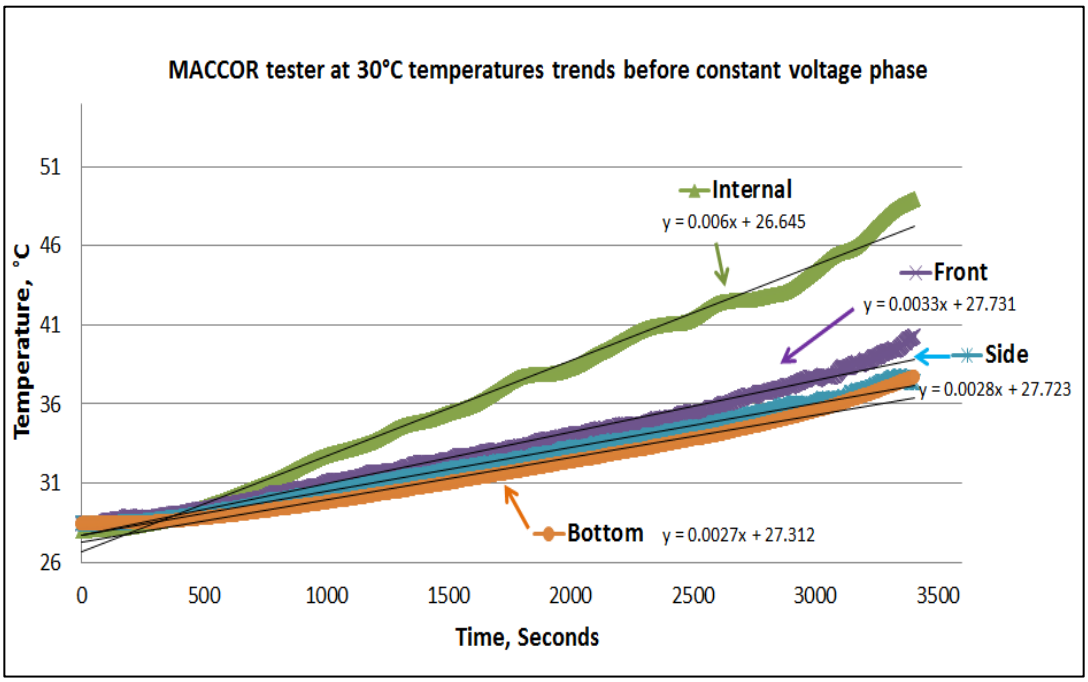

Figure 4.14 1C Charge Temperature trend

Figure 4.14 shows temperature trends for charge test in several measured locations before period which the temperature dropped at the constant voltage phase. Here, the temperature trends were shown to follow the same sense with discharge test temperature response. The surface temperatures (front, side and bottom) are in closed range with each other. For the trend internal temperature, it can be seen that the gradient steeper than the surface temperatures. This means the battery heats up faster from the inside. It is also observed that the temperature-time gradients of internal temperature in the discharge and charge test are closed to each other at around 0.006 to 0.007 from comparing this figure to figure 4.9. The surface temperatures measured from discharge and charge tests also produced the gradient in the same sense around 0.003 comparing to the same figure. Therefore, it can be concluded that the different test protocol (charge or discharge) can leads to the similar results of temperature response. Furthermore, the similar linear trend will also be observed in the test which combines both charge and discharge protocols in order to maintain the battery at the targeted state of charge. In this test, temperature-time gradient will be used for the calculation of one of the most important thermal properties, the heat capacity. In the next section, pulse current test will be performed to observe temperature trends, open circuit voltage recovery and internal resistance.

4.1.2 Pulse Current Test Results

From figure 4.15, the battery is discharged with 5 minute pulse rest by Agilent device at C/2 (30A) rate as recommended by the manufacturer (see specifications in Appendix A for reference). The result shows that voltage dropped dramatically to about 2.3 V (directly measured) after current was applied. Compared to actual voltage, the effect from resistance in battery cables makes the difference of 1 V. When load is off, voltage quickly recovered to 3.24 V which is closed to actual value. At the end of test, voltage reading from Agilent Electronic load was closed to 0.5 V but the actual voltage was about 2.2 V. It is also observed that voltage started to decrease quicker after the depth of discharge at 100%. To explain on the depth of discharge value of higher than 100%, the capacity applied in this test is according to the specification (60 Ah) but the results from this test found the capacity to be higher than expected. This is similar to the case of constant current discharge test with the results in figure 4.2, showing the depth of discharge at the end of test went over 100%. The results of discharge test after IR thermal sensor installation may show voltage drop before 100% due to the capacity reduction from the effect of reduction in active material as the battery was exposed to open air. The inaccuracy of voltage reading of Agilent device which resulted from internal resistance in the cable is observed again in this test. To eliminate this, MACCOR battery system was used because it has separated voltage cables in the system and thus provides simpler setup.

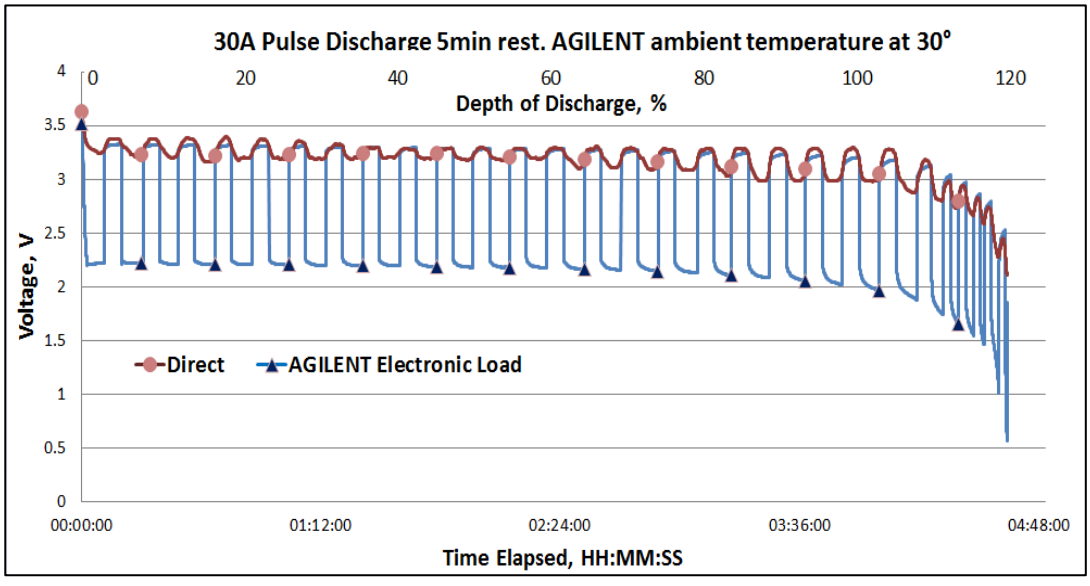

Figure 4.15 Pulse discharge curve from Agilent device

In figure 4.16, pulse test results performed on MACCOR battery system is shown. Here, it is observed the voltage started to drop quicker in 70% depth of discharge (DOD). This can be seen from the steeper curve of voltage reduction while loaded with current. At 90% DOD, when the battery was loaded, voltage dropped with steepest curve which approach the end condition of test at 100%.

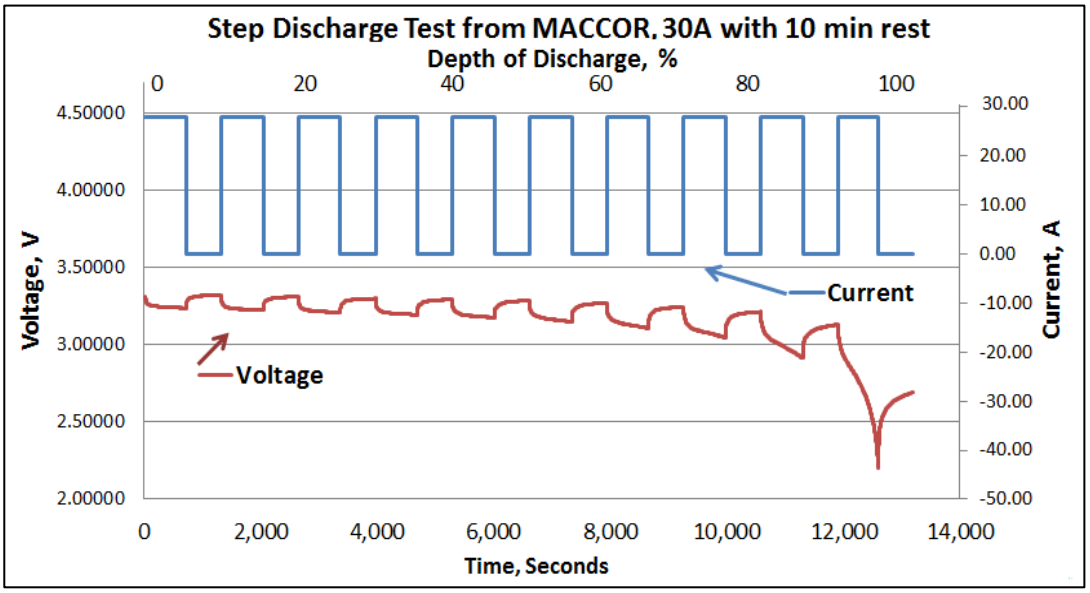

Figure 4.16 30A Pulse Current Test Voltage profile

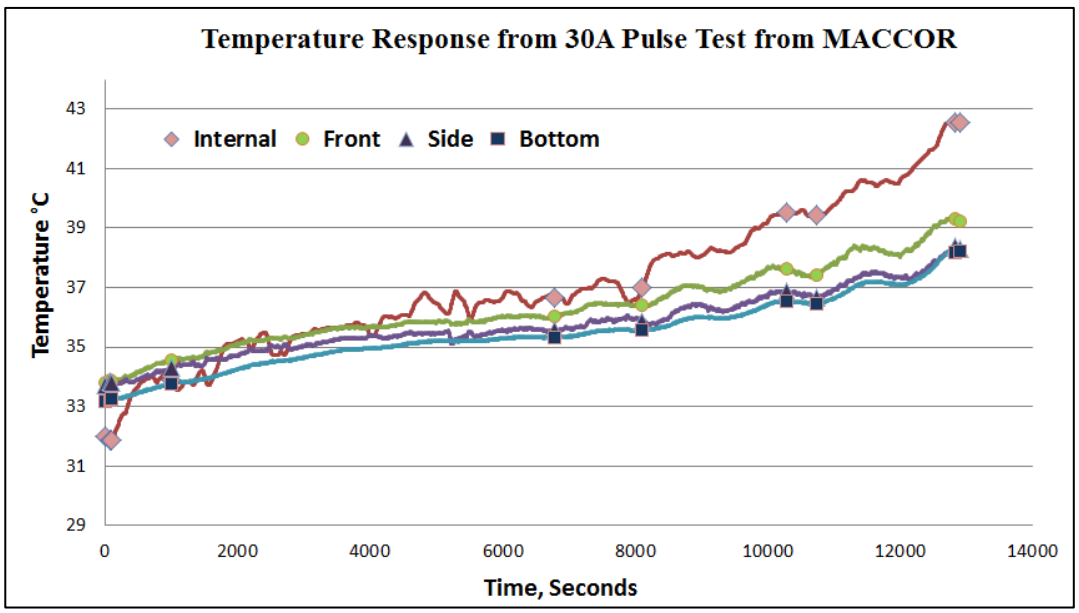

Figure 4.17 Temperature responses 30A Pulse Test

In figure 4.18, voltage and temperatures are plotted together. The temperature is shown to be related to the discharge and rest profile applied. The temperature fluctuated up and down to the current loaded and unloaded respectively. This behavior is more obvious from 60% depth of discharge and onwards as the temperature decreased at rest period (I = 0). The curve of internal temperature produced more fluctuated trend compared to the surface temperature because internal temperature was acquired from infrared sensor which got interruption from noise in the signal. Nevertheless, the temperature curve still shows same sense of trend as the surface temperature from 60% DOD as the voltage recover at rest period, internal temperature was also reduced.

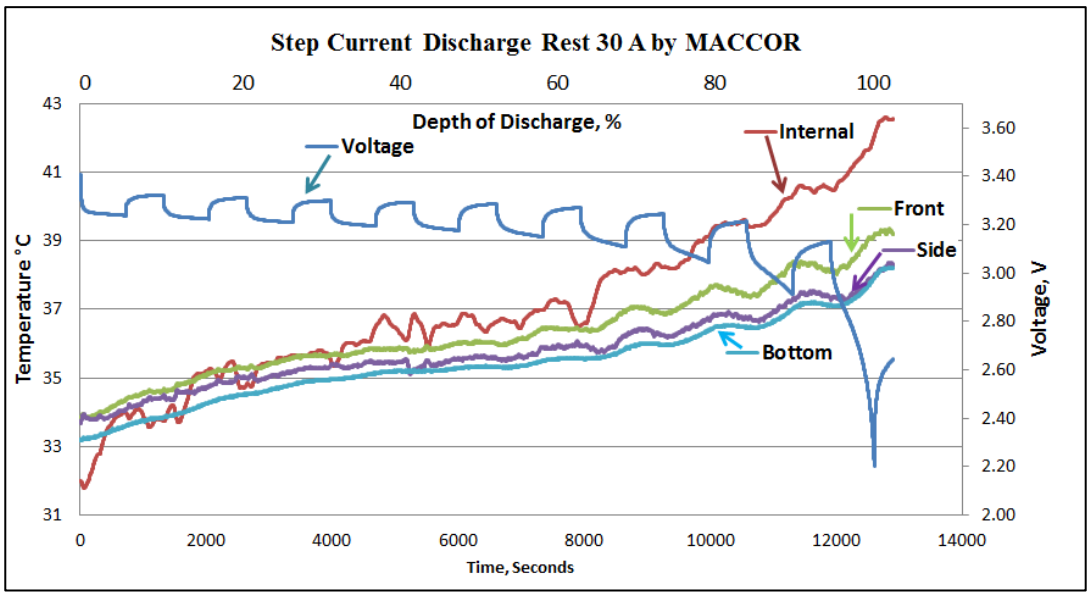

Figure 4.18 30A Pulse Test Voltage and Temperature response

4.1.3 Temperature (Entropic) Coefficient Test

In this test, the battery is put into thermal chamber in order to test to see the change in open circuit voltage effect on the change in surrounding temperature. This is performed for each state of charge from 0 -100% with 10% incremental. The result shown in figure 4.19 is from when the battery is in 20% state of charge. It can be seen that as the temperature increased, E_{eq} decreased. This makes the value of temperature or temperature coefficient becomes negative. On the other hand, at 60% SOC in figure 4.20, while the temperature is increased, E_{eq} also increased. This makes temperature coefficient becomes positive.

The selection of open-circuit voltage is from when the temperature of the battery becomes equilibrium. In this case of experiment, the condition is set to when the battery temperature reaches the environment temperature as to minimize the time. In table 4.1, open circuit voltage (E_{eq}) results are shown from each temperature coefficient test conditions. Note that the steady-state condition in each temperature can be time-consuming and therefore some of the data points were marked as dash (-) due to their unsteady condition.

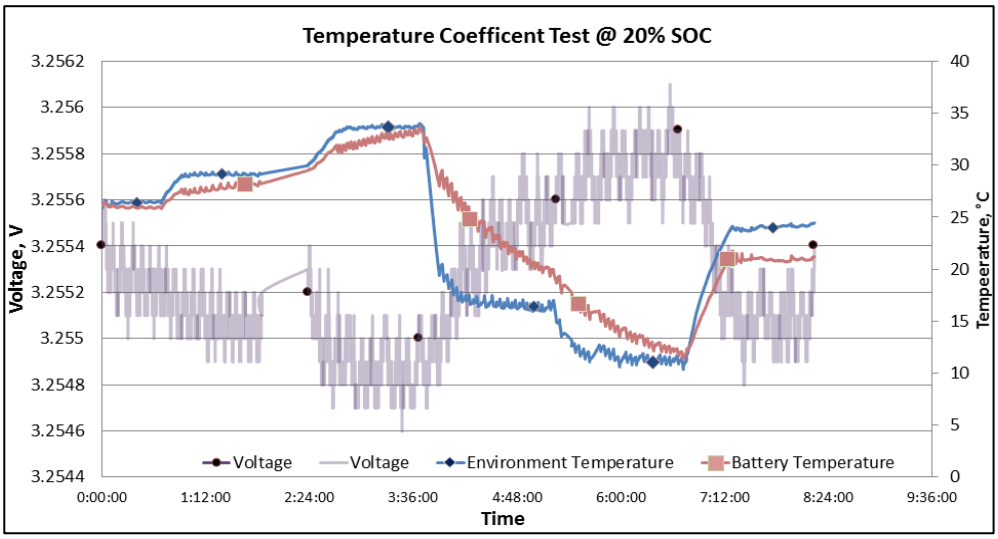

Figure 4.19 Temperature Coefficient Test at 20% SOC

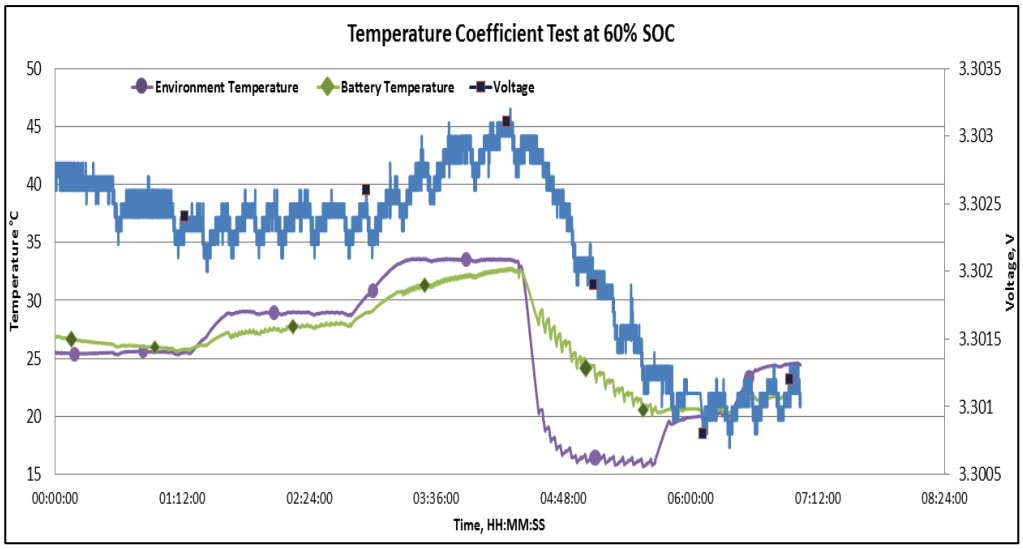

Figure 4.20 Temperature Coefficient Test at 60% SOC

Table 4.1 Open Circuit voltage at several conditions from temperature coefficient test

SOC/Temperature	10°C	20°C	25°C	30°C	35°C
0	3.042	-	3.0411	-	3.0387
10%	3.2152	3.2146	3.2139	-	3.2131
20%	3.2559	3.2554	3.2554	3.2552	3.255
30%	3.2794	-	3.2793	-	3.2791
40%	3.2936	3.2945	3.2958	-	3.2965
50%	3.295	3.2964	-	-	3.2989
60%	-	3.3013	3.302	3.3022	3.3029
70%	3.3061	3.3074	-	3.3091	3.3101
80%	3.3328	3.3335	-	3.3343	-
90%	3.3344	3.335	-	-	3.3359
100%	3.3409	3.342	-	-	3.3458

Table 4.2 Actual battery temperature measured from temperature coefficient test

SOC/Target Temperature	10°C	20°C	25°C	30°C	35°C
0	12.8°C	19.6°C	-	-	33.28°C
10%	12.152°C	20.3°C	27.21°C	-	32.9826°C
20%	12.2°C	20.8°C	26°C	29°C	33.59°C
30%	13°C	-	29.14°C	-	34.1°C
40%	13°C	18°C	24.5478°C	-	31°C
50%	11.69°C	19.72°C	-	-	33.15°C
60%	-	20.3°C	25.69°C	27.8°C	32.43°C
70%	11.19°C	19.7°C	-	27.12°C	33.57°C
80%	13.67°C	18.36°C	-	23.68°C	-
90%	12.1°C	20.2686°C	-	-	33.13°C
100%	11.694°C	15.4464°C	-	-	33.25°C

The measured temperatures of the battery which were closed to target temperature condition are shown in table 4.2. This is the temperature measured from the surface of the battery which approach to the condition of steady-state quicker than the internal temperature. So the surface temperature is regarded as the battery temperature as to save test time. The end results of

dE_{eq}/dT (temperature coefficients) are compared with the literature that use the similar type of battery and were found to follow the similar sense and values are in the same range. The calculation of dE_{eq}/dT was performed by plotting open circuit voltage with the battery temperature.

Linear regression of the plots provides the slopes which express the values of temperature coefficients. Figure 4.21 and 4.22 demonstrates the plot according to the 20% and 60% SOC conditions. From both figures, results of dE_{eq}/dT slopes are -0.04023 at 20% SOC and 0.13057 mV/°C at 60% SOC. To see these results for all SOC conditions, see Appendix F.

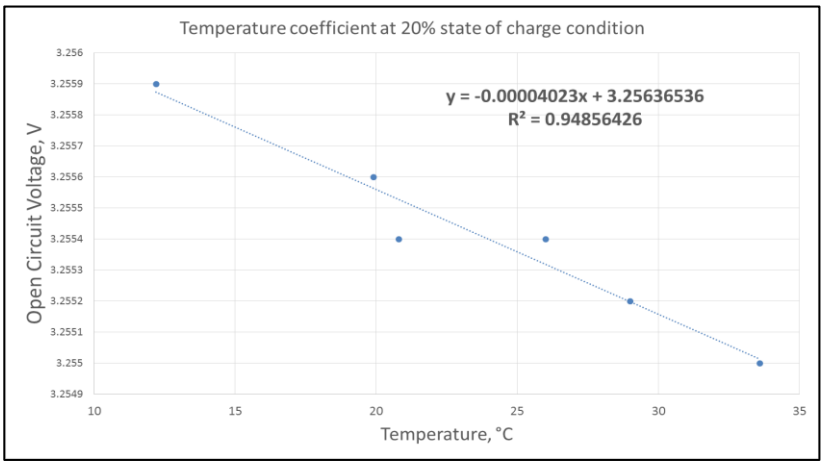

Figure 4.21 Plot of temperature vs. E_{eq} from 20% SOC equilibrium data points

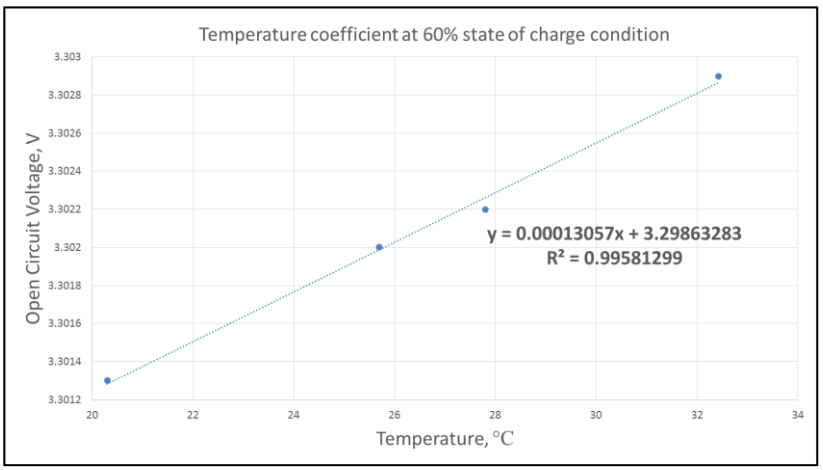

Figure 4.22 Plot of temperature vs. E_{eq} from 60% SOC equilibrium data points

When experiments are performed on all SOCs, the result according to above methods to acquire temperature coefficient (dE_{eq}/dT) is summarized in table 4.3 below for each SOC condition. It can be seen that from state of charge of 0 – 30%, the plot of voltage vs. open circuit voltage produce negative slopes (thus negative dE_{eq}/dT) and vice versa for SOC conditions from

40 – 100% (positive dE_{eq}/dT). Refer to the research with the similar battery type [42], the trend between dE_{eq}/dT and SOC does not show any relationship with each other. The result of dE_{eq}/dT compared to this literature also follow the same sense as negative values are produced from 0 – 30% SOC and positive values from 40 – 100%.

Table 4.3 Temperature coefficients results in each state of charge conditions

State of Charge	dE_{eq}/dT (mV/°C)
0	-0.1632
10%	-0.09978
20%	-0.04023
30%	-0.09326
40%	0.16462
50%	0.18219
60%	0.13057
70%	0.18358
80%	0.14986
90%	0.07121
100%	0.22295

4.1.4 Heat Capacity Test

From figure 4.23, the heat capacity test regarding to procedures explained in chapter 3, section 3.4.3 is presented. Here, it can be observed that the voltage is changing according to the current applied to maintain the average state of charge at 50% with pulse current of 1 C (see figure 4.24 for current load profile). The initial E_{eq} of the battery is at 3.22 V then it was discharged to reduce SOC by 4% to 3.10 V and charged to gain SOC by 4% to 3.45 V. Both trends of internal and surface temperatures of battery are increased in linear relationship and the temperature-time slope from linear regression will be used for heat capacity calculation. The calculation part will be shown in analysis part in chapter 5.

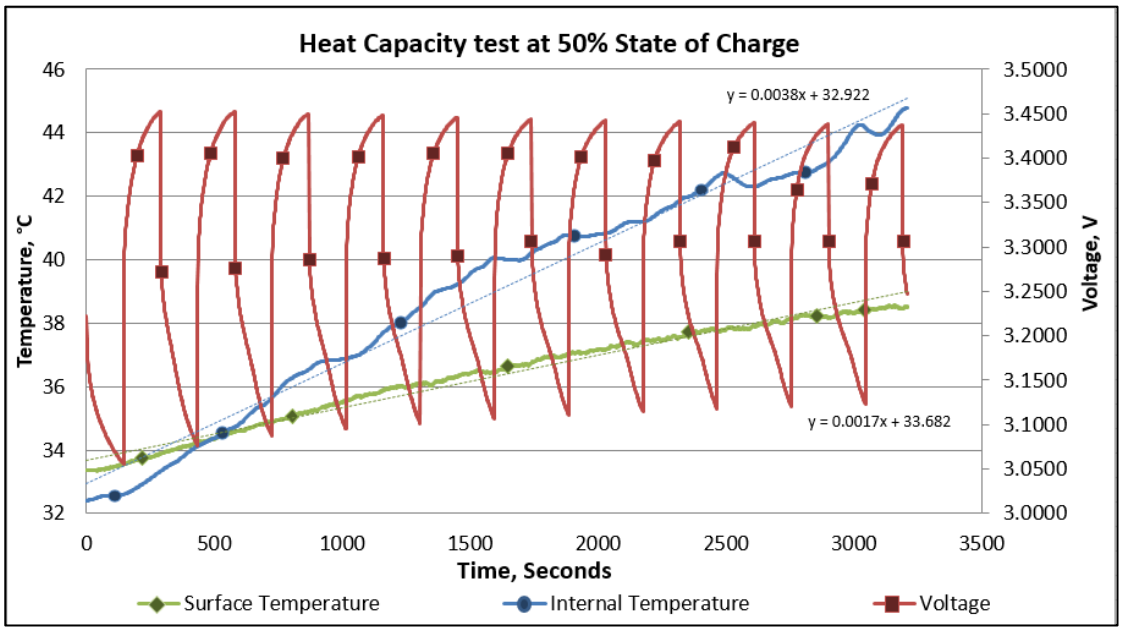

Figure 4.23 Results from heat capacity test

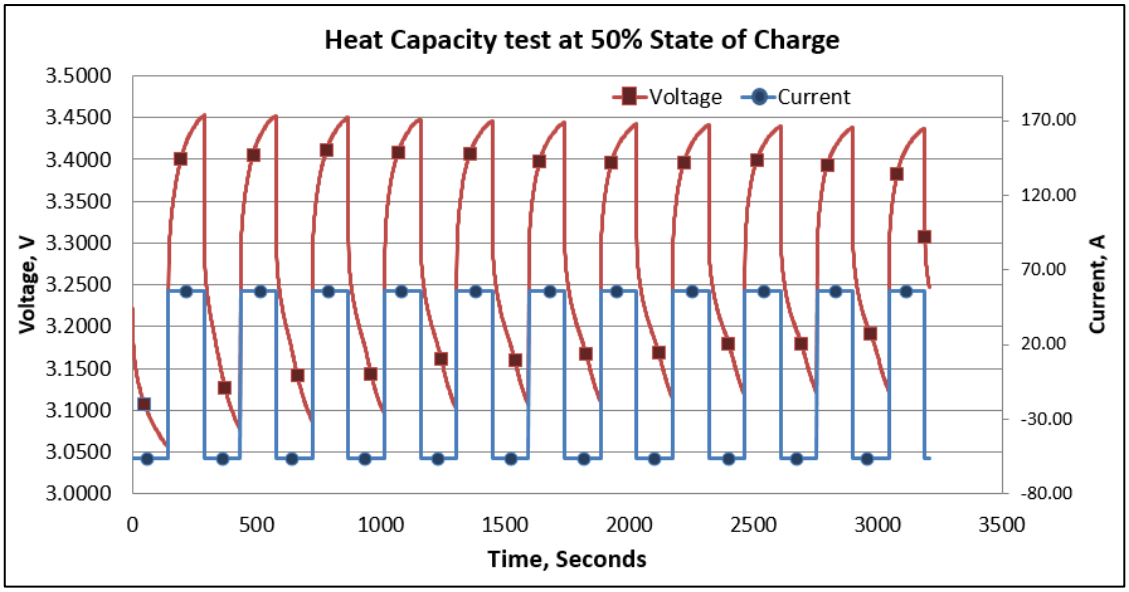

Figure 4.24 Voltage response from current applied in heat capacity test

CHAPTER 5

DISCUSSIONS AND ANALYSIS

5.1 Heat Generation from the Battery

From thermal model in equation 2.9, heat generation can be calculated from using the data in constant current test. Firstly, the over-potential term which depends on the difference between open circuit voltage (E_{eq}) and battery voltage (E) is focused. Table 5.1 shows parameters of calculation for this term in each state of charge (SOC). Here, electric current (I) is set to be negative value because the battery was discharged. From table 5.1, heat generated from over-potential fluctuated between 11 to 12 Watts at depth of discharge (SOC) from 90 to 50%. Then it made a significant rise from 15.1 – 26.4 Watts from 40 to 0% state of charge.

$$\dot{Q} = I(E - E_{eq}) + IT\frac{dE_{eq}}{dT} \tag{2.9}$$

Table 5.1 Parameters for calculating first term heat generation (I = 60 A)

SOC, %	E_{eq}, V	E, V	I, A	**I(E - E_{eq}), W**
100	3.5090	3.423	-60	**5.181963836**
90	3.3357	3.150	-60	**11.13765118**
80	3.3346	3.132	-60	**12.15198993**
70	3.3085	3.114	-60	**11.68463951**
60	3.3027	3.095	-60	**12.47191073**
50	3.2988	3.073	-60	**13.51966857**
40	3.2966	3.044	-60	**15.1455079**
30	3.279	3.002	-60	**16.63471275**
20	3.2554	2.940	-60	**18.91749966**
10	3.2139	2.832	-60	**22.92784298**
0	3.041	2.600	-60	**26.45176013**

Next, the chemical reaction term which is the second term of heat generation is analyzed (results shown in table 5.2). Here, this heat term mainly depends on the temperature coefficient (dE_{eq}/dT) which can be positive or negative, depends on the state of charge of the battery. According to heat generation equation, temperature must be in Kelvin scale and same to over-potential term, current is set to be negative due to discharge condition. The heat generated for this term of chemical reaction is positive (exothermic) and negative (endothermic) when temperature coefficient is negative and positive respectively. Table 5.3 summarizes both terms together.

Table 5.2 Parameters for calculating second term of heat generation (I = 60 A, 1C)

SOC, %	I, A	dE_{eq}/dT, mV/K	T_{in}, °C	T_{in}, K	**IT(dEeq/dT), W**
100	-60	0.22295	30.2038816	303.203882	**-4.055958324**
90	-60	0.07121	32.9649281	305.964928	**-1.307265752**
80	-60	0.14986	34.6679675	307.667967	**-2.766427296**
70	-60	0.18358	36.619032	309.619032	**-3.410391714**
60	-60	0.13057	38.7746245	311.774625	**-2.442504763**
50	-60	0.18219	40.3162326	313.316233	**-3.424985065**
40	-60	0.16462	42.6359487	315.635949	**-3.117599392**
30	-60	-0.01224	46.1132874	319.113287	**0.234356798**
20	-60	-0.04023	48.1826634	321.182663	**0.775270713**
10	-60	-0.09978	50.6727584	323.672758	**1.93776407**
0	-60	-0.1632	51.2990294	324.299029	**3.175536096**

For a sample calculation at state of charge of 50%, the parameters of calculations are battery voltage (E) = 3.073 V, open circuit voltage (E_{eq}) = 3.2988 V, temperature coefficient (dE_{eq}/dT) = 0.18219 mV/K and battery internal temperature (T_{in}) = 40.32 °C = 313.32 K. Then, first and second term of heat generation can be calculated according to equation 2.8 as below. Finally, the two terms are summed together as shown in table 5.3 in next page.

Over-potential heat term = $I(E - E_{eq}) = -60\times(3.073 - 3.2988) = 13.519$ W. Chemical Reaction heat term = $IT\frac{dE_{eq}}{dT} = (-60)\times(313.32)\times(0.18219\times10^{-3}) = -3.425$ W. Therefore, sum of both terms is 13.519 + (-3.425) = 10.094 W.

Table 5.3 Summation of heat generation in each state of charge (I = 60 A)

SOC, %	I(E - E_{eq}), W	IT(dEeq/dT), W	$\dot{Q}$ (W)
100	5.181963836	-4.055958324	1.126005512
90	11.13765118	-1.307265752	9.830385427
80	12.15198993	-2.766427296	9.385562633
70	11.68463951	-3.410391714	8.274247792
60	12.47191073	-2.442504763	10.02940597
50	13.51966857	-3.424985065	10.09468351
40	15.1455079	-3.117599392	12.0279085
30	16.63471275	0.234356798	16.86906955
20	18.91749966	0.775270713	19.69277037
10	22.92784298	1.93776407	24.86560705
0	26.45176013	3.175536096	29.62729622

At the start of discharge test from SOC 100% - 40%, the chemical reaction term of heat generation is negative (endothermic) due to the positive values of temperature coefficients and negative value of current discharged. At highest value of temperature coefficient at 100% SOC results in highest endothermic heat generation around 4 W but was compensated by over potential heat of around 5.18 W which produces the total exothermic heat generation of around 1.13 W. The rising temperature is also one of the main parameters which affect the heat generation. This can be seen from table 5.2 where the temperature rise when battery is running out of charges (0% SOC), the chemical reaction heat generation is increased from 1.94 to 3.18 W (by nearly 1 W) comparing to 10% state of charge.

The most affecting parameter on heat generation is the battery voltages. As time passed during the discharge test, the gap between battery voltage and open-circuit voltage become larger. With larger gap between two said voltages, over-potential heat generation becomes larger accordingly and therefore peaked at 0% SOC or 100% DOD (depth of discharge). As current is set to be constant in this test, it can be noticed that from Ohm's law that battery resistance plays that major role in this heat generation term as well. This will be investigated later as heat generation and battery resistance are compared together.

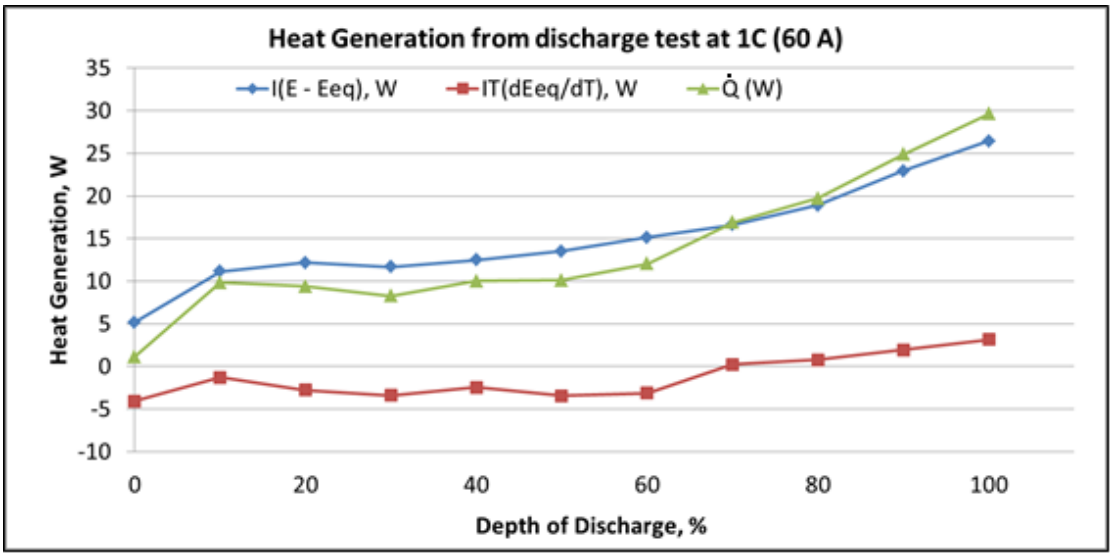

Figure 5.1 Calculated Heat Generation from 1C discharge test

It could be seen from figure 5.1 that at high loads of 1 C, the irreversible term of over-potential heat dominates the heat from chemical reaction which is resulted from the entropy change. However, comparing with lower loads, the chemical reaction heat has more effect on the total heat generation. Figure 5.2 shows the comparison of total heat generation at different current loads. The peaked value at 1 C rate is about 30 W which is much higher than the other two cases. The results of heat generation of both 30A (C/2) and 20A (C/3) loads have similar trend to each other from 10% - 60% depth of discharge. Then heat gradually increased from 60% (20A) and 70% (30A) but the peak values are far from that of 60A test. This shows that constant load at 1C or higher can create high temperature rise in the battery which can be harmful to the system.

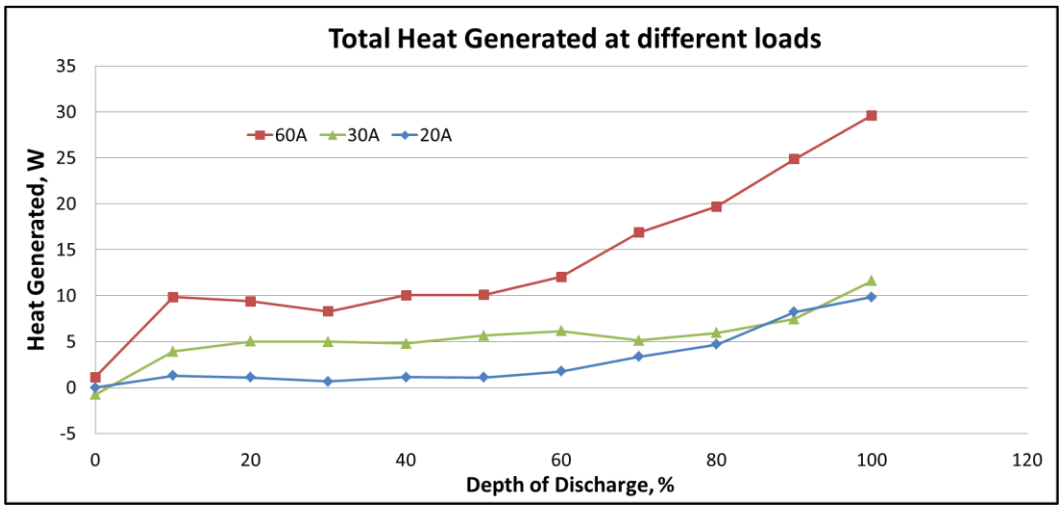

Figure 5.2 Calculated Total Heat Generation at different loads

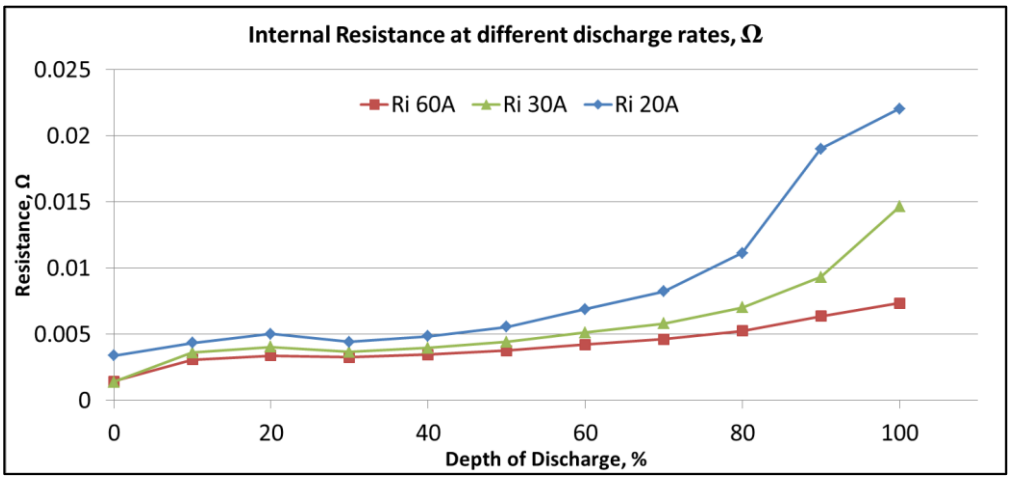

Figure 5.3 Calculated Internal Resistance from different discharge rate tests

Using ohm's law, figure 5.3 shows battery internal resistances at different discharge rates. This was calculated by using the difference between open circuit voltages at each state of charge (SOC) or depth of discharge (DOD) divided by the current rate applied for the discharge test. From the displayed result, the trends from 0 – 50% DOD are quite close to each other. From 60% DOD onwards, trend at 20A rate increased at higher rate than other conditions and peaked at 0.022 Ω. While at the highest discharge rate in the figure (60A) shows lowest peak internal resistance of 0.007 Ω. This confirms the better performance (lower resistance) under higher temperature operation (also higher heat generated) due to higher reaction speed. Figure 5.4 shows temperature trend which is in reverse of the resistance trend from figure 5.3.

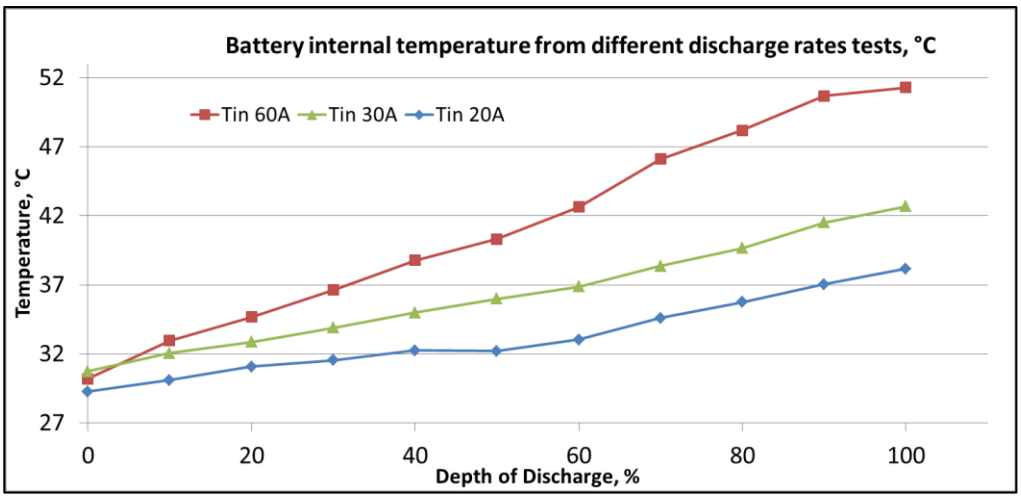

Figure 5.4 Calculated Internal Temperature from different discharge rate tests

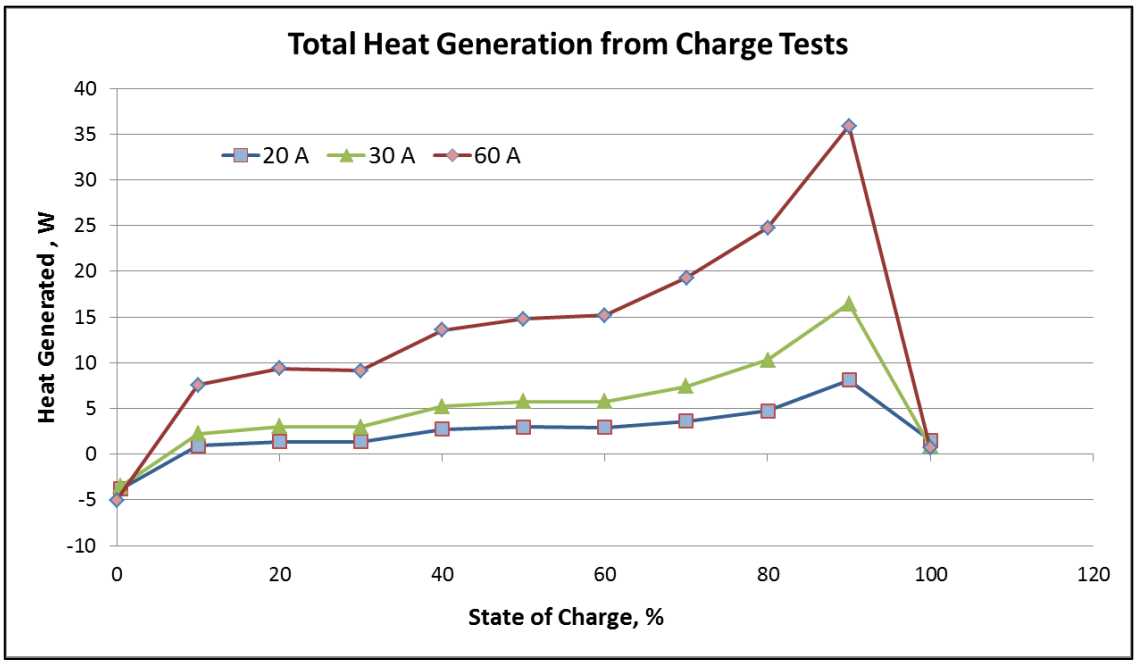

Figure 5.5 Calculated Heat Generated from charge tests

Using the same approach with the discharge test, heat generated in each test condition were calculated and plotted as shown in figure 5.5. It can be observed that at the SOC 0%, total heat generated is in negative value which is in endothermic mode for all charging current conditions. This is due to battery voltage is lower than open circuit voltage, causing the over-potential heat to be negative. Furthermore, the temperature coefficient is negative which cause chemical reaction term to be negative as well. Then it changed to exothermic mode (7.57 W at 60A) from 10% SOC onwards which shows the same trend as discharge tests where highest current supplied resulted in highest heat generation. The peak value of heat generation from the figure is about 35 W at 60A (1 C) current supplied and 90% SOC. However, when the battery was nearly fully charged to 100% SOC, current was reduced to nearly 1 A at constant voltage mode, causing the heat generation at fully charge (from over-potential and chemical reaction terms together) to be reduced to nearly 0. This demonstrates that current supplied or loaded has a major influence on the total heat generation.

5.2 Heat Transferred to the surroundings

From using the heat flux sensors mounted in three surfaces of the battery (see figure 3.19), the heat transferred to the surrounding can be calculated by using equation 2.13. The condition of ambient temperature is kept at approximately 30˚C. From the specification of the heat flux sensors, thermal resistance per unit area is 0.004 m^2·K/W with the surface area of the sensor is 0.001 m^2. Therefore, thermal resistance is 4 K/W. This results in outside heat transfer coefficient (h_{out}) to be 0.25 W/K. Surrounding heat was calculated for each axis and summarized in table 5.4. Figure 5.3 compares this heat term in different current rate.

$$\dot{Q}_B = h_{in}\left(T_{in} - T_{surf}\right) = h_{out}\left(T_{surf} - T_{amb}\right) \tag{2.13}$$

Table 5.4 Parameters for calculating heat transfer to the surroundings

DOD, %	T_x, °C	T_y, °C	T_z, °C	T_{amb}, °C	$\dot{Q}_B$, W
0	31.0255	30.9043	30.6050	30.2010	0.8652
10	31.9435	31.6736	31.2158	30.2010	1.8619
20	33.0785	32.7644	32.0026	30.2010	3.1720
30	34.1338	33.8725	32.8466	30.2010	4.4651
40	35.0903	34.7940	33.6842	30.2010	5.6139
50	36.1637	35.8145	34.5863	30.2010	6.8869
60	37.2761	36.8985	35.5236	30.2010	8.2199
70	38.4094	38.0345	36.6276	30.2010	9.6310
80	39.4671	39.0886	37.8828	30.2010	11.0012
90	41.3703	40.4827	39.5605	30.2010	13.0700
100	41.9043	41.4459	40.7703	30.2010	14.1214

Refer to table 5.4, a sample calculation at state of charge of 50%, temperatures at x (T_x), y (T_y) and z (T_z) axis measured according to figure 3.19 are 36.1637, 35.8145 and 34.5863 °C, with ambient temperature (T_{amb}) maintained at around 30°C. From equation 2.13 with outside thermal resistance known, heat transferred to the surrounding in each axis was calculated accordingly.

For x axis; $\dot{Q}_{B,x} = h_{out}(T_{surf,x} - T_{amb}) = 0.25 \times (36.1637 - 30.3586) = 1.4513$ W

For y axis; $\dot{Q}_{B,y} = h_{out}(T_{surf,y} - T_{amb}) = 0.25 \times (35.8145 - 30.3586) = 1.3640$ W

For z axis; $\dot{Q}_{B,z} = h_{out}(T_{surf,z} - T_{amb}) = 0.25 \times (34.5863 - 30.3586) = 1.0570$ W

The total sum of heat transfer to the surrounding in this case (50% SOC) then equal to the sum of heat in each side. There are two sides for x and y axis surfaces which heat can dissipate through. However for z axis only bottom surface is considered for the calculation because the top surface contains air gap between the core and the battery case, thus heat is assumed to dissipate to the sides instead (see figure 3.20 and 3.21 for battery internal structure). Thus the total heat transfer to the surrounding, $\dot{Q}_B$ is $(2 \times 1.4513) + (2 \times 1.3640) + (1.0570) = 6.6869$ W. Figure 5.6 shows surrounding heat resulted from this calculation at different discharge rate conditions. This parameter of heat depends on how much the battery surface temperature shift away from the ambient temperature. In the 60A discharge condition, temperature elevated at the fastest rate comparing to other conditions, thus heat dissipated to surrounding is highest which jumped to around 14 W at the end of test condition.

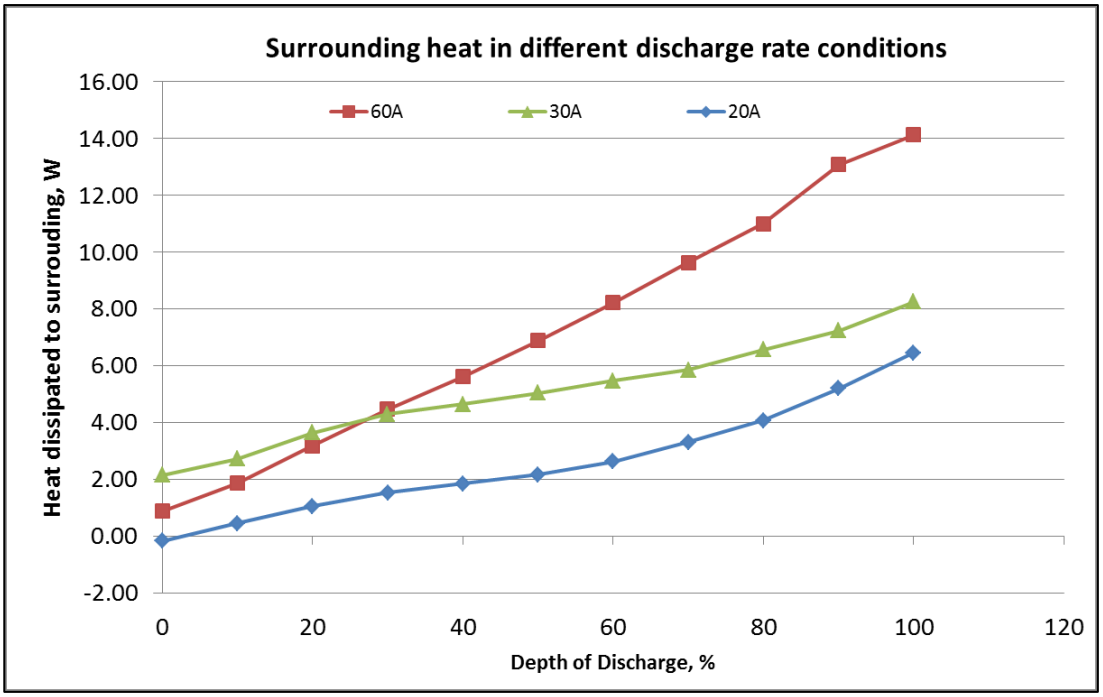

Figure 5.6 Calculated Heat Transferred to the surrounding at different discharge load

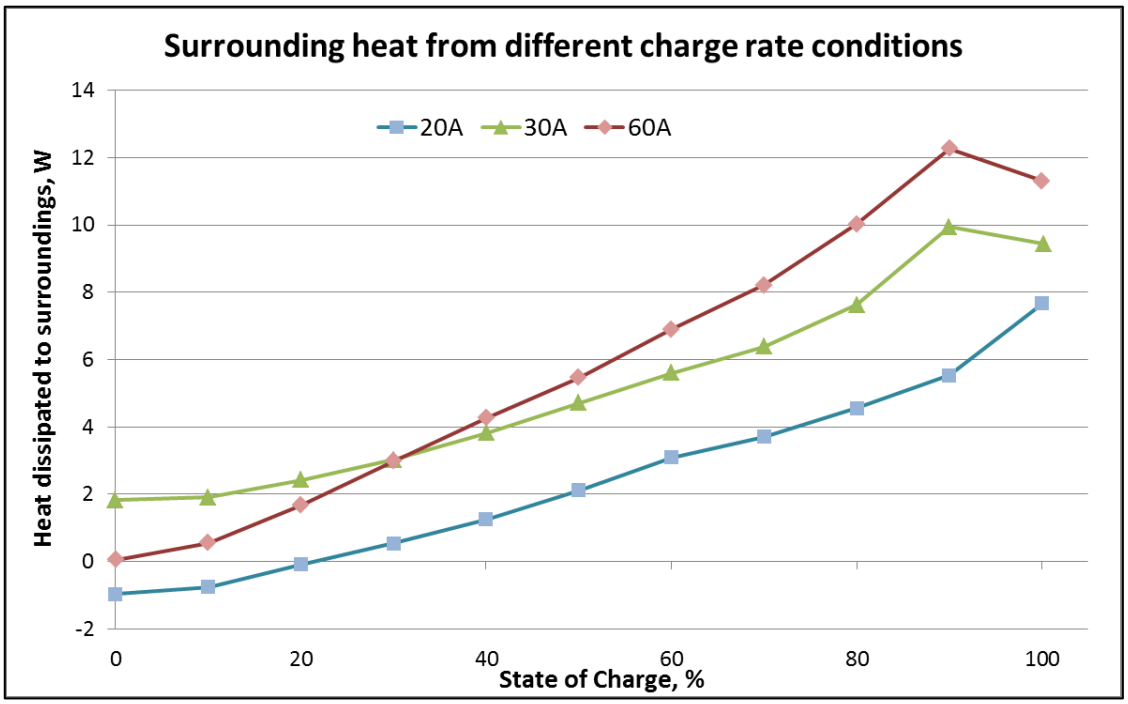

Figure 5.7 Calculated Heat Transferred to the surrounding at different charging condition

By applying the same method as discharge test explained previously, the surrounding heat dissipated in different charging conditions were calculated and plotted as shown in figure 5.7 above. The similarity between the two results from figure 5.6 and 5.7 is the heat trend which shows that peak value heat dissipated is from the highest current applied. However, at the start of the test for both charging and discharging, heat from 30A is higher than 60A condition. This is from the initial temperature of the battery surface is higher than the surrounding temperature. Then after 30% SOC, surrounding heat dissipated at 60A grew above the 30A condition. For charge test at 60A and 30A, heat is dropped at 100% SOC, this is from the temperature reduction near the end of test due to current is reduced in charging with constant voltage mode. It is also observed at 100% SOC of charging test at 20A, heat kept increasing due to the slower temperature reduction when current reduced in constant voltage charging process was triggered. This demonstrated that with lower charging current, it takes shorter time to reduce current in constant voltage mode and thus temperature reduction becomes slower in the process. Note that in discharge test, heat dissipated is peaked at 100% DOD (0% SOC) because there is no temperature reduction due to current stay constant for the whole process. Therefore, heat dissipated resulted from discharge test is shown with higher peak than that from charge test.

5.3 Heat Capacity

This thermal property was approached by using the pulse test method which includes both charging and discharging to maintain the battery average state of charge (SOC) to be constant (refer to figure 3.40 for test process). From figure 4.23, battery SOC was maintained at average of 50%, current is loaded and supplied to maintain the SOC between 48% and 52% (±2%). To calculate for heat capacity, equation 2.12 was used with the data at which the battery was at 50% SOC. To seek the state of charge at 50%, amp-hour values charged and discharged were observed. In this case, the battery capacity is 60 Ah then 2% of this is 1.20 Ah. Thus, data points at 1.20 Ah charged and discharged were used for the heat capacity calculation. Note that capacity was reduced due to infrared sensor installation which exposed the battery core to air and thus disturbed the active material. Figure 5.8 below shows the voltage profile from this experiment and the rhombus shape points are when battery was maintained at SOC of 50%.

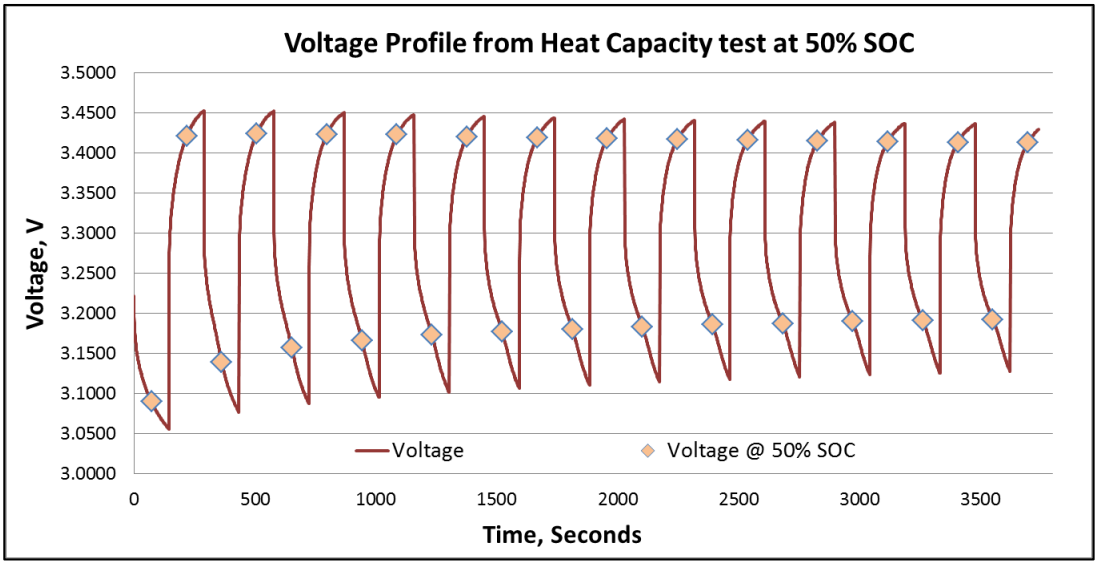

Figure 5.8 Voltage profile from heat capacity test

The calculation in this case starts with heat generation for both over-potential and chemical terms with same approach explained previously. Then heat transfer to the surrounding is also calculated in the same manner. Then the battery temperature from this test is plotted against time to find the temperature-time gradient, dT/dt (see figure 4.25). Finally with all parameters together, heat capacity is calculated from equation 2.12. Table 5.5 shows parameters for this calculation.

Table 5.5 Parameters for calculating heat capacity (SOC maintained at 50%)

Time elasped (s)	(OCV-V)I, W	IT(dV/dT), W	Q_B, W	dTsurf/dt	C_p, (J/K)	$C_{p\ Avg}$, (J/K)
363	8.926748813	-3.104295158	3.400064606	0.0017	1424.9347	2112.838087
1088	6.949812345	3.139070753	5.279222081	0.0017	2829.2124	2112.838087
1378	6.830181613	3.158211664	5.844344805	0.0017	2437.6756	2112.838087
1523	6.807610498	-3.16499287	6.17436027	0.0017	1489.2604	2112.838087
1668	6.761600097	3.167887803	6.422347035	0.0017	2063.024	2112.838087
1813	6.636820752	-3.173320799	6.760340291	0.0017	1939.3178	2112.838087
1958	6.676370672	3.17549737	6.929874608	0.0017	1718.8197	2112.838087
2103	6.483115802	-3.179672633	7.217275163	0.0017	2302.2541	2112.838087
2248	6.625100359	3.183739874	7.374255086	0.0017	1432.1089	2112.838087
2393	6.329095395	-3.189782461	7.644549656	0.0017	2650.1392	2112.838087
2683	6.226556444	-3.193815619	8.055343384	0.0017	2954.4721	2112.838087

From table 5.5, the temperature-time gradient (dT/dt) from battery surface temperature measurement is used because the whole battery to the surface is considered for calculation boundary. The average value of heat capacity ($C_{p\ Avg}$) is then approximately 2112.84 J/K. Figure 5.9 shows the trend of calculated heat capacity compared to battery temperature trend. Also, the average value of heat capacity is plotted in dashed line. This shows no significant trend between heat capacity and battery temperature.

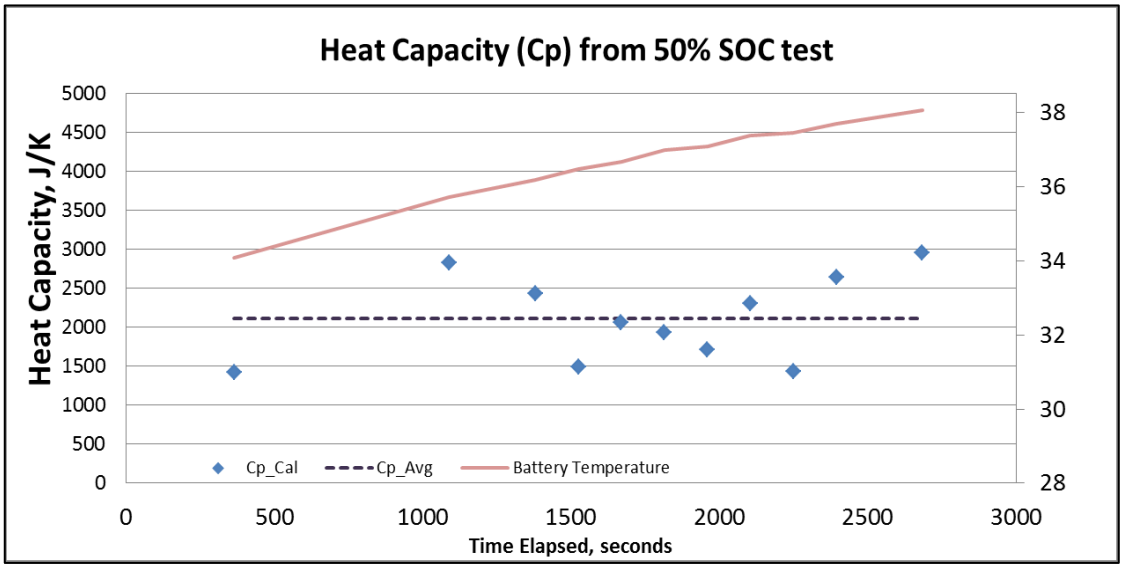

Figure 5.9 Calculated Heat Capacity from 50% SOC test

The external heat transfer coefficient which is a part of surrounding heat ($\dot{Q}_B$) calculation according to equation 2.13 can be obtained from the specification of heat flux sensor. Such specification is called "thermal resistance" (R_{in}) which is reciprocal to heat transfer coefficient. With this value known with measurable temperatures (surface and surrounding), surrounding heat can be calculated. To find internal heat transfer coefficient, equation 2.12 is also considered in steady-state condition ($\frac{dT_{in}}{dt} = 0$). In this condition, equation will be left with heat generation and heat surrounding terms. Therefore, temperature trend from heat capacity test is plotted (figure 5.10) to observe steady-state condition in the test.

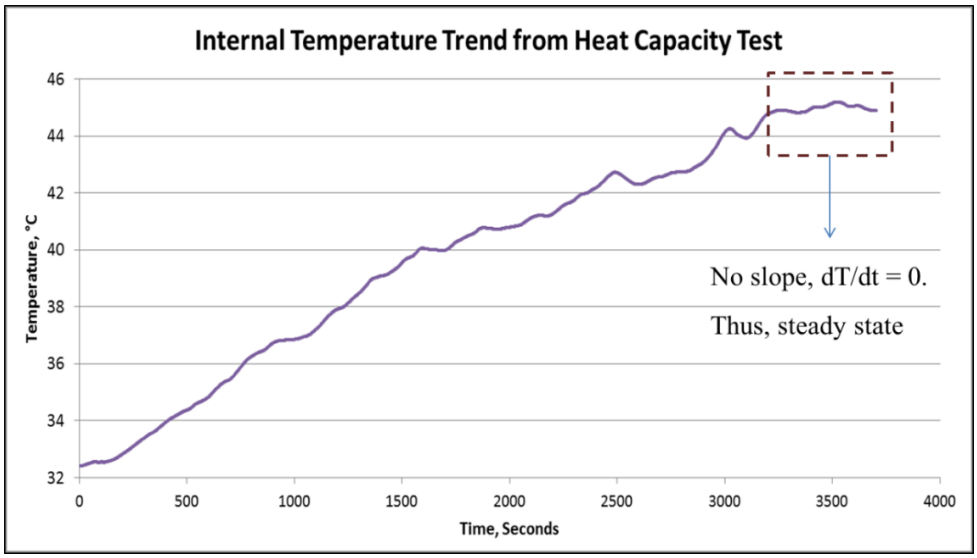

Figure 5.10 Internal temperature trend from heat capacity test

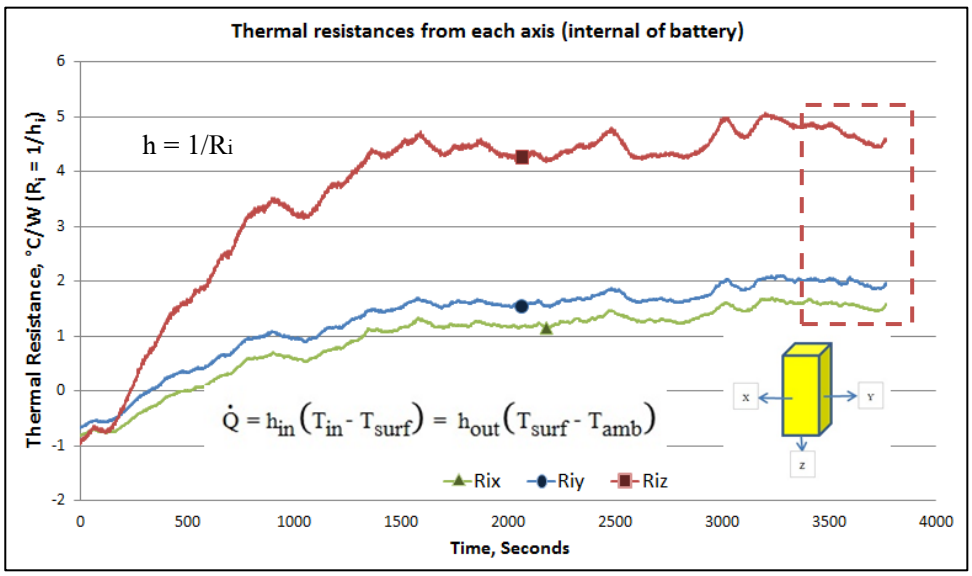

Figure 5.11 Calculated Battery Internal Thermal resistance

From figure 5.10, the steady state condition was shown to be about 3500 seconds later after running the heat capacity test. Here, the information of voltage, current, temperatures and external heat transfer coefficient are applied to the shown equation in figure 5.11 to find h_{in}. At the steady state point where dT/dt becomes zero , thermal resistances at axis x, y and z are calculated as 1.61 °C/W , 1.96 °C/W and 4.89 °C/W respectively. Table 5.6 shows the result for internal heat transfer coefficient for each axis. For better understanding, figure 5.12 is formed to explain on the process of heat transfer coefficient approach. In next chapter, analysis will be put on obtained data for further calculations of important thermal parameters such as heat generation and heat capacity.

Table 5.6 Internal heat transfer coefficient from heat capacity test at 1C (60 A) current pulse and 50% state of charge

Axis (Orientation)	Thermal Resistance °C/W	Heat Transfer Coefficient W/°C
X (Front)	1.61	0.62
Y (Side)	1.96	0.51
Z (Bottom)	4.89	0.20

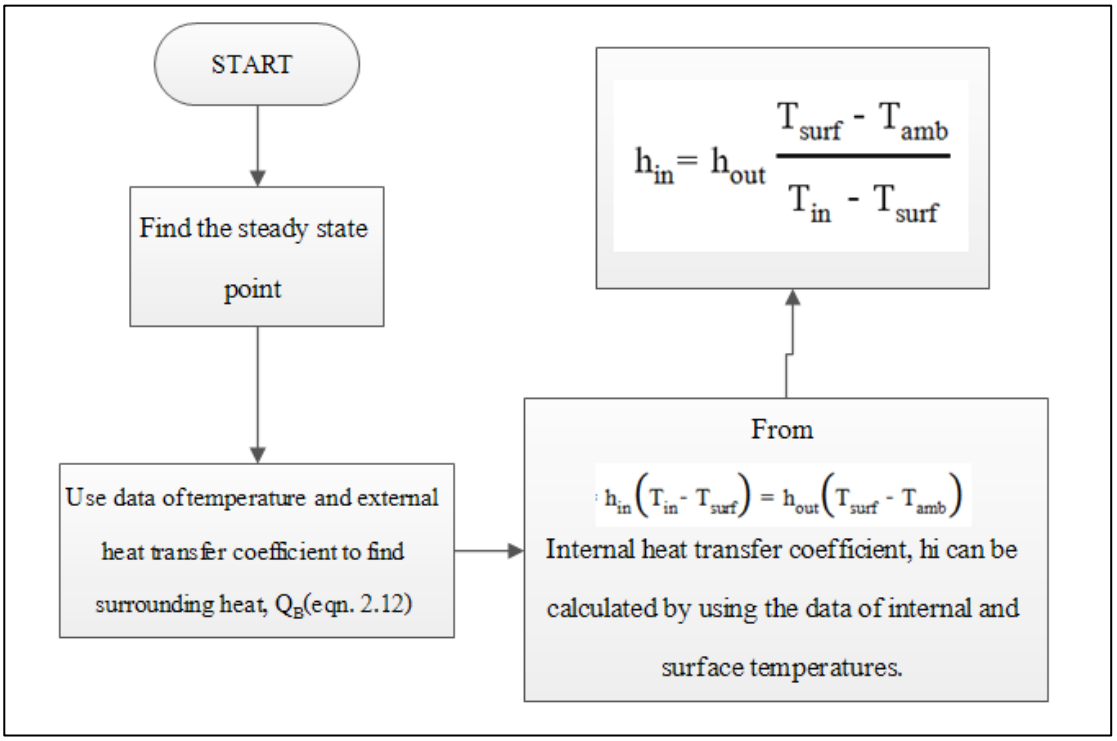

Figure 5.12 Process of the internal heat transfer coefficient approach

Table 5.7 Summarize of thermal properties from this work

Thermal properties	Values
Heat Generation ($\dot{Q}$)	1.126 – 29.627 W
Heat Capacity (C_p)	2112.84 J/K
Coefficient of heat transfer (h_{in})	0.2 – 0.62 W/°C

To summarize the thermal properties, table 5.7 is formed. The purpose is to compare them with the data obtained from the literatures (summarized in table 2.6). Note that the heat generation is taken from 60A discharge test. For heat generation per unit area, the tested battery in this work yields peak value of 348.06 W/m^2, this use the dimension of the battery specified in figure 3.1 for the calculation. The heat capacity per unit mass is 0.917 kJ/kg·K based on the battery mass of 2.3 kg. The coefficient of heat transfer per unit area is 26.552 W/m^2K, calculated based on dimensions stated in figure 3.1 also. Comparing to results from reviewed literatures, the chosen battery in this work tends to generate higher heat rate [38, 40, 41]. The factors which affect this can be from size, chemistry, dimension, test conditions and environment conditions. However, the results of heat capacity per unit mass are relatively comparable to each other, especially for similar type of battery from the work of Forgez et al [42] (Lithium iron phosphate, $LiFePO_4$) and also close to the calculated heat capacity from material percentage described in the instruction manual (see Appendix A). The coefficient of heat transfer to the surrounding per unit area is higher than results reviewed also. This indicates that heat can transfer better from internal to surface of the battery and thus, temperature can rise at quicker rate compare to other types.

From the designed experiments for thermal properties of selected lithium ion battery, heat generation was calculated and analyzed by referring directly to the battery thermal model unlike some review literatures [3], [41]. The result of higher heat generation compared to reference literature is due to the bigger size. The approach to calculate surrounding heat and heat capacity was simplified by using heat flux gauge. Then calculation of battery heat capacity could be done without considering the steady-state temperature condition because the coefficient of external heat transfer to surroundings (h_{out}) is already known from the specification of heat flux sensor. However, steady-state condition is considered for internal heat transfer coefficient (h_{in}) analysis and summarized in table 5.7. Above all, the whole process of thermal properties analysis was done without using calorimeter device which requires complex setup and financial support for materials and equipment for the system.

5.4 Open Circuit Voltage Prediction

In the analysis for open circuit voltage (E_{eq}), results from pulse test is considered. This will look into the dynamic of E_{eq} change from the change of battery SOC. As well as the determination of rest time to see the steady point when E_{eq} remains constant. The focused period in the test is from when pulse load is terminate and introduce the rest period to the battery until the point when it is loaded again (see figure 5.13 in the dash line area). Here, the behavior of voltage recovery will be observed and analyzed for the fitting equation. To obtain the voltage profile data, the battery is discharged with current load of C/3 of its capacity until the DOD reached up by 10%. Then the load is stopped so the voltage can recover to steady open circuit voltage. In this case, 2 hours of rest time is applied. Notice from figure 5.13 that when current load was turned off, the voltage profile tends to be quite flat. This is because voltage recovered suddenly at the time of load termination and then slowly progressed to open circuit voltage. When the battery was discharged to 90% DOD and rest, obvious trend of voltage recovery is shown and the recovery profile is not as flat as earlier conditions. When the battery is discharged to 100% DOD, voltage was reduced rapidly to around 2.6 V. This also shows the obvious trend of voltage recovery to approximately 2.9 V. Next, data at 50% DOD will be focused as a sample of analysis to determine voltage recovery behavior.

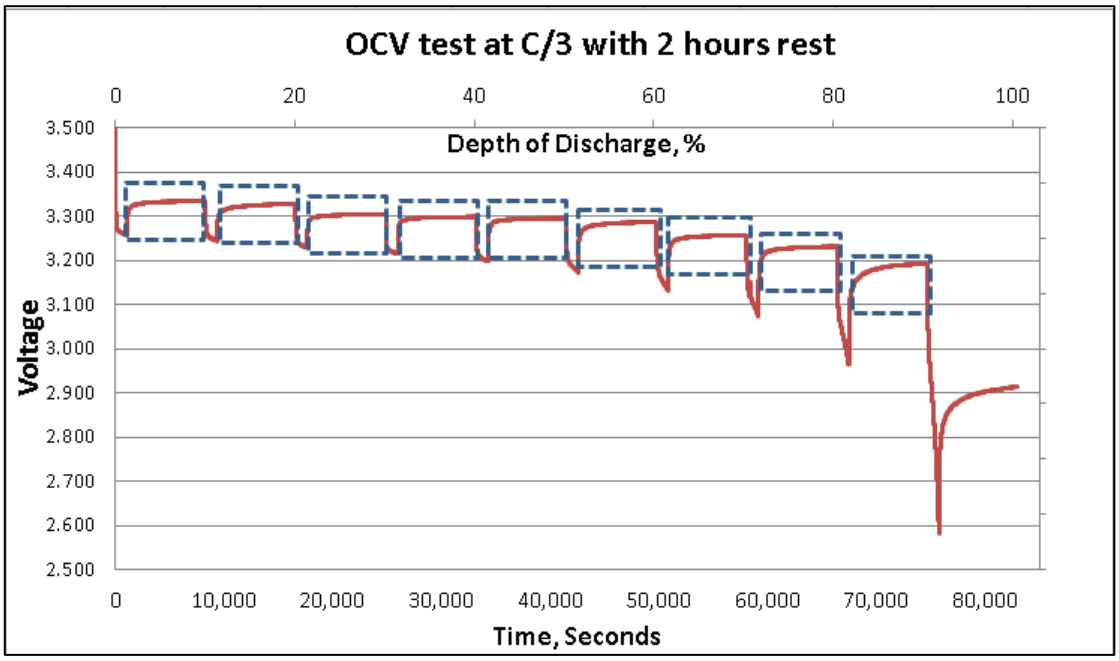

Figure 5.13 Voltage profile from C/3 (20A) pulse test for E_{eq} prediction

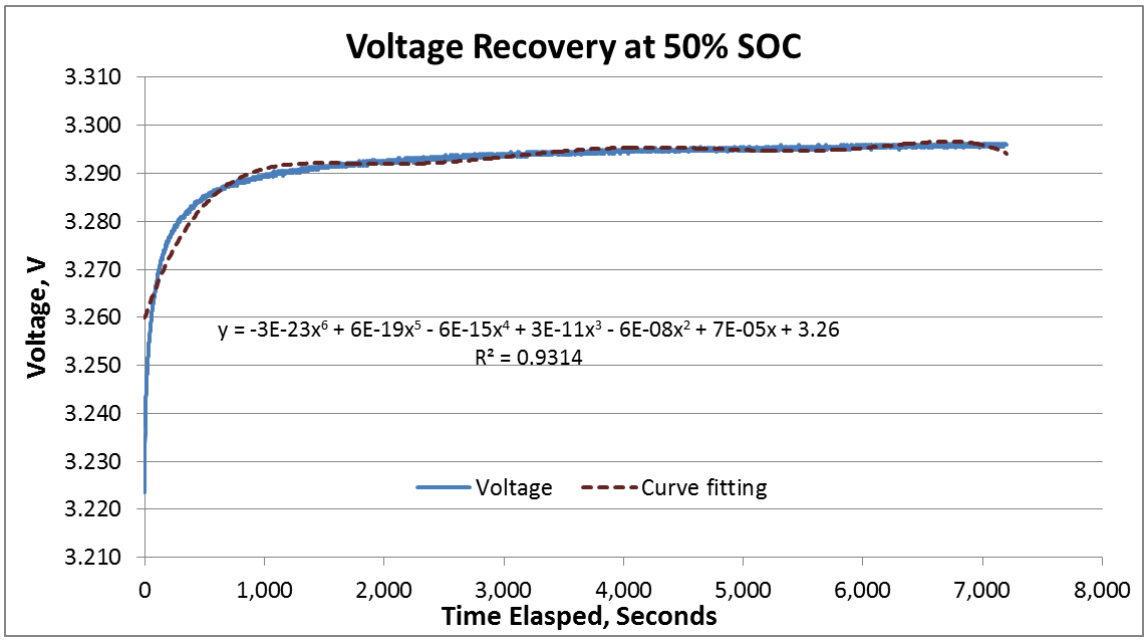

Figure 5.14 Voltage recovery at 50% SOC

The analysis of voltage recovery behavior at 50% SOC is shown in figure 5.14 above. The x-axis shows elapsed time since it was put to rest mode for two hours (current, I = 0) up until it current was applied again. The normal line shows the plot of actual E_{eq} recovery and dashed line shows the trend line of fitted curve. From the figure, voltage started to recover from 3.224 V which increased to 3.295 V in about 3600 seconds or 1 hour. From this point, it took another hour to recovery to 3.296. In the scale of 3 decimal points, the steady point of voltage is uncertain but if considers 2 decimal point scale which is the standard for most typical volt-meter, voltage was recovered to 3.33 V with the rest time of about 1 hour. Sixth order polynomial relationship is demonstrated between voltage (y-axis) and time (x-axis) in the same figure. It can be observed that this model is quite accurate when the voltage starts to reach 3.26 V. This is suitable for E_{eq} analysis because the purpose of this is to determine the value of fully recovered E_{eq}, thus the earlier part which is not applicable to the fitted equation can be ignored. Take note that in battery specification, the standard discharge current is C/2 which applied in previous pulse test. However, for better understanding in open circuit voltage recovery behavior, C/3 discharge rate was applied here to allow the voltage to recovery faster due to less voltage reduction while discharging. For data in other SOC and table of open circuit voltage by SOC, please refer to the Appendix F.

CHAPTER 6

CONCLUSIONS AND SUGGESTIONS

6.1 Conclusions

- Experimental procedures for determining thermal performance and properties of selected lithium ion battery was proposed and developed. The approach for this is to modify from the combination of procedures which performed in similar research works. This designed procedure proposed to obtain heat generation and heat capacity by using results from charge and discharge tests applied to thermal model. Therefore, this does not need to use calorimeter for analysis which reduces equipment expense, simpler and applicable to other types of batteries.

- Trend of discharge and charge test results proves to be accurate according to theory. Results from constant discharge test shows that the peak temperature at 1C discharge rate does not exceed the limit which suggested in the specification manual (60 ºC). It was found that the temperature rise rate depends on the rate of current applied to the battery and proved to be linear relation with time.

- The result of heat generation in different discharge rates shows that chemical reaction heat term only affects at the start of the test. After that, over-potential term is the main factor which impact the total heat generation. For surrounding heat transferred, the value directly depends on the temperature rise of the battery. The internal heat transfer coefficient was calculated and also found to be relatively close to reviewed literature. It is also observed that higher current discharge applied can produce less internal resistance calculated from ohm's law.

- For heat generation in charge test, same trend as discharge test was shown except at the end which the value dropped because of current reduction in constant voltage phase. This also applied to surrounding heat transferred which reduced at the end of test (except for 20A condition) due to temperature drop as a result from current reduction.

- The calculated heat capacity was averaged to be about 2112 J/K. This is relatively close to reviewed literature with the similar lithium ion battery chemistry.

- Study of open circuit voltage shows that the E_{eq} recovery can be expressed in the function of sixth degree polynomial but the derived model is application after a period of recovery time.

6.2 Suggestions

Although this work was finished, it was only the first step for studying the thermal properties in lithium ion batteries. Following suggestions can be applied to improve this work:

- Infrared thermal sensor output should have the proper filter to obtain more accurate temperature results with less or no noise disturbance. Thermocouple output is recommended in this case.
- Programmable Thermal chamber can be applied to battery for more data on open circuit voltage vs. environment temperature for calculating temperature coefficient and assist in this time consuming procedure as to let the system run automatically.
- Other means of determining the internal resistance can be applied such as impedance spectroscopy for more accurate result.
- Since the selected lithium ion battery is for the purpose of powering converted electric vehicle. Actual power profile from driving cycle can be applied when discharging the battery. This can help to observe the actual heat generation in driving condition.
- The simulation program can be used to compare and support with heat generation analysis and prediction when the battery is performed in various conditions. This can help to save time and cost of experimental setup.

REFERENCES

[1] Buchmann, Isidor. Batteries in a Portable World. 2 ed: Cadex Electronics Inc., 2001. Print.

[2] Lawson, Barrie. "Cell Construction". 2005. <http://www.mpoweruk.com/cell_construction.htm>.

[3] Kazuo Onda, Takamasa Ohshima, Masata Nakayama, Kenichi Fukuda, Takuto Araki. "Thermal Behavior of Small Lithium-Ion Battery During Rapid Charge and Discharge Cycles." Journal of Power Sources 158 (2005): 535 - 42. Print.

[4] De-Leon, Samuel. "Battery Seminar Battery Technology Mid Term Forecast". 2011. Shmuel De-Leon Energy Ltd. <http://www.sdle.co.il/AllSites/809/Assets/20%20-%20battery%20mid%20term%20forcast%20v1.pdf>.

[5] Dinger, Andreas. "Batteries for Electric Cars: Challenges, Opportunies, and the Outlook to 2020." (2009): 18 pp. <https://www.bcg.com/documents/file36615.pdf>.

[6] Richmond, Randy. "Lithium-Ion Batteries for Off-Grid Systems." (2013). <http://www.homepower.com/articles/solar-electricity/equipment-products/lithium-ion-batteries-grid-systems>.

[7] Buchmann, Isidor. "Types of Lithium-Ion". 2015. CADEX Electronics. <http://batteryuniversity.com/learn/article/types_of_lithium_ion>.

[8] Muratori, Matteo. "Thermal Characterization of Lithium-Ion Battery Cell." POLITECNICO DI MILANO, 2009. Print

[9] Linden, David. Handbook of Batteries. 3 ed: R. R. Donnelley & Sons Company, 1995. Print.

[10] Schweiger, Hans-Georg. "Comparison of Several Methods for Determining the Internal Resistance of Lithium Ion Cells." Sensors 10 (2010): 5604-25. Print.

[11] Lawson, Barrie. "Lithium Battery Failures." (2005). <http://www.mpoweruk.com/lithium_failures.htm>.

[12] Fuller, John. "What Is the History of Electric Cars?" (2009). <http://auto.howstuffworks.com/fuel-efficiency/hybrid-technology/history-of-electric-cars1.htm>

[13] "General Motors Ev1." (2015). <http://en.wikipedia.org/wiki/General_Motors_EV1>

[14] Buchmann, Isidor. "Comparison Table of Secondary Batteries." (2015). <http://batteryuniversity.com/learn/article/secondary_batteries>.

[15] "List of Modern Production Plug-in Electric Vehicles." (2015). <http://en.wikipedia.org/wiki/List_of_modern_production_plug-in_electric_vehicles>.

[16] Yevgen Barsukov, Jinrong Qian. Battery Power Management for Portable Devices. Artech House, 2013. Print.

[17] Pop, Valer. Battery Management Systems Accurate State-of-Charge Indication for Battery Powered Applications. Philip Research. Vol. 9: Springer, 2008. Print.

[18] Lawson, Barrie. "Battery Life (and Death)." (2005). <http://www.mpoweruk.com/life.htm#arrhenius>.

[19] Matthew Zolot, Ahmad Pesaran, Mark Mihalic. "Thermal Evaluation of Toyota Prius Battery Pack." SAE International (2002). Print.

[20] "The Chevrolet Volt Cooling/Heating Systems Explained." (2010). <http://gm-volt.com/2010/12/09/the-chevrolet-volt-coolingheating-systems-explained/>.

[21] Siddique A. Khateeb, Shabab Amiruddin, Mohammed Farid, J. Robert Selman, Said Al-Hallaj. "Thermal Management of Li-Ion Battery with Phase Change Material for Electric Scooters: Experimental Validation." Journal of Power Sources 142 (2005): 345 - 53. Print.

[22] Heyer, Benjamin. Battery Testing Apparatus. 1937.

[23] Benham, Harold. Battery Thermal Runaway Monitor. 1977.

[24] Esrom, Hilmar. High-Temperature Storage Battery. 1985.

[25] Harm, Charles. Battery Charger with Thermal Runaway Protection. 1993.

[26] Stephen McShane, Oak Brook, Mark, Hlavac, New Lenox. Method and Apparatus for Detection and Control of Thermal Runaway in a Battery under Charge. 1996.

[27] John Eugene Waters, Andrew Borne. Battery Pack. 1997.

[28] Barry Lake, Lawrence Ziehr, Bruce Siekkinen. System for Cooling Electric Vehicle Batteries. 2000.

[29] Salah Oweis, Peter Allen, Guy Chagnon. Thermal Management Blanketing and Jacketing for Battery System Modules. 2002.

[30] Takashi Oda, Hideki Okajima, Tatsuhito Horiuchi. Power Supply Apparatus. 2003.

[31] Christopher Yahnker, Daniele C Brotto, Erik Ekstrom, Adrew Seman Jr. Thermal Management Systems for Battery Packs. 2007.

[32] Zhou, Peng. Electric Vehicle Thermal Management System. 2010.

[33] Rolf Schaller, School Kwak. Battery Thermal Management with Phase Transition. 2012.

[34] Todd Bandhauer, Joseph Farmer. Li-Ion Battery Thermal Runaway Suppression System Using Microchannel Coolers and Refrigerant Injections. 2013.

[35] Battery Thermal Management in EVs and HEVs: Issues and Solutions. First Annual Advanced Automotive Battery Conference. 2001. Print.

[36] Ahmad Pesaran, John Ireland, Dirk Long, Kandler Smith, Gi-Heon Kim, Yoon Seok Jung. Nrel Battery Thermal and Life Test Facility: National Renewable Energy Laboratory, 2011. Print.

[37] Keyser, Matthew. Large-Volume Battery Calorimeter: National Renewable Energy Laboratory, 2011. Print.

[38] Jong Sung Hong, Said Al Hallaj. "Electrochemical-Calorimetric Studies of Lithium-Ion Cells." Journal of The Electrochemical Society 145.5 (1998): 1489 - 501. Print.

[39] Hossein Maleki, Said Al Hallaj, J. Robert Selman, Ralph B. Dinwiddle, H. Wang. "Thermal Properties of Lithium-Ion Battery and Components." Journal of The Electrochemical Society 146.3 (1999): 947 - 54. Print.

[40] Hari Vaidyanathan, William H. Kelly, Gopalakrishna Rao. "Heat Dissipation in a Lithium Ion Cell." Journal of Power Sources 93 (2001): 112 - 22. Print.

[41] Kazuo Onda, Hisashi Kameyama, Takeshi Hanamoto, Kohei Ito. "Experimental Study on Heat Generation Behavior of Small Lithium-Ion Secondary Batteries." Journal of The Electrochemical Society 150.3 (2003): A285 - A91. Print.

[42] Christophe Forgez, Dinh Vinh Do, Guy Friedrich, Mathieu Morcrette, Charles Delacourt. "Thermal Modeling of a Cylindrical Lifepo4/Graphite Lithium-Ion Battery." Journal of Power Sources 195 (2010): 2961 – 68. Print.

[43] Bernardi, Dawn. "A General Energy Balance for Battery Systems." Journal of Electrochemical Society 132.1 (1985): 5 - 12. Print.

[44] Karen Thomas, John Newman. "Thermal Modeling of Porous Insertion Electrodes." Journal of Electrochemical Society 150.2 (2003): A176 - A92. Print.

[45] Carolyn Pals, John Newman. "Thermal Modeling of the Lithium/Polymer Battery : I Discharge Behavior of a Single Cell." Journal of Electrochemical Society 142.10 (1995): 3274-81. Print.

[46] Hallaj, Said Al. "Thermal Modeling and Design Considerations of Lithium-Ion Batteries." Journal of Power Sources 83 (1999): 1 - 8. Print.

[47] Rouse, Margaret. "Seebeck Effect." (2008). <http://searchnetworking.techtarget.com/definition/Seebeck-effect>.

[48] OMEGA. "The Thermocouple." <http://www.omega.com/temperature/z/pdf/z021-032.pdf>.

[49] MICRO-EPSILON. "Basics of Non Contact Temperature Measurement." <http://www.micro-epsilon.com/download/products/dat--infrared-basics--en-us.pdf>.

[50] Corp, AA Portable Power. "Li-Ion 18650 Rechargeable Cell: 3.7v 2200mah (8.14wh) - Made in China - Un38.3 Passed (0.66)". 1995. <http://www.batteryspace.com/li-ion-18650-rechargeable-cell-3-7v-2200mah-8-14wh---made-in-china---un38-3-passed-0-66.aspx>.

[51] MOLICEL. "Product Data Sheet Model: Imr 26650c". <http://www.power-guide.com/pdf/IMR-26650.C.pdf>.

[52] Battery, Winston. "WB-LYP60AHA". 2014. <http://en.winston-battery.com/index.php/products/power-battery/item/wb-lyp60aha?category_id=176>.

[53] Technologies, Keysight. "Keysight Technologies N3300 Series Dc Electronic Loads". 2014. <http://literature.cdn.keysight.com/litweb/pdf/5980-0232E.pdf>.

[54] Technologies, Keysight. "Keysight Technologies Models 6690a-6692a System Dc Power Supply". 2014. <http://literature.cdn.keysight.com/litweb/pdf/5988-3149EN.pdf>.

[55] Technologies, Keysight. "Keysight Technologies Gpib, Usb and Instrument Control for Easy Pc-to-Instrument Connections". 2014. <http://literature.cdn.keysight.com/litweb/pdf/5989-1889EN.pdf>.

[56] Instruments, National. "Ni 9205 ±200 Mv to ±10 V, Analog Input, 250 Ks/S, 32 Ch Module". 2014. < http://www.ni.com/pdf/manuals/374188d.pdf>.

[57] Instruments, National. "Ni 9213 16-Channel Thermocouple Module". 2014. <http://www.ni.com/pdf/manuals/374916a.pdf>.

[58] Instruments, National. "Ni 9211 ±80 Mv Thermocouple Input, 14 S/S, 4 Ch Module". 2014. < http://www.ni.com/pdf/manuals/373466e.pdf>.

[59] Instruments, National. "Ni Compactdaq Usb Data Acquisition System Ni Cdaq-9172". 2014. < http://www.ni.com/pdf/manuals/371747f.pdf>.

[60] OMRON. "S8vs-06024". 2014. <http://www.ia.omron.com/product/item/s8vs0068g/>.

[61] USA, MICRO-EPSILON. "Thermometer Non-Contact Ir Temperature Sensors". <http://www.micro-epsilon.com/download/products/_temperature/dax--thermoMETER-CSmicro--en-us.html>.

[62] Engineering, OMEGA. "Hfs-3 and Hfs-4 Thin Film Flux Sensors". <http://www.omega.com/manuals/manualpdf/M1844.pdf>.

[63] MACCOR. "Series 4000 Automated Test System". 2014. <http://www.maccor.com/ProductDocs/Data%20Sheet%20for%20Series%204000%20Test%20System.pdf>.

[64] Sky, Thunder. "Instruction Manual". <http://www.thunderstruck-ev.com/Manuals/Thundersky%20Product%20Manual.pdf>.

APPENDIX A

BATTERY SPECIFICATIONS

Battery	3.7V 18650 size Cylindrical Li-Ion Cell
Nominal Voltage	Average 3.7 V
Nominal Capacity	2200mAh, Minimum 2150mAh
Maximum Charging Current	2.2A Max.
Maximum Discharging Current	4.3 A max.
Dimensions (Dia x H)	(0.72") 18.3 mm (Max 18.4) x (2.56") 64.9 mm (Max 65.1)
Weight	1.57 oz (44.5 g)
Internal Impedance	Internal Impedance: less or equal to 90 mohm (with PTC)
Cycle Performance	80% of initial capacity at 300 cycles

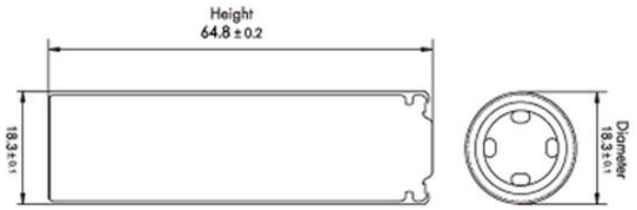

Figure A.1 18650 Li-Ion Cell Specifications [50]

Parameter	75% $LiCoO_2$, 25% $LiNiO_2$ cell
Mass (g)	42.57
Volume (cm^3)	16.54
Diameter (cm)	1.8
Height (cm)	6.5
Electrical capacity (A h)	
0°C, *C*/5 rate	0.945
10°C, *C*/5 rate	1.162
25°C, *C*/5 rate	1.277
25°C, *C*/2 rate	1.252
35°C, *C*/5 rate	–
Impedance (mΩ)	130
Self-discharge in 72 h (%)	3.39

Figure A.2 Cell specification from Vaidyanathan et al [40]

PRODUCT DATA SHEET
MODEL : IMR-26650C pg 1/2

MOLICEL®

Custom design the MOLICEL® lithium-ion rechargeable battery into your mobile device.

The IMR-26650 cylindrical cell consists of a manganese dioxide positive electrode material and a graphitic carbon negative electrode providing 3.8 volts and 3300 mAh.

LITHIUM-ION RECHARGEABLE BATTERY

CELL SPECIFICATIONS	
Capacity (Nominal)	3300 mAh
Nominal Voltage	3.8 V
Energy	12.5 Wh
Size	ϕ26 x 65 mm
Weight	93 grams
Energy Density Volumetric Gravimetric	 354 Wh/l 131 Wh/kg
OPERATING SPECIFICATIONS	
Operating Voltage	4.2 V to 3.0 V
Charge Voltage	4.2 V ± 50 mV
Cutoff Voltage	2.5 V
Temperature Range Discharge Charge	 -20°C to 60°C 0°C to 45°C
Maximum Discharge Current (Continuous)	5.0 A
Maximum Charge Current	3.0 A

Figure A.3 26650 Cell specification [51]

ThunderSky
LITHIUM BATTERY
E-mail: thunder@thunder-sky.com Http: // www.thunder-sky.com
TEL: 86-755-86026789 FAX: 86-755-86026678

雷天牌稀土鈆鐵鋰動力電池性能説明
THUNDER SKY LiFeYPO4 POWER BATTERY SPECIFICATIONS

單體電池尺寸 DIMENSIONS

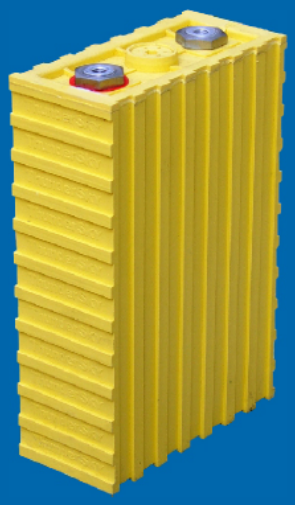

型号(MODEL)：TS-LFP60AHA

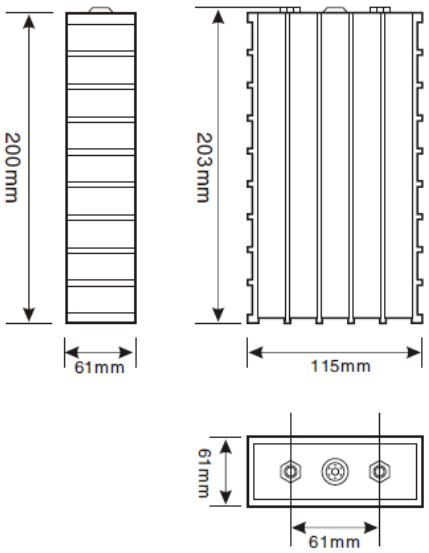

技術參數 SPECIFICATIONS

型号(MODEL)：TS-LFP60AHA		
標稱容量 Nominal Capacity	60Ah	
工作電壓 Operation Voltage	充電 (Charge)	4.0V
	放電 (Discharge)	2.8V
最大充電電流 Max Charge Current	≤3CA	
最大放電電流 Max Discharge Current	恒電流 (Constant Current)	≤3CA
	脉衝式 (Impulse Current)	≤20CA
標准充放電電流 Standard Charge/ Discharge Current	0.5CA	
循環壽命 Cycle Life	(80DOD%)	≥3000Times
	(70DOD%)	≥5000Times
殼體耐温性 Temperature Durability Of Case	≤200℃	
適應環境 Operating Temperature	充電 (Charge)	-45°C~85°C
	放電 (Discharge)	-45°C~85°C
自放電率(月) Self-discharge Rate	≤3% (Monthly)	
單體電池重量 Weight	2.3kg±50g	

Figure A.4 Thunder Sky Battery Specifications [52]

Material	Specific Heat Capa (J/g K)	%	c, Molar Heat Capa (J/mol·K)	Atomic Weight	c x % (J/g·K)
Yttrium	0.298	40.5	26.53	88.906	12.085
Lithium	3.582	16	24.86	6.940	57.314
Manganese	0.479	4.4	26.32	54.938	2.108
Calcium	0.647	0.3	25.929	40.078	0.194
Carbon (Graphite)	0.709	8.1	8.517	12.011	5.744
Sodium	1.228	1.5	28.23	22.990	1.842
Iron	0.449	3.4	25.1	55.845	1.528
Potassium	0.757	1.7	29.6	39.098	1.287
Fluorine	1.632	3.3	31	18.998	5.385
Strontium	0.301	1.5	26.4	87.620	0.452
Sum		**80.7**			**87.939**
	Specific Heat Capacity (J/g·K) =		***(Σ c x %) / % =***	***1.090***	
	Heat Capacity (J/K) =		***1.0897*Mass =***	***2506.316***	

Figure A.5 Thunder Sky Battery Heat Capacity calculated from material percentage [64]

APPENDIX B

TEST EQUIPMENT SPECIFICATIONS

	N3302A	N3303A	N3304A	N3304-J01 Special order option	N3305A	N3306A	N3307A
Input ratings							
Current	0–30 A	0–10 A	0–60 A	0–60 A	0–60 A	0–120 A	0–30 A
Voltage	0–60 V	0–240 V	0–60 V	0–80 V	0–150 V	0–60 V	0–150 V
Maximum power @ 40 °C[1]	150 W	250 W	300 W	300 W	500 W	600 W	250 W
Input characteristic							

Operating contour

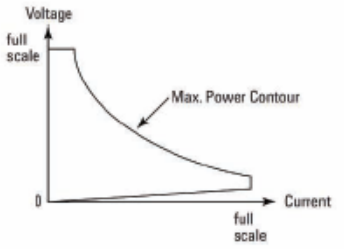

Derated current detail

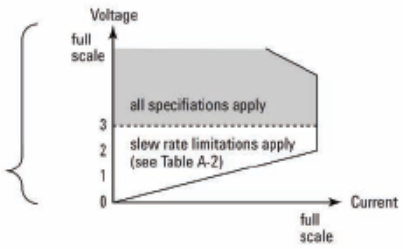

	N3302A	N3303A	N3304A	N3304-J01 Special order option	N3305A	N3306A	N3307A
Specified current @ low voltage operation							
2.0 V	30 A	10 A	60 A	60 A	60 A	120 A	30 A
1.5 V	22.5 A	7.5 A	45 A	45 A	45 A	90 A	22.5 A
1.0 V	15 A	5 A	30 A	30 A	30 A	60 A	15 A
0.5 V	7.5 A	2.5 A	15 A	15 A	15 A	30 A	7.5 A
0 V	0 A	0 A	0 A	0 A	0 A	0 A	0 A

1. *Maximum continuous power available is derated linearly from 100% of maximum at 40 °C, to 75% of maximum at 55 °C.*

Table A-1 states that maximum current is available down to 2 volts. Typically, however under normal operating conditions, the load can sink the maximum current down to the following voltages:

	N3302A	N3303A	N3304A	N3304-J01 Special order option	N3305A	N3306A	N3307A
Typical minimum operating voltage @ full scale current							
	1.2 V	1.2 V	1.2 V	1.2 V	1.4 V	1.4 V	1.4 V

		N3302A	N3303A	N3304A	N3304-J01 Special order option	N3305A	N3306A	N3307A
Constant current mode[1]								
Low range/High range		3 A/30 A	1 A/10 A	6 A/60 A	6 A/60 A	6 A/60 A	12 A/120 A	3 A/30 A
Regulation		10 mA	8 mA	10 mA	10 mA	10 mA	10 mA	10 mA
Low range accuracy	0.1% +	5 mA	4 mA	7.5 mA	7.5 mA	7.5 mA	15 mA	7.5 mA
High range accuracy	0.1% +	10 mA	7.5 mA	15 mA	15 mA	15 mA	37.5 mA	15 mA
Constant voltage mode[1]								
Low range/High range		6 V/60 V	24 V/240 V	6 V/60 V	8 V/80 V	15 V/150 V	6 V/60 V	15 V/150 V
Regulation		5 mV	10 mV	10 mV	10 mV	10 mV	20 mV	10 mV
Low range accuracy	0.1% +	3 mV	10 mV	3 mV	5 mV	10 mV	3 mV	10 mV
High range accuracy	0.1% +	8 mV	40 mV	8 mV	12 mV	20 mV	8 mV	20 mV
Constant resistance mode[1]								
Range 1 (I > 10% of current rating)		0.067–4 Ω	0.2–48 Ω	0.033–2 Ω	0.033–2.6 Ω	0.033–5 Ω	0.017–1 Ω	0.067–10 Ω
Range 2 (I > 1% of current rating)		3.6–40 Ω	44–480 Ω	1.8–20 Ω	2.4–26 Ω	4.5–50 Ω	0.9–10 Ω	9–100 Ω
Range 3 (I > 0.1% of current rating)		36–400 Ω	440–4800 Ω	18–200 Ω	24–260 Ω	45–500 Ω	9–100 Ω	90–1000 Ω
Range 4 (I > 0.01% of current rating)		360–2000 Ω	4400–12000 Ω	180–2000 Ω	240–2600 Ω	450–2500 Ω	90–1000 Ω	900–2500 Ω
Current measurement[1]								
Low range/High range		3 A/30 A	1 A/10 A	6 A/60 A	6 A/60 A	6 A/60 A	12 A/120 A	3 A/30 A
Low range accuracy[2]	0.05% +	3 mA	2.5 mA	5 mA	5 mA	5 mA	10 mA	3 mA
High range accuracy[2]	0.05% +	6 mA	5 mA	10 mA	10 mA	10 mA	20 mA	6 mA
Voltage measurement[1]								
Low range/High range		6 V/60 V	24 V/240 V	6 V/60 V	8 V/80 V	15 V/150 V	6 V/60 V	15 V/150 V
Low range accuracy	0.05% +	3 mV	10 mV	3 mV	5 mV	8 mV	3 mV	8 mV
High range accuracy	0.05% +	8 mV	20 mV	8 mV	12 mV	16 mV	8 mV	16 mV
Power measurement[1]								
Accuracy	0.1% +	0.4 W	1.2 W	0.6 W	0.8 W	1.6 W	1.3 W	0.9 W

Figure B.1 Agilent N3306A Specifications [53]

Parameter			Keysight model number		
			6690A	6691A	6692A
Output ratings					
	Voltage		0-15 V	0-30 V	0-60 V
	Current*		0-440 A	0-220 A	0-110 A
	*Derated linearly 1%/°C from 40 to 55 °C				
Programming accuracy (@ 25 ±5 °C)					
	Voltage	0.04% +	15 mV	30 mV	60 mV
	Current	0. 1% +	230 mA	125 mA	65 mA
Ripple & noise					
	(from 20 Hz to 20 MHz with outputs ungrounded, or with either output terminal grounded)				
	Constant Voltage	rms	2.5 mV	2.5 mV	1.5 mV
	Constant Voltage	p-p	15 mV	25 mV	25 mV
	Constant Current**	rms	200 mA	50 mA	30 mA
	**With load inductance > 5 µH				
Readback accuracy					
	(from front panel or over GPIB with respect to actual output @ 25 ±5 °C)				
	Voltage	0.05% +	22.5 mV	45 mV	90 mV
	±Current	0.1% +	300 mA	165 mA	80 mA
Load regulation					
	(change in output voltage or current for any load change within ratings)				
	Voltage	0.002% +	650 µV	1.1 mV	2.2 mV
	Current	0.005% +	40 mA	17 mA	9 mA
Line regulation					
	(change in output voltage or current for any line change within ratings)				
	Voltage	0.002% +	650 µV	650 µV	650 µV
	Current	0.005% +	40 mA	17 mA	9 mA
Transient response time					
	(for the output voltage to recover to within 150 mV following any step change from 100% to 50% or 50% to 100% of the rated output current): < 900 µs				

Supplemental characteristics	
DC floating voltage	Output terminal can be floated up to ±60 VDC from chassis ground
Remote sensing	Up to half the rated output voltage can be dropped in each load lead. The drop in the load leads subtracts from the voltage available at the load.
Command processing time	Average time required for the output voltage to begin to change following receipt of digital data is 20 ms for power supplies connected directly to the GPIB.
Modulation:	(analog programming of output voltage and current): Input signal: 0 to –5 V for voltage, and 0 to +5 V for current. Input impedance: 30 kΩ or greater.
AC input (47 to 63 Hz)	180 to 235 VAC (line-to-line 3 phase) 36 Arms maximum worst case, 28 Arms nominal; 360 to 440 VACX, 18 Arms maximum worst case, 14 Arms nominal. (Maximum line current includes 5% unbalanced phase voltage condition).
CD ships with	IVI and VXI Plug n Play drivers, Operating, Programming, Service and Quick Start Guides.
Input power	9000 VA and 7950 W maximum; 175 W at no load.
Size	425.5 W x 221.5 H x 674.7 mm D (16.75 x 8.75 x 25.56 in).

Specifications (at 0 to 55 °C unless otherwise specified) Supplemental Characteristics (Non-warranted characteristics determined by design that are useful in applying this product)		6690A	6691A	6692A
Ripple and noise constant current mode from 20 Hz to 20 MHz				
rms		200 mA	50 mA	30 mA
Average programming resolution				
Voltage		4.1 mV	8.1 mV	16 mV
Current		118.5 mA	59 mA	30 mA
OVP		90 mV	170 mV	330 mV
Output voltage programming response time (excludes command-processing time) Full-load programming rise or fall time (10 to 90% or 90 to 10%, resistive load)		45 ms	60 ms	100 ms
Output common-mode noise current (to signal-ground binding post)	rms	3 mA	3.5 mA	4 mA
	peak-to-peak	20 mA	20 mA	25 mA

Figure B.2 Agilent N6692A Specifications [54]

Boosting performance with simplest connectivity

82357B technical specifications	
General requirements	
Minimum system requirements	Refer to page 4 for requirements in using the Keysight IO Libraries software (included with the instrument control hardware)
Supported standards	– Supports USB 2.0 high speed – Standard USB endpoints supported – IEEE-488.1 and IEEE-488.2 compatible – SICL and VISA 2.2
Unsupported GPIB modes of operation	– Pass Control – Non-System Controller mode
General characteristics	
Power	USB bus-powered device, +5 V, 500 mA (maximum), 200 mA (typical)
Maximum data rate (GPIB)	1.15 MB/s
Connectors	– Standard 24-pin IEEE-488 (GPIB) – Standard USB A
USB hubs	Self-powered hubs
Parallel polling	A single parallel poll can easily check up to eight individual devices at once, corresponding to the number of data lines on the GPIB
Cable	2.5 meters, shielded, connector rated for 1,500 insertions
LED indicators	READY, ACCESS, FAIL
Maximum instrument connection	14 instruments—daisy chain via GPIB. A maximum of 4 converters can be connected to the PC.
Configuration	Plug-and-play
Warranty	1 year
EMC and safety	– IEC 61010-1: 2001/EN 61010-1: 2001 – USA: UL61010-1: 2004 – Canada: CSA C22.2 No. 61010-1: 2004
Dimensions	
Length, width, and height	105 mm (L) x 64 mm (W) x 30 mm (H) (including connectors)
Weight	215 grams
Environmental specifications	
Operating environment	0 °C to 55 °C
Operating humidity	Up to 90% at 40 °C non-condensing
Storage environment	–40 °C to 70 °C
Storage humidity	Up to 90% at 65 °C non-condensing
Ordering information	
Includes	Keysight IO Libraries Suite and VISA/SICL programming manuals on CD-ROM
Accessories	GPIB cables/adapter (see page 12)

Figure B.3 Agilent 82357B Specifications [55]

NI 9205

32-Channel, ±200 mV to ±10 V, 16-Bit Analog Input Module

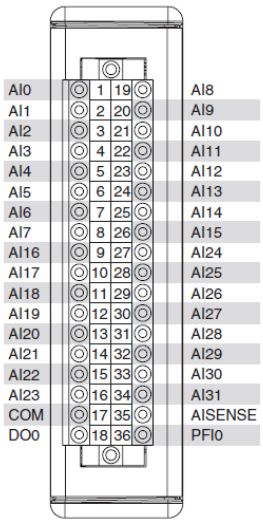

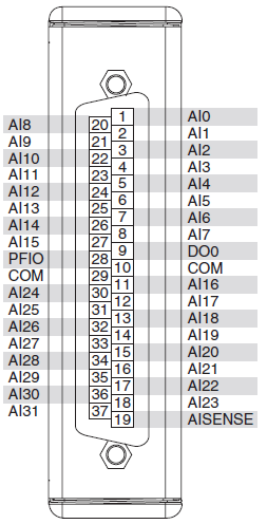

Analog Input Characteristics

Number of channels ..... 32 single-ended or 16 differential analog input channels, 1 digital input channel, and 1 digital output channel

ADC resolution ..... 16 bits

DNL ..... No missing codes guaranteed

Conversion time

R Series Expansion chassis ..... 4.50 µs (222 kS/s)

All other chassis ..... 4.00 µs (250 kS/s)

Input coupling ..... DC

Nominal input ranges ..... ±10 V, ±5 V, ±1 V, ±0.2 V

Minimum overrange (for 10 V range) 4%

Maximum working voltage for analog inputs (signal + common mode) ..... Each channel must remain within ±10.4 V of common

Physical Characteristics

If you need to clean the module, wipe it with a dry towel.

Spring-terminal wiring ..... 18 to 28 AWG copper conductor wire with 7 mm (0.28 in.) of insulation stripped from the end

Weight

NI 9205 with spring terminal ..... 158 g (5.8 oz)

NI 9205 with DSUB ..... 148 g (5.3 oz)

Figure B.4 NI 9205 Module Specifications [56]

OPERATING INSTRUCTIONS AND SPECIFICATIONS

NI 9213

16-Channel Thermocouple Input Module

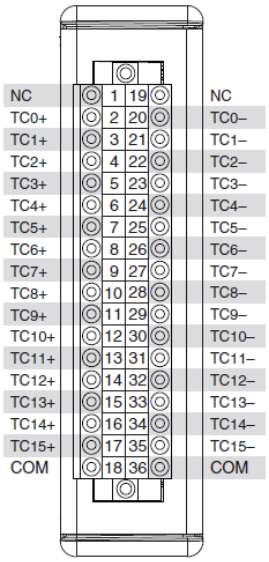

Input Characteristics

Number of channels ..... 16 thermocouple channels,
1 internal autozero channel,
1 internal cold-junction compensation channel

ADC resolution ..... 24 bits

Type of ADC ..... Delta-Sigma

Sampling mode ..... Scanned

Voltage measurement range ..... ±78.125 mV

Temperature Measurement Accuracy

Measurement sensitivity[1]

High-resolution mode

Types J, K, T, E, N ..... <0.02 °C

Types B, R, S ..... <0.15 °C

High-speed mode

Types J, K, T, E ..... <0.25 °C

Type N ..... <0.35 °C

Type B ..... <1.2 °C

Types R, S ..... <2.8 °C

Figure B.5 NI 9213 Module Specifications [57]

OPERATING INSTRUCTIONS AND SPECIFICATIONS

NI 9211

4-Channel Thermocouple Input Module

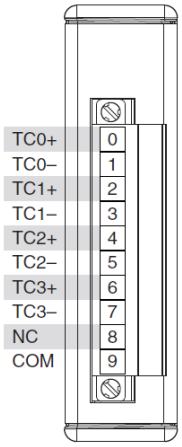

Input Characteristics

Number of channels	4 thermocouple channels, 1 internal autozero channel, 1 internal cold-junction compensation channel
ADC resolution	24 bits
Type of ADC	Delta-Sigma
Sampling mode	Scanned
Voltage measurement range	±80 mV
Temperature measurement ranges	Works over temperature ranges defined by NIST (J, K, T, E, N, B, R, S thermocouple types)
Conversion time	70 ms per channel; 420 ms total for all channels including the autozero and cold-junction channels
Common-mode voltage range	
Channel-to-COM	±1.5 V
COM-to-earth ground	±250 V

Temperature Measurement Accuracy

Measurement sensitivity[1]

With autozero channel on

Types J, K, T, E, N	<0.07 °C
Types B	<0.25 °C
Types R, S	<0.60 °C

With autozero channel off

Types J, K, T, E, N	<0.05 °C
Type B	<0.20 °C
Types R, S	<0.45 °C

Figure B.6 NI 9211 Module Specifications [58]

NI cDAQ-9172

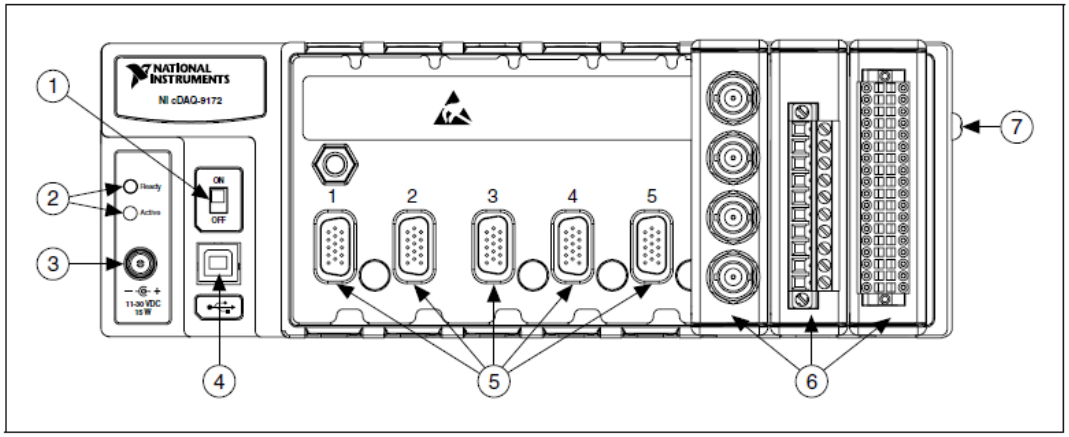

1	Power Switch	5	Empty Module Slots
2	Ready/Active LEDs	6	Installed C Series I/O Modules
3	Power Connector	7	Screw for Ground Connection
4	USB Connector		

Analog Input

Input FIFO size ..... 2,047 samples

Sample rate[1]

Maximum..... 3.2 MS/s (multi-channel, aggregate)

Minimum ..... 0 S/s

Timing accuracy[2] ..... 50 ppm of sample rate

Timing resolution[2] ..... 50 ns

Number of channels supported ..... Determined by the C Series I/O modules

Analog Output

Numbers of channels supported

In hardware-timed task 16

In non-hardware-timed task ..... Determined by the C Series I/O modules

Maximum update rate ..... 1.6 MS/s (multi-channel, aggregate)

Timing accuracy..... 50 ppm of sample rate

Timing resolution..... 50 ns

Output FIFO size..... 8,191 samples shared among channels used

Figure B.7 NI 9172 Module Specifications [59]

S8VS-06024

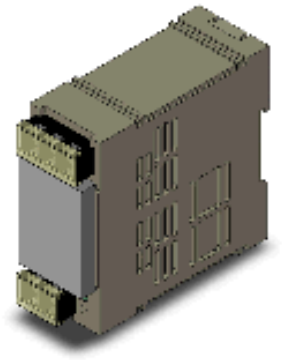

Standard Model , Input 100 to 240 VAC , 60 W , Output 24 V 2.5 A

Power rating	60 W
Efficiency	84 % TYP. （At 100 VAC input) 83 % TYP. （At 200 VAC input)
Rated input voltage	100 to 240 VAC
Allowable-input voltage variable range	85 to 264 VAC 80 to 370 VDC
Note at DC input	The range for compliance with EC Directives and safety standards (UL, EN, etc.) is 100 to 240 VAC (85 to 264 VAC).
Frequency	50/60 Hz （47 to 450 Hz Single-phase）
Rated input current	1.3 A TYP. （At 100 VAC input) 0.68 A TYP. （At 200 VAC input)
Harmonic Current	EN61000-3-2
Leakage current	0.5 mA Max. (At 100 VAC input) 1.0 mA Max. (At 200 VAC input)
Inrush current	14 A TYP. （At 100 VAC input (For cold start at 25 CEL)) 28 A TYP. （At 200 VAC input (For cold start at 25 CEL))
Output voltage	24 VDC
Output voltage variable range	-10 to +15 % (With V. ADJ) (The output voltage may increase beyond the allowable voltage range (up to +15% of the rated voltage) depending on the operation of the output voltage adjuster (V.ADJ). When adjusting the output voltage, check the output voltage of the Power Supply and be sure that the load is not damaged.)
Ripple	2 %(p-p) Max. (Under the rated I/O conditions.) 70 mV Max. (Under the rated I/O conditions.)

Figure B.8 OMRON 58VS-06024 Specifications [60]

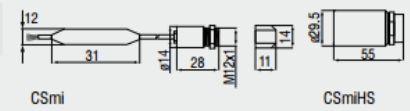

CSmi CSmiHS

Product identification

CSmi - SF15 - C1
- Cable length
- Fokus [SF / CF]
- thermoMETER CSmi

Model	CSmi-SF02-C1	CSmi-SF15-C1	CSmiHS-SF15-C4
Optical resolution	2:1	15:1	15:1
Temperature range	-40°C to 1030°C [1]		-20°C to 150°C
Spectral range	8 to 14µm		
System accuracy	±1.5% or ±1.5°C [3]		±1.0% or ±1.0°C [4]
Repeatability	±0.75% or ±0.75°C [3]		±0.3% or ±0.3°C [4]
Temperature coefficient	± 0.05 K/K or ± 0.05% K [5]		
Temperature resolution	0.1°C [6]		0.025°C [6]
Response time (90%)	30ms (adjustable up to 999s via optional programming device)		150ms (adjustable up to 999s via optional programming device)
Emissivity/gain	0.100 to 1.100 [2]		0.100 to 1.100 [1]
Transmissivity/gain [1]	0.100 to 1.100		
Signal processing [1]	peak hold, valley hold, average; extended hold function with threshold and hysteresis		
Dimensions controller	length 35mm; ø12mm		
Outputs/analog	0 to 5V or 0 to 10V 1/10/100 mV/°C		4 to 20mA
Loop resistance	-		1000Ω [7]
Outputs/alarm	Alarm (50mA / 24V)		0-30V / 500mA (open collector)
Outputs/digital (optional)	uni/bidirectional, 9.6 kBaud, 0/3V digital level/USB optional		
Inputs	programmable functional input for external emissivity adjustment (0 - 5VDC), hold function or USB communication		programmable functional input for triggered signal output or peak-hold function
LED functions	alarm indication, automatic aiming support, self diagnostic, temperature indication (via temp. code)		
Cable length	1m (standard); 0.5m between sensor and controller; 0.4m between controller and terminal		**4m (0.5m sensor-controller) sensor with massive housing TM-MHS-CT ø29.5mm x 55mm**
Power supply	9mA (5 to 30VDC)		4...20mA (5 to 30VDC)
Environmental rating	IP 65 (NEMA-4) sonsor head		
Ambient temperature	Sensor: -20°C to 120°C Controller: -20°C to 80°C		Sensor -20°C to 75°C Controller: -20°C to 75°C
Storage temperature	-40°C to 85°C (sensor and controller)		
Relative humidity	10 - 95%, non condensing		
Vibration	IEC 68-2-6: 3G, 11-200Hz, any axis		
Shock	IEC 68-2-27: 50G, 11ms, any axis		
Weight	42g		200g

[1] adjustable via software
[2] adjustable via 0 - 5VDC input or software
[3] ± at ambient temperature 23±5°C; object temperature >0°C; whichever is greater
[4] at ambient temperature 23±5°C; object temperature >20°C; whichever is greater
[5] object temperature <100°C; and time constant >0.2s
[6] object temperature > 20°C; and time constant >0.2s
[7] in dependence on supply voltage

Figure B.9 Micro Epsilon Infrared Thermometer Specifications [61]

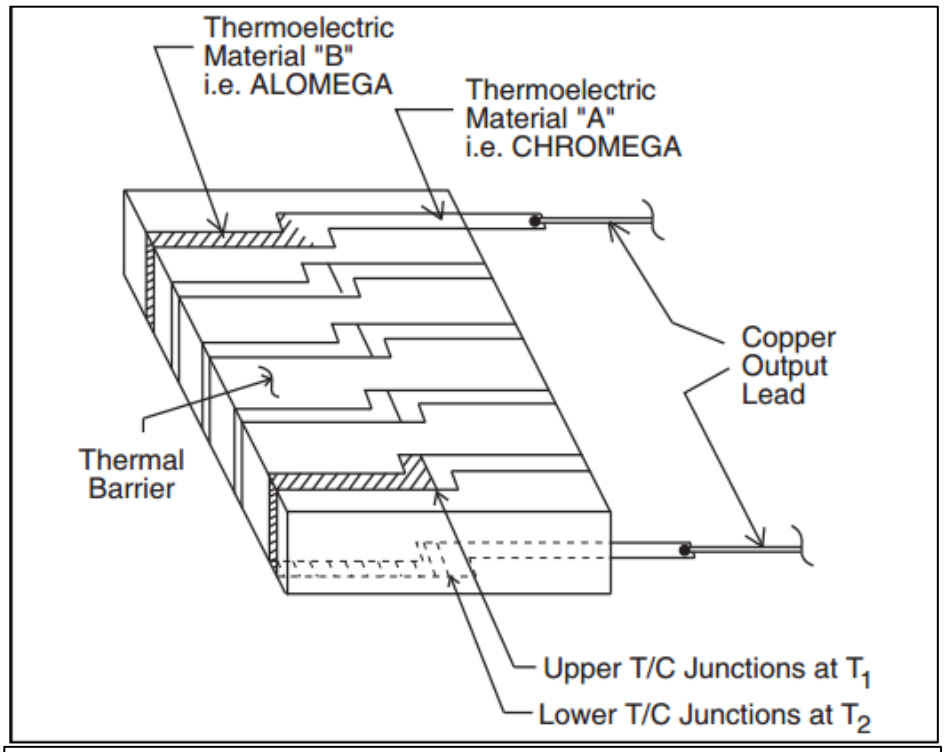

Upper Temperature Limit:	300°F
Number of Junctions:	50+
Carrier:	Polyimide film (Kapton)
Sensor Resistance:	160 approximately
Lead Wires:	#30 AWG Solid, Teflon insulated color coded, 10 feet long
Dimensions:	See Figure 5-1

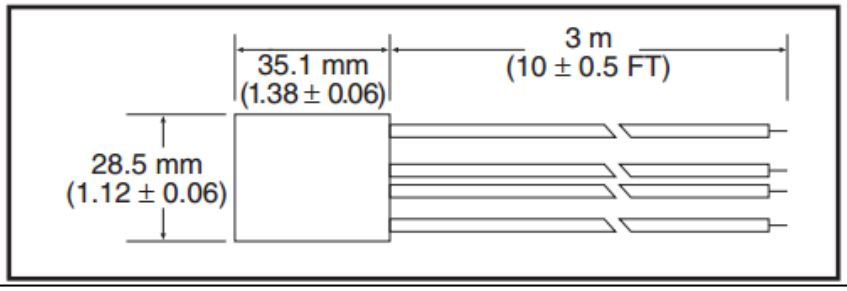

Figure B.10 HFS-3, HFS-4 Thin Film Flux Sensors Specifications [62]

Multi-Current Range

Range 1	150 µA Full Scale ±0.03 µA
Range 2	5 mA Full Scale ±1.0 µA
Range 3	150 mA Full Scale ±30.0 µA
Range 4	5000 mA Full Scale ±1.0 mA
Current Control Range	300 ηAmps to 5 Amps

Voltage (multi-current range channels)

Measurement Range	-2V to +8 Volts or 0V to +10 Volts
Accuracy	±0.02% Full Scale Range
Resolution	16 bit

Single-Current Range

Current Range	Per Your Specifications, currents up to 2000A available
Current Accuracy	±0.05% Full Scale

Dual-Current Range

Current Range	Any combination of two single-current ranges
Current Accuracy	±0.05% Full Scale Range

Voltage (single-current range and dual- current range channels)

Measurement Range	Per Your Specifications, voltages up to 180V available
Accuracy	±0.02% Full Scale
Resolution	16 bit

Modes of Operation

Fixed (Constant) Current	Fixed (Constant) Power
Fixed (Constant) Resistance	Fixed (Constant) Voltage
1kHz AC Impedance Measurement	
Voltage Ramp (Cyclic Voltammetry)	
Functions – functions can be used as set points, end conditions, or set as variables. The function is entered in the function field and valid mathematical functions, measured values, and custom values are selected and added from the valid key words.	
Waveform – allows the streaming of an external test file (i.e. FUDS drive cycle test) to the test system.	

AC Power Input

For each system, two separate AC inputs are required, one to power the electronics and one for the charge power.

Power for Electronics	Power for Charge
110 or 220/240 VAC Single-Phase 50/60 Hertz	186 to 265 VAC Single-Phase or 186 to 265 VAC Three-Phase 50/60 Hertz

Figure B.11 MACCOR Series 4000 Specifications [63]

APPENDIX C

LabVIEW BLOCK DIAGRAM FOR ELECTRONIC LOAD

Note: The whole block diagram is the combination of of page 123 to 126 altogether.

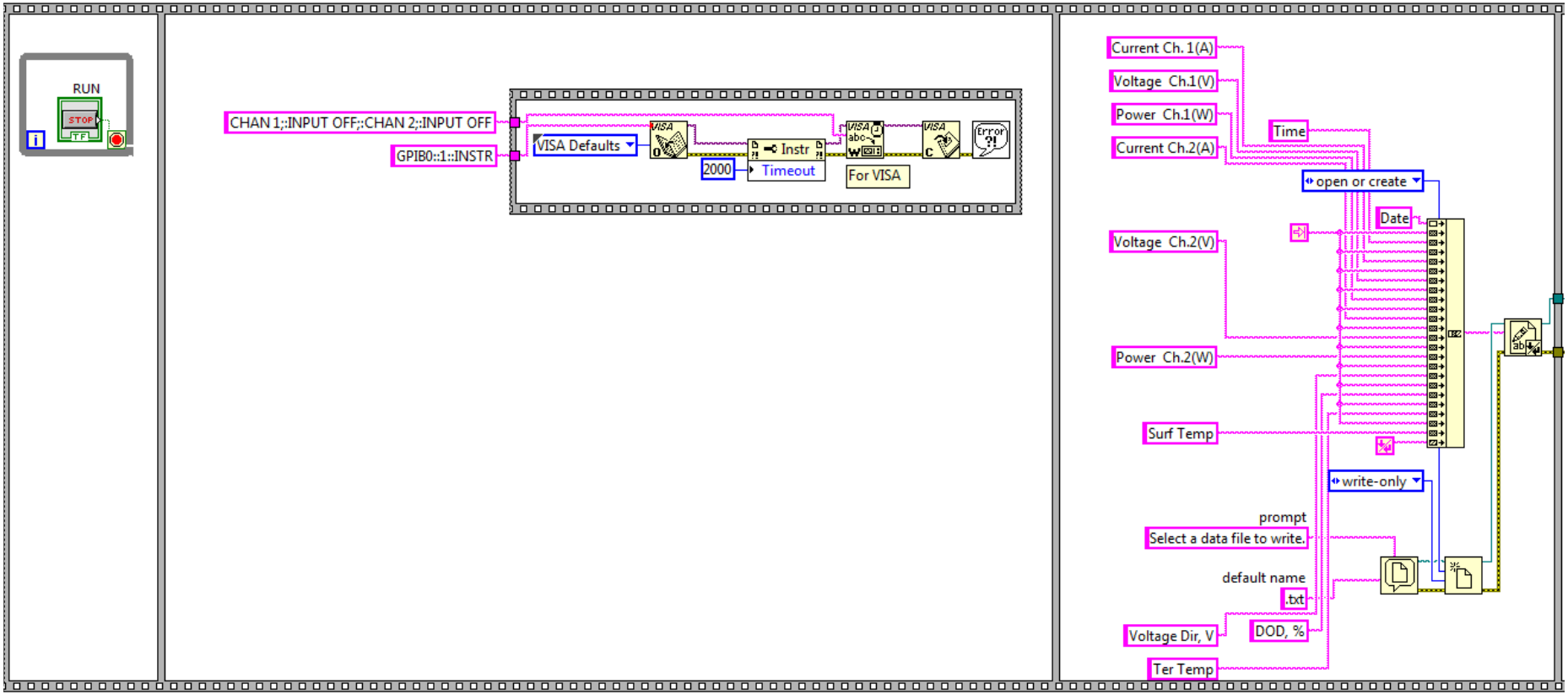
RUN
STOP
TF
CHAN 1;:INPUT OFF;:CHAN 2;:INPUT OFF
GPIB0::1::INSTR
VISA Defaults
VISA
Instr
2000
Timeout
For VISA
Error ?!
Current Ch. 1(A)
Voltage Ch.1(V)
Power Ch.1(W)
Current Ch.2(A)
Time
open or create
Date
Voltage Ch.2(V)
Power Ch.2(W)
Surf Temp
write-only
prompt
Select a data file to write.
default name
.txt
Voltage Dir, V
DOD, %
Ter Temp

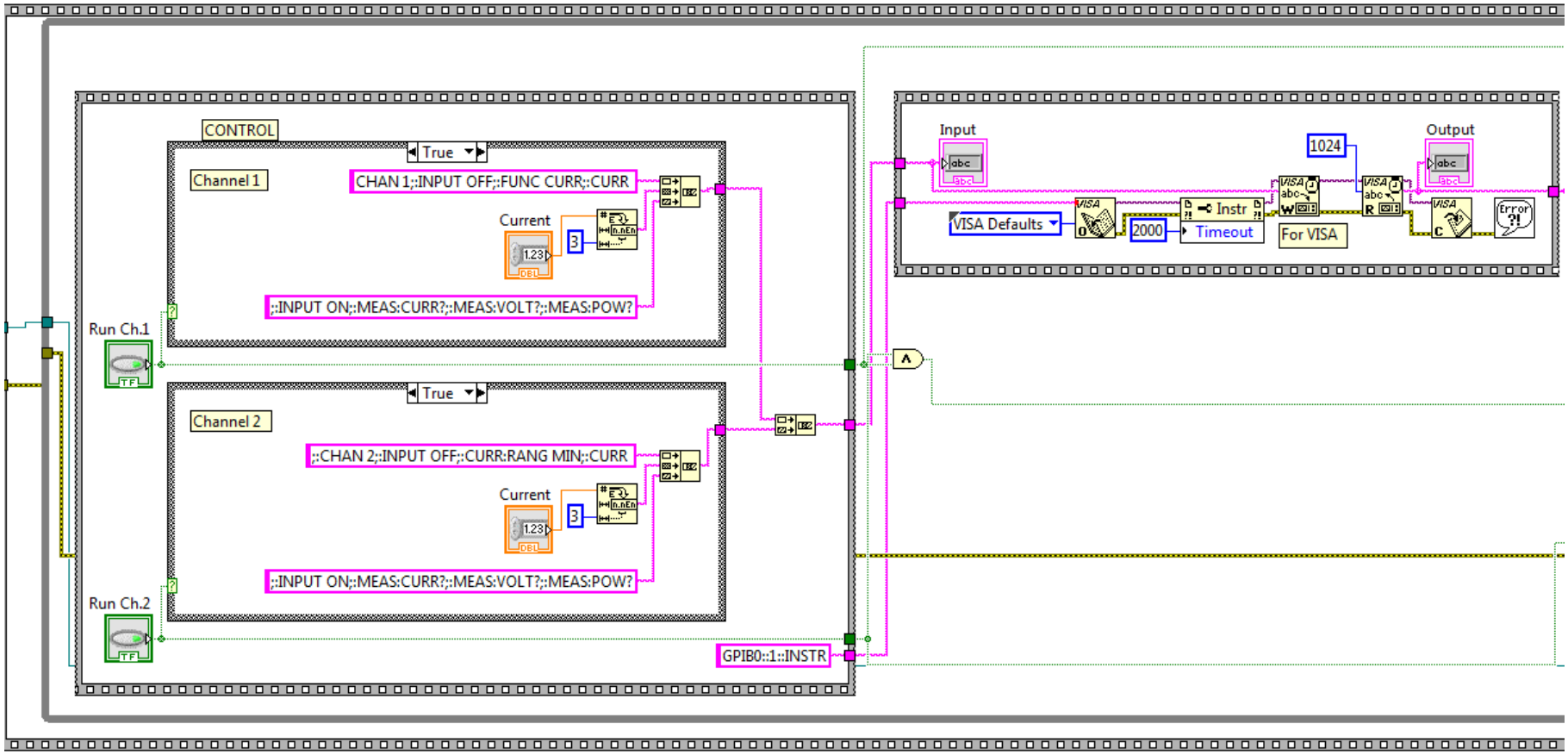
CONTROL
True
Channel 1
CHAN 1;:INPUT OFF;:FUNC CURR;:CURR
Current
1.23
3
;:INPUT ON;:MEAS:CURR?;:MEAS:VOLT?;:MEAS:POW?
Run Ch.1
True
Channel 2
;:CHAN 2;:INPUT OFF;:CURR:RANG MIN;:CURR
Current
1.23
3
;:INPUT ON;:MEAS:CURR?;:MEAS:VOLT?;:MEAS:POW?
Run Ch.2
GPIB0::1::INSTR
Input
1024
Output
VISA Defaults
2000
Instr
Timeout
For VISA
Error

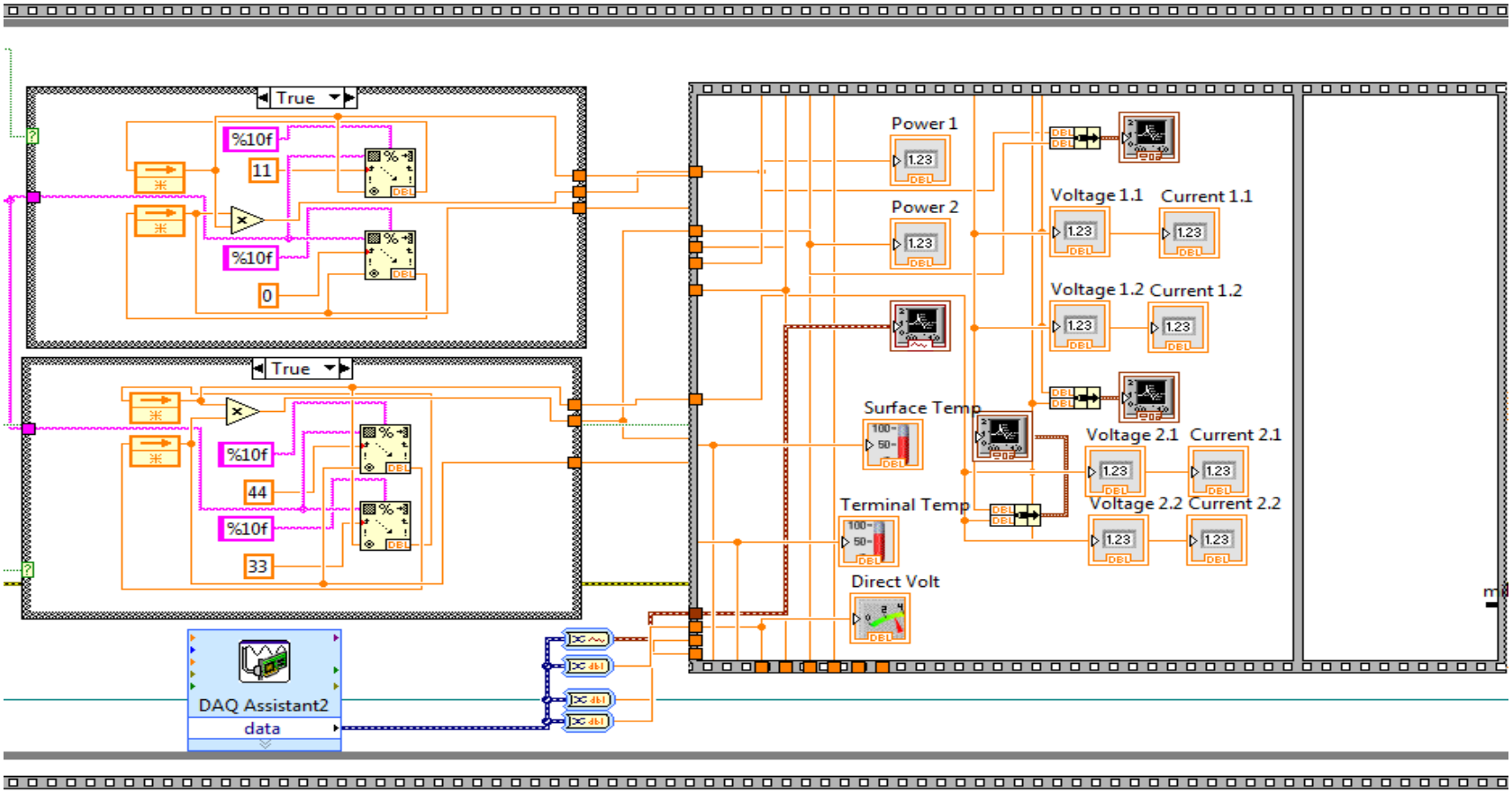
True
%10f
11
%10f
0
True
%10f
44
%10f
33
DAQ Assistant2
data
Power 1
Power 2
Surface Temp
Terminal Temp
Direct Volt
Voltage 1.1
Current 1.1
Voltage 1.2
Current 1.2
Voltage 2.1
Current 2.1
Voltage 2.2
Current 2.2

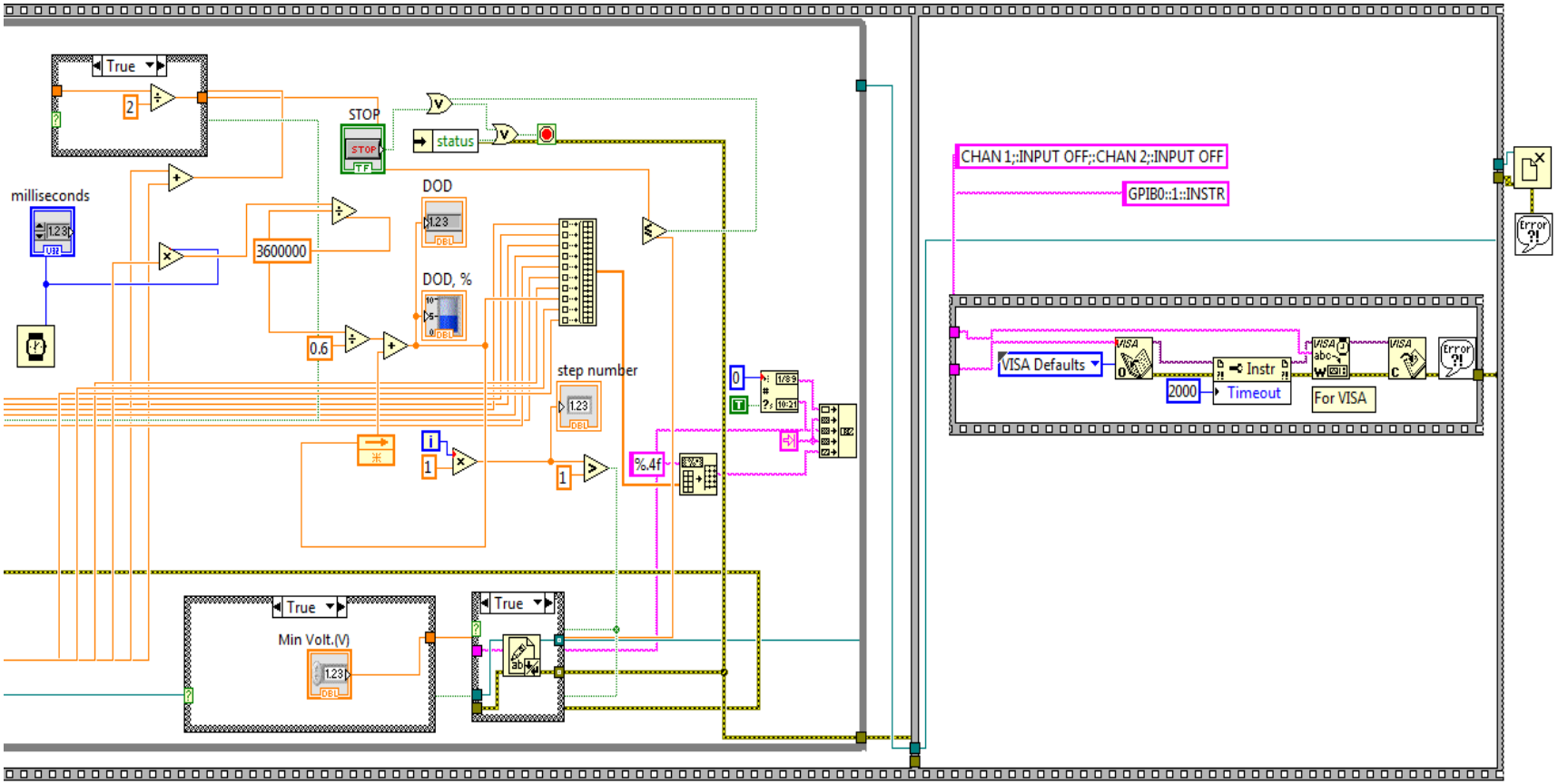
True
2
STOP
STOP
TF
status
milliseconds
DOD
1.23
DBL
3600000
DOD, %
0.6
step number
1.23
DBL
0
1
1
%.4f
True
Min Volt.(V)
1.23
DBL
True
CHAN 1;:INPUT OFF;:CHAN 2;:INPUT OFF
GPIB0::1::INSTR
VISA Defaults
VISA
Instr
2000
Timeout
VISA
abc
VISA
C
Error
?!
For VISA
Error
?!

APPENDIX D

LabVIEW BLOCK DIAGRAM FOR POWER SUPPLY

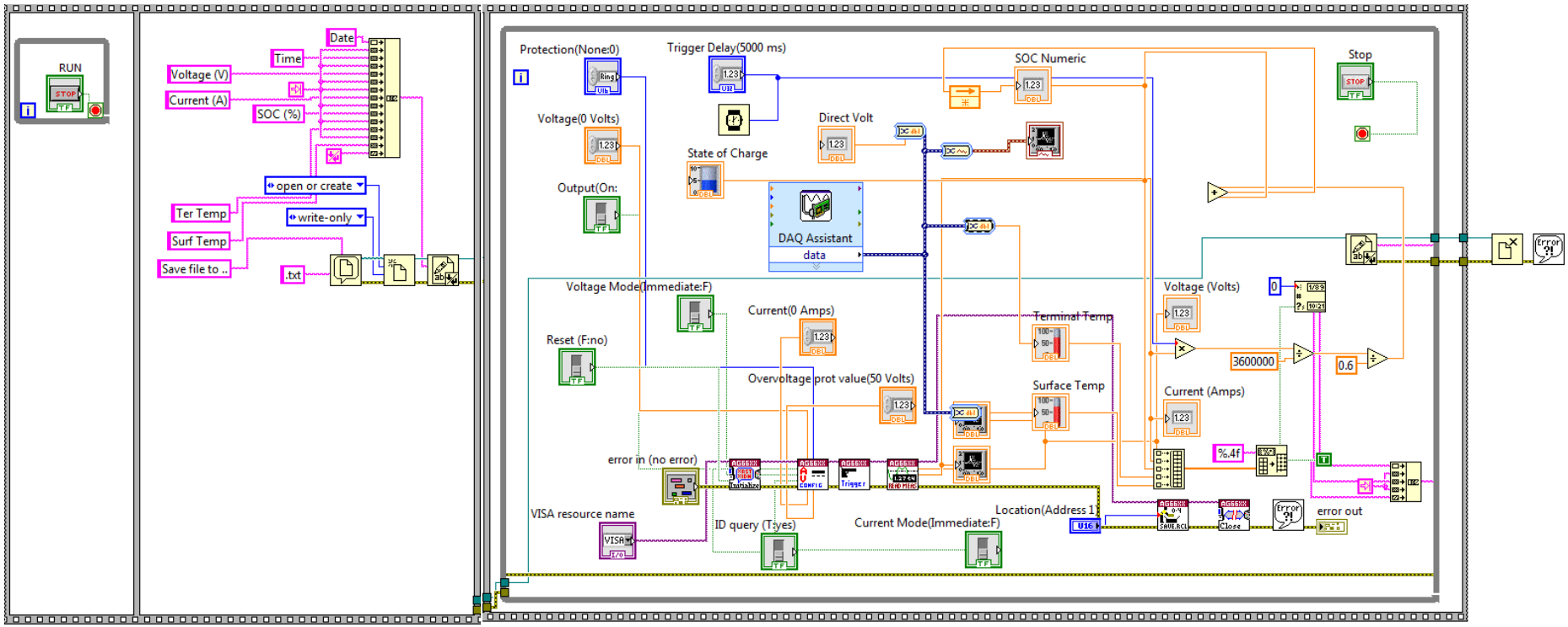
RUN
Date
Time
Voltage (V)
Current (A)
SOC (%)
open or create
write-only
Ter Temp
Surf Temp
Save file to ..
.txt
Protection(None:0)
Trigger Delay(5000 ms)
SOC Numeric
Stop
Voltage(0 Volts)
Direct Volt
State of Charge
Output(On:
DAQ Assistant
data
Voltage Mode(Immediate:F)
Current(0 Amps)
Terminal Temp
Voltage (Volts)
Reset (F:no)
Overvoltage prot value(50 Volts)
Surface Temp
Current (Amps)
3600000
0.6
%.4f
error in (no error)
VISA resource name
ID query (T:yes)
Current Mode(Immediate:F)
Location(Address 1)
error out

APPENDIX E

MATLAB Codes for Low pass filter

```
%%% Filtering (low pass filter)
%%% x = input signal
%%% x_new = filtered signal
%%% para = filter parameter --> change this value
para = 100;
[b,a]=butter(1,0.01);   %%% using frequency = 1/100 = 0.01
volt_filt=filtfilt(b,a,volt);
%% put the unfiltered voltage data named as volt
%% press run
```

APPENDIX F

Experimental Data

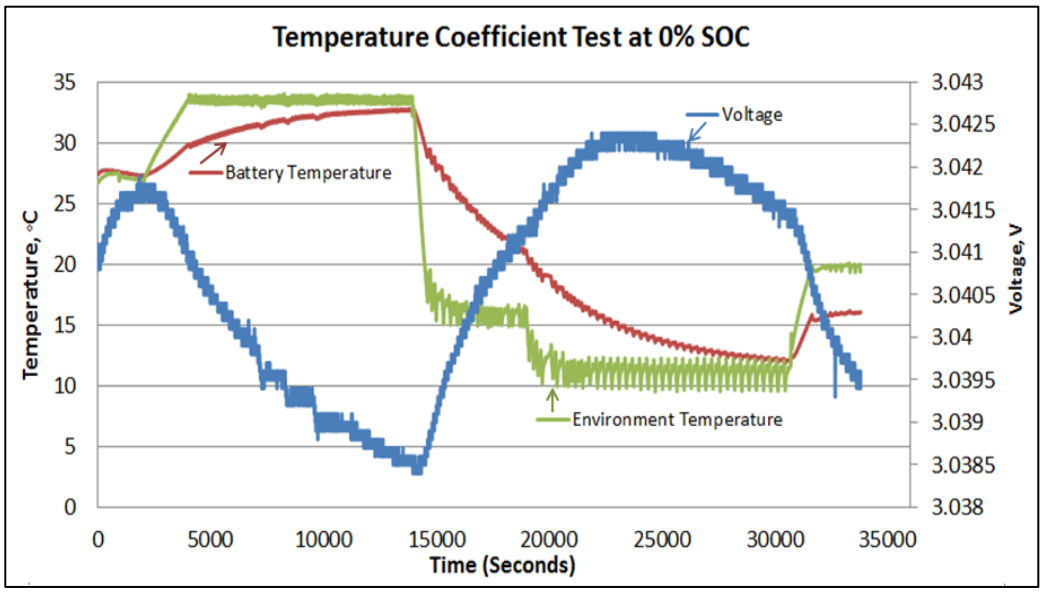

Figure F.1 Temperature Coefficient Test at 0% SOC

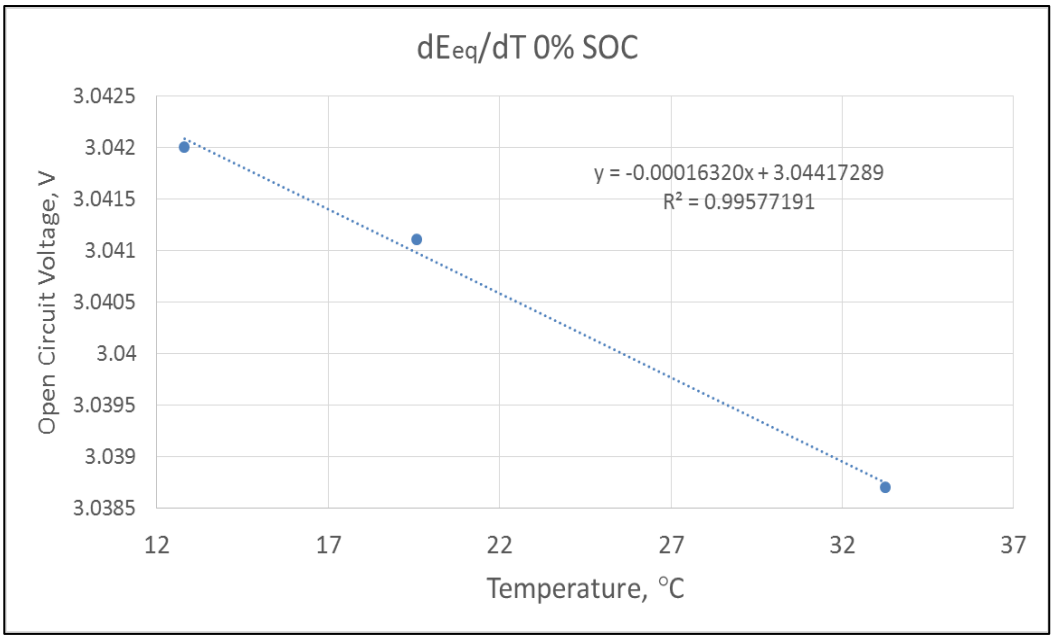

Figure F.2 Plot of Temperature vs. E_{eq} from 0% SOC equilibrium data points

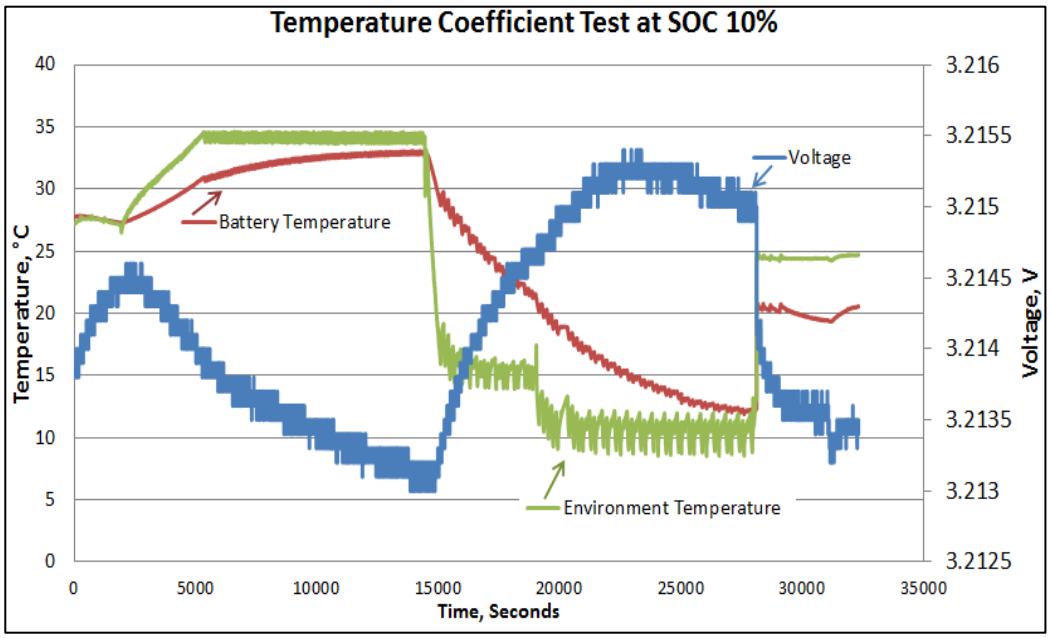

Figure F.3 Temperature Coefficient Test at 10% SOC

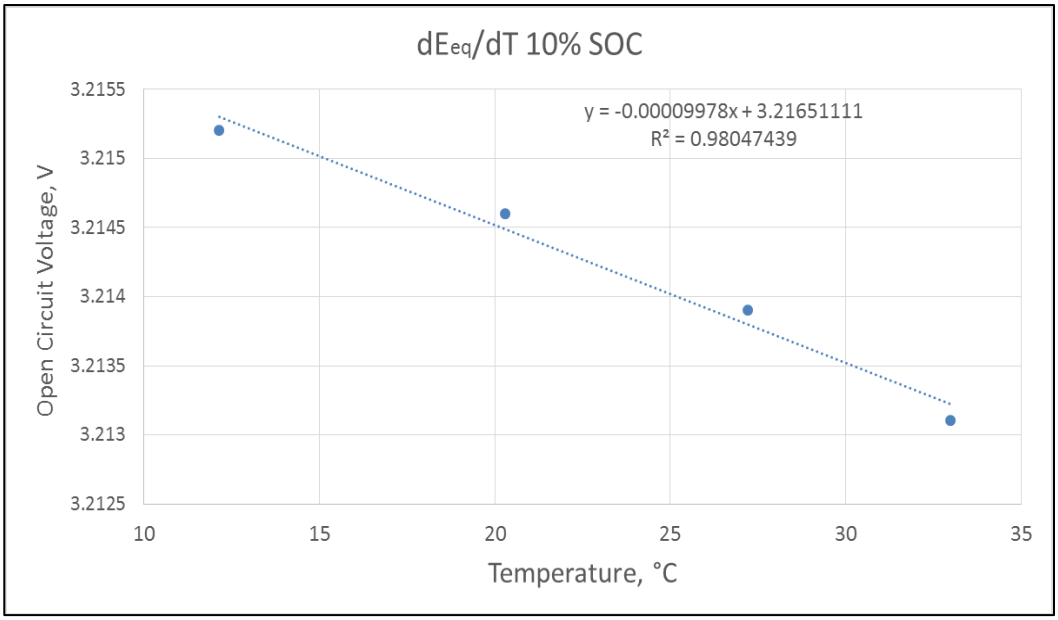

Figure F.4 Plot of Temperature vs. E_{eq} from 10% SOC equilibrium data points

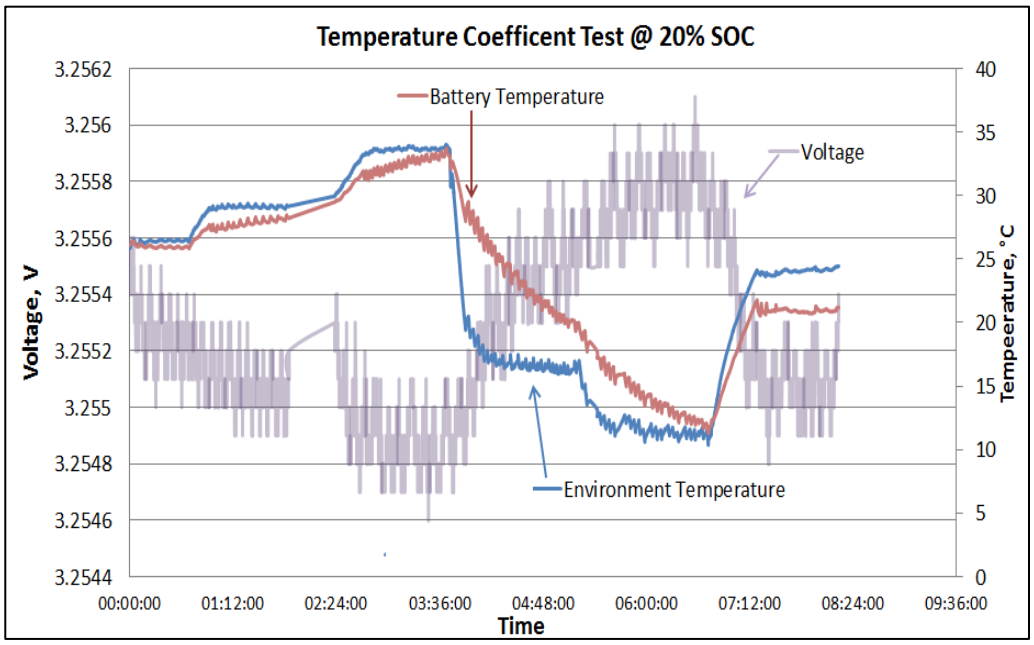

Figure F.5 Temperature Coefficient Test at 20% SOC

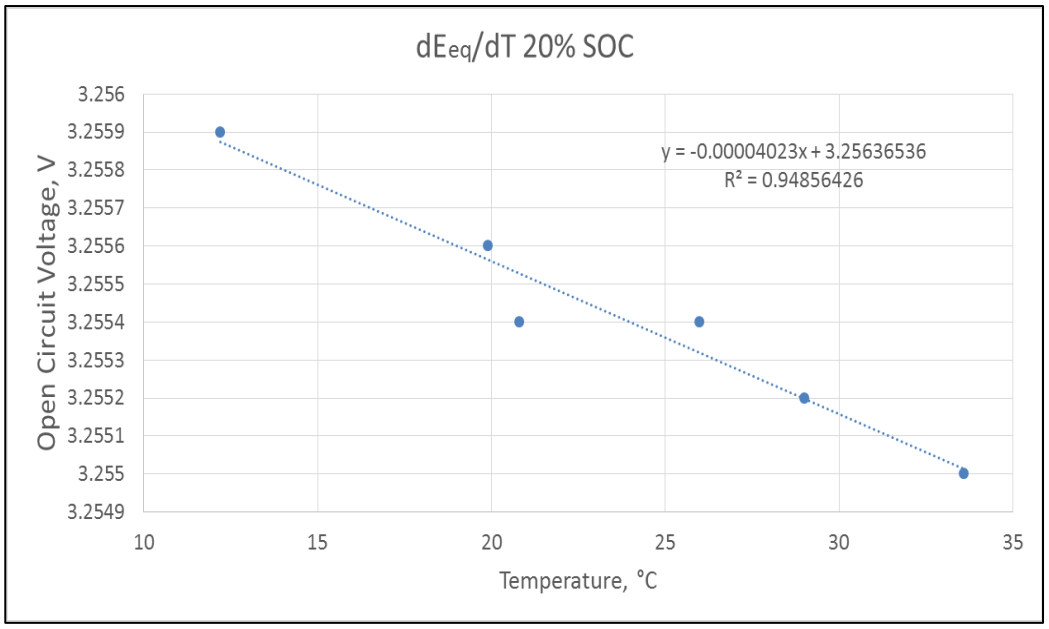

Figure F.6 Plot of Temperature vs. E_{eq} from 20% SOC equilibrium data points

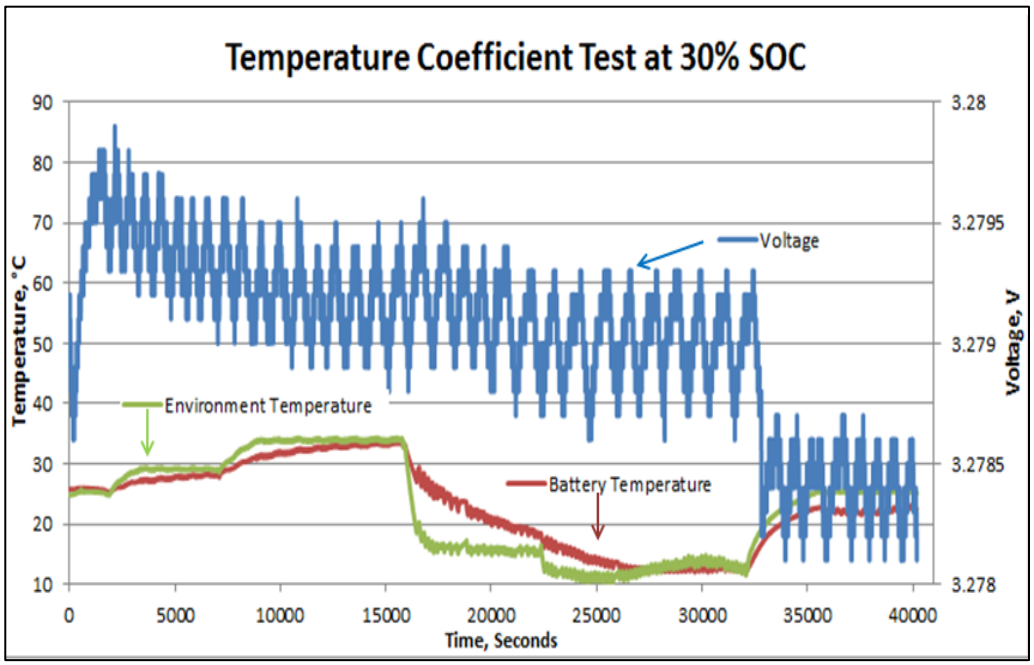

Figure F.7 Temperature Coefficient Test at 30% SOC

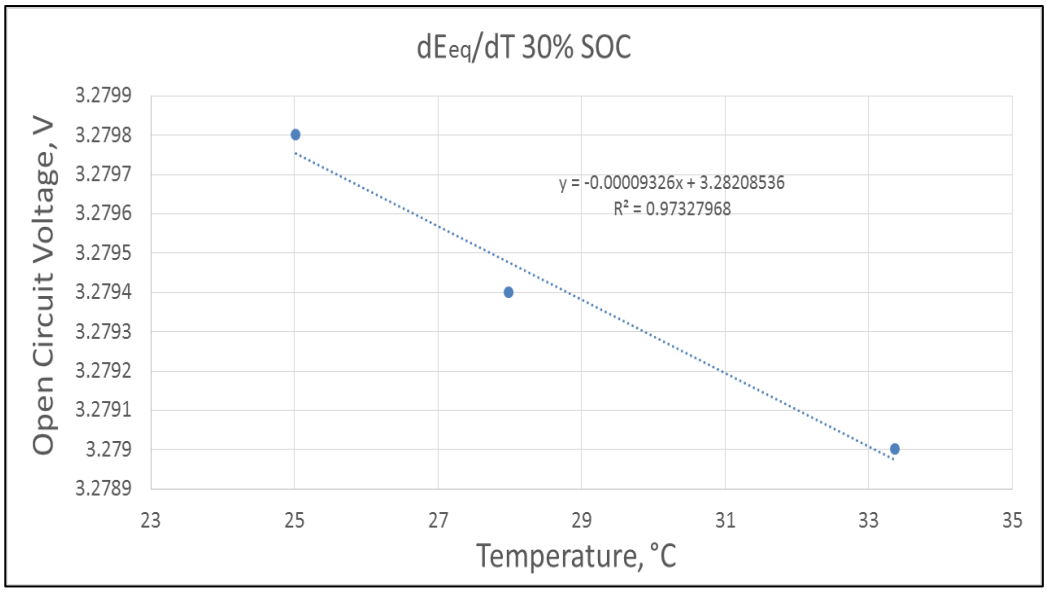

Figure F.8 Plot of Temperature vs. E_{eq} from 30% SOC equilibrium data points

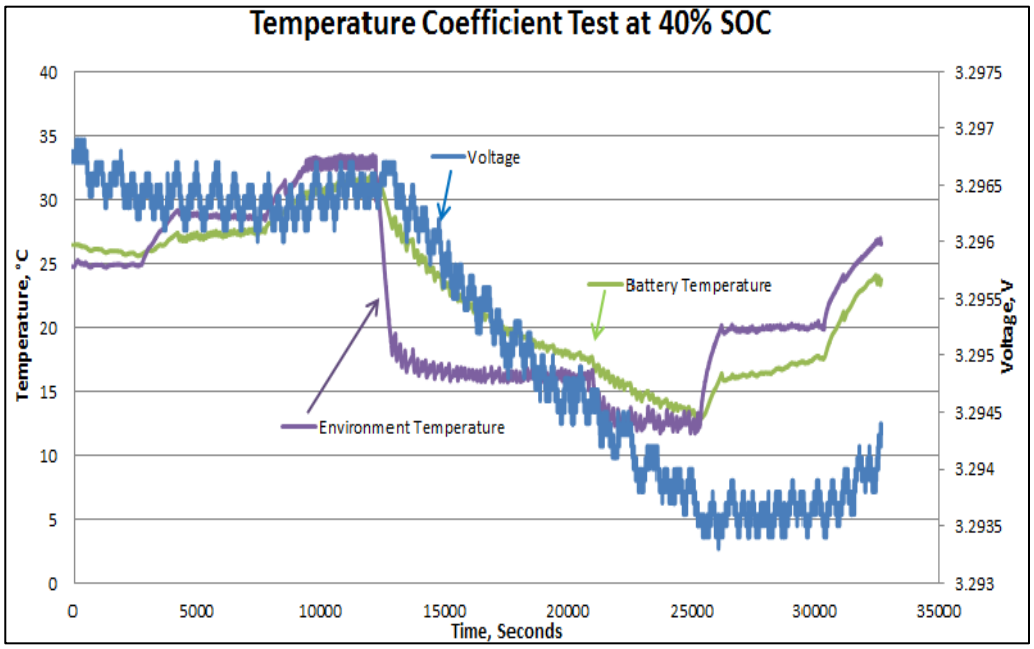

Figure F.9 Temperature Coefficient Test at 40% SOC

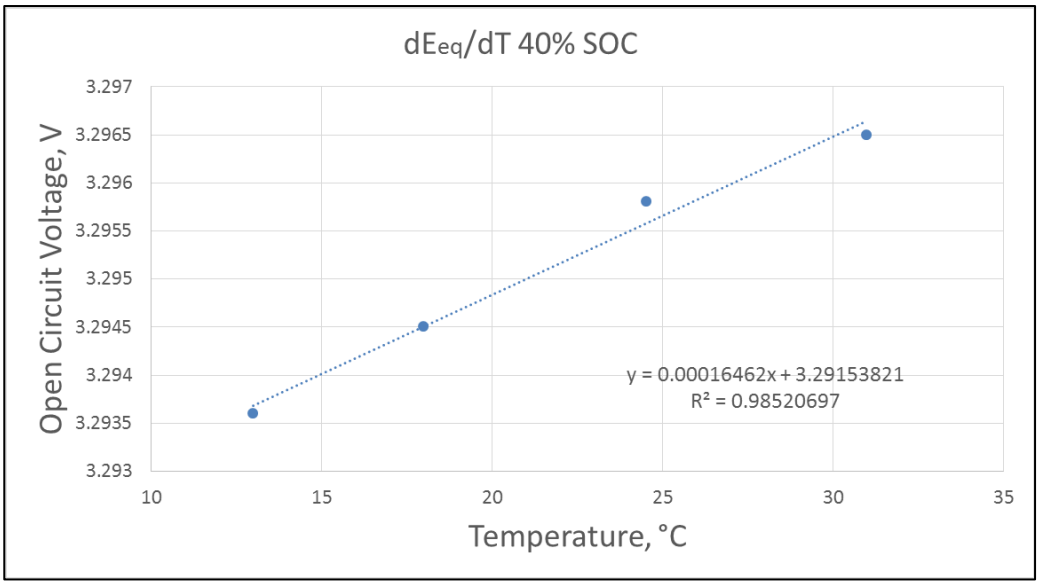

Figure F.10 Plot of Temperature vs. E_{eq} from 40% SOC equilibrium data points

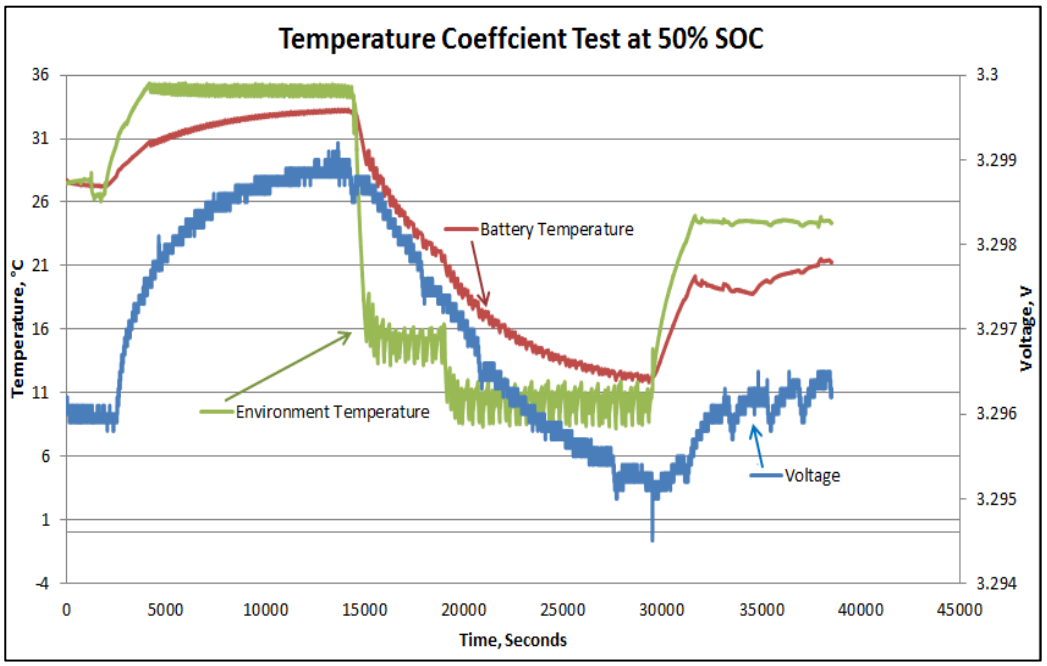

Figure F.11 Temperature Coefficient Test at 50% SOC

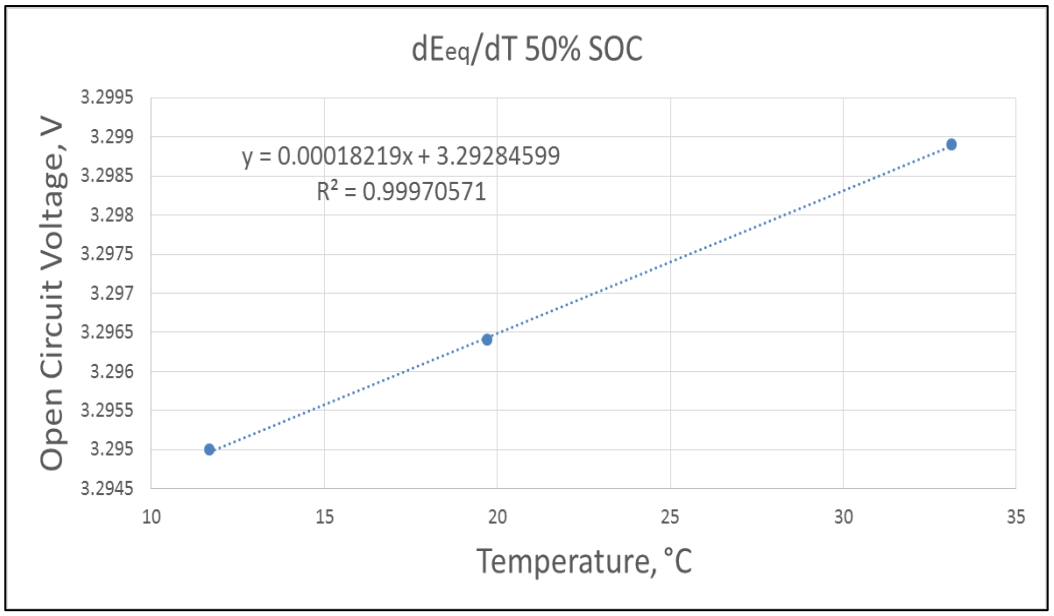

Figure F.12 Plot of Temperature vs. E_{eq} from 50% SOC equilibrium data points

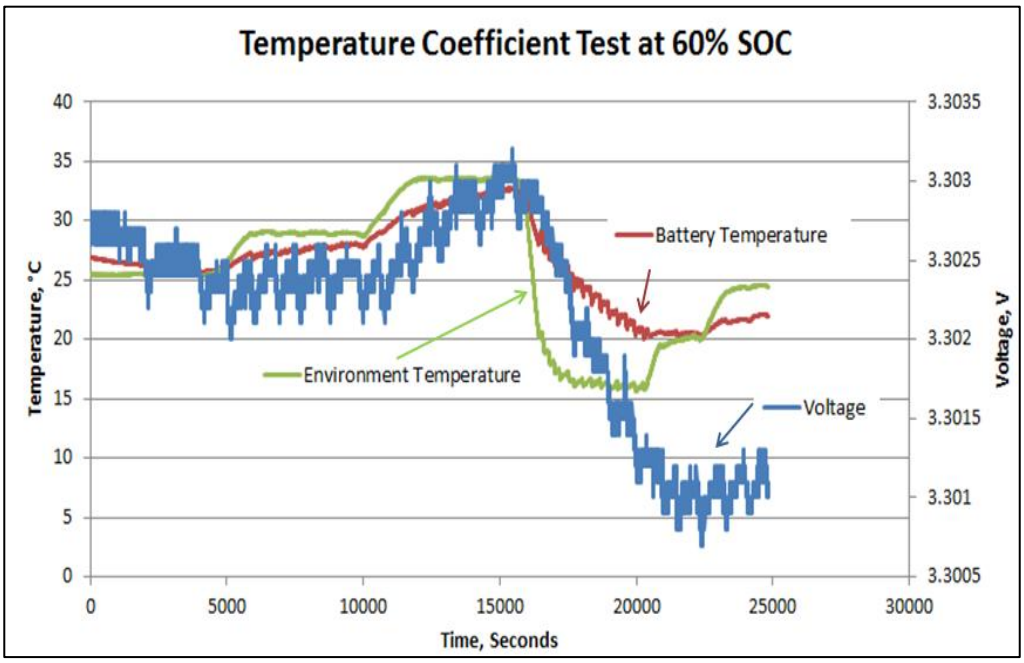

Figure F.13 Temperature Coefficient Test at 60% SOC

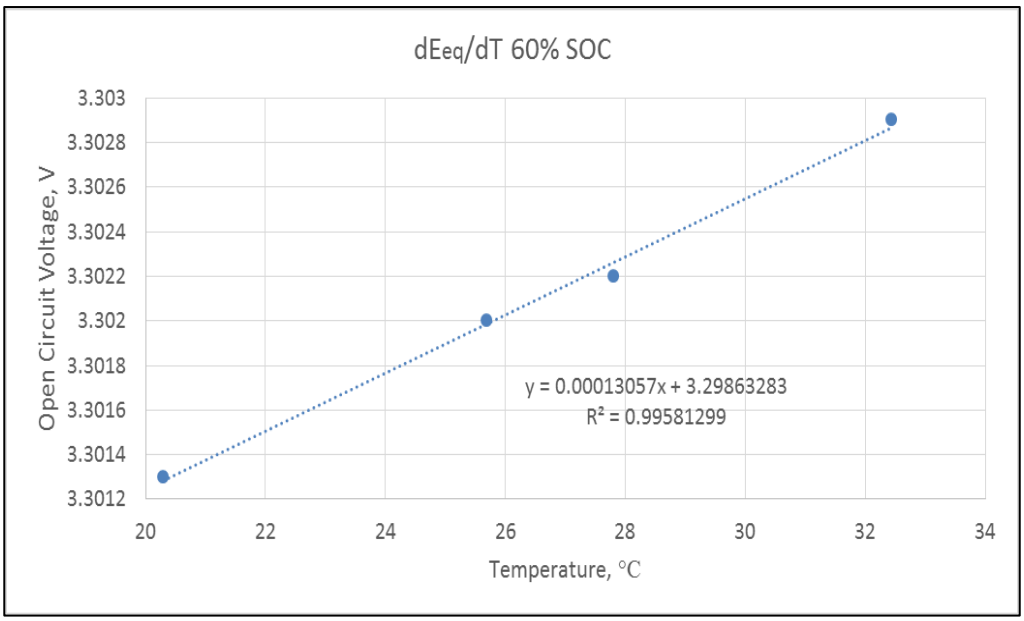

Figure F.14 Plot of Temperature vs. E_{eq} from 60% SOC equilibrium data points

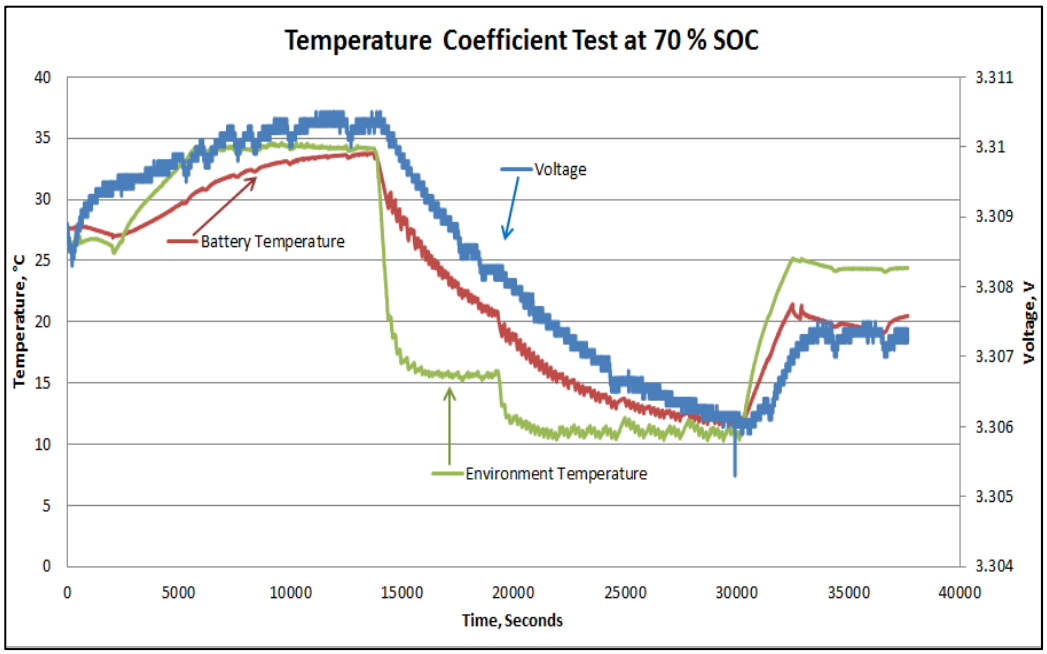

Figure F.15 Temperature Coefficient Test at 70% SOC

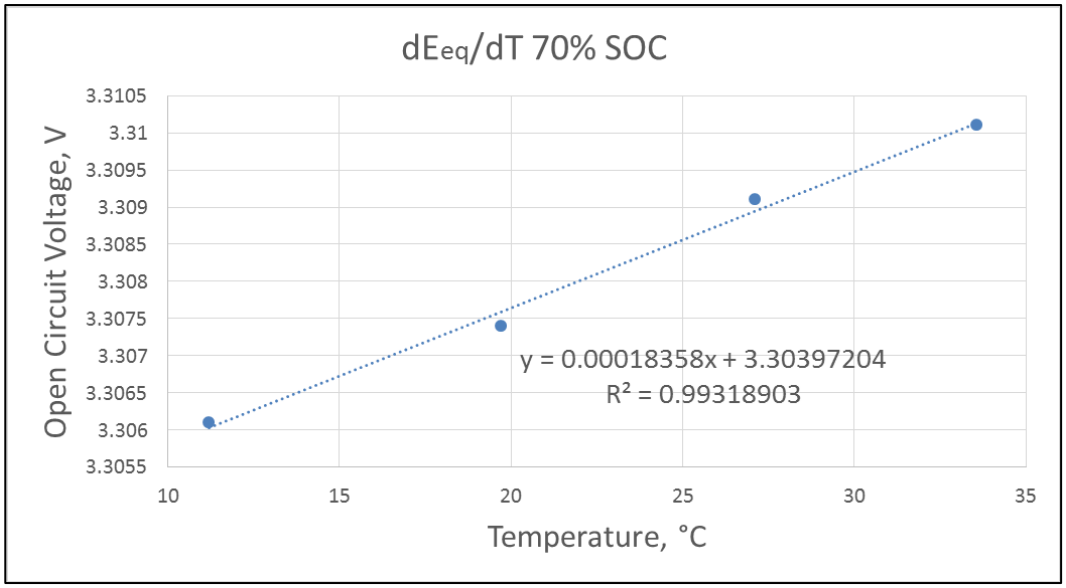

Figure F.16 Plot of Temperature vs. E_{eq} from 70% SOC equilibrium data points

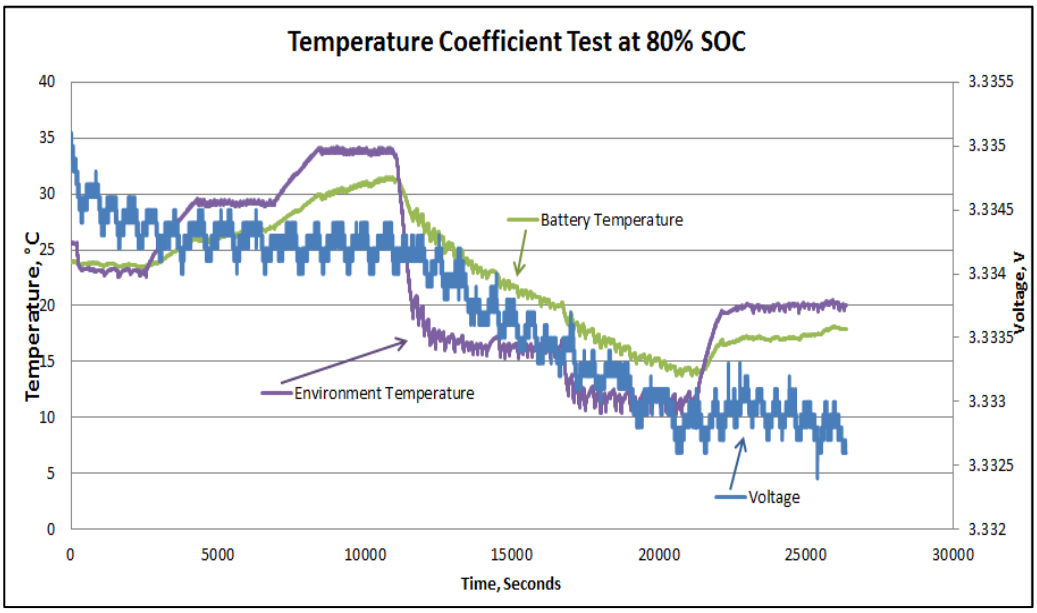

Figure F.17 Temperature Coefficient Test at 80% SOC

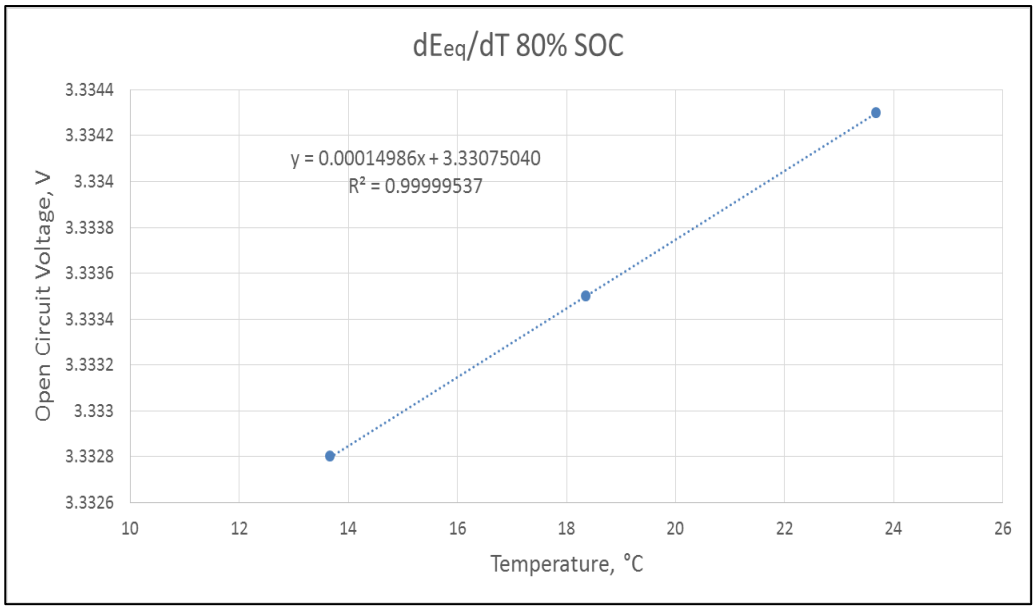

Figure F.18 Plot of Temperature vs. E_{eq} from 80% SOC equilibrium data points

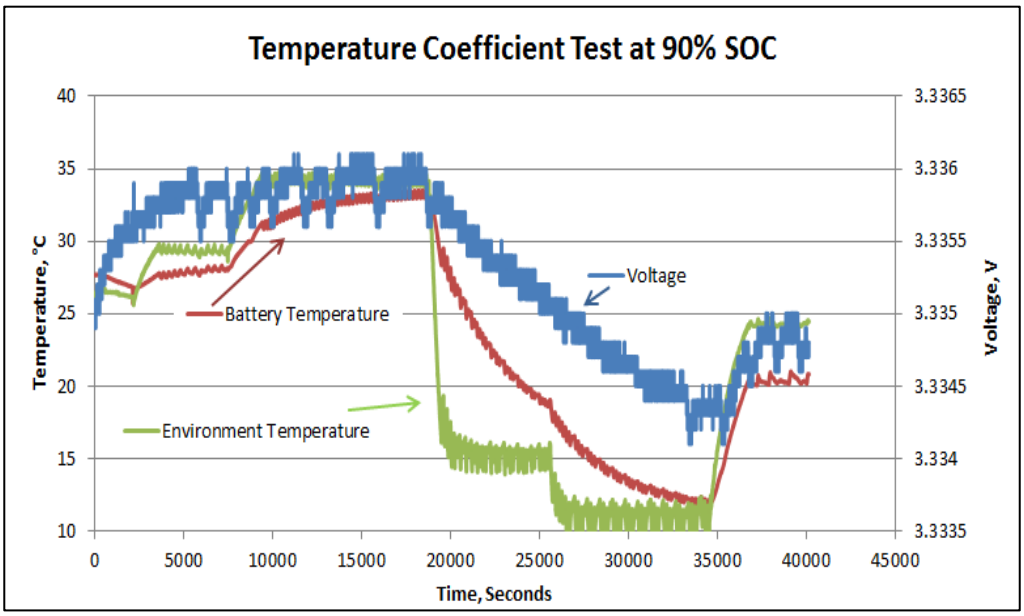

Figure F.19 Temperature Coefficient Test at 90% SOC

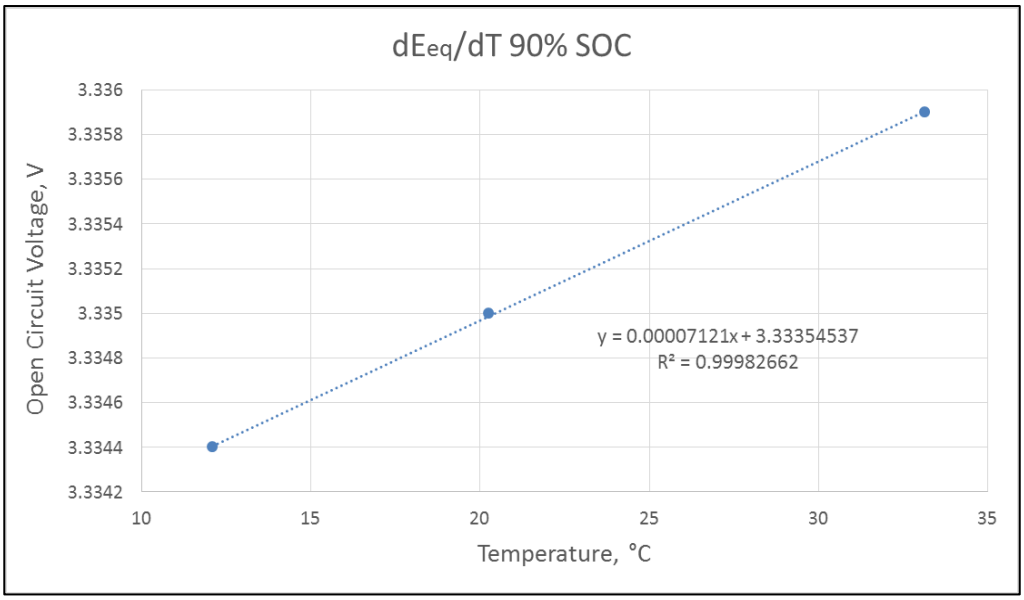

Figure F.20 Plot of Temperature vs. E_{eq} from 90% SOC equilibrium data points

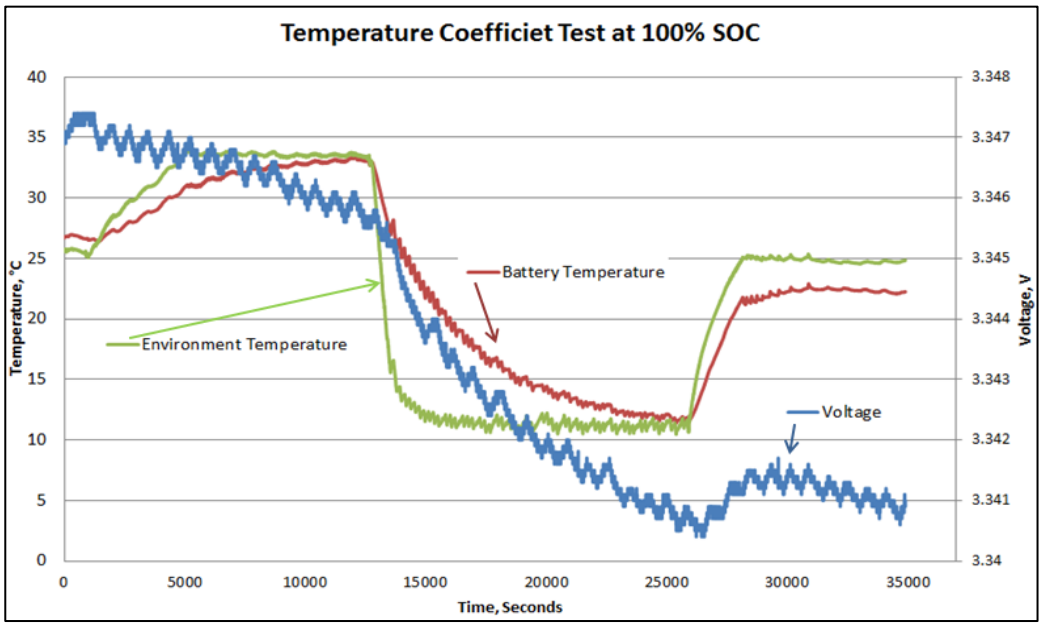

Figure F.21 Temperature Coefficient Test at 100% SOC

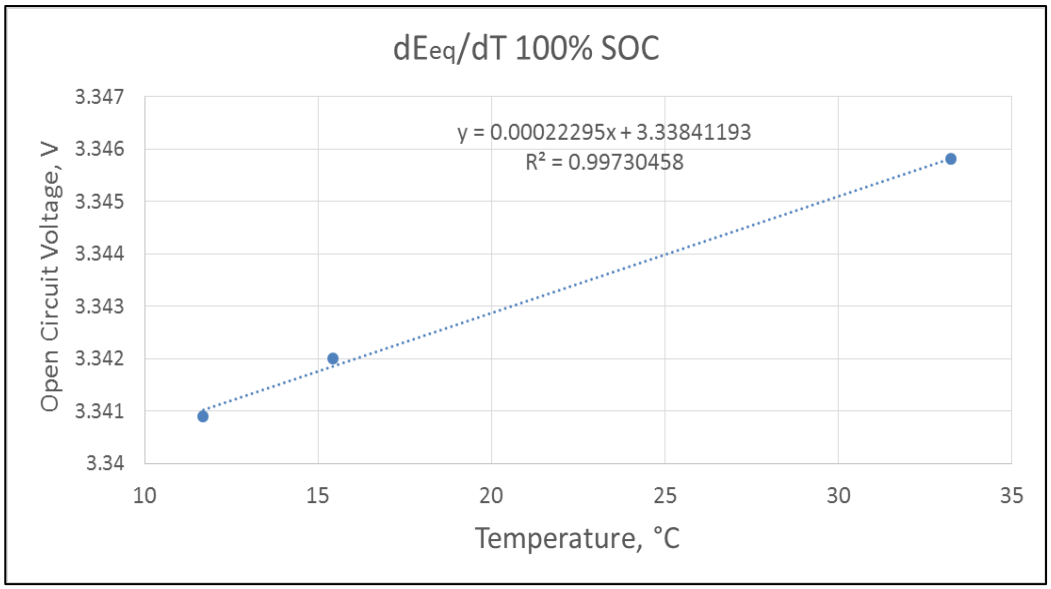

Figure F.22 Plot of Temperature vs. E_{eq} from 100% SOC equilibrium data points

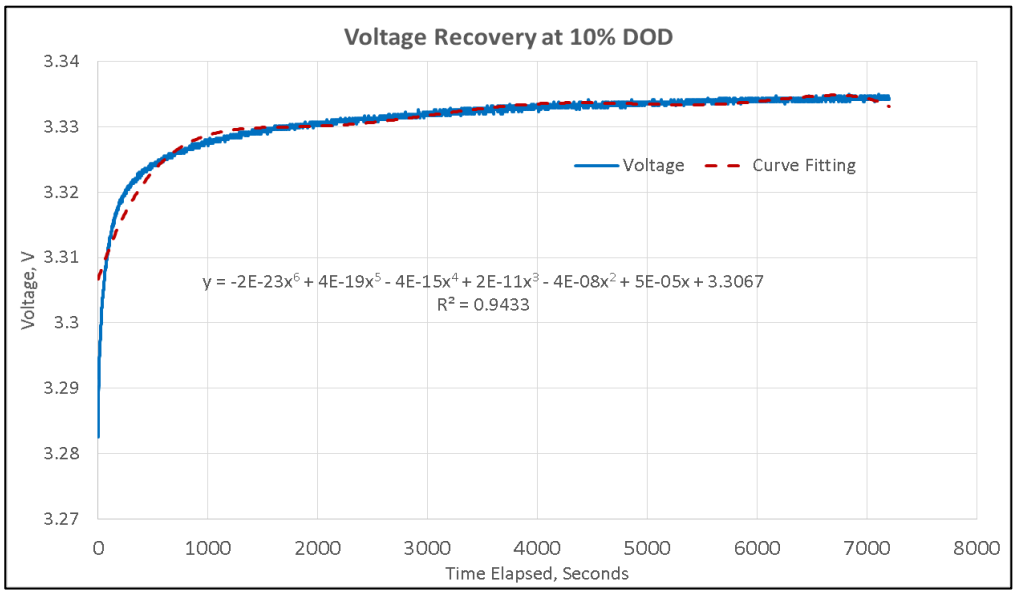

Figure F.23 Voltage Recovery from C/3 and 2 hour rest pulse test at 10% DOD

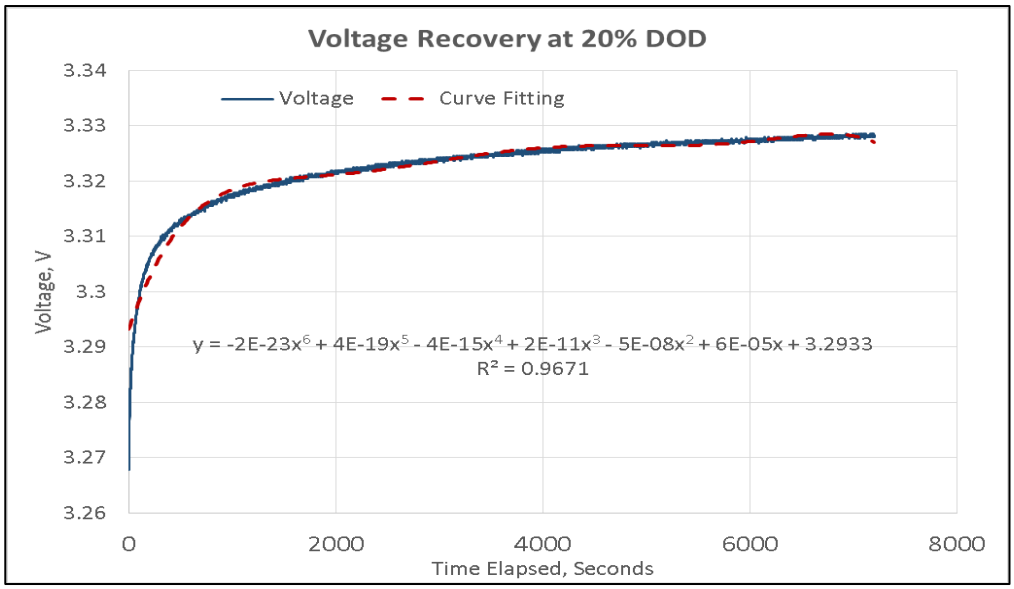

Figure F.24 Voltage Recovery from C/3 and 2 hour rest pulse test at 20% DOD

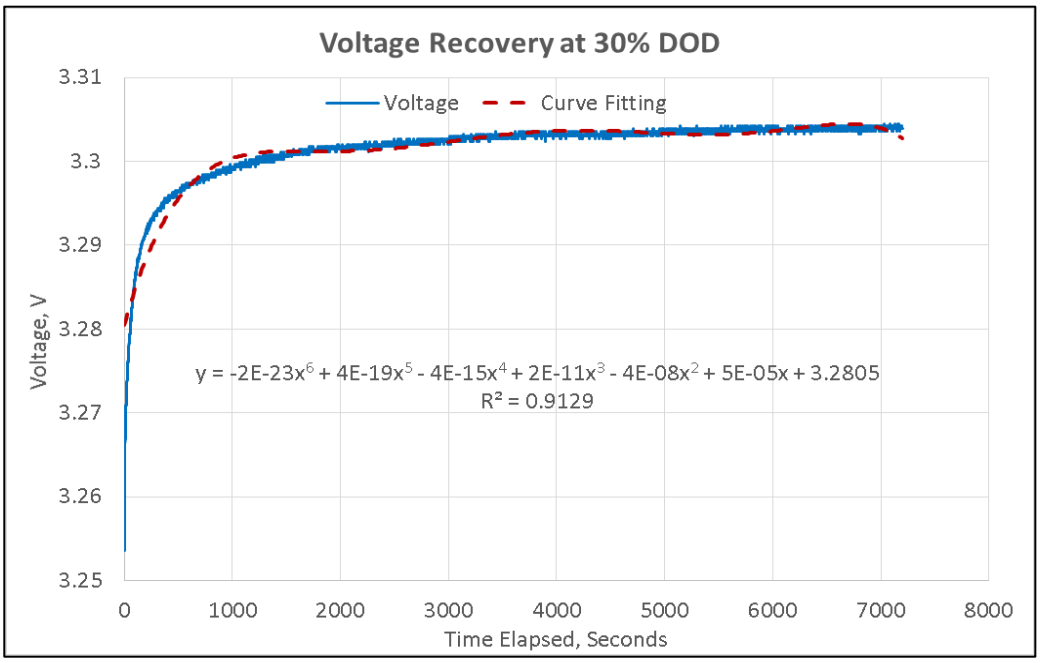

Figure F.25 Voltage Recovery from C/3 and 2 hour rest pulse test at 30% DOD

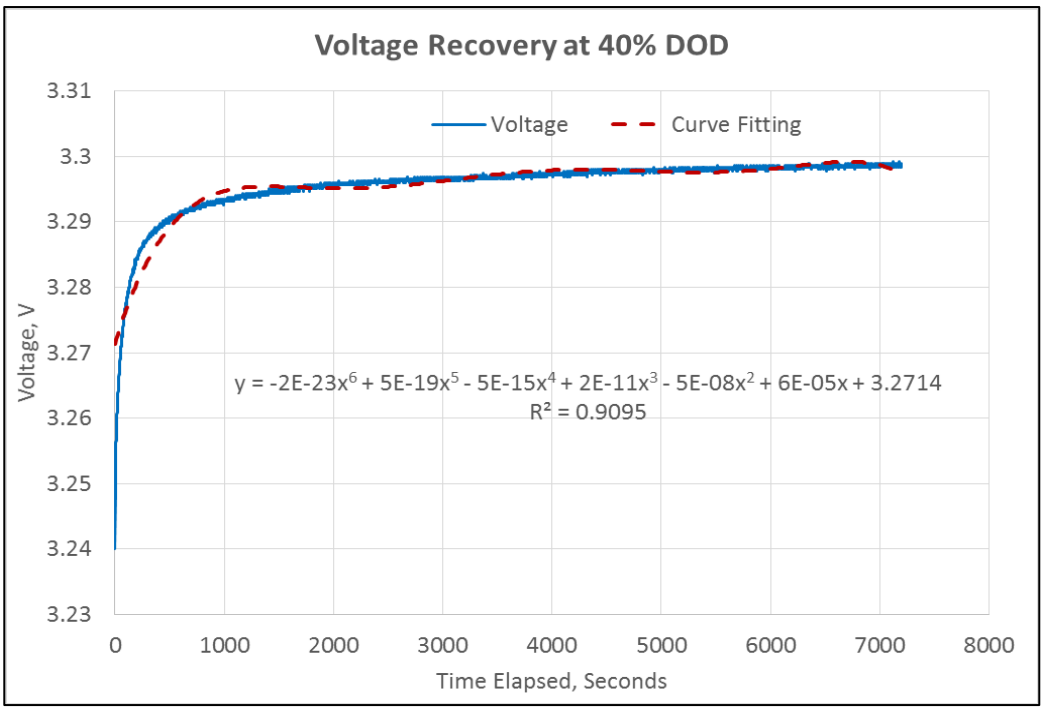

Figure F.26 Voltage Recovery from C/3 and 2 hour rest pulse test at 40% DOD

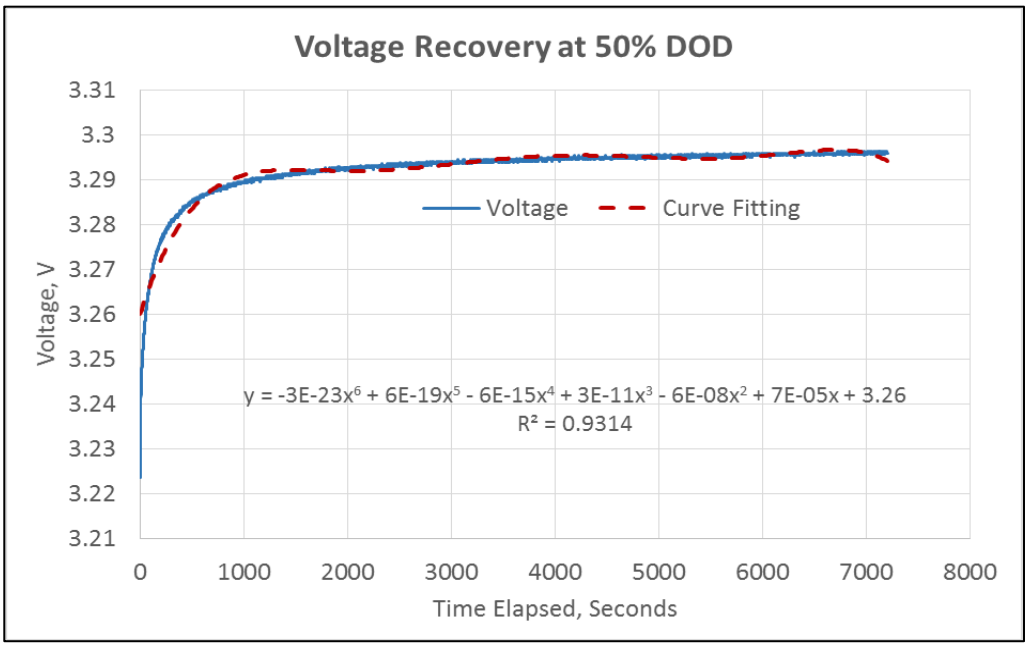

Figure F.27 Voltage Recovery from C/3 and 2 hour rest pulse test at 50% DOD

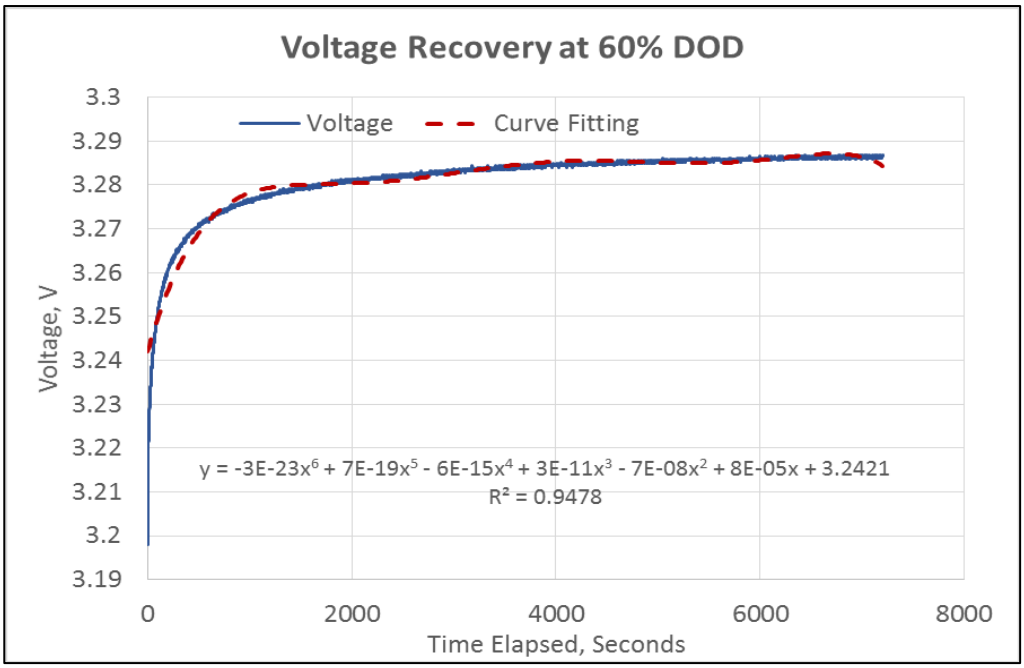

Figure F.28 Voltage Recovery from C/3 and 2 hour rest pulse test at 60% DOD

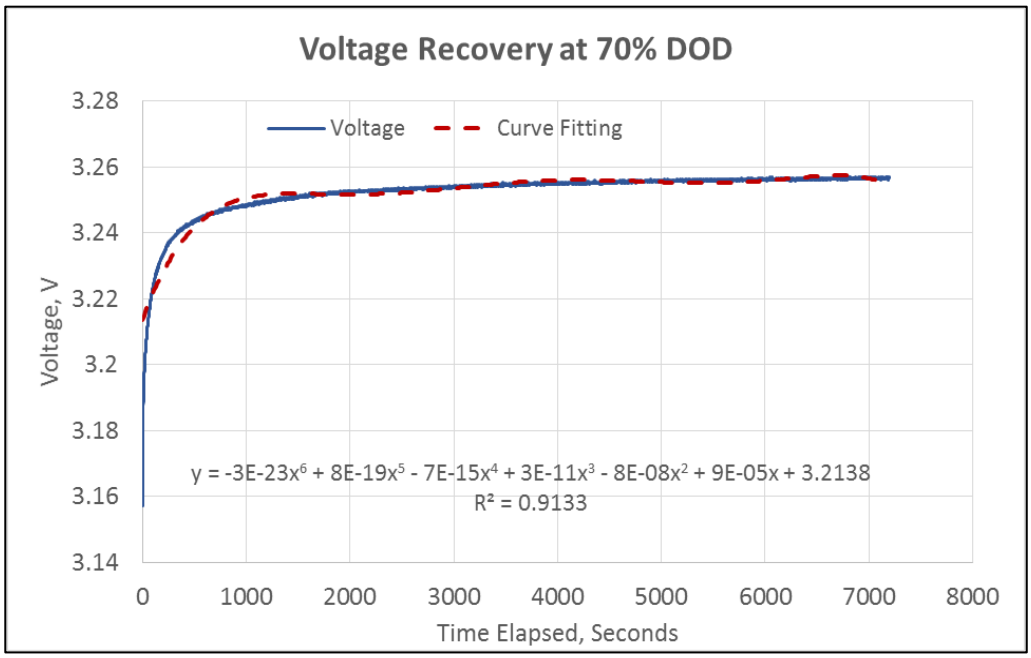

Figure F.29 Voltage Recovery from C/3 and 2 hour rest pulse test at 70% DOD

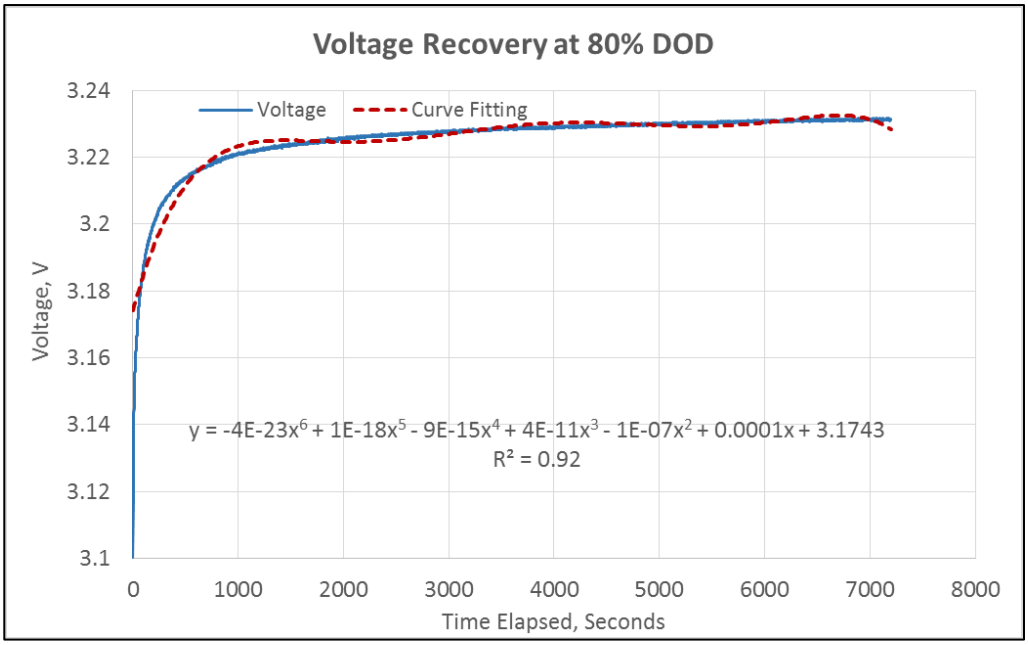

Figure F.30 Voltage Recovery from C/3 and 2 hour rest pulse test at 80% DOD

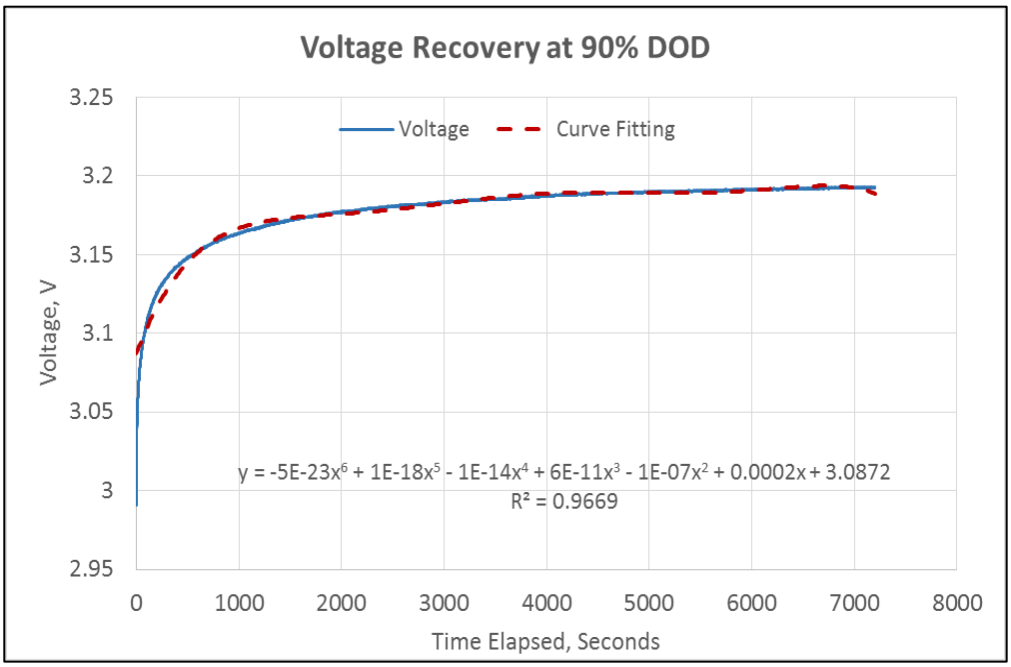

Figure F.31 Voltage Recovery from C/3 and 2 hour rest pulse test at 90% DOD

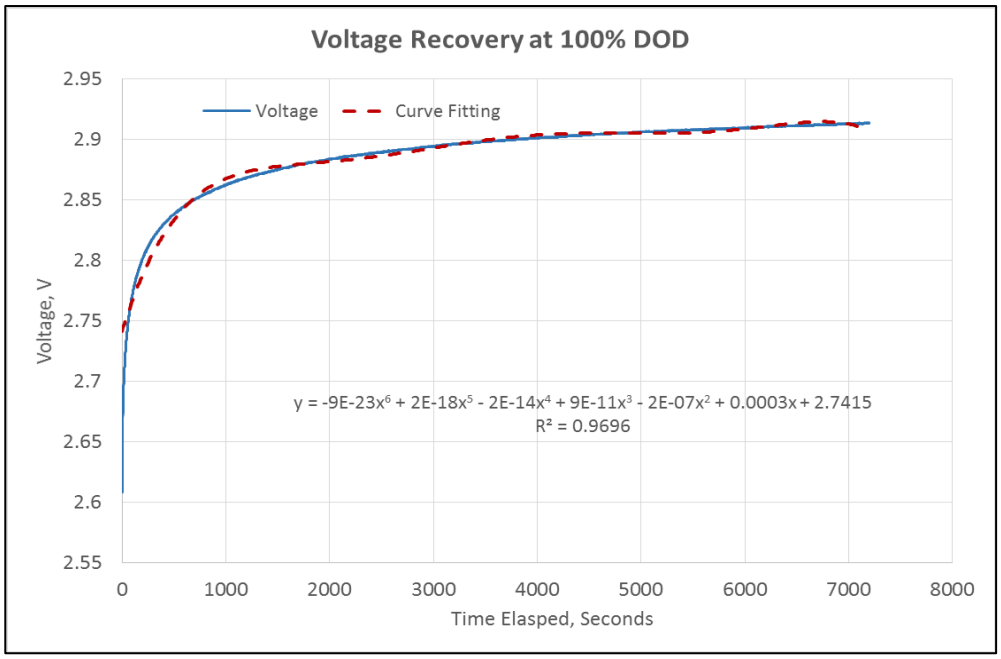

Figure F.32 Voltage Recovery from C/3 and 2 hour rest pulse test at 100% DOD

Depth of Discharge, %	Equilibrium Voltage, V
10	3.334
20	3.328
30	3.304
40	3.299
50	3.296
60	3.286
70	3.257
80	3.232
90	3.192
100	2.914

Table F.1 Equilibrium Voltage from Voltage Recovery C/3 and 2 hour rest pulse test

APPENDIX G

PROCEEDINGS


FISITA
2012
World Automotive Congress
27-30 November, Beijing, China
Final
Programme
FISITA 2012 World Automotive Congress
27th-30th November, Beijing, China
www.fisita2012.com
Automobiles and Mobility in a Low Carbon Economy
– China and the World
SAE
CHINA
FISITA

F2012-B04-007

DESIGN OF THE EXPERIMENTAL PROCEDURES FOR ANALYSIS OF THERMAL AND ELECTRICAL PROPERTIES OF A PRISMATIC LiFeYPO4 BATTERY IN A MODIFIED ELECTRIC CAR

[1]Sanguanwatana, Chayangkun[*]; [1]Srisurangkul, Chadchai; [2]Pimsarn, Monsak;
[3]Tsushima, Shohji
[1]Automotive Laboratory, National Metal and Materials Technology Center, Thailand;
[2]King Mongkut's Institute of Technology Ladkrabang, Thailand;
[3]Research Center for Carbon Recycling and Energy, Tokyo Institute of Technology

KEYWORDS – Lithium ion battery, Electric Vehicle, Lithium ion battery Thermal Characterization, Battery Thermal Management System, Battery Thermal Model

ABSTRACT
As being the most important part in the energy supply system, the battery must be carefully monitored in order to optimize the performance and to prolong its life. The most affected parameter to the battery is the operating temperature as the higher operating temperature increase the performance but shorten the life and with lower operating temperature can ensure longer life but reduce the performance. With this, the battery thermal management system is created in order to keep the operating temperature at the suitable range. In order to achieve this, thermal behaviour in loaded condition must be analysed beforehand. A series of experimental procedures is designed for the selected lithium iron phosphate battery to determine the thermal properties such as heat capacity, heat generation, and cell temperature according to the electrical load applied. Derived thermal model of lithium ion battery was utilized for this purpose as it shows the relationship between the thermal, electrical properties and other parameters such as voltage, current and cell temperature. When the battery is applied with electrical load, the data of voltage, current, and surface cell temperature can be used to determine the thermal properties and at the same time, electrical properties such as open circuit voltage, state of charge and internal resistance are also obtained for the performance evaluation.

INTRODUCTION

Electric vehicle has become one of the alternatives for replacing the fossil-fuel vehicle due to the rapid decrease in the energy source and increase in the automobile utilization. Also, with the zero pipe-tail emission, the replacement of electric vehicle can decrease a great deal of the amount of green house gas released into the earth's atmosphere. National Metal and Materials Technology Center, Thailand (MTEC) joined with Electricity Generating Authority of Thailand (EGAT) in order to form the electric car project modified from the conventional gasoline powered car. This has the conventional components replaced with the electrical ones such as motor and batteries. The benefits from this includes the reduced cost of purchasing a brand new electric car and this can demonstrate that in the future, used gasoline cars can be modified into electric cars which is a merit in terms of materials recycling.

Many tests are required in order to maximize the performance of the vehicle. In this paper, the main focus is put on the battery which is the most important component in the power supply system. With the proper design of battery management system, the performance of the battery can be maximized. Also, it is known that the greatest enemy of the battery is heat because heat is the main factor which impacts the battery's performance directly.

The sudden change in temperature can change the form of active chemicals in the battery. This result in many serious consequences depends on the temperature level. Extremely low operating temperature can cause lithium plating while charging the battery. On the other hand extremely high operating temperature can build up the pressure due to gassing inside the cell, cathode material breakdown and possibly thermal runaway. To keep the suitable operating temperature, battery thermal management system or in short BTMS can be a great help. BTMS is the system which monitors the battery temperature, provide the battery with the proper cooling system in order to prolong battery's life and maximize its performance. However, before the design of BTMS, it is best to understand the thermal behavior of the selected battery or to perform thermal characterization of the battery. This includes the determination of thermal properties of the battery which includes heat capacity and heat generation while the battery is loaded. As different amount of load is applied to the battery, it is expected to see the different results of thermal properties with different electrical load. With the data of thermal properties of the battery, thermal characterization can be performed to see the change in cell temperature and then BTMS can be designed based on those results.

LITHIUM IRON PHOSPHATE BATTERY

As known that lithium ion battery contains many attributes which has a lot of advantages over the other types of battery such as higher working voltage comparing to aqueous batteries, less self-discharge rate, higher energy density and contains no memory effect. With this, it was selected to be used for the modified electric car. The cell chemistry of the battery is "lithium iron yttrium phosphate" which has additional advantages comparing to the other types of lithium ion batteries. This includes the long life span, great thermal stability and less impact to the environment comparing to the cobalt cells. With great thermal stability, it becomes the safest lithium ion battery type because under the situation where the battery is misused such as in a very hot environment, lithium iron phosphate battery will not decompose at high temperature.

Cathode Material	Typical Voltage (V)	Energy Density		Thermal Stability
		Gravimeric (Wh/Kg)	Volumetric (Wh/L)	
Cobalt Oxide	3.7	195	560	Poor
Nickel Cobalt Aluminum Oxide (NCA)	3.6	220	600	Fair
Nickel Cobalt Manganese Oxide (NCM)	3.6	205	580	Fair
Manganese Oxide (Spinel)	3.9	150	420	Good
Iron Phosphate (LFP)	3.2	90-130	333	Very Good

Table 1: Characteristics of several types of lithium ion batteries[1]

From table 1, it can be seen that even though the operating voltage of lithium iron phosphate battery is the lowest among the others, the (thermal) stability is the best. As

invented by John Goodenough's research group at the University of Texas in 1996[2], it gradually became popular and is utilized many applications such as One Laptop per Child Program in China, Solar Powered Path Lights and many electrical-converted vehicle projects.

BATTERY THERMAL SAFETY ISSUES AND THERMAL MANAGEMENT SYSTEM

Abusive or uncontrolled use of a battery can lead to serious consequences. Cell voltage and operating temperature are the most affected parameters towards the failure of lithium batteries. It is needed to be controlled at some range. Figure 1 shows the safe area for using lithium ion cell.

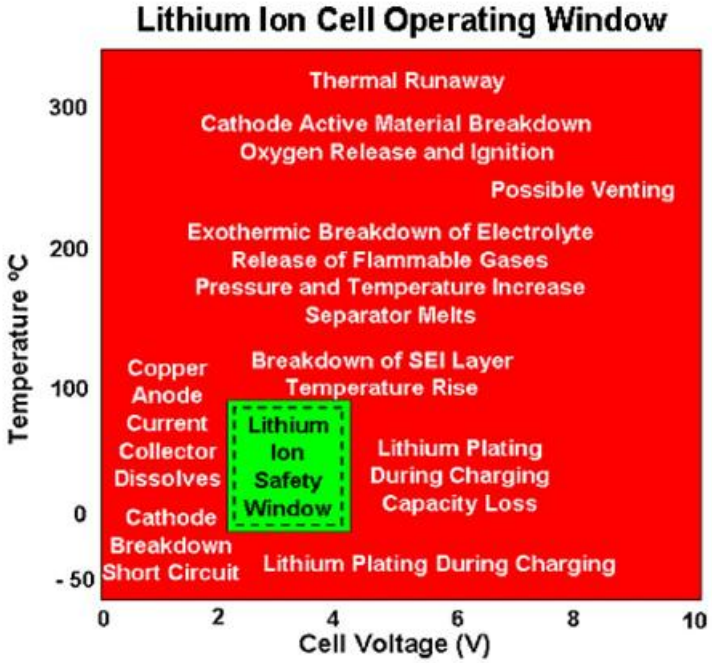

Figure 1: Lithium ion cell operating window[3]

From figure 1, it shows that many consequences from several abusive situation (dealing with voltage and temperature). This means that the user have to maintain the suitable range of operating voltage and temperature at the same time. For example, if the battery is used at room temperature but the battery was overcharged (overvoltage), it may result in lithium plating which permanently reduce the capacity. Or if the voltage is at 3.3 V but the operating temperature is well over 100°C, it will surely melts the separator inside the cell and short circuit the whole system. Thermal runaway is the most severe consequences which could ever happen because it can lead to the explosion of the battery.

At this point, the consequences of using the battery outside the temperature range can be more severe than using it outside the voltage range as it will not only damage the battery but also damage the user. Therefore, it is important that the operating temperature is kept at the optimized range.

Battery Thermal Management System (BTMS) is therefore designed for this purpose. It can be used to observe and regulate the temperature not to exceed the limit. This can help prolonging the life of the battery, maximize the performance and also ensure the highest degree of safety of the user. However, some procedures are needed before the construction of BTMS. According to NREL, following issues are to be discussed: cell characteristics, module cooling strategy, operating conditions and battery thermal responses.

In this case, the battery thermal response is the main focus. Various tools can be used in the development of the battery thermal management system. This includes thermal analysis (CAD), fluid and heat transfer experiments and simulations (CFD), thermal characterization and vehicle testing[4].

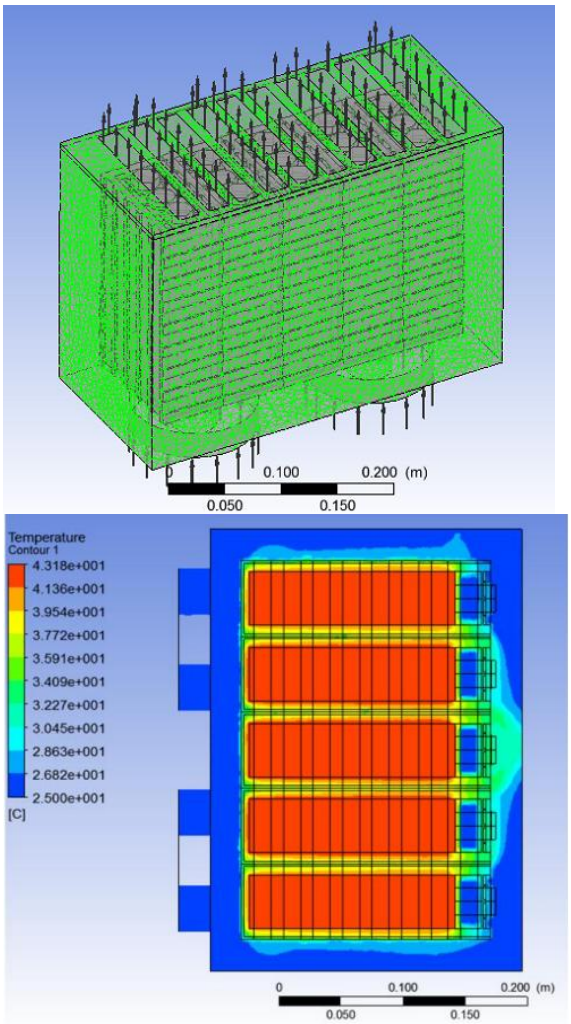

Figure 2: Simulation of fluid and heat transfer with thermal analysis of the battery[5]

An amount of work has been done in order to see how heat is transferred from the battery in the designed cooling method[5]. However, thermal properties of the battery used for this simulation is simply averaged from the data of chemistry structure of the cell in the manual from the manufacturer. To improve the accuracy of the results, thermal properties should be obtained by using thermal model of the battery.

BATTERY THERMAL MODEL

From the work of Newman et al[6] , it was found that many researchers[7][8][9] used the thermal model for a single cell in order to capture thermal behavior of the battery

while being loaded. Few assumptions are needed for applying this model such as the uniform temperature distribution throughout the cell and stable chemical reactions. It is summarized as followed:

$$I(V_{oc} - V) + IT_{cell}\frac{\partial V_{oc}}{\partial T_{cell}} = h\left(T_{surf} - T_{amb}\right) + C_p\frac{dT}{dt} \quad \text{---------- (1)}$$

I = Current (A), V_{oc} = Open Circuit Voltage (V), V = Cell Voltage (V)
T_{cell} = Internal Temperature (°C), T_{amb} = Ambient Temperature (°C),
T_{surf} = Surface Temperature (°C), C_p = Heat Capacity (J/°C), h = Surrounding heat coefficient (W/°C)

This equation is a result of a heat balance which considering the battery as a control volume. It can be seen that there are two terms on the left hand side. The first term is the overpotential resistance term which results from the electrical power applied, it is always positive. The second terms deal with the chemical reaction in the cell, the charge and discharge reaction can result in endothermic and exothermic condition for the battery respectively in which it can be related to the enthalpy change and Gibb's free energy. This second term on the left hand side is usually called the reversible entropic term and it can either positive or negative.

As for the right hand side, the first term represents the heat transfer from the battery to the surroundings, it can also be considered in terms of the difference between the cell surface and the ambient temperature. Surrounding heat transfer coefficient, h will also be one of the properties to be investigated before the calculations of heat capacity C_p. In the second term on the right hand side, heat capacity represents the amount of heat required for changing the temperature of the battery. It is the main focus for this research work.

DESIGN OF THE EXPERIMENTAL PROCEDURES

The main objective of this work is to determine thermal properties of the selected Li-ion battery at different loads and thermal environments. To simplify the procedures, the block diagram below shows the overall picture of this work.

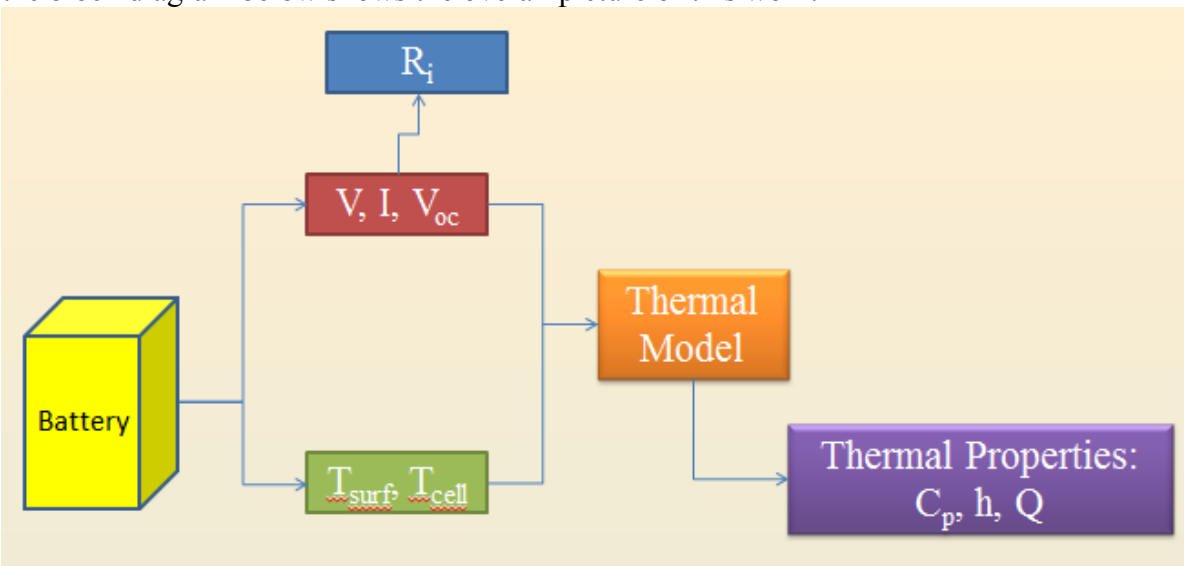

Figure 3: Block diagram shows overall picture of this research work

As illustrated in figure 3, to serve the main purpose of this work, it is needed to design the procedures in order to obtain the voltage and current load data while the battery is loaded and at the same time surface and cell temperature are also monitored. This is

based on the thermal model shown in the previous section which requires those data in order to determine thermal properties of the battery. Furthermore, R_i or internal resistance is included for evaluating the battery's performance and is calculated from the data of voltage and current load.

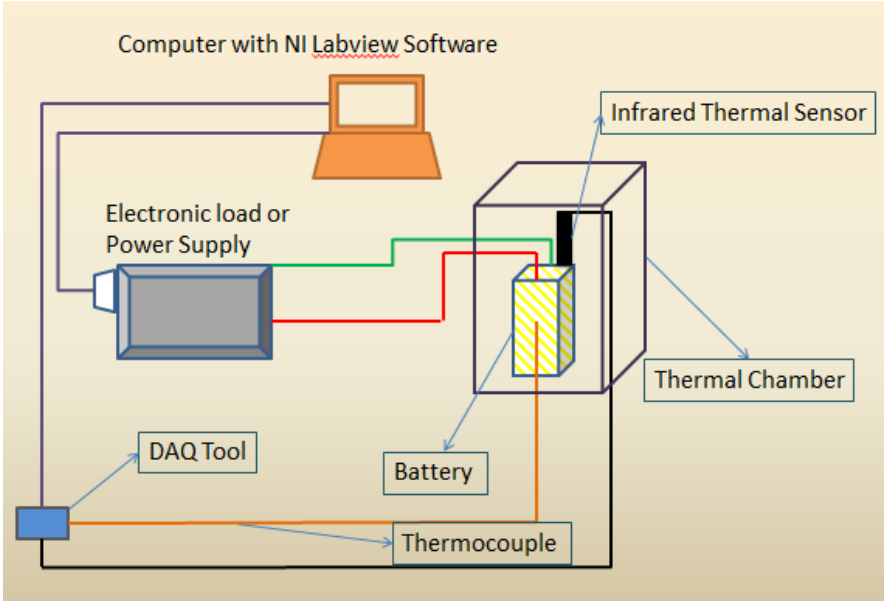

Figure 4: Schematic diagram for the experimental setup.

From figure 4, a selected battery is connected to the electronic load/power supply with thermocouple probe attached to the surface and infrared temperature sensor attached at the top of the cell in order to measure the internal temperature. The electronic load and power supply are used for discharging and charging the battery respectively. The infrared thermal sensor for measuring the cell internal temperature. Thermocouple cannot be used for measuring internal temperature is because it is required to contact the core of the cell which can lead to short circuit. Therefore, using the non-contact measurement is more suitable. The small blue box represents the Data Acquisition tool where it is used for recording the temperature measured at the surface and the cell. A computer is used for storing the experimental data for the analysis. The transparent purple box is the thermal chamber where it will be used for regulating the environmental temperature around the battery, this deals with the temperature coefficient which will be explained in the next section.

The selected lithium ion battery is the Thunder Sky lithium iron phosphate battery with the capacity of 60 Ah. Specifications are shown below:

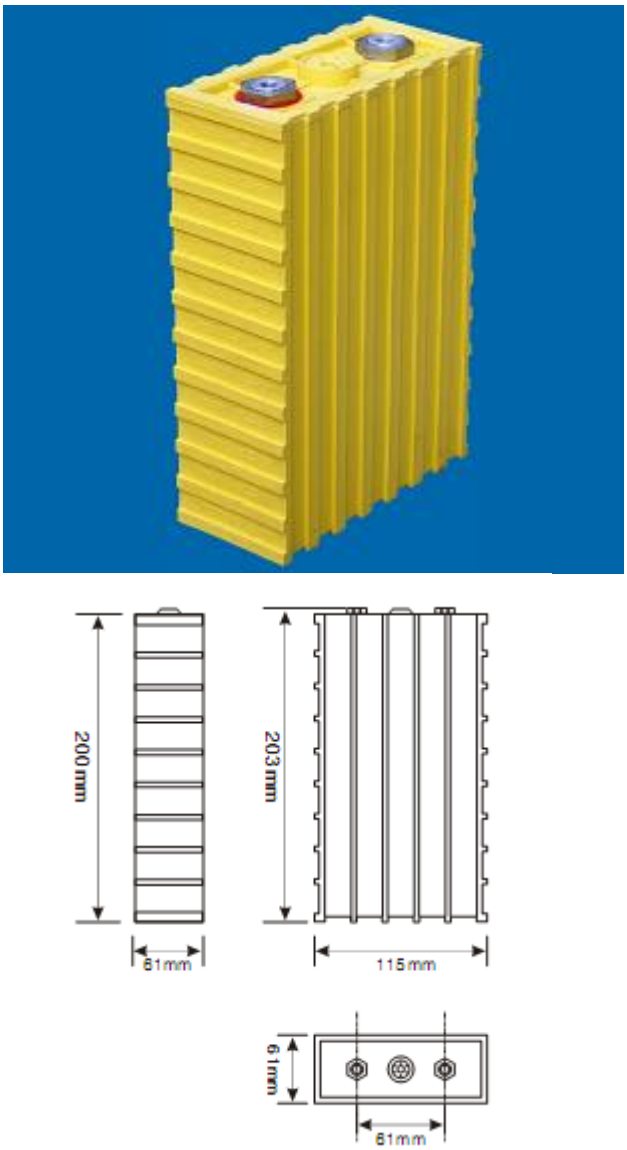

Figure 5: The selected battery for the experiment[10]

Model	TS-LFP60AHA
Nominal Capacity	60Ah
Operation Voltage	Charge: 4.0V, Discharge: 2.8V
Maximum Charge Current	Less or equal to 3CA
Maximum Discharge Current	3CA or less for constant current 20CA or less for impulse current
Standard Charge/Discharge Current	0.5CA
Cycle Life	(80DOD%) ≥3000 times (70DOD%) ≥5000 times
Temperature Durability of case	≤200°C
Operating temperature	-45°C ~ 85°C for both charge and discharge
Self-discharge rate	≤3% (Monthly)
Weight	2.3kg ±50g

Table 2: Specifications of the selected battery for the experiment[10]

The design of experimental procedures is based on the thermal model of the battery and also the specifications of the battery. The procedures are divided into two main parts:

1. Determination of heat generated from the cell
2. Calculations of thermal properties of the cell

In the first part, the heat generated from the cell is the combination of all terms on the left hand side in equation 1. This can be obtained from recording the voltage, current and cell temperature while the battery is being charged or discharged. The main parameter here is the current load applied (I), which can be 1CA. 0.5CA or 2CA.

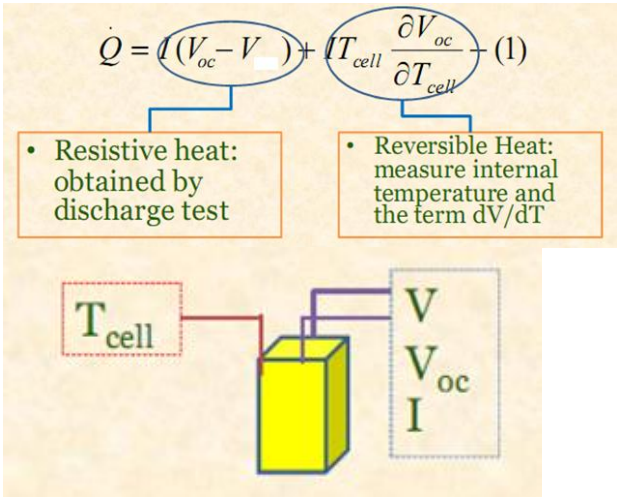

Figure 6: Determination of heat generated from the cell

However, in the second term, dV/dT or the temperature coefficient is present. This has to be determined in a separated experiment. See figure below for illustrations:

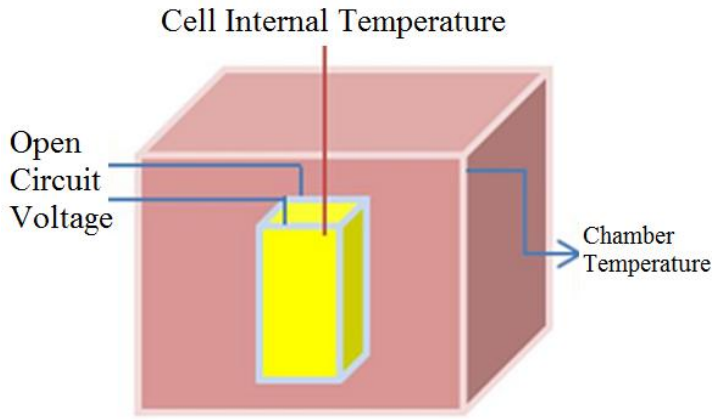

Figure 7: Experiment for the temperature coefficient.

The battery is put inside the adjustable temperature thermal chamber and while the environmental temperature is adjusted, the cell temperature and open circuit voltage will be observed and recorded. This will be used for the calculation of temperature coefficient.

In the second part, when the battery is charged or discharged and the voltage, current and temperature data are gathered, thermal properties can be determined. From equation 1, it can be seen that there are two variables to be determine. They are heat capacity (C_p) and surrounding heat transfer coefficient (h).

With the steady state condition, where the cell temperature stay constant with time ($\partial T_{cell}/\partial t = 0$), the term with heat capacity will be eliminated and thus, surrounding heat transfer coefficient (h) can be determined and while this depends on the current load applied to the battery, I (and also the heat generated, Q). Therefore, when surrounding heat coefficient is determined, it can be applied in the transient condition ($\partial T_{cell}/\partial t \neq 0$) to find the heat capacity of the battery.
The initial condition has the 100% charged battery stored in the room temperature. As the battery is put through the discharge test, the value of $V\text{-}V_{oc}$ will be changed as the depth of discharge increases. Also, the cell temperature here will also be increased, then, the value of Q will be different in the different state of charges. This will also apply on surrounding heat transfer coefficient and heat capacity and explained in the previous paragraph. This will also include the other experiment with different amount of current load applied to see the change in the focused thermal properties.

PRELIMINARY STUDY AND RESULTS

At this stage, performance characteristics of the battery were studied. These include the charge and discharge profile (constant and pulsed current). The surface and terminal temperature were also recorded.

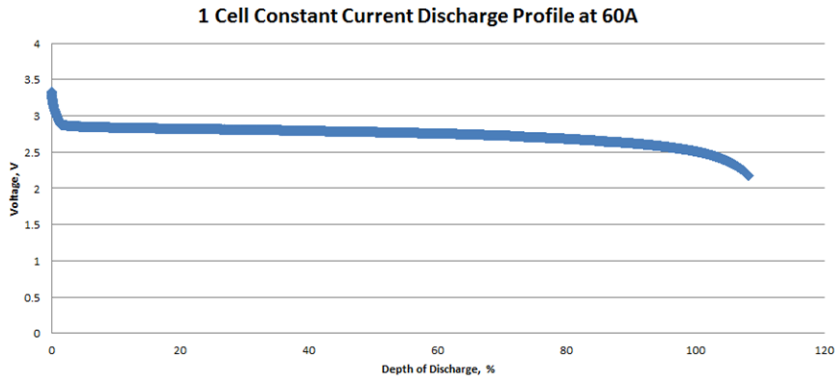

Figure 8: Constant current discharge profile

From the figure, the voltage response from the constant current discharge shows that it tends to be flat from 10% - 80% depth of discharge. This is suitable for the electric vehicle application due to its voltage stability. Furthermore, the chemistry of lithium iron phosphate gives the advantage in terms of thermal stability as it is unlikely to reach the stage of thermal runaway unless is extremely abused.

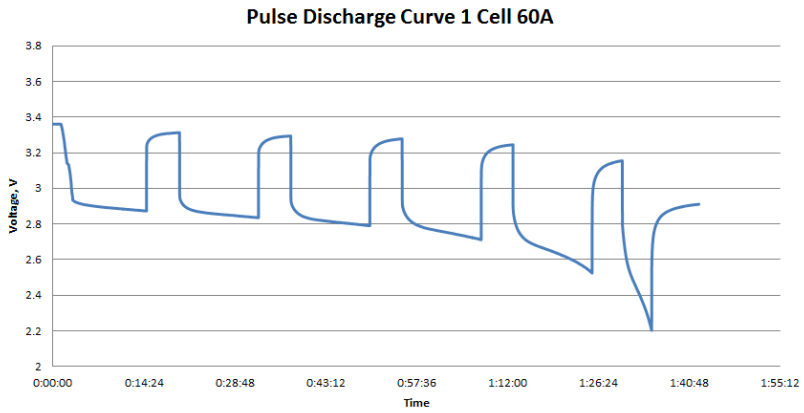

Figure 9: Pulse discharge curve profile

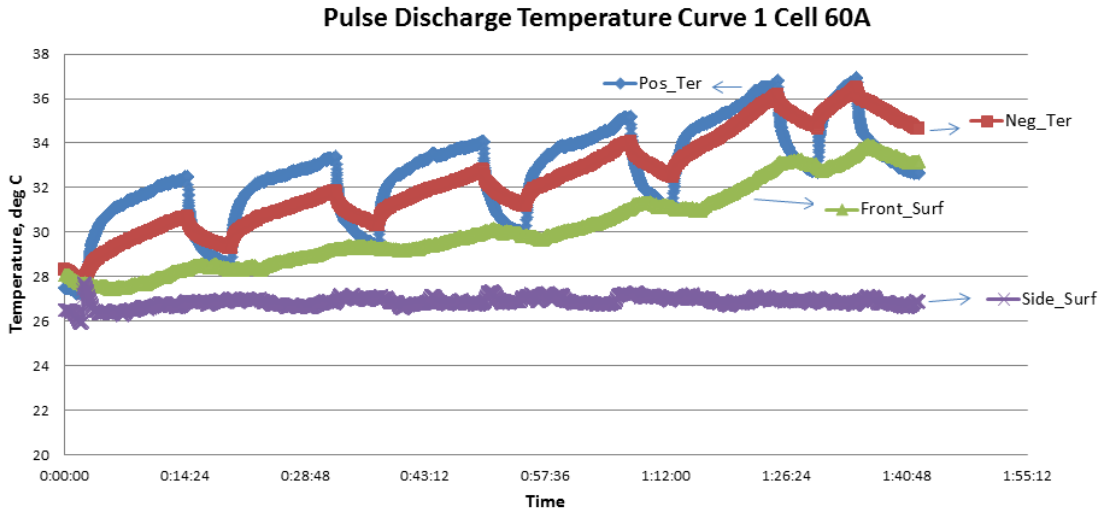

Figure 10: Battery surface and terminal temperature response from pulse discharge test.

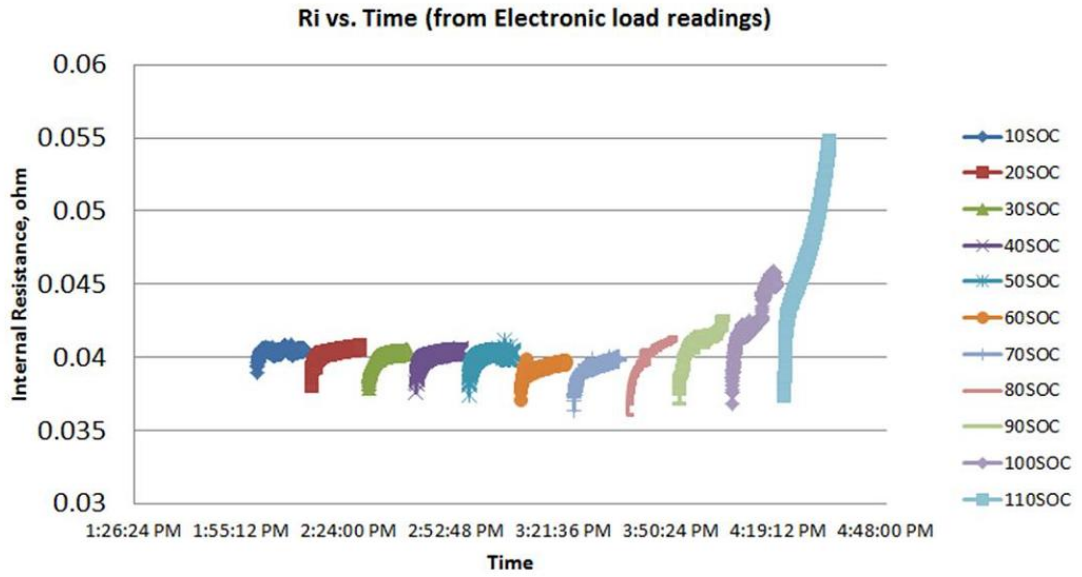

Figure 11: Internal Resistance calculated from the pulse test result (60A)

From figure 9 and 10, the temperature response from the pulse test shows that terminal temperature is more sensitive than surface temperature because when the load is put to zero, surface temperature dropped until the load is turned back on again.

The advantages of conducting pulse current test are that more data can be obtained and the dynamic of temperature change can also be captured. In this test, open circuit voltage can be observed as used for calculating heat generation as noted in thermal model. Furthermore, the data obtained from the pulsed discharge curve can be used to calculate the internal resistance which can also estimate battery's life as shown in figure 11.

Note that in this test, surface temperature is only measured at two points in front of and on the side of the battery. Also, it is observed that the positive terminal gives out heat more than that of negative terminal. This concludes that positive terminal is the point of heat concentration.

CONCLUSIONS

Experimental procedures have been designed for the determination of thermal properties of the selected battery for the modified electric vehicle. Currently, the charge and discharge characteristics of the battery are obtained and in the same time surface and terminal temperature are monitored. In the next step, infrared temperature sensor will be installed at the top of the battery for internal temperature measurement. This is the main key towards the goal of this research work because the data of internal temperature of the battery can be used to calculate for thermal properties of the battery. Finally, when the data of thermal properties are obtained, it will be hand over to the design team of BTMS of the modified electric car and the cooling system of the battery.

REFERENCES

[1] Woodbank Communication. "Rechargeable Lithium Batteries"[W]. Electropaedia: Battery and Energy Technology, 2005, http://www.mpoweruk.com/lithiumS.htm
[2] A.K. Padhi, K.S. Nanjundaswamy, J.B. Goodenough . "$LiFePO_4$: A Novel Cathode Material for Rechargeable Batteries" [J]. Electrochimical Society Meeting Abstracts, 1996, 96-1, pp 73
[3] Woodbank Communication. "Lithium Battery Failures"[W]. Electropaedia: Battery and Energy Technology, 2005, http://www.mpoweruk.com/lithium_failures.htm
[4] A.Pesaran. "Battery Thermal Management, Battery Modeling and Validation, Ultracapacitor Modeling and Hybridization"[J]. National Renewable Energy Laboratory, 2002
[5] V.Vuthiwongvarakorn. N. Taychavinijudom. "Design of a Battery Thermal Management system for Electric Vehicle"[R]. 2010
[6] K.E.Thomas. J.Newman. "Thermal Modeling of Porous Insertion Electrodes"[J]. Journal of The Electrochemical Society, 2003, 150(2), pp 176- 192
[7] C.Forgez. "Thermal modeling of a cylindrical $LiFePO_4$/graphite lithium-ion battery"[J]. Journal of Power Sources, 2009, 195, pp 2961-2968
[8] K. Onda. "Thermal behavior of small lithium-ion battery during rapid chage and discharge cycles"[J]. Journal of Power Sources, 2006, 158, pp 535-542
[9] N.Sato. "Thermal behavior analysis of lithium-ion batteries for electric and hybrid vehicles"[J]. Journal of Power Sources, 2001, 99, pp70-77
[10] ThunderSky Lithium Battery. "THUNDER SKY LiFeYPO4 POWER BATTERY SPECIFICATIONS"[M]. ThunderSky

Note: [M]: Manual
[R]: Report
[W]: Website
[J]: Journal

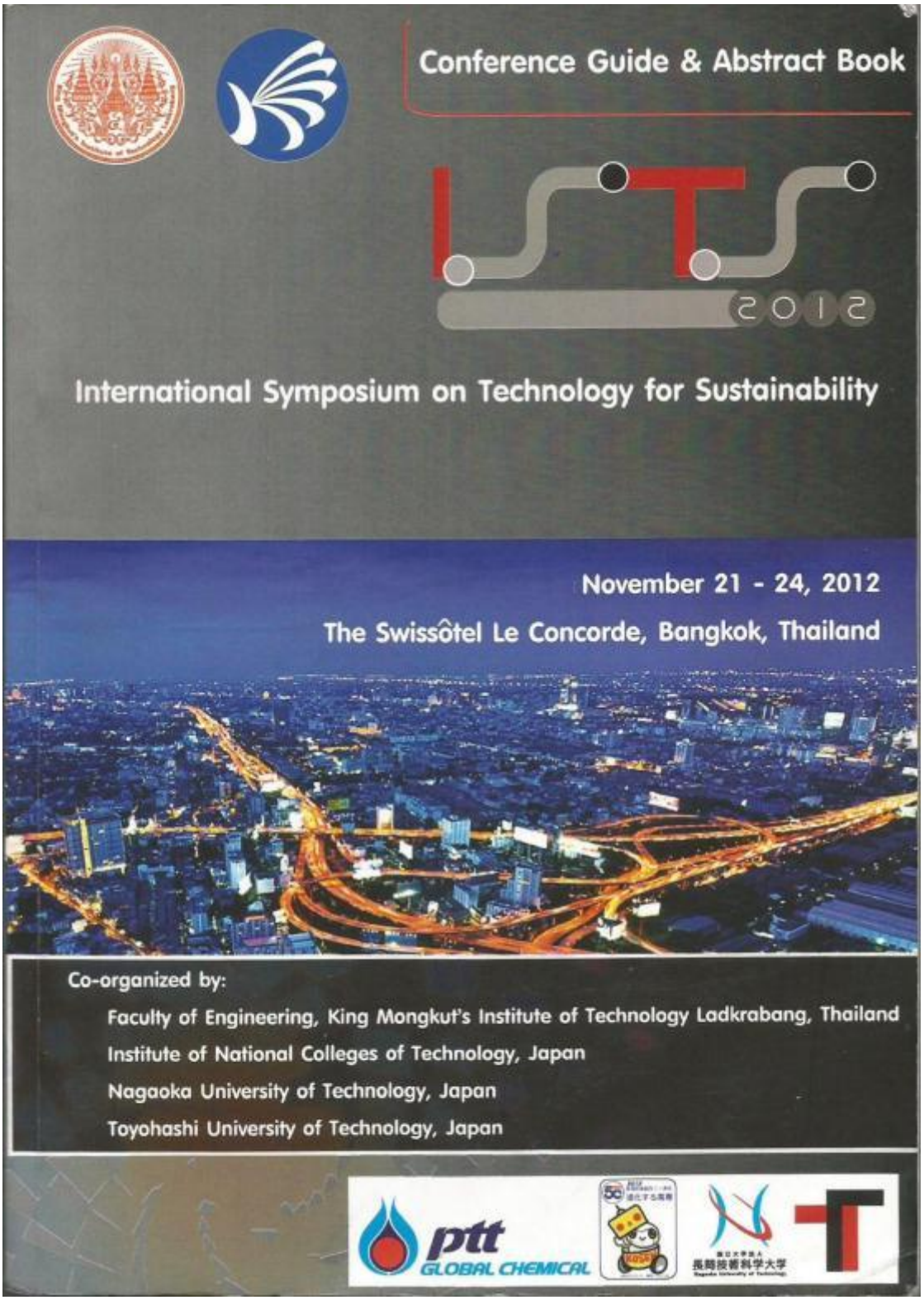
Conference Guide & Abstract Book
ISTS
2012
International Symposium on Technology for Sustainability
November 21 - 24, 2012
The Swissôtel Le Concorde, Bangkok, Thailand
Co-organized by:
Faculty of Engineering, King Mongkut's Institute of Technology Ladkrabang, Thailand
Institute of National Colleges of Technology, Japan
Nagaoka University of Technology, Japan
Toyohashi University of Technology, Japan
ptt
GLOBAL CHEMICAL

Design of Experimental Procedures for Thermal Properties Analysis of Lithium-ion Battery for EV

Chayangkun Sanguanwatana
Thailand Advance Institute of Science and Technology (TAIST), Tokyo Tech
Bangkok, Thailand
Email: aura_win@hotmail.com

Monsak Pimsarn
Faculty of Mechanical Engineering
King Mongkut's Institute of Technology Ladkrabang
Bangkok, Thailand

Chadchai Srisurangkul
National Metals and Materials Technology Center
Bangkok, Thailand
Email: chadchas@mtec.or.th

Tsushima Shohji
Research Center for Carbon Recycling and Energy
Tokyo Institute of Technology
Tokyo, Japan

***Abstract*— A series of experimental procedures were designed in order to capture thermal and electrical properties of a selected lithium ion battery for electric vehicles. Derived thermal model for lithium ion battery were mainly used for the design. These thermal properties include heat capacity, heat generation and cell temperature at the different amount of electrical load applied. Electrical properties such as internal resistance and open circuit voltage are also analyzed. The data from experiment will be used to serve the future design of battery thermal management system in the electric vehicle in order to preserve battery's life and maximize its performance.**

Keywords-component; Lithium ion battery, Electric Vehicle, Lithium ion battery Thermal Characterization, Battery Thermal Management System, Battery Thermal Model

INTRODUCTION

Realizing that the effect global warming is increasing and fossil fuel is decreasing rapidly due to the elevated amount of automobiles used today, electric vehicle become one of the alternative vehicles for sustaining the environment. Electric vehicle produce zero pipe-tail emission and therefore can reduce the amount of greenhouse gas such as carbon dioxide released into the air. To reduce the cost of buying brand new vehicle and to recycle the material, MTEC (National Metals and Materials Technology Center, Thailand initiated the modified electric vehicle project which has a conventional components in a used gasoline car with electrical components such as motor and battery. With this, many tests and experiments are required to maximize the performance of the overall system. In this paper, the main focus is on the battery which is the most important part in the energy supply system.

THE BATTERY

Lithium Iron Phosphate Battery

Many types of batteries were invented to store energy for various purposes but comparing to the other types such as lead acid or nickel metal hydride, lithium ion battery is considered to be more advantageous. These advantages include higher working voltage, less self-discharge rate, higher energy density and it contains no memory effect. John Goodenough and his research group in University of Texas invented the "Lithium iron phosphate" as a new chemistry for lithium ion battery[1] which contains more benefits than the usual Lithium Cobolt chemistry in terms of environmental friendly and thermal stability. It is becoming gradually popular and used in many applications such as One Laptop per Child project in China and many electric car conversion projects.

Battery Safety Issues

The manufacturer can never know how the users utilize the battery. When the battery is misused, the consequence can be severe. This may include overcharging/discharging, penetration, excessive operating environment temperature or failure of battery management system. It is noticed that all of those can be related to thermal issue. Overcharging can create the rise in temperature inside the battery, causing the pressure from gassing inside and the pressure might cause the battery to explode. Excessively low operating temperature can also permanently destroy the battery as it causes lithium plating. Operation outside the working voltage is also harmful to the battery for example of over discharging which can permanently reduce the capacity. Figure below illustrates the safe operation window for lithium ion battery.

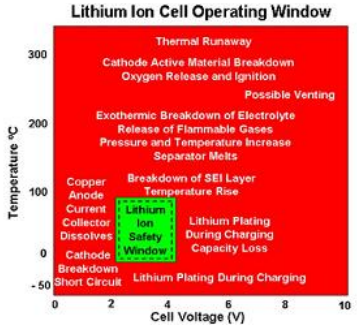

Figure 1: Lithium Ion Cell Operating Window[2]

Many protection mechanisms were built inside the battery such as integrated circuits, pressure vents, thermal fuses and etc. This is to protect the user from being harmed as the battery is misused. However, it is best that the battery does not show any signs of harm and therefore, proper management system is required.

Battery Thermal Management System

Being the greatest enemy to the battery, heat must be carefully monitored in the surroundings. As noted in the previous section, two main causes from battery failures are over-voltage and over-temperature. However, it can be seen that the latter can produce much more severe consequence. This is when the thermal management system for the battery comes in to regulate the operating temperature of the battery to prolong its life and maximized its performance. According to NREL (National Renewable Energy Laboratory, USA), some procedures are needed before designing the thermal management system. Thermal response of the battery can be captured by using various methods such as thermal analysis (CAD), fluid and heat transfer simulation (CFD), thermal characterization and vehicle testing[3]

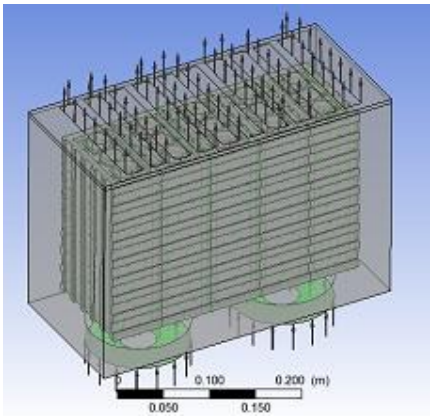

Figure 2: CFD simulation for cooling system of the battery[4]

In this case, thermal characterization is the main focus. This is to acquire thermal properties from the battery. Thermal model will be used for this purpose. The data of thermal properties can be used for the design of battery thermal management system as it can

Battery Thermal Model

As derived by Newman et al[5], a single cell thermal model of lithium ion battery is used by many researcher to study thermal properties of the battery[6] and thermal behavior of the battery at rapid charge/discharge cycles[7]. The model is summarized as below;

$$I(V_{oc}-V)+IT_{cell}\frac{\partial V_{oc}}{\partial T_{cell}}=h(T_{surf}-T_{amb})+C_p\frac{dT_{cell}}{dt} \quad (1)$$

Where; I = Current (A), V_{oc} = Open circuit voltage (V),

V = Cell voltage (V), T_{surf} = Surface Temperature (°C),

T_{amb} = Ambient Temperature (°C), t = Time (s),

T_{cell} = Cell Temperature (°C), C_p = Heat Capacity (J/°C),

h = Surrounding heat transfer coefficient (W/°C)

Here, some assumptions are required such as uniform temperature distribution inside the battery and stable chemical reactions.

The battery is considered as the control volume in the heat balance for this thermal model. On the left hand side, there are two main terms. First term is called overpotential resistance which is always positive because it always generates heat from the battery, it is the result of heated resistance inside the battery due to charge or discharge process. In the second term on the left hand side, it is the reversible entropic heat which is related to the Gibb's free energy and battery's chemical reactions. This term can either be positive or negative depends on the heat transfer whether it is endothermic or exothermic. For the right hand side, surrounding heat is expressed in the first term and can be calculated if the surface and ambient temperature is known. The second term represents the heat capacity of the battery which will be the main properties for the analysis. However, the experimental designs are required beforehand.

EXPERIMENTAL DESIGN

Prelimanry Design of the Experimental Setup

To determine thermal properties of the selected Lithium ion battery at different loads and environments, a setup of experiment is prepared as illustrated in the figure below;

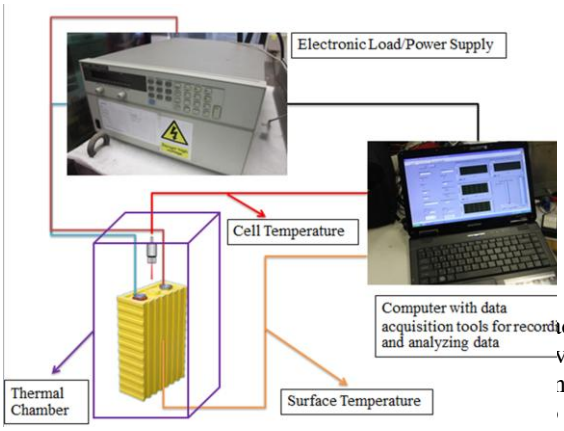

T d or
pow vely.
In t n be
obta the
batte also
monitored by using infrared and thermocouple respectively. Overall design is based on the thermal model of the battery (equation 1). The electronic load can be programmed to either perform constant current or pulse current discharge and temperature response from both internal cell and surface can be observed and analyzed according to the thermal model. Thermal chamber is required for regulating environment temperature around the battery and also for a separated experiment in order to determine the term called "temperature coefficient" which will be explained in the next section.

Analysis of Thermal Properties of the Battery Using Thermal Model and Results from the Designed Experiment

The analysis of thermal properties of the battery is done considering one term by another. The first part considers heat generation from the cell and thermal properties are analyzed in the second part. As noted from equation 1, the left hand side shows heat generated from the battery while it is being loaded.

$$\dot{Q} = I(V_{oc} - V) + IT_{cell}\frac{\partial V_{oc}}{\partial T_{cell}} \qquad (2)$$

The first term for calculating heat generated from the battery is called "resistive" or "overpotential" heat which is the can be calculated from the voltage and current load data while being charged or discharged. The current load can be altered to see the change to 1CA, 0.5CA or 2CA to see how much resistive heat dissipate. In the second term, noted as "reversible entropic" term which is the product of current loaded, cell temperature and the temperature coefficient (dV_{oc}/dT_{cell}) which need a separated experiment.

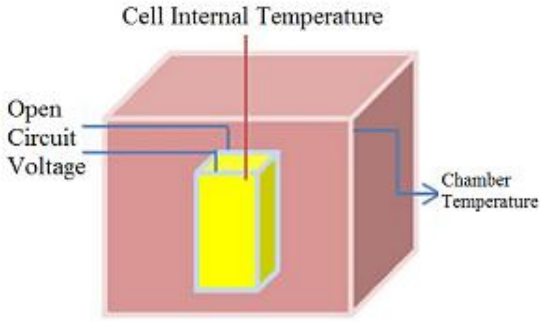

Figure 4: Schematic of experimental setup for temperature coefficient

To obtain the value of temperature coefficient, the battery is put inside thermal chamber which its temperature can be adjusted. Voltmeter or similar device is attached to the terminals and infrared temperature sensor is attached at the top of the cell. The temperature of the chamber is adjusted according to the actual operating conditions and then the internal temperature and open circuit voltage are observed. The data is obtained from the state of charge of 10% - 100%.

With the heat generated analyzed at the different current loads, surrounding heat coefficient (h) is firstly analyzed considering the steady state condition while the battery is loaded. This can be noticed from the temperature curve with time while the temperature stays constant at a certain period. With this condition the heat capacity term becomes zero as $\delta T_{cell}/\delta t = 0$. With this, the surrounding heat coefficient is determined at the different amount of current load applied.

At the transient condition, where temperature do not stay constant with time or $\delta T_{cell}/\delta t \neq 0$, the data corresponding to the current load applied can be used to determine the heat capacity of the battery. The initial condition is at 100% state of charge at room temperature. As the battery is discharged the value of $V-V_{oc}$ will keep changing and so as the value of Q due to elevated temperature but the heat capacity will depend on the load.

RESULTS FROM PRELIMINARY EXPERIMENTS

At this point, performance characteristics such as charge and discharge curve are obtained. Surface and terminal temperature response from the discharge test are also captured. Also, with the results from pulse discharge test, internal resistance and open circuit voltage of the battery are also analyzed.

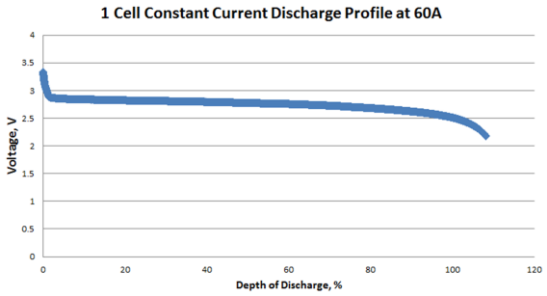

Figure 5: Constant current discharge profile

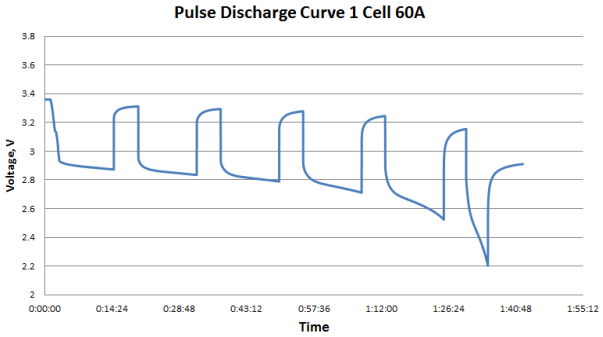

Figure 6: Pulse discharge test result

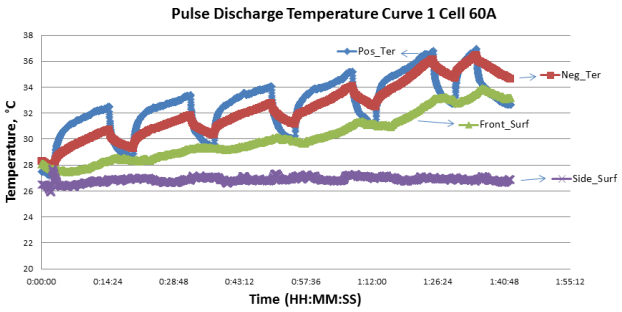

Figure 7: Temperature response from pulse test

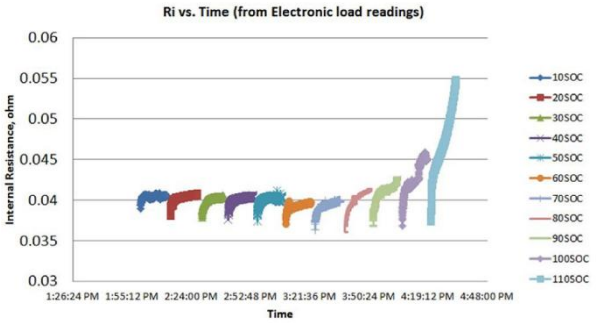

Figure 8: Internal Resistance calculated from pulsed test results

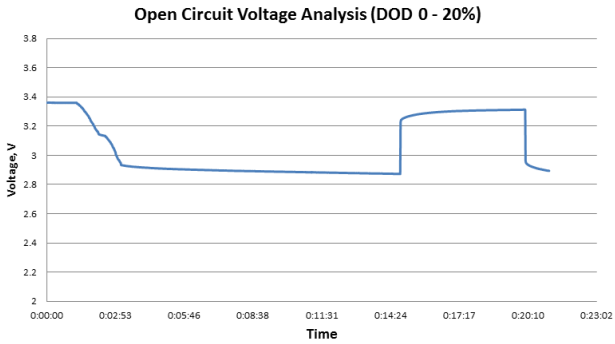

Figure 9: Open circuit voltage observation at depth of discharge of 0 – 20%.

In figure 5, constant current discharge curve which has the "flat" profile from depth of discharge from 10% to 80%. This makes it complicate to learn the state of charge just by looking at the voltage. Therefore, pulse current discharge experiment is applied (results shown in figure 6). The result of pulse discharge test benefits in many ways such as ease of monitoring battery's state of charge, calculating the internal resistance and can be used to study the temperature dynamics with the step load as in figure 7. In this case, internal resistance is calculated by using the ohm's law from the result of pulse current discharge test, results shown in figure 8. As noted in thermal model, open circuit voltage is one of the important values in calculating heat generation. The dynamic of open circuit voltage in each stage of charge is observed from the pulse discharge test with the results shown in figure 9 (depth of discharge from 0 – 20%).

In the next step, it is aimed to have the battery installed with the infrared thermal sensor to measure its internal temperature. When the behavior of internal cell temperature is observed while the battery is loaded, thermal properties can be calculated. Then the data from this can be used to perform thermal characterization to the battery and battery thermal management system can be designed to the maximum efficiency for the electric vehicle.

• ACKNOWLEDGMENT

The author would like to express the appreciation to his advisors; Dr. Chadchai Srisurangkul of MTEC, Dr. Monsak Pimsarn of KMITL and Dr. Tsushima Shohji of Tokyo Tech for providing knowledge and directions towards the success of this work.

• REFERENCES

K.E.Thomas. J.Newman, "Thermal Modeling of Porous Insertion Electrodes", Journal of The Electrochemical Society, 2003, 150(2), pp 176- 192.

Woodbank Communication. "Lithium Battery Failures", Electropaedia: Battery and Energy Technology, 2005, http://www.mpoweruk.com/lithium_failures.htm.

A.Pesaran. "Battery Thermal Management, Battery Modeling and Validation, Ultracapacitor Modeling and Hybridization", National Renewable Energy Laboratory, 2002.

V.Vuthiwongvarakorn. N. Taychavinijudom, "Design of a Battery Thermal Management system for Electric Vehicle", 2010.

K.E.Thomas. J.Newman, "Thermal Modeling of Porous Insertion Electrodes", Journal of The Electrochemical Society, 2003, 150(2), pp 176- 192.

C.Forgez, D.Vinh Do, G.Friedrich, M.Morcrette, C.Delacourt "Thermal modeling of a cylindrical $LiFePO_4$/graphite lithium-ion battery", Journal of Power Sources, 2009, 195, pp 2961-2968.

K. Onda, "Thermal behavior of small lithium-ion battery during rapid chage and discharge cycles", Journal of Power Sources, 2006, 158, pp 535-542.

BIOGRAPHY

Name: Mr. Chayangkun Sanguanwatana

Date of Birth: May 8, 1988

Place of Birth: Bangkok, Thailand

Education:

2006-2009 B. ME. School of Manufacturing Systems and Mechanical Engineering, Sirindhorn International Institute of Technology, Thammasat University

2010-2014 M.Eng. in Automotive Engineering (International program), International College, King Mongkut's Institute of Technology Ladkrabang (KMITL)

Honour and Scholarships:

2010-2012 Full scholarship for study in the master degree from National Science and Technology Development Agency (NSTDA)

Publications:

1. Sanguanwatana C., Srisurangkul C., Tsushima S., and Pimsarn M., "Design of Experimental Procedures for Thermal Properties Analysis of Lithium-ion Battery for EV", 2012, 8th International Symposium on Technology for Sustainability (ISTS 2012), November 27 - November 30, 2012, Impact, Swissôtel Le Concorde, Bangkok, Thailand
2. Sanguanwatana C., Srisurangkul C., Tsushima S., and Pimsarn M., "Design of the experimental procedures for analysis of thermal and electrical properties of a prismatic LiFeYPO4 battery in a modified electric car", The 2012 World Automotive Congress (FISITA 2012), November 27 - November 30, 2012, China National Convention Center (CNCC), Beijing, Chinad.